Phase 2 Final Report

A Phosphorus/Eutrophication Water Quality Model for Cayuga Lake, New York

Submitted December 2016

Revised January 2017

This page intentionally left blank

Phase 2 Final Report

A Phosphorus/Eutrophication Water Quality Model for Cayuga Lake, New York

Prepared for
Cornell University

Submitted December 2016
Revised January 2017

Prepared by

Upstate Freshwater Institute
Syracuse, NY

Department of Biological and Environmental Science
Cornell University
Ithaca, NY

This page intentionally left blank

Table of Contents

Appendices Listing

Appendices are hyperlinked to text below. Clicking on the title will open the relavent appendix.

List of Tables

List of Figures

Executive Summary (arranged by report section)

Section 1: Background – Modeling Goals, Progress from Phase 1, and Organization of the Phase 2 Findings

This section presented background for this study of Cayuga Lake, to support management deliberations and advance the understanding of phosphorus (P)-eutrophication and water column sediment. The design and planning of this four year, two phase study was reviewed. The summary of findings from the approved Phase 1 report was reviewed, as it importantly influenced the foci and approaches adopted for Phase 2. A schematic representing the approach and major elements of the Phase 2 work presents a logic pattern for the interaction of the work topics, and serves to provide organization for the reported findings.

Written documentation has been a central feature of meeting regulatory requirements and providing insights for management deliberation, and advancing the understanding of key limnological processes. It has been apparent from the outset that the P and sediment issues are interactive on the shelf of Cayuga Lake and the near-shore waters proximate to tributary inflows, similar to the setting in many other lakes. This interaction has been conceptually recognized, but now quantitatively resolved at Cayuga Lake, as documented in project reports and advanced through publication of key findings in the peer-reviewed literature (e.g., Effler et al. 2014, Peng and Effler 2015, Gelda et al. 2016b; others on Table 1-3 in Section 1). These challenging water quality issues have received two extensive and independent forms of written documentation. The first form is related to regulatory needs for such projects/studies, including (1) scientific proposals, (2) QAPP(s), (3) presentations on progress, (4) final reports of Phases of work, and (5) preparation of written responses by the study team to review comments prepared by the regulatory review team.

The second form of written communication for this project has been publication of key findings, insights, advancements of understanding, and mechanistic mathematical models, in peer-reviewed journals. These published articles have been critical in establishing the credibility of the findings of this project. Moreover, these papers have advanced related research for Cayuga Lake and other lakes with similar issues.

Finally, the organization of the various primary study elements of the Phase 2 work is presented in Figure 1-2 in Section 1. This schematic diagram also serves as the organizational framework for this report.

Section 2: Two-Dimensional Hydrothermal/Transport Submodel

A two-dimensional longitudinal-vertical hydrothermal/transport model (the hydrothermal/ transport submodel of CE-QUAL-W2, version 3.72) has been set-up, rigorously tested, and applied for Cayuga Lake (Gelda et al. 2015, Gelda et al. 2016a, 2016b). Robust testing of the

model was supported by rich monitoring data sets of (1) temperature profiles at multiple lake sites for ten years; (2) near-surface temperatures at one end of the lake for 16 years, including irregular occurrences of upwelling events; (3) the timing and magnitude of seiche activity (oscillations of stratified layers) for two years; and (4) transport of a conservative tracer. The model demonstrated excellent temporal stability, maintaining good performance in uninterrupted simulations over a period of 15 years (Gelda et al. 2015). The large aspect ratio (length:width ratio) of Cayuga Lake (like the other Finger Lakes) contributes to these positive performance features.

In addition to application of the hydrothermal/transport sub-model in water quality modeling in Phase 2, it was also applied in Phase 1 to resolve features of transport known to influence water quality in Cayuga Lake. These applications addressed: (1) residence times of stream inputs within the shelf and the entire lake, (2) transport and fate of negatively buoyant (i.e., plunging) streams, and (3) the extent of transport from the hypolimnion to the epilimnion. This hydrothermal/transport model is particularly appropriate for addressing longitudinal differences in water quality, including the shelf vs. pelagic waters, and issues involving multiple time scales.

Section 3: Bioavailable Phosphorus Loads to Cayuga Lake, other Constituent Loads, and Representing the Effects of the Cayuga Inlet Channel

The important phosphorus (P) bioavailability concept was integrated into a comprehensive P loading analysis for the larger tributaries of Cayuga Lake. Components of the analysis of Phase 1 included (Prestigiacomo et al. 2016) the (1) monitoring of particulate P (PP), soluble unreactive P (SUP), and soluble reactive P (SRP), supported by bi-weekly and runoff event-based sampling of the lake's four largest tributaries over the April-October interval of 2013; (2) development of relationships between tributary P concentrations and flow rate (Q); (3) algal bioavailability assays of PP, SUP, and SRP for the primary tributaries and the three largest point sources; and (4) development of P loading estimates to apportion contributions according to individual non-point and point sources for the overall and bioavailable fractions and to provide a representation of the effects of interannual variations in tributary flows on P loads.

Tributary SRP, SUP, and PP were found to be completely, mostly, and less bioavailable, respectively (Prestigiacomo et al. 2016). The highest mean bioavailability for PP was observed for Salmon Creek, the stream with the highest agriculture land use. Point source contributions to the present total bioavailable P load (BAP_L) are minor (5%), reflecting the benefit of reductions from recent treatment upgrades. The BAP_L represented only about 25% of the total P load received during the 2013 study period, because of the large contribution of the low bioavailable PP component. Most of BAP_L (>70% in study period of 2013) is received during high flow intervals. The common large variations in BAP_L, that doubtless accompany those in tributary

flow, will tend to mask future responses to changes in individual sources (Prestigiacomo et al. 2016).

The pursuit of representative loading estimates was expanded in Phase 2 in support of the testing and application of the water quality model and sub-models. Related work in Phase 2 included (1) addition of other constituents (along with P) to support broader capabilities and issues with the water quality model, (2) review of other data sets to identify potential systematic changes in the quality of these tributary inputs since the late 1990s, (3) resolution of the concentration-flow dependencies of the constituents for multiple large tributaries in support of analyses of consistency of data sources and loading estimates, and (4) development of loading estimates for model testing and application.

Daily loading estimates for forms of P were made for the April-October interval of 2013 with widely used software, FLUX32 (Method 6; Prestigiacomo et al. 2016), with the logarithmic concentration-flow (C-Q) relationship stratified seasonally. A somewhat different time stratification strategy was applied with FLUX32 in Phase 2 that included additional constituents and extended loading estimates year-round. Relationships of C-Q were investigated for each case. Distinct shifts in these relationships were not observed with wide changes in Q for dissolved constituents. Thus uniform C-Q dependencies were used (though different among the tributaries) to estimate the loads of these dissolved materials, driven by measured daily flow rates for the various tributaries. In contrast, two strata were invoked for the particulate constituents, reflecting their abrupt increases in concentration with Q. The stratified relationships were used, in combination with Q records to estimate external loads of these materials.

Availability of historic concentration data for the Cayuga Lake tributaries was generally limited, but differed with respect to constituent and tributary. Despite the occurrence of some differences, similar C-Q relationships for the other data sources were indicated. These consistent relationships have provided support for the assumed unchanged C-Q dependencies for the tributaries over the monitored interval (1998-2013) adopted here. Accordingly, the C-Q relationships developed from 2013 observations supported the first approximations of constituent loads for the 1998-2013 period, which varied dramatically year-to-year in this period because of wide interannual differences in Q.

The Cayuga Inlet Channel, constructed in 1977, receives the inflows of Cayuga Inlet, Sixmile Creek, and Cascadilla Creeks, and modifies their loading to the lake within the channel, representing a complication for loading estimates. The contemporary effects of the channel on the loading were evaluated based on 2013 observations through (1) continuous instrumentation measurements (velocity, turbidity, and temperature), (2) laboratory measurements (e.g., forms of P), and (3) analyses of these data. The goal was to appropriately modify the loads from these tributaries during the study interval of 2013 according to what reaches the southern end of the lake via the Channel, and develop a basis to represent this effect based on differences in Q levels.

The vertical profile measurements of flow adjoining the mouth of the channel directly resolved occurrences of bi-directional flow during low Q intervals. However, outflow from the channel to the lake was recurring during runoff events.

The Channel acted as a source of particulate constituents (e.g., PP) during dry weather intervals, suggesting inputs from channel deposits. The Channel acted as a sediment sink overall during major runoff events; i.e., tributary inputs to the Channel exceeded outputs to the lake. The Channel acted as a source of SRP_L (compared to summed tributaries) for most of the 2013 monitoring, but a sink for the largest runoff events. In contrast, the Channel remained a source of SUP throughout the study. Load estimates from the Channel were developed using the same method as adopted for the major tributaries; i.e., based on C-Q relationships kept uniform over Q ranges for dissolved constituents, but stratified (2 strata) for particulate forms. In development of overall loading estimates from the watersheds to the lake, the Channel source replaced those that had been attributed separately to Cayuga Inlet, Sixmile Creek, and Cascadilla Creek.

Section 4 Minerogenic Particles and a PAV_m Submodel

Minerogenic (inorganic) particles play important ecological and water quality roles in freshwaters by presenting reactive surfaces, affecting the concentrations and stoichiometry of particulate constituents, influencing metabolic activity, contributing to net sedimentation, and degrading optical water quality through the process of light scattering (Effler et al. 2014). These issues are important in Cayuga Lake, and many other New York lakes. When concentrations are high, these minerogenic particles (sediment) affect other water quality metrics of concern, including P concentrations (Prestigiacomo et al. 2016, Gelda et al. 2016b), turbidity (Tn; Effler et al. 2014), and water clarity (Secchi disk depth, Z_{SD}; Effler et al. 2014, 2016).

Quantification of minerogenic particles, and their effects, was limited previously by the use of common gravimetric measurements. The transition was made in this study to the use of a scanning electron microscopy technique (SAX) instead that provides quantitative characterizations of minerogenic particle populations. SAX analyses can resolve the important effects of these particles on water quality issues related to both P and sediment. Minerogenic particles are a dominant component of tributary inputs (Prestigiacomo et al. 2016, Gelda et al. 2016b). Advantages of SAX over gravimetric analyses for the minerogenic particle populations of lakes include (1) improved analytical performance, (2) insight from the more robust size and composition information, (3) theoretical advantages to assess optical impacts, and (4) stronger relationships with water quality metrics.

In the context of contributions of minerogenic particles to common metrics of water quality, the primary summary result of SAX characterizations is the projected area of the minerogenic particles per unit volume of water (PAV_m). SAX provides resolution of the contributions of both multiple size classes and generic geochemical particle types (e.g., clays, calcite) to PAV_m and bulk measurements of light scattering (Peng and Effler 2016a, b), Secchi disk depth (Z_{SD}) (Effler

et al. 2016), turbidity (Tn) (Effler et al. 2014), and the minerogenic form of PP (PP_m) (Effler et al. 2014, Gelda et al. 2016b). The contributions of these particles are substantial, particularly on the shelf. There is legitimate concern for increased PAV_m inputs, driven by predicted increases in the occurrence and severity of major runoff events in this region from climate change. Clay minerals, received primarily from the tributaries during runoff events, dominate lake PAV_m, though calcite precipitated internally is important in late summer ("whiting event"; Effler and Peng 2014, Peng and Effler 2016b). The clay inputs may be linked to anthropogenic influences in the watershed, while an interaction between whiting events and human activities has not been established (Peng and Effler 2016b).

A mass balance model for PAV_m, partitioned according to the contributions of four size classes of terrigenous particles (mostly clays), has been developed and successfully tested for Cayuga Lake, supported by long-term monitoring of PAV_m (Gelda et al. 2016a). The model represents the source of PAV_m as tributary inputs, using loading rate estimates developed according to protocols described in Section 3. The two-dimensional, laterally averaged hydrothermal/transport sub-model was adopted as the transport sub-model for the overall PAV_m model. The PAV_m model represents the effects of three in-lake loss processes for the minerogenic particles (1) size-dependent settling, (2) enhancement of settling through aggregation, and (3) filter feeding by Dreissenid mussels (Gelda et al. 2016a).

The central roles of major runoff events and local external loads of minerogenic sediment at the southern end of the lake in driving patterns of PAV_m in time and space were successfully simulated, including (1) the higher PAV_m levels on the shelf, relative to pelagic waters, following runoff events; and (2) the positive dependence of the shelf increases on the magnitude of the event (Gelda et al 2016a). Analyses with the model established that settling, with aggregation enhancement, dominated the loss of PAV_m from the water column of the shelf following runoff events, while mussel filtration increased in relative importance in pelagic waters. The PAV_m model can be used as a quantitative basis to resolve the effects of the minerogenic particles on optical properties and phosphorus concentrations (Gelda et al. 2016b).

Section 5: Water Quality Optics Sub-models

Secchi disk depth (Z_{SD}) is one of the three most widely adopted metrics of trophic state, but particle types other than phytoplankton, including minerogenic particles, can also importantly influence this metric of water clarity (Effler et al. 2016a). An optics theory-based mechanistic model that represents the effects of multiple particle types on Z_{SD} was developed, tested, and applied for Cayuga Lake (Effler et al. 2016a). Robust data sets supported this initiative at Cayuga Lake, including (1) Z_{SD} observations at multiple sites, over an extended period; (2) modern optical instrumentation measurements of the beam attenuation (c) and particulate scattering (bp) coefficients; and (3) measures of constituents responsible for contributions to b_p by phytoplankton (b_o) and minerogenic particles (b_m; $b_p = b_o + b_m$). The model features two serially connected links. The first link supports predictions of b_p from those for b_o and b_m. The

second link provides predictions of Z_{SD} based on those for b_p, utilizing an earlier optical theory radiative transfer equation. Recent advancements in mechanistically strong estimates of b_m, empirical estimates of b_o, and more widely available bulk measurements of c and b_p, have enabled a transformation from a theory-based conceptual model to this implementable Z_{SD} model for lacustrine waters. The successfully tested model was applied to quantify the contributions of phytoplankton biomass, and minerogenic particle groups, such as terrigenous clay minerals and autochthonously produced calcite, to recent b_p and Z_{SD} levels and dynamics (Effler et al. 2016a).

The best metrics of the b_o component are concentrations of particulate organic carbon (POC) and chlorophyll *a* (Chl-*a*); POC demonstrated better performance. The best metric for b_m is PAV_m (from SAX; see Section 4), the projected area of minerogenic particles per unit volume of water. Reasonably good performance was demonstrated with each of the two links of the model and overall (e.g., predictions of Z_{SD} from paired measurements of POC and PAV_m; Effler et al. 2016a). The successfully tested model was applied separately through predictions of shifts in Z_{SD} distributions associated with (1) reasonable shifts in Chl-*a* concentrations (i.e., $b_o \pm 20\%$), (2) the contribution of minerogenic particles (PAV_m; i.e., b_m, elimination), and (3) the present contribution of calcite (a fraction of b_m). The adopted change in Chl-*a* was predicted to cause 10% (inverse) shifts in Z_{SD}. In the absence of minerogenic particles ($b_m = 0$) the average Z_{SD} was predicted to be 35% greater in pelagic waters and 42% higher on the shelf. In the absence of internally produced calcite the Z_{SD} would be ~15% higher on average in late summer. The Z_{SD} model developed and tested here is expected to be highly transferable to many other lakes, and has been integrated into the larger water quality model for Cayuga Lake.

Turbidity (Tn) is another important optical metric of water quality, particularly with respect to water supplies. Z_{SD} depends primarily on overall particle scattering (b_p), in contrast to the regulation of Tn by the side-scattering coefficient (b_{sc}), approximately measured by a turbidimeter (Effler et al. 2014). Minerogenic particles have a greater effect on Tn than Z_{SD} because of the greater dependence of b_{sc} than bp on the higher refractive index values of such particles. Variations in the relative contributions of phytoplankton vs. minerogenic particles to the overall particle population are a primary source of variations in their relative contributions to these optical measures; e.g., noise in the Z_{SD} vs. Tn relationships.

The dependence of Tn on the contributions of minerogenic (PAV_m) vs. bioseston (e.g., phytoplankton, Chl-*a*) in Cayuga Lake was developed through an empirical stoichiometric approach based on paired observations for both shelf and pelagic sites over the 1998-2007 period (Effler et al. 2014). The higher Tn levels on the shelf following runoff events was found to be a result of elevated PAV_m associated with allochthonous inputs. The empirical model for Tn performed well, particularly on an annual basis. Predictions generally tracking observations, and higher shelf vs. pelagic values were resolved, particularly after runoff events. Regulation of Tn by minerogenic particles is consistent with optical theory and the PAV_m levels, based on the much greater efficiency of side-scattering for minerogenic vs. organic particles (Effler et al. 2014).

Section 6: Simulation of the Contribution of Minerogenic Particles to Particulate Phosphorus

Phosphorus (P) associated with minerogenic particles delivered from watersheds can interfere with the common use of total P (TP) concentration as a metric of trophic state in lakes, particularly proximate to tributary entries. The concentration of biologically unavailable minerogenic particulate P ($PP_{m/u}$), where it is noteworthy, should be subtracted from TP in considering primary production potential and trophic state levels (Gelda et al. 2016b). A mass balance model for $PP_{m/u}$ was developed and tested for Cayuga Lake (Gelda et al. 2016b). This model was supported by a rare combination of detailed information, collected as part of this project, for minerogenic particle dynamics for the tributaries and lake (Peng and Effler 2015; Section 4), the bioavailability of tributary particulate P (PP) (Prestigiacomo et al. 2016; Section 3), and previously tested hydrothermal/transport (Gelda et al. 2015; Section 2) and minerogenic particle concentration (Gelda et al. 2016a; Section 4) submodels. The central roles of major runoff events and localized tributary loading at the southern end of the lake in driving patterns of $PP_{m/u}$ in time and space were well simulated, including (1) the high $PP_{m/u}$ levels on the shelf proximate to multiple large tributary inflows, relative to pelagic waters, following runoff events, and (2) positive dependence of the shelf increases on the magnitude of the event. The $PP_{m/u}$ component was primarily responsible for the higher summer average TP on the shelf versus pelagic waters and the exceedances of the TP guidance value of 20 g/Lon the shelf.

This work has important implications for appropriate use of P measurements in management of trophic state conditions in Cayuga Lake and other lacustrine waters. The concentrations of $PP_{m/u}$ in the pelagic waters in this lake only make a modest contribution to TP, establishing TP is not compromised as a trophic state metric in the open waters by this unavailable form of P. However, TP is severely compromised as a trophic state metric on the shelf because of temporally irregular and much higher $PP_{m/u}$ levels, caused by runoff event inputs from local tributaries enriched in $PP_{m/u}$ (Gelda et al. 2016b). The occurrences of high $PP_{m/u}$ levels on the shelf were well simulated with the $PP_{m/u}$ model. The irregular exceedances of the 20 g/L guidance value on the shelf in high runoff summers (Effler et al. 2010, 2014) are caused by locally elevated levels of non-bioavailable $PP_{m/u}$. This systematically compromises TP as a quantitative trophic state metric for that area. An "adjusted" summer average TP for the shelf ($TP_{adjusted\ shelf}$), calculated by subtracting the $PP_{m/u}$ concentration difference between the shelf and pelagic waters from the shelf TP concentration, would be more meaningful relative to trophic state

$$TP_{adjusted\ shelf} = TP_{shelf} - (PP_{m/u\ shelf} - PP_{m/u\ pelagic})$$

where TP_{shelf} is the summer average TP value on the shelf, and $PP_{m/u\ shelf}$ and $PP_{m/u\ pelagic}$ are the summer average $PP_{m/u}$ values for the shelf and pelagic waters, respectively (Gelda et al. 2016b). The limitation of TP as a metric of trophic state on the shelf is not unique to Cayuga Lake. The localization of tributary inputs at one end of a lake and their enrichment in inorganic

sediment during runoff events (Prestigiacomo et al. 2007; Peng and Effler 2015) is common (Wetzel 2001).

Applications of this model call into question the appropriateness of TP as a trophic state metric for the shelf. These model results are generally consistent with limnological analyses, which together have demonstrated the short-comings of using TP as a metric of trophic state on the shelf. Findings of the related limnological analyses have included (Effler et al. 2010; 2014; Peng and Effler 2015; Prestigiacomo et al. 2016) : (1) the coupling of both high TP and lower Z_{SD} on the shelf compared to pelagic waters, but without noteworthy differences in Chl-*a*, (2) high PP:Chl-*a* ratios on the shelf compared to pelagic waters, (3) a low f_{BAP} (bioavailability fraction) value (0.02) for a shelf PP sample collected after a major runoff event, (4) low f_{BAP} values for PP delivered in large quantities from the shelf tributaries during runoff events, (5) coincidence of high PAV_m and $PP_{m/u}$ levels on the shelf following runoff events, and (6) application of an empirical model for temporal and spatial patterns of $PP_{m/u}$ in Cayuga Lake based on paired PAV_m and Chl-*a* observations. These findings make it clear that TP should not be applied as an equivalent metric of trophic state on the shelf and in pelagic waters. Moreover, rapid flushing of the shelf, promoted by active lake-wide mixing, further limits impacts on local phytoplankton levels from the local tributary inputs (Effler et al. 2010; Gelda et al. 2015).Concentrations in Cayuga Lake

Section 7: Cayuga Lake Hydrothermal and Water Quality Modeling

The overarching goal of this study was to develop and test a water quality P-eutrophication model for Cayuga Lake. The integrated model (CLM-2D) is capable of supporting a phosphorus TMDL analysis for Cayuga Lake, including the southern shelf. The model incorporates the bioavailability concept for external P inputs and the potential importance of the phytoplankton, zooplankton, and dreissenid mussel communities. The New York State Department of Environmental Conservation listed the southern end of Cayuga Lake (e.g., shelf) as an impaired segment with respect to phosphorus and silt/sediment in 2002. Findings from the study of Cayuga Lake have supported a unified scientific position of the absence of a reliable signature of cultural eutrophication for the water column of the shelf, despite frequently high TP levels. TP, chlorophyll a (Chl-*a*), and Secchi disk depth (Z_{SD}) have limitations as reliable trophic state indicators and targets for management, as they can be importantly influenced by processes and constituents not directly coupled with primary production. Minerogenic particles can complicate relationships between trophic state metrics because have associated P and contribute to diminished Z_{SD}.

We have adopted the modeling philosophy of parsimony in development of this P-eutrophication model for Cayuga Lake. The model structure and capabilities are consistent with our scientific understanding of Cayuga Lake and suitable for the regulatory task of conducting a P TMDL analysis. CLM-2D is an integrated two dimensional model utilizing the hydrothermal/transport portion of CE-QUAL-W2 (version 3.72; Cole and Wells 2015) and a

separately developed water quality model described in Section 7 of this report. The overall water quality (P-eutrophication) model has a robust array of model state variables that address the water quality issues targeted by this study. Multiple forms of P are predicted, including particulate and dissolved fractions, which are partitioned according to labile and refractory, and organic versus inorganic, components. Phytoplankton biomass and organic carbon are simulated, and Chl-*a* is derived from algal carbon. Secchi disk depth was predicted by the optics sub-model. Nitrate+nitrite (NO_x) and silica (Si) were added to the Phase 1 list of model state variables because both had distinctive depletion signatures in the pelagic waters of the lake. CLM-2D includes kinetic sub-models representing algae, zooplankton, the effects of dreissenid mussels, and four major algal constituents: (1) carbon, (2) phosphorus, (3) nitrogen, and (4) silica. Sub-models are also included for minerogenic particles and optics (e.g., Secchi depth).

The upgraded hydrothermal/transport model was calibrated for 2013 and validated for two years (1999, 2006) with very different forcing conditions. The summer of 1999 was quite dry and the summer of 2006 was extremely wet. The wide range of meteorological forcing conditions included in the calibration and validation data sets represents a robust test of the hydrothermal/transport model. The hydrothermal model simulated T observations well for the calibration year of 2013. Features of thermal stratification were simulated accurately, including surface temperature, mixed layer depth, near-bottom temperature, and overall profile shape. The model also performed well in simulating temperatures for the two years of model validation, 1999 and 2006. Under these different hydrologic and meteorological forcing conditions the model continued to accurately simulate thermal stratification as well as simulating longitudinal temperature differences in the lake.

The P-eutrophication model, CLM-2D, was successfully calibrated to the robust data set collected in 2013 as part of Phase 1. Following calibration, CLM-2D was validated by applying it for two additional years (1999 and 2006) with a wide range of conditions for precipitation, flow, phosphorus loads, and flushing rate. The model performed very well in matching observations of TP, Chl-*a*, SRP, and Z_{SD} in both model validation years. Model performance criteria were met for each of these parameters. A sensitivity analysis was conducted to identify important model parameters and their influence on model predictions. We varied eight key model coefficients and two sub-models, one at a time, and observed the impact of each change on 2013 model predictions for Chl-*a*, POC, and TP. Model predictions of Chl-*a* and POC were sensitive to changes in the stoichiometric coefficients P:C and C:Chl-*a*. This is not surprising given that these stoichiometric ratios establish the composition of the modeled algal community. Turning off the dreissenid mussel sub-model resulted in a 14.5% decrease in Chl-*a*, suggesting that nutrient recycling by these filter feeders stimulates algal growth.

Three example applications of CLM-2D were conducted to demonstrate capabilities of the model for evaluating the effects of various potential management initiatives on water quality in Cayuga Lake. The first application consisted of comparing predicted water quality conditions for 2013 with a scenario of zero flow to the lake from the LSC facility. In the second

application, the impact of eliminating P loading from the six WWTPs that discharge to Cayuga Lake was evaluated. Finally, we assessed predicted water quality impacts associated with a hypothetical 30% reduction in non-point sources of P from the watershed. These scenarios are entirely hypothetical and are not intended as management recommendations. Model simulations indicated that water quality impacts associated with the LSC facility are negligible. These results are not surprising given that the LSC contribution to P loading is also quite small. Model simulations indicated that elimination of P loading from WWTPs located on Cayuga Lake would result in extremely small improvements in water quality. These results are consistent with the minor contribution of point sources to P loading to Cayuga Lake. A 30% reduction in non-point source P loading was predicted to result in water quality improvements that are modest (<20% for the shelf, <8% for pelagic waters) relative to the magnitude of the loading reduction.

Constituent concentrations input to CLM-2D may be modified based on output from the watershed/land use model (SWAT; Section 8). For example, a SWAT management scenario that predicted a 10% reduction in TP loading for Fall Creek would be translated to CLM-2D as a 10% reduction in the TP concentrations for this inflow. Note that concentrations are modified rather than loads or flows. This represents a linkage of the models that is attractive for evaluating land use management alternatives.

Section 8: Modeling the Cayuga Lake Watershed with SWAT

A SWAT (Soil and Water Assessment Tool v2012) model was developed for the Cayuga Lake watershed to (1) estimate current precipitation driven discharge and loading of total suspended solids (TSS), nitrate + nitrite (NO_x) and total phosphorus (TP) to Cayuga Lake, and (2) evaluate best management practices in reducing TP loading to Cayuga Lake. Model development and calibration was first performed for the Fall Creek watershed, which has an extensive period of record of observed precipitation (NRCC 2016), streamflow (USGS 2016), and estimated water quality constituents (Prestigiacomo et al. 2016). Further, details on the spatial and temporal distributions of agricultural fertilizer applications were available for the Fall Creek watershed. Hydrologic parameters defining the precipitation-runoff response of the watershed derived from calibration of the Fall Creek watershed were extrapolated to the entire Cayuga Lake watershed.

Known fertilizer spreading schemes for the Fall Creek watershed were extrapolated to the entire Cayuga Lake watershed and the temporal distribution of fertilizer applications throughout the Cayuga Lake watershed was assumed to be consistent with the management practices within Fall Creek. Further it was assumed that the total mass of fertilizer applied was proportional based on area by land use and that all row crops throughout the watershed were actively fertilized as in Fall Creek with the same mass per unit area. Similarly, it was assumed that the same proportion of pastures throughout the watershed received fertilizer spreading schedules defined for Fall Creek.

The 30-meter National Elevation Dataset (NED) digital elevation model was used to define watershed land surface elevations (USGS 2016a). Land-use information was obtained from the National Land Cover Database (NLCD) (Fry et al 2011) and the 30-meter 2009 New York Cropland Data Layer (USDA 2010). The NLCD dataset was modified to include more specific agricultural land uses common to the Finger Lakes region.

The SWAT model was corroborated for the period of 1998 – 2010 against observed daily flows and estimated total suspended solids (TSS), NO_x (NO_3 + NO_2), Particulate Phosphorus (PP), and Total Dissolved Phosphorus (TDP) loads. For model corroboration the Fall Creek model was forced with daily precipitation, and minimum and maximum air temperatures measured at the Northeast Regional Climate Center weather station (NRCC 2016). Relative humidity, solar radiation, and wind speed were solved internally by SWATs weather generator.

Model calibration consisted of manually adjusting 19 SWAT model parameters. Nash-Sutcliffe Model Efficiency (NSE) values for daily flows were above the recommended value of 0.5 (Moriasi et al. 2013) for 10 of the 13 years used for model corroboration. The commonly accepted NSE of 0.5 is defined for a monthly time step, which is a considerably more relaxed metric than NSE calculated at a daily time step. Simulation of flow was good for all months with some overestimation occurring from spring snowmelt.

Daily estimates of TSS are highly variable due to uncertainty in the estimation of daily flow and the relative simplicity of the governing equation in SWAT. The seasonality of TSS loading was reproduced reasonably well with slight over-estimation of summer loads. There was an underestimation of April TSS loads associated with spring snowmelt. Similar to TSS, the model adequately estimates the long term trend in annual NO_x loading and reproduces the seasonality, but underestimates the spring snowmelt NO_x runoff. We manually adjust the PHOSKD and ERORGP parameters to reproduce the estimated TDP and PP loads for Fall Creek. The seasonality in TDP and PP loads for Fall Creek were well produced with a slight underestimation of spring P loads owing largely to the simplified snowmelt hydrology incorporated within SWAT.

Section 1. Background - Modeling Goals, Progress from Phase 1, and Organization of the Phase 2 Findings

1.1. Description of Cayuga Lake and study goals

Cayuga Lake (42º 41′ 30″ N; 76º 41′ 20″ W) is the fourth easternmost of the New York Finger Lakes (Figure 1-1), and has the second largest surface area (172 km^2) and volume (9.4 x 109 m^8) of this group of lakes. The mean and maximum depths are 55 m and 133 m, respectively. This long and narrow system has an aspect ratio (length along its major axis ÷ average width) of 22 (11, if maximum width is used), and is positioned along a

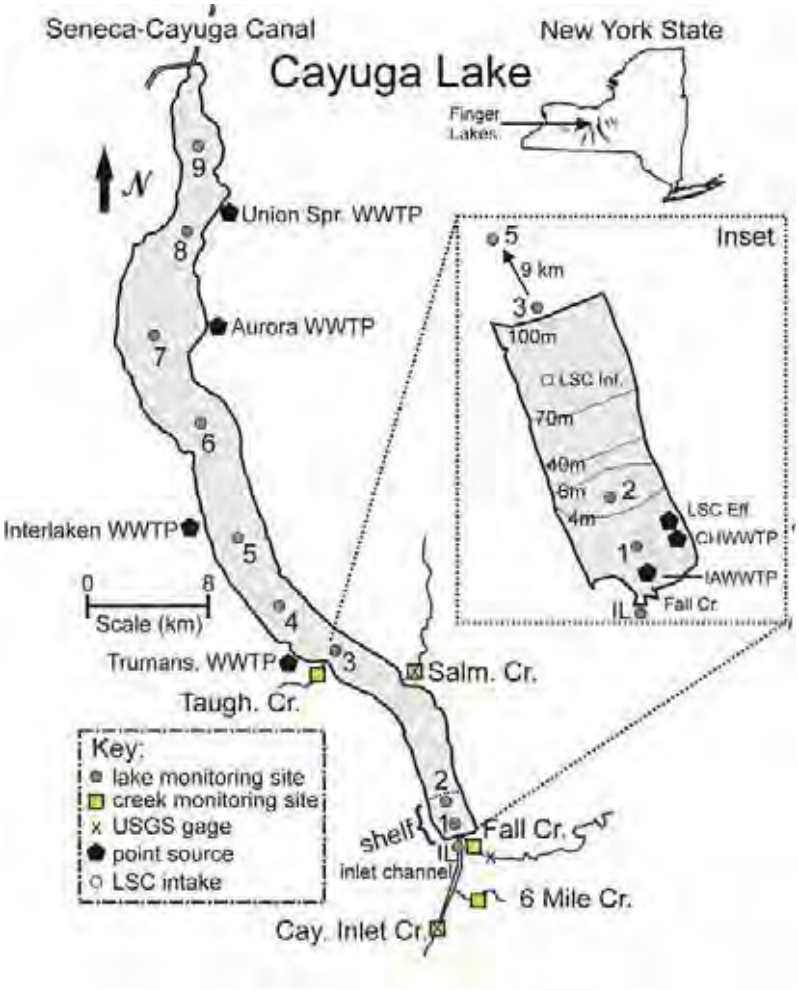

Figure 1- 1. Cayuga Lake, position within New York, and the 11 Finger Lakes. Shown are five monitored tributaries, WWTPs Lake Source Cooling (LSC) facility discharge, four USGS gages, nine lake monitoring sites, and the shelf portion of the lake at its southern end.Cauga Lake

mostly north-south axis that coincides with prominent wind directions (Figure 1-1). Cayuga Lake has a warm monomictic stratification regime, stratifying strongly in summer through mid-fall, but only rarely developing complete ice cover (Schaffner and Oglesby 1978). Internal seiches (e.g., lake-scale tilting of the metalimnion), internal waves (oscillations in stratified layers), and upwelling events occur in the lake in response to wind energy inputs. These events are promoted by the elongated shape of the lake and the common wind directions (Effler et al. 2010, Gelda et al. 2015). The average hydraulic retention time of the lake, calculated by dividing its volume by the total volumetric inflow rate (e.g., completely mixed assumption), is nine years.

Nearly 40% of the total tributary inflow to the lake enters the southern end, specifically from Fall Creek, Cayuga Inlet, and Sixmile Creek (Table 1-1; Figure 1-1). Two other tributaries of noteworthy size enter the lake further north—Salmon Creek enters from the east and Taughannock Creek enters from the west (Figure 1-1). Thirty smaller streams, draining ~ 40% of the overall watershed, flow into the lake; the associated individual watersheds are small (< 3.5% of the total; Haith et al. 2012). Fall Creek, the largest of the tributaries, has the longest record of gaged flow (since 1925). Cayuga Inlet, Sixmile Creek, and Salmon Creek are also gaged. Agricultural land use is particularly high in the Salmon Creek watershed (68%), but is also substantial in portions of the watershed with small tributaries and Fall Creek (Table 1-1).

Effluent from two domestic wastewater treatment plants (Ithaca Area WWTP (IAWWTP) and Cayuga Heights WWTP (CHWWTP)), serving the City of Ithaca and bordering suburbs, also enter the southern end of the lake (Figure 1-1). Treatment targeting phosphorus (P) removal has been upgraded at the two WWTPs over the last decade. In May 2006, IAWWTP, the largest of the WWTPs (Table 1-1), implemented micro-sand ballasted flocculation, that uses ionic polymer and ferric chloride for P removal. The CHWWTP as well as several smaller WWTPs that enter the lake further north (Figure 1-1) have chemical P treatment. The “lake source cooling” (LSC) facility withdraws cold water from a depth of 73 meters to meet cooling demands for Cornell University (i.e., greater withdrawals in summer) and returns the spent cooling water to the shelf.

Cayuga Lake is mesotrophic (moderately productive) with algal growth limited by the availability of phosphorus (Effler et al. 2010, Schaffner and Oglesby 1978). The localized entry of such a large fraction of the tributary flow delivers locally high loads of various constituents, including phosphorus, to the southern end of the lake. In particular, large quantities of phosphorus (Prestigiacomo et al. 2016), sediment (Peng and Effler 2015), and dissolved organic carbon (DOC) and dissolved color (Effler et al. 2015a), are delivered to the southern end of the lake by these tributaries during runoff events. Conditions in the shallow southern end, designated the “shelf” (Figure 1-1; earlier demarcated by the 6 m contour of depth, now by the 10 m contour of depth), have generally been considered degraded relative to the pelagic zone (Schaffner and Oglesby 1978, Effler et al. 2010, Effler et al. 2014). Lake monitoring since the late 1990s has established that two trophic states metrics, total phosphorus (TP) and Secchi disk

(SD), are significantly higher and lower, respectively, on the shelf compared with pelagic waters, and that chlorophyll a (Chl-*a*) concentrations are not significantly different (Effler et al. 2010). In 2013, the most intensely monitored year, the number of pelagic sampling locations along the main axis of the lake was increased to seven (sites 3 – 9; Fig. 1.1). Summer (June-September) average concentrations of TP on the shelf (but not in pelagic waters) have irregularly exceeded the New York State guidance value of 20 g/L. The New York State Department of Environmental Conservation (NYSDEC) has listed the southern end of Cayuga Lake (e.g., shelf) as an impaired segment with respect to P and sediment in "The Final New York State 2012 Section 303(d) List of Impaired Waters Requiring a TMDL/Other Strategy".

Table 1- 1. Average stream flow, watershed areas, and land use for Cayuga Lake tributaries.

Tributary	Flow Information			Watershed		Land Use Percent[1]		
	USGS Gage	Record (years)	Mean Q (m^3/s)	Area (km^2)	%	A	F/B, R	U
Fall Creek	04234000	89	6.1	330.9	18%	49%	40%	11%
Cayuga Inlet[2]	04233255	77	2.7	240.8	13%	29%	56%	15%
Salmon Creek	0423401815	8	3.6	233.8	13%	68%	25%	7%
Taughannock Creek[3]	-	-	3.4	173.0	9%	49%	40%	11%
Sixmile Creek	04233300	19	2.1	134.1	7%	22%	63%	15%
Unmonitored Tributaries[4]	-	-	14.3	758.1	41%	62%	23%	15%
Total	-	-	28.8	1870.7	100%	60%	26%	14%

[1] A – agriculture, F/B – forest/brush, R – other rural, U – urban (from Haith et al. 2012);
[2] gage moved in 2011;
[3] ungaged, flow estimates from VSA watershed model (Archibald et al. 2014);
[4] estimated from product of total gaged flow (sum) and ungaged: gaged watershed area ratio.

The overarching objective of this project was to develop and test watershed and water quality phosphorus/eutrophication models for Cayuga Lake. It was intended that these models would be capable of supporting a phosphorus (P) TMDL analysis for the shelf, though pelagic waters conditions can also be addressed. This initiative accommodates the bioavailability of external P inputs and its importance for phytoplankton growth, as well as the potential importance of other biological (zooplankton and mussel) communities. The lake model was also designed to have comprehensive predictive capabilities for water column sediment (primarily minerogenic particles), because of its influence on both P and clarity levels in this lake (Effler et al. 2014, Peng and Effler 2015, Prestigiacomo et al. 2016, Effler et al. 2016).

1.2. Phasing of project components and Phase 1 findings

1.2.1. Project components.

The Cayuga Lake Modeling Project has been partitioned into five technical components

1. tributary monitoring to support specification of dynamic loading conditions, including the bioavailability of the external phosphorus loads for a eutrophication model,
2. lake monitoring of water quality variables and related biological communities,
3. setup and testing of a two-dimensional hydrothermal/transport model for the lake,
4. setup and testing of a watershed/land use model that will quantify the dependence of tributary loading on land use and meteorological drivers, and
5. development, testing, and application of a phosphorus/eutrophication water quality model, and appropriate sub-models, for the lake.

This work was conducted in a phased manner. Technical components (1)-(4) were part of Phase 1 of this two-phase project. Item (4) was completed in Phase 2 by Cornell's co-investigators. Items (4) and (5) are contained in this Phase 2 report. The scope, key findings, and progress, as well as other supporting documentation, has appeared in a series of project-specific presentations and reports, as well as in professional peer-reviewed papers. Project-specific documents submitted prior to this Phase 2 report have been accepted by NYSDEC. The contents of these reports, and professional peer-reviewed papers, have supported the resolution of key findings and the approaches that were adopted in the design and conduct of Phase 2. In particular, the Executive Summary of the Phase 1 Final Report, included below (with comment), served as a valuable guide for the approaches adopted in Phase 2.

1.2.2. Executive summary of Phase 1 report

The executive summary of the Phase 1 Report, describes findings from the first four technical components of the project. It is repeated here to provide valuable context, as indicated findings had a guiding role to approaches of Phase 2, described subsequently in this report. Several numbered footnotes and italic bolded designations provide added insights that evolved from the progression of Phase 2 work and are briefly commented on here (refer to subsection 1.2.3.). The text from the Phase 1 report is presented below in italics.

Introduction

This report documents progress in the study of phosphorus (P) and trophic state metrics in Cayuga Lake, NY. The overarching goal of the study is to develop and test a water quality model for this lake that represents P-eutrophication dynamics. It is intended that this model will be capable of supporting a P Total Maximum Daily Load (TMDL) analysis for the shallow southern end of the lake that receives 40% of the lake's total inflow, described as the "shelf". The model will also have predictive capabilities for inorganic (minerogenic) sediment, because these particles also influence metrics of trophic state, including P concentrations and water clarity.

The study has five technical elements: (1) monitoring of the five largest tributaries for forms of P, sediments, and related metrics, (2) monitoring of the lake for multiple forms of P, metrics of trophic state, sediment metrics, and selected biological communities, (3) setup and testing of a two-dimensional hydrothermal/transport model for the lake, (4) setup and testing of a watershed/landuse model to quantify the dependence of tributary constituent loading on landuse, and (5) ***development, testing, and application of a P-eutrophication water quality model for the lake that will be suitable to support a P TMDL[1]****. The study is being conducted in two phases, with the first phase including the first four of the above elements. This report documents the findings of the first phase, and considers how these influence development of the model in the second phase.*

2013 Monitoring Program

The tributary and lake monitoring programs were conducted concurrently over the April through October interval of 2013. These were both temporally intensive and spatially extensive. Five tributaries were monitored, Fall Creek, Cayuga Inlet Creek, Six Mile Creek, Salmon Creek and Taughannock Creek (first four gaged for flow), that together represent 60% of the lake's watershed. There were two primary components of tributary monitoring (1) fixed frequency, bi-weekly collections, and (2) runoff event-based collections, to represent changes in concentration over the time course of the events.

Lake monitoring included: (1) the conduct of in situ measurements, (2) sampling for laboratory measurements of an array of water quality constituents to address the P-eutrophication and related sediment issues, (3) sampling and characterization of phytoplankton and zooplankton communities, and (4) the conduct of a spatially detailed dreissenid (quagga and zebra) mussel survey. Water quality monitoring was conducted at nine sites along the entire length of the lake, with two sites (No.'s 1 and 2) located on the shelf. Lake wide monitoring was conducted bi-weekly at all sites over the April-October interval. The frequency was increased to twice per week in summer (June-September), at shallow sites 1 and 2, and at site 3, the nearest deep water ("pelagic") location.

Tributaries: Concentrations, P Bioavailability and Loads

The robust tributary data sets were analyzed, and together with flow rate (e.g., with units of m^3/d) information, were used to estimate constituent loading rates (e.g., with units of kg/d), that are necessary to drive mass balance type mechanistic models. The central element of this work was the development of loads that were calculated based on the bioavailability of each P form (ability of each form to support algal growth). Bioavailability bioassay experiments were conducted for three forms of P that sum to total P, soluble reactive P (SRP), soluble unreactive P (SUP), and particulate P (PP), for the major tributaries (Fall Creek, Cayuga Inlet Creek, Six Mile Creek and Salmon Creek) and two point sources. Tributary SRP, SUP, and PP were found to be completely, mostly, and less bioavailable, respectively. The estimated total bioavailable P load (BAP_L) for the study interval was only about 25% of the total P load, because the low bioavailability PP fraction dominated. Most of the BAP_L (> 70%) is received during high flow intervals. Point source contributions to the BAP_L are minor (~ 5%), reflecting the benefit of reductions from recent treatment upgrades. Salmon Creek represents a particularly potent source of P with a high BAP_L relative to its contribution to total inflow.

Reasonably strong empirical relationships between concentration and tributary flow (Q) were observed for forms of P, as well as a number of other constituents, that supported specification of concentrations on days without measurements for calculations of loading rates. The study period of 2013 had an above average flow, ranking 32nd in the 89 year record for Fall Creek, but the summer interval had particularly high flow ranking 6th highest of the record. Concentrations of particulate constituents increased dramatically in all of the tributaries during intervals of high Q; each of the tributaries demonstrated strong positive dependencies on Q for these constituents. The sediment delivered to Cayuga Lake was dominated by inorganic (minerogenic) material. Constituent loads were calculated at a time step of daily, to be consistent with the needs of the future mechanistic water quality model for the lake.

Cayuga Lake Watershed Modeling

The watershed model development for this project involved compiling the necessary meteorological, land cover, and land management data for the 860 square mile Cayuga Lake Watershed. Because there is interest in both particulate and soluble phosphorus, the decision was made to focus on the USDA Soil and Water Assessment Tool (SWAT), because it includes modules designed to simulate the necessary landscape phosphorus (P) transformations and in-stream P processes. The model has been set-up and tested for the major tributaries in the southern-end of the watershed. A primary focus has been the Fall Creek sub-watershed, because of the copious historical and on-going monitoring that provide data for calibrating and testing the model, and because it represents the largest sub-watershed area for Cayuga Lake. Additionally, the model team is working with local Soil and Water Conservation Districts, Pro-Dairy, and the New York State Soil and Water Conservation Committee to develop a land management algorithm for Fall Creek and a strategy for extending it to the entire watershed. At this time, we have a preliminary land management algorithm that we are testing in collaboration

with the aforementioned stakeholders and a preliminary model calibration. We will continue to refine these through early 2015. Currently there are two issues with the SWAT model that we need to correct: (1) the storm flow-to-base-flow ratio is too high and (2) the organic-to-inorganic phosphorus ratio is not agreeing with the UFI measurements. SWAT model files will be submitted as soon as these two issues are resolved.

Hydrothermal/Transport Submodel

A two-dimensional longitudinal – vertical hydrothermal/transport model (W2/T; the transport submodel of CE-QUAL-W2) was set up, tested, and preliminarily applied for Cayuga Lake. The model was supported by long-term monitoring of meteorological and hydrologic drivers and calibrated and validated using in-lake measurements made at multiple temporal and spatial scales over sixteen years. Measurements included (1) temperature profiles at multiple lake sites for ten years, (2) near-surface temperatures at one end of the lake for sixteen years, including irregular occurrences of upwelling events, (3) timing and magnitude of seiche activity (oscillations of stratified layers) for two years, and (4) transport of a conservative tracer. The model demonstrates excellent temporal stability, maintaining good performance in uninterrupted simulations over a period of fifteen years. Performance is better when modeling is supported by on-lake versus local land-based meteorological measurements.

The validated model has been applied through numeric tracer experiments, to evaluate various features of transport of interest to water quality issues for the lake, including (1) residence times of stream inputs within the entire lake and the shelf, (2) transport and fate of negatively buoyant (i.e., tending to plunge) streams, and (3) the extent of transport from the hypolimnion to the epilimnion. Multiple factors contribute to making W2/T an appropriate transport submodel for the P-eutrophication model for Cayuga Lake, including (1) the basin morphology and associated transport characteristics, (2) longitudinal differences in water quality metrics imparted from localized inputs, particularly extending from the southern end, and (3) the demonstrated performance of W2/T in representing transport in this lake across multiple time scales.

Limnology

A number of noteworthy limnological signatures were resolved through routine in situ instrumentation measurements, including (1) the development of strong thermal stratification in summer, (2) occurrences of seiche activity, (3) entry of turbid waters from the shelf area toward northern areas, (4) occurrences of deep chlorophyll maxima (DCM) in metalimnetic depths, and (5) abrupt changes on the shelf coupled to runoff events. Conditions on the shelf with respect to optical metrics of water quality, including Secchi depth (SD, a measurement of clarity), were on average degraded relative to the deeper pelagic portions of the lake. These conditions were particularly acute following runoff events, primarily associated with inorganic (minerogenic) sediment received from the local streams. Differences between the pelagic sites for these metrics

were generally minor, a recurring feature also observed for most of the laboratory measurements of collected samples. Spatial patterns for the upper waters for laboratory measurements for the nine sites were resolved on a time-averaged basis. A gradient in concentrations was observed for most parameters including multiple forms of P and metrics of sediments, with tributaries > site 1 (shelf, adjoining tributaries) > site 2 (shelf) > pelagic sites. Particularly noteworthy exceptions were chlorophyll a (Chl-a) and nitrate nitrogen (NO_3^-), for which no significant differences between the shelf and pelagic sites were observed. The New York State guidance value for the summer average concentration of total P (TP) of 20 μgP/L was exceeded at site 1 (shelf) and approached at site 2 (shelf).

Strong temporal variations were resolved for the shelf for most laboratory analytes that were linked to runoff events, during which the greatest differences with pelagic conditions prevailed. A key metric of the effects of minerogenic particles was demonstrated to be the projected area of minerogenic particles per unit volume (PAV_m). PAV_m is reported to be linearly related to contributions of minerogenic particles to PP, the minerogenic component of turbidity, the scattering and beam attenuation coefficients, and inversely related to SD. ***The vast majority of PAV_m delivered to the lake and found within the lake is clay mineral particles[2]*** *from the watershed. Increases in PAV_m on the shelf following runoff events, and lake-wide for the major events, were clearly resolved. The contributions of four particle size classes to PAV_m were represented in anticipation of the need for such an apportionment in model simulations of this attribute in the lake. The large contributions of these particles to PP on the shelf following runoff events and the low bioavailability of this P is not supportive of inclusion of such shelf observations in assessments of trophic state (e.g., state guidance value) status for that portion of the lake. A number of signatures were resolved for other metrics in pelagic waters that will be valuable to support testing of the water quality model for lake-wide conditions, including (1) depletions of soluble reactive P (SRP), dissolved silica (Si), and nitrate nitrogen (NO_3^-) in the upper waters over the spring to early summer interval, (2) increases in soluble unreactive P (SUP) in the upper waters in early summer, (3) mid-summer increases in particulate (PP) and particle organic carbon (POC) in the upper waters, and (4) increases in SRP in the near-bottom waters through early fall.*

The DCM observed in the lake's metalimnion was not indicative of phytoplankton biomass maxima in those stratified layers. The relationship between the two common measures of phytoplankton biomass, POC and Chl-a, in the lake's upper waters was weak. POC was a better predictor of light scattering, SD, and PP than Chl-a. The long-term monitoring data associated with Cornell's Lake Source Cooling (LSC) facility was analyzed in an effort to identify trends. Higher TP concentrations and lower SD on the shelf were compared to pelagic conditions, based on summer average values, were recurring over the entire record (1998-2012). However, the lack of noteworthy differences in summer average Chl-a values between these areas was also recurring over the same period. Multiple statistical analyses were conducted on the three common trophic state metrics, TP, SD, Chl-a, to test for significant changes in the lake's upper

waters. The only indication of a change was an increase in Chl-a in pelagic waters. However, given the indicated weakness of the trend and the inherent limitations in the metric, the change is not considered noteworthy. Significant increases in deep (hypolimnetic) water concentrations of SRP, and thereby total dissolved P (TDP) and TP, starting in 2004, as assessed by monitoring of the LSC discharge, have occurred.

The spring increase in phytoplankton (bloom) was dominated by the diatom group in 2013. The termination of this bloom was consistent with both limitation of this group by decreased Si concentrations and the timing of an increase in grazing zooplankton, patterns that are typical of north-temperate zone lakes in general. Cyanobacteria (previously blue-green algae) did not become sufficiently dense to form nuisance blooms or floating scums. Large Daphnia, a particularly efficient grazing zooplankton, capable of causing near-elimination of phytoplankton and other particles, and associated major increases in SD, were not present.

Quagga mussels were collected at all depths and in 96% of the samples collected in the extensive September-October survey of 2013. Zebra mussels were only collected at shallow depths (< 10 m), in 24% of the samples. Overall, dreissenid (includes quagga and zebra mussels) biomass decreased with depth in the lake from levels of 95 g/m^2 to less than 10 g/m^2 at depths deeper than 80 m. Application of literature-based and site specific P excretion rates to the lake wide biomass estimate support the hypothesis that mussel excretion has made a large contribution to the SRP increase in the hypolimnion. Although historic data are limited, the timing of the mussel expansion in the lake is consistent with that of the increase in hypolimnetic SRP after 2004.

Approach for Phase 2 Water Quality Modeling

The presentation and analyses of monitoring information for Cayuga Lake, particularly the detailed data set collected in 2013 as part of this study (Phase 1), have provided invaluable insights to guide Phase 2 of this study. In Phase 2 a mechanistic P-eutrophication model will be developed, tested and preliminarily applied to address the potential cultural eutrophication issue for the lake, with particular focus on the shelf. Extensive data analysis confirms that the P and sediment issues cannot be separated for this system.

The character of the conspicuous "disconnect" in the three common trophic state metrics (the concentration of TP, Chl-a, and Secchi depth) that has emerged in the limnological analyses established model attributes that will be necessary to adequately address these features. The disconnect refers to the lack of significant differences in Chl-a between the shelf and pelagic waters of the lake, despite clearly degraded TP (higher) and SD (lower) conditions on the shelf. The disconnect has two primary elements (1) the greater contributions of minerogenic particles to TP and SD levels on the shelf from local tributary inputs, and (2) the absence of locally greater phytoplankton growth on the shelf despite higher concentrations of immediately bioavailable forms of P. The first element requires a robust treatment of minerogenic particles

in the model. The second element requires attributes that appropriately represent the effects of (1) the short residence time of tributary inflows on the shelf, (2) the more limited availability of light on the shelf, particularly following runoff events, and (3) the diluting effect on local phytoplankton biomass concentrations from tributary inputs. Given that the Chl-a patterns for the shelf generally track lake-wide pelagic conditions, there are several nutrient and phytoplankton biomass signatures that were identified for pelagic waters that will be valuable in testing the P-eutrophication model for the entire lake.

Modeling activities in Phase 2 will embrace the principle of parsimony. Accordingly, there will be an effort to avoid overly complex components and submodels that can be accompanied by greater uncertainty and excessive computational demands. Robust temporal and spatial scales will be represented to address the primary signatures resolved in monitoring related to the project goals. Short-term patterns in response to runoff events, which are primary drivers of the shelf versus pelagic waters differences, need to be resolved, as well as the seasonality in phytoplankton growth manifested lake-wide, and the potential effects of year-to year differences in runoff. Spatial structure must resolve longitudinal differences on the shelf, between the shelf and pelagic waters, and lake-wide mixing and the effects of the thermal stratification regime. The two-dimensional model (W2/T) and the adopted segmentation scheme will provide a robust representation of these features. Drivers for the water quality model will include (a) local meteorological data, (2) hydrologic data for primary tributaries, and (3) loading rate estimates for multiple constituents, as described in this report.

***A tentative listing of model state variables (n~30) has been presented that establishes that the water quality model to be developed and tested in Phase 2 will have robust predictive capabilities. The overall water quality model will be composed of several submodels[3]**, that include: (1) the two-dimensional hydrothermal/transport submodel, (2) a minerogenic particle submodel, (3) an optics submodel, (4) **a phosphorus submodel[4]**, and (5) a phytoplankton growth/biomass submodel. Conceptual models depicting structural features are presented for each of the submodels in this report, which reflect insights and results of analyses derived from the Phase 1 work. However, the focus of the model remains P-eutrophication; specifically, **the sediment sub-model is not being designed explicitly to support a sediment TMDL[5]**, which is outside the scope of this project.*

1.2.3. Comments on selected aspects of the Phase 1 Executive Summary (according to footnote numbers in subsection 1.2.2, above)

The bulleted numbers of the following comments correspond to the footnoted text identified in bold above (subsection 1.2.2.)

(1) Both clarifications and updates are valuable here. The inclusion of the term "application" for the modeling of Phase 2 will not include the specific scenarios necessary to evaluate management goals and alternatives, such as a P TMDL. Rather these would be limited

to selected example scenarios to establish the capabilities for the more detailed and focused analyses conducted as part of a P TMDL.

The "P-eutrophication" description suggests only a capability of the model for this single issue, and therefore is overly limited. Multiple issues can be addressed (e.g., water column sediments). The model is now more appropriately described as a water quality model that importantly addresses the P-eutrophication process. This broadening naturally evolved from the findings of both Phases 1 and 2. The design of the model enables further growth with respect to more issues (e.g., potential addition of other state variables). The limited model title – "P-eutrophication" appears in multiple locations of the Phase 1 Executive Summary.

(2) Recent research has established that internally produced (autochthonous; e.g., chemical precipitation) calcite ($CaCO_3$) makes important, though shorter-term compared to clay, contributions to PAV_m in late-summer in Cayuga Lake (Effler and Peng 2014). The intensity of the process, and therefore the relative contributions to light scattering and Secchi disk depth, varies substantially year-to-year (Peng and Effler 2016). The effects of calcite on Secchi disk depth has been integrated into the water quality model for the lake in Phase 2. No clear anthropogenic connection of the calcite precipitation ("whiting") phenomenon has been established here or for other lakes (Peng and Effler 2016b).

(3) The substantial number of state variables and sub-models justifies describing the product as a water quality model, rather than limiting the description to P-eutrophication.

(4) A second phosphorus sub-model has been created and tested in the Phase 2 work that simulates the concentration of particulate phosphorus that is associated with minerogenic particles and unavailable to support phytoplankton growth ($PP_{m/u}$; Gelda et al. 2016a). Unavailable minerogenic particulate P ($PP_{m/u}$) concentrations are higher on the shelf, particularly after runoff events, and are responsible for the documented exceedances of the summer average total phosphorus (TP) guidance value of 20 g/L.

(5) The value of the term sediment sub-model would be improved by some clarification. In this case, the "sediment" refers to material in the water column of the lake, received from tributary inputs of minerogenic particles (Peng and Effler 2015). This sub-model (Gelda et al. 2016b) does not address deposition and accumulation rates. The capabilities of this sub-model are likely suitable to address most management concerns related to water column sediment.

1.2.4. Project review and oversight

This four year study included extensive oversight and review by regulators, technical review panels and committees (Table 1-2). This started with submission of a "scope of work" by UFI in 2012, on behalf of Cornell, that evolved from system-specific limnological analyses. This was followed by preparation of a Quality Assurance Project Plan (QAPP) for the Phase 1 work (mostly detailed monitoring and associated limnological analyses) and periodic progress

presentations. Extensive technical responses to reviewer comments on progress presentations thoroughly addressed all questions, and modest revisions were made. An extensive final report for Phase 1, prepared by UFI and co-investigators, was approved by the regulatory parties and their review panels. Similarly, an addendum to the first QAPP for Phase 1 to conduct the Phase 2 (final) portion of the work, prepared and submitted by UFI and co-investigators, was approved, including exchanges with reviewers (Table 1-2).

1.3. Publications in the peer-reviewed literature

Publication in the peer-reviewed literature, including scientific and engineering journals, is an important pathway for advancing the understanding and protection of freshwaters. Accordingly, publication of key findings was a primary goal of this project. Positive reviews by independent (and usually anonymous) experts represent support for the published work, including both the scientific approaches and advancements. Our understanding of Cayuga Lake and its water quality issues benefitted from both the preparation of these papers and the input from independent experts.

The list of peer-reviewed publications by UFI concerning Cayuga Lake is presented in Table 1-3. Most were published during this project. The listing is partitioned according to priorities (1 and 2). The priority 1 papers provided key documentation and insights on important components central to this project. These papers have been integrated into the primary sections of this report. The priority 2 papers have secondary roles in supporting the primary features of the report, but continue to provide valuable information for this project.

1.4. Project work elements and organization of the Phase 2 report

The primary elements of the Phase 2 work, and key underpinnings from Phase 1, are presented in a schematic format (Fig. 1.2). A numbering system identifies seven major elements, numbered 2 through 8, that represent the technical sections of this report according to topic. This "background" section has been designated Section 1 (Fig. 1.2). Peer-reviewed manuscripts appearing in this report are organized in a consecutive alphabetic order. A summary of the most noteworthy findings of Phase 2 is presented in the Executive Summary.

Table 1- 2. Technical documents prepared and meetings held to communicate key findings and modeling approaches for the Cayuga Lake Modeling Project.

Item No.	Date(s)	Document Title	Function/Category
1	September 7, 2012	Lake Monitoring and Modeling for a Cayuga Lake TMDL	original proposal for Phase 1 work
2	January 30, 2013	QAPP Phase 1 workshop	informational meeting
3	March 15, 2013	Quality Assurance Project Plan Addendum for Phase 1: Monitoring and Modeling Support for a Phosphorus/Eutrophication Model for Cayuga Lake	QAPP, Phase 1; protocols for sampling
4	June 12, 2013	CLMP[1] progress meeting	project update
5	July 16, 2013	CLMP progress meeting	project update
6	September 9, 2013	CLMP progress meeting	project update
7	October 15, 2013	CLMP progress meeting	project update
8	December 2, 2013	CLMP progress meeting	project update
9	December 31, 2013	CLMP progress meeting	project update
10	January 15, 2014	MEG[2]/TAC[3] meeting	project update
11	May 19, 2014	MEG/TAC meeting	project update
12	June – August, 2014	(on-going) responses to MEG/TAC comments	responses to reviewers comments/questions
13	July 17, 2014	CLMP public meeting	project update
14	October 22, 2014	Phase 1 final presentation(s) of findings to MEG/TAC/EPA	project presentation regarding salient findings of Phase 1 work
15	November 5, 2014	MEG/TAC meeting	project update
16	December 19, 2014	Phase 1: Monitoring and Modeling Support for a Phosphorus/Eutrophication Model for Cayuga Lake	Phase 1 final report
17	December 29, 2014	Phase 2 TMDL modeling scope of work	proposal for Phase 2 modeling work
18	January 15, 2015	Quality Assurance Project Plan Addendum for Phase 2: A Water Quality Model for the Phosphorus/Eutrophication Issues for Cayuga Lake	QAPP documenting protocols for modeling
19	December 14, 2015	Responses from project team to comments by NYSDEC, TAC, MEG, EPA	responses to questions on October 22, 2015 project presentation
20	January – December, 2015	Approximately monthly teleconference calls with Cornell	project updates
21	January – December, 2016	Approximately monthly teleconference calls with Cornell	project updates
22	December 31, 2016	Phase 2 Final Report (this document)	Phase 2 final report documenting model results

Table 1- 3. Listing of peer-reviewed papers by UFI concerning Cayuga Lake, and priority of support for this project

Priority Status	Listing of Peer-Reviewed Manuscript of Reference	Origin This (✓) Project	UFI Contrib. No.
1	Effler, S. W., A. R. Prestigiacomo, D. A. Matthews, R. K. Gelda, F. Peng, E. A. Cowen and S. A. Schweitzer. 2010. **Tripton, trophic state metrics, and near-shore versus pelagic zone responses to external loads in Cayuga Lake, New York.** Fundamental and Applied Limnology 178(1):1-15.	-	270
1	Effler, S. W., A. R. Prestigiacomo, F. Peng, R. K. Gelda and D. A. Matthews. 2014. **Partitioning the contributions of minerogenic particles and bioseston to particulate phosphorus and turbidity.** Inland Waters 2(2):179-192.	✓	317
1	Prestigiacomo, A. R., S. W. Effler, D. A. Matthews, M. T. Auer, B. E. Downer, A. Kuczynski and M. T. Walter. 2016. **Apportionment of bioavailable phosphorus loads entering Cayuga Lake, New York.** Journal of the American Water Resources Association. 52(1), 31-47.	✓	323
1	Gelda, R. K., A. T. King, S. W. Effler, S. A. Schweitzer and E. A. Cowen. 2015. **Testing and application of a two-dimensional hydrothermal/transport model for a long, deep and narrow lake with moderate Burger number.** Inland Waters:387-402.	✓	327
1	Peng, F. and S. W. Effler. 2015. **Quantifications and water quality implications of minerogenic particles in Cayuga Lake and its tributaries.** Inland Waters 5:403-420.	✓	330
1	Gelda, R. K., S. W. Effler, A. R. Prestigiacomo, F. Peng and J. M. Watkins. 2015. **Simulations of Minerogenic Particle Populations in Time and Space in Cayuga Lake, New York, in Response to Runoff Events.** Water Air Soil Pollution 227(10), 1-20.	✓	332
1	Gelda, R. K., S. W. Effler, A. R. Prestigiacomo, F. Peng, M. T. Auer and A. Kuczynski. 2016. **Simulation of the Contribution of Minerogenic Particles to Particulate Phosphorus Concentration in Cayuga Lake, New York.** Water Air Soil Pollution 227:365.	✓	333
1	Effler, S. W., C. M. Strait, A. J. P. Effler, F. Peng, D. M. O'Donnell, A. R. Prestigiacomo, S. M. O'Donnell, M. Perkins, and S. C. Chapra. 2016. **A mechanistic model for Secchi disk depth: Driven by light scattering constituents.** Water Air Soil Pollution (in review).	✓	337
2	Effler, S. W., M. T. Auer and N. A. Johnson. 1989. **Modeling Cl concentration in Cayuga Lake, USA.** Water, Air and Soil Pollution 44:347-362.	-	92
2	Matthews, D. A., S. V. Stehman and S. W. Effler. 2002. Limnological and Statistical **Issues for Monitoring the Impact of a Lake Source Cooling Facility: Cayuga Lake, NY.** Lake and Reservoir Management 18(3):239-256.	-	141
2	Effler, S. W., D. A. Matthews, M. G. Perkins, D. L. Johnson, F. Peng, M. R. Penn and M. T. Auer. 2002. **Patterns and impacts of inorganic tripton in Cayuga Lake.** Hydrobiologia 482:137-150.	-	207
2	Effler, S. W. and F. Peng. 2014. **Long-term study of minerogenic particle optics in Cayuga Lake, New York.** Limnology and Oceanography 59(2):325-339.	0.5	315
2	Peng, F. and S .W. Effler. 2016. **Characterization of calcite particles and evaluations of their optical effects in lacustrine systems.** Limnology and Oceanography (in press; 2017).	0.5	336
2	Peng, F. and Effler, S. W. 2016. **Advancing two-component partitioning of light scattering in Cayuga Lake, New York.** Limnology and Oceanography 61, 298-315.	✓	331
2	Effler, A. J. P., C. M. Strait, S. W. Effler, M. G. Perkins, A. R. Prestigiacomo and K. L. Schulz. 2015. **Linking CDOM patterns in Cayuga Lake, New York, USA, to terrigenous inputs.** Inland Waters 5(4), 355-370.	-	322
2	Effler, A. J. P., F. Peng, S. W. Effler, C. M. Strait, M. G. Perkins and K. L. Schulz. 2015. **Light absorption by phytoplankton and minerogenic particles in Cayuga Lake, New York.** Inland Waters 5(4), 433-450.	-	324
2	Effler, S. W., A. R. Prestigiacomo, N. G. Hairston, M. T. Auer and S. C. Chapra. 2016. **Analytical protocol-based differences in phosphorus concentration and implications.** Lake and Reserv. Manag.32(4):392-401.	✓	326

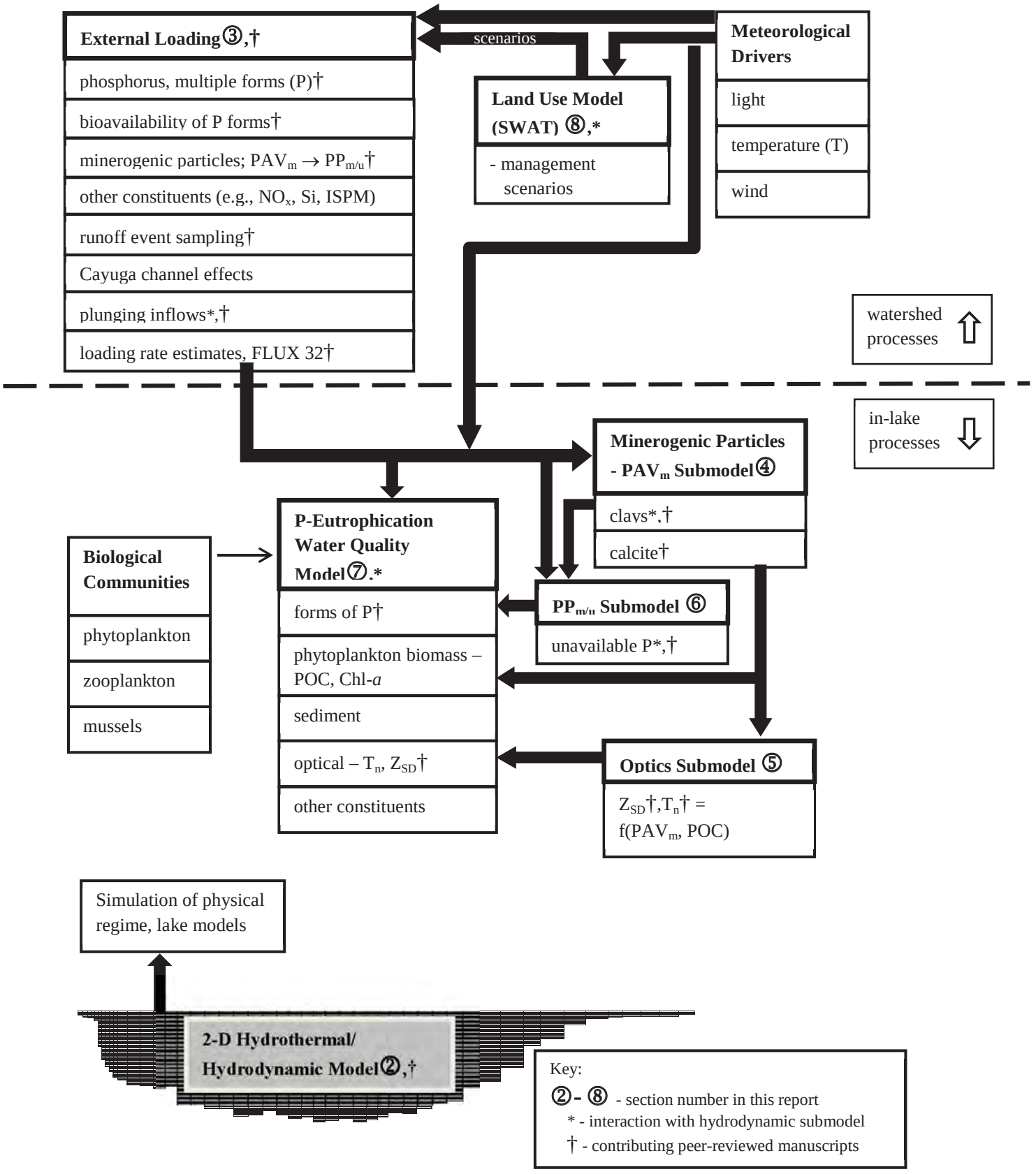

Figure 1-2. Schematic depicting the study approach supporting the development of the water quality model for Cayuga Lake, including interactions, the order of presentation in this report, and areas supported by peer-reviewed publication.

Sections 2 through 8 are presented in an order consistent with the organization depicted in the schematic format (Figure 1-2). Section 2 describes the 2-dimensional hydrothermal sub-model for Cayuga Lake (the hydrothermal/transport sub-model in CE-QUAL-W2). External loading estimates, important to driving the lake models are presented in Section 3. This section addresses external loads of forms of phosphorus, other constituents, modifications from the Cayuga Channel, interaction with the lake, and methodology for loading rate estimates from that input.

Sections 4 through 7 describe in-lake processes and modeling (Figure 1-2). Section 4 describes the quantification of PAV_m and its partitioning of minerogenic particle components and the development and testing of the PAV_m sub-model. Section 5 describes the development and testing of an optics sub-model that quantifies the contribution of phytoplankton and minerogenic particles to Secchi disk depth (Z_{SD}) and turbidity (Tn). Section 6 describes the development and testing of a sub-model for unavailable minerogenic particle P ($PP_{m/u}$). Section 7 documents the development and testing of the P-eutrophication water quality model for the lake. A primary focus of this project is the P-eutrophication issue, though the capabilities of this water quality model extend substantially beyond this single issue. Characterizations of the zooplankton and Dreissenid mussel communities were available to guide modeling of their water quality effects.

A SWAT (Soil and Water Assessment Tool v2012) model was set-up and tested by Cornell co-investigators for the Cayuga Lake watershed (Section 8). The SWAT model will be used to evaluate best management practices for reducing P loading to Cayuga Lake from its watershed. Simulations from the watershed model are used to inform the lake water quality model through adjustments to input files. For example, a SWAT model run that predicted a 10% reduction in TP loading from Fall Creek would be translated to the lake water quality model via input files as a 10% decrease in Fall Creek TP concentrations.

Section 2. Two-Dimensional Hydrothermal/Transport Submodel

2.1. Peer-reviewed Manuscript: Gelda RK, King AT, Effler SW, Schweitzer SA, Cowen E.A. 2015. Testing and application of a two-dimensional hydrothermal/ transport model for a long, deep, and narrow lake with moderate Burger number. Inland Waters. 5:387-402

Selected Salient Findings:

- CE-QUAL-W2 hydrothermal submodel (v.3.70) was calibrated for 2013
- Simulations for the validation years were year-round and continuous (no re-initialization) for 1998 – 2012
- Model captured both longer –term (seasonal and multi-year) dynamics of the thermal stratification regime and short-term oscillations of stratified layers associated with seiche activity
- Model predicted the median and average residence time of tributary inputs on the shelf to be 3.54 and 3.66 days, respectively
- Model demonstrated the high flushing rate of the shelf relative to net phytoplankton growth rates; an important factor in the lack of localized high phytoplankton biomass concentrations on the shelf despite higher available nutrient concentrations
- Model demonstrated the occurrence of plunging inflow; which diminishes the occurrence of effective loading from tributary sources to the productive upper waters

Manuscript Errata

Please note the following typographic corrections to the original attached publication.

1. There was a typographic error in Table 1 of the following manuscript (Testing and application of a two-dimensional hydrothermal/transport model for a long, deep, and narrow lake with moderate Burger number). The value for the coefficient of bottom heat exchange was listed as 7.0×10^{-8} W/m^2/s. The coefficient value should have read 0.3 W/m^2/s
2. The model used in the original manuscript was originally cited as Cole and Wells, 2013. The correct citation is Cole and Wells, 2010. (Cole, T.M. and Wells, S.A. 2014. CE-QUAL-W2: A Two-Dimensional, Laterally Averaged, Hydrodynamic and Water Quality Model, Version 3.70 User Manual. Portland (OR): Portland State University, Department of Civil and Environmental Engineering.)

Article

Testing and application of a two-dimensional hydrothermal/transport model for a long, deep, and narrow lake with moderate Burger number

Rakesh K Gelda,[1] Alexandra T. King,[2] Steven W. Effler,[1]* Seth A. Schweitzer,[2] and Edwin A. Cowen[2]

[1] *Upstate Freshwater Institute, NY, USA*
[2] *DeFrees Hydraulics Laboratory, School of Civil and Environmental Engineering, Cornell University, Ithaca, NY, USA*
* *Corresponding author: sweffler@upstatefreshwater.org*

Received 17 October 2014; accepted 13 July 2015; published 9 October 2015

Abstract

Setup, testing, and application of a 2-dimensional longitudinal vertical hydrothermal/transport model (the transport submodel of CE-QUAL-W2) was documented for Cayuga Lake, New York, where the Rossby radius is on the order of the lake's width. The model was supported by long-term monitoring of meteorological and hydrologic drivers and calibrated and validated using in lake temperature measurements made at multiple temporal and spatial scales over 16 years. Measurements included (1) temperature profiles at multiple lake sites for 10 years, (2) near-surface temperatures at one end of the lake for 16 years, (3) high frequency temperature at multiple depths for 2 years, and (4) seasonal measurements of a conservative passive tracer. Seiche activity imparted prominent signatures within these measurements. The model demonstrated excellent temporal stability, maintaining good performance in uninterrupted simulations over a period of 15 years. Performance was improved when modeling was supported by on-lake versus land-based meteorological measurements. The validated model was applied through numeric tracer experiments to evaluate various features of transport of interest to water quality issues for the lake, including (1) residence times of stream inputs within the entire lake and a smaller region defined bathymetrically as a shallow shelf, (2) transport and fate of negatively buoyant streams, and (3) the extent of transport from the hypolimnion to the epilimnion. This hydrothermal/transport model is appropriate to serve as the transport submodel for a forthcoming water quality model for this lake and for other high aspect (length to width) ratio lacustrine systems for which the internal Burger number is order one or greater.

Key words: Burger number, calibration, lake, model, Rossby radius, seiche, thermal stratification, transport, 2-dimensional, validation

Introduction

Temperature is a fundamental regulator of the physical character of water and thereby the ecology and quality of surface waters because it structures biological communities and affects the rates of biochemical processes (Wetzel 2001). Seasonal thermal stratification is ubiquitous in deep, temperate lakes and reservoirs and is an important regulator of transport processes (Imboden 2004). The critical dependence of lake metabolism and related metrics of water quality on stratification and associated transport regimes has been widely acknowledged (e.g., Lam and Schertzer 1987, Wetzel 2001, Imboden 2004). Water motion and features of stratification in lakes and reservoirs depend on a number of factors, including basin morphometry, setting, hydrology, and meteorological conditions (Csanady 1973, Imboden 1990, 2004, Imberger 1994). Internal seiches (successive oscillations of stratified layers) are particularly prominent features of water motion in long, narrow (high aspect ratio) lakes (Hunkins and Fliegel 1973, Lemmin and Mortimer 1986), promoting turbulence and thus vertical

DOI: 10.5268/IW-5.4.804

Inland Waters (2015) **5**, pp. 387–402

Click here to load Gelda et al. 2015 manuscript.

Section 3. External Loads of Bioavailable Phosphorus and Other Constituents to Cayuga Lake, NY

3.1. Peer-reviewed Manuscript:

Prestigiacomo AR, Effler SW, Gelda RK, Matthews DA, Auer MT, Downer BE, Kuczynski A, Walter MT. 2016. Apportionment of bioavailable phosphorus loads entering Cayuga Lake, New York. J. Amer. Water Resources Association 52: 31-47.

Selected Salient Findings:

- SRP, SUP, and PP were completely, mostly, and low in their bioavailability, respectively
- Unavailability of SUP in the LSC discharge
- Nearly complete unavailability of PP in the IAWWTP effluent appears to be an attribute of micro-sand ballasted flocculation treatment
- Low fBAP values for PP in local tributaries during runoff events are responsible for the bioavailable load being much smaller than the TP load
- Low fBAP value of tributary loads in conjunction with low fBAP value on shelf soon after an event are not supportive of inclusion of such shelf observations of TP in assessments of trophic state (e.g., state TP guidance value)
- Estimates of bioavailable loads were only 26% of the TP loading estimates

JOURNAL OF THE AMERICAN WATER RESOURCES ASSOCIATION

Vol. 52, No. 1 AMERICAN WATER RESOURCES ASSOCIATION February 2016

APPORTIONMENT OF BIOAVAILABLE PHOSPHORUS LOADS ENTERING CAYUGA LAKE, NEW YORK[1]

Anthony R. Prestigiacomo, Steven W. Effler, Rakesh K. Gelda, David A. Matthews, Martin T. Auer, Benjamin E. Downer, Anika Kuczynski, and M. Todd Walter[2]

ABSTRACT: The integration of the phosphorus (P) bioavailability concept into a P loading analysis for Cayuga Lake, New York, is documented. Components of the analyses included the: (1) monitoring of particulate P (PP), soluble unreactive P (SUP), and soluble reactive P (SRP), supported by biweekly and runoff event-based sampling of the lake's four largest tributaries, (2) development of relationships between tributary P concentrations and flow, (3) algal bioavailability assays of PP, SUP, and SRP from primary tributaries and the three largest point sources, and (4) development of P loading estimates to apportion contributions according to individual nonpoint and point sources, and to represent the effects of interannual variations in tributary flows on P loads. Tributary SRP, SUP, and PP are demonstrated to be completely, mostly, and less bioavailable, respectively. The highest mean bioavailability for PP was observed for the stream with the highest agriculture land use. Point source contributions to the total bioavailable P load (BAP_L) are minor (5%), reflecting the benefit of reductions from recent treatment upgrades. The BAP_L represented only about 26% of the total P load, because of the large contribution of the low bioavailable PP component. Most of BAP_L (>70%) is received during high flow intervals. Large interannual variations in tributary flow and coupled BAP_L will tend to mask future responses to changes in individual inputs.

(KEY TERMS: environmental impacts; rivers/streams; point sources; lakes; nutrients; phosphorus; load estimates; bioavailability.)

Prestigiacomo, Anthony R., Steven W. Effler, Rakesh K. Gelda, David A. Matthews, Martin T. Auer, Benjamin E. Downer, Anika Kuczynski, and M. Todd Walter, 2016. Apportionment of Bioavailable Phosphorus Loads Entering Cayuga Lake, New York. *Journal of the American Water Resources Association* (JAWRA) 52(1): 31-47. DOI: 10.1111/1752-1688.12366

INTRODUCTION

Despite advancements in wastewater treatment and control of nonpoint sources over the last 30 years, cultural eutrophication and its attendant water quality problems continue to be an issue for many lakes in the United States (Cooke *et al.*, 2005). Reductions of phosphorus (P) inputs remain a primary management objective as it is the limiting nutrient in the vast majority of freshwater systems (Cooke *et al.*, 2005). Partitioning external loads of P according to sources is fundamental information to support related rehabilitation initiatives, such as the

[1]Paper No. JAWRA-14-0155-P of the *Journal of the American Water Resources Association* (JAWRA). Received July 7, 2014; accepted September 15, 2015.

[2]Research Scientist (Prestigiacomo) and Research Engineer (Effler, Gelda, Matthews), Upstate Freshwater Institute, P.O. Box 506, Syracuse, New York 13214; Professor (Auer) and Graduate Student (Downer, Kuczynski), Department of Civil and Environmental Engineering, Michigan Technological University, Houghton, Michigan 49931; and Associate Professor (Walter), School of Civil and Environmental Engineering, Cornell University, Ithaca, New York 14853 (E-Mail/Prestigiacomo: tony@upstatefreshwater.org).

3.2. Loading estimates for constituents other than phosphorus and expansion to long-term (a UFI report)

3.2.1. Loading estimates for constituents other than phosphorus and expansion for long-term

3.2.1.1. Summary

The pursuit of representative loading estimates was expanded in Phase 2 in support of the testing and application of the water quality model (and submodels). Evolutionary steps taken were: (1) inclusion of other constituents (along with P) to support broader capabilities and issues with the water quality model, (2) review of other data sets to identify potential systematic changes in the water quality of inputs since the late 1990s, (3) resolution of the concentration-flow dependencies of the constituents for multiple large tributaries in support of temporal data consistency, and (4) development of loading estimates for model testing and application. During the study interval of 2013, daily loading estimates for forms of P were made with widely used software, FLUX32 (FLUX32 Load Estimation Software 2013; Method 6; Prestigiacomo et al. 2016), with the logarithmic concentration-flow (C-Q) relationship stratified seasonally. A somewhat different strategy for long-term loading estimates was applied with FLUX32 in Phase 2 that included both the P forms and other constituents that extended year-round (instead of April-October only, Phase 1) over the 1998-2013 time period. Relationships of C-Q were investigated for each case (i.e., tributary and constituent specific). Uniform C-Q dependencies were used (though different among the tributaries) to estimate the loads of dissolved materials, driven by measured daily flow rates for the various tributaries. In contrast, a two flow strata approach was used for the particulate constituents, reflecting their abrupt increases in concentration with Q. The stratified relationships were used, in combination with Q records, to estimate external loads of these materials for the desired time interval. This approach assumes C-Q (stream and constituent specific) consistency in time, an assumption that is supported by analyses in Phase I and here in Phase II.

3.2.1.2. Background

Representative estimates of external loads of key constituents important to lake water quality are critical elements in the development and testing of mass balance water quality models. Loading rates (e.g., kg/d) are calculated as the product of the constituent concentration (C) and the corresponding flow rate from an input (Q, m^3/d). Daily loading estimates are necessary to satisfy the temporal driver requirements for the model of this project (Cayuga Lake Model 2D; (CLM-2D; refer to Section 7 for more information), and similar modeling initiatives elsewhere (Chapra 1997). Such lake water quality models require quantification of inputs from both tributaries and point sources. Presently, tributary inputs dominate in Cayuga Lake because: (1) tributary inflows dominate the overall hydrologic budget of the lake and (2) recent upgrades

have resulted in much lower concentrations (especially P) in the largest point sources that enter the southern end (shelf area) of the lake. Management actions to improve water quality most often focus on reductions in external loading.

The number and timing of measurements of constituents, the number of tributaries and point sources tracked, and loading estimate protocols employed, are fundamental features for the credibility of the estimates. The 2013 Cayuga Lake monitoring program for the tributaries and point sources was the most comprehensive conducted for this system to date relative to the P-eutrophication issue and related features of water quality, with respect to coverage of tributaries including runoff events (Prestigiacomo et al. 2016 and UFI 2014). The development of tributary loading estimates was conducted with the FLUX32 software. This software is designed to support loading estimates for the common case of available continuous daily flow (Q) records (e.g., gaged tributaries) and temporally incomplete concentration observations (i.e., not available for every day). This software calculates loads directly for days of measurements, and generates estimates for those without measurements. Estimates for intervals (daily) between observations were based on log (natural) concentration (C) – LN flow (Q) regression relationships (Vogel et al. 2003) and interpolated residuals (observed loads minus regression predicted loads). The daily load estimates for days without observations were calculated as the sums of the regression estimates and interpolated residuals. Loading estimates for the point sources were simpler, based on interpolation of the most frequently available flow and concentrations data (i.e., monthly or weekly) obtained directly from these sources.

Subsection 3.3 documents the development of loading estimates required by the model, using approaches similar to those described in the Phase 1 report (UFI 2014) with slight modifications. The 2013 concentration-flow (C-Q) relationships serve as the basis for loading rate estimates, not only for the 2013 study period (the year with detailed tributary information) but the development of long-term (1998-2013) estimates (including for forms of P) to support model development, testing, and application. Historical P data (from UFI 2003-2006) was used to supplement 2013 C-Q relationships when available. The use of 2013 C-Q relationships was validated by comparison with historical C-Q relationships developed (tributary and constituent specific) for selected constituents from other sources (NYSDEC in 2007, Community Science Institute (CSI), albeit in modest quantities, since the early 2000s). Also, a new site was analyzed as part of Phase II at the mouth of the Cayuga Inlet Channel (IL). This site is the most downstream site in the Channel. Because IL receives input from Cayuga Inlet Creek, Sixmile Creek, and Cascadilla Creek, this site replaces those previousy mentioned streams. IL was monitored in 2013 as part of the Cayuga Lake Monitoring program. For more information see subsection 3.3.

3.2.1.3. Observations and protocols for tributary loading estimates

Model input requirements exceeded the 2013 monitoring program described in Phase I (UFI 2014). Table 3-1 lists the stream measurements conducted in 2013 in the context of model requirements and describes the calculation techniques or assumptions used to approximate concentrations not explicitly monitored.

Table 3- 1. Summary of stream parameters monitored in 2013, CE-QUAL-W2 hydrothermal input requirements, and assumptions to meet unmonitored requirements

	Concentration Input Requirements for Water Quality Model												
Stream	DOC	POC	tNH3	NOx	PON	DON	PP	SRP	SUP	Diss. Si	Part. Si	FSS	VSS
Fall Creek (FC)[a]	✓	1	✓	✓	2	3	✓[4]	✓[4]	✓[4]	✓	5	✓	✓
Cayuga Inlet Channel Mouth (IL)[a,b]	6	✓	6	6	2	3	✓[4]	✓[4]	✓[4]	6	5	✓	✓
Salmon Creek (SC)	✓	1	✓	✓	2	3	✓[4]	✓[4]	✓[4]	✓	5	✓	✓
Taughannock Creek (TC)	✓	1	✓	✓	2	3	✓[4]	✓[4]	✓[4]	✓	5	✓	✓
Unmonitored and Ungaged Inputs (UG)	estimated from gaged loading estimates and ratio of gaged to ungagged watershed areas as described in Phase 1 and Prestigiacomo et al. 2016												
Seneca River (SR)	assumed from Site 9 surface concentrations												

✓ estimated directly using paired flow and concentration measurements in FLUX32

1: not measured, concentrations estimated from observed VSS and empirical POC/VSS regression relationship from 2013 IL data (Appendix 1)

2: not measured, concentrations estimated from POC estimate and a C:N ratio of 10.89 (Hecky 1988)

3: refer to Appendix 1

4: fraction bioavailable coefficient from site and P-form specific bioassay as described in Phase 1 (UFI 2014) and Prestigiacomo et al. 2016

5: no information, assumed to be zero

6: assumed to be the sum of Cayuga Inlet Creek, Sixmile Creek, and Cascadilla Creek

a: data sets were modified by the inclusion of historical P data over the 2003-2006 time period (UFI unpublished data). Over the 2003-2006 interval, 59 P observations were added to the 2013 Fall Creek data set and 33 observations were added to the IL data set. This data was determined to be consistent with the 2013 data (see below on data validation).

b: site added in Phase 2 to replace Cayuga Inlet Creek, Sixmile Creek, and Cascadilla Creek (see subsection 3.3)

3.2.1.4. Support for the use of 2013 concentration data for long-term estimates

Since only limited data existed for years prior to 2013; 2013 C-Q relationships were used to generate all historical inputs (1998-2013) to the water quality model. To validate this approach, 2013 C-Q scatterplots were generated on common axes with available historical data (stream and constituent specific). TP was the most abundant parameter measured historically as it was available from multiple sources over the period of interest (CSI from early 2000-2013, NYSDEC in 2007, and UFI for 2003-2006). Comparative results for Fall Creek TP were presented in Phase 1 and it was concluded that 2013 was representative of historic P conditions, validating the use of 2013 C-Q relationships to estimate P load for previous years. This analysis was expanded in Phase 2 to include other streams and more parameters. Some limited PP, SRP, SUP, TSS, Tn, NOX, and T-NH3 data was available for analysis. These other data sets were observed to be consistent with the 2013 C-Q relationships, as illustrated here for Fall Creek for PP (Figure 3-1a), SRP (Figure 3-1b), SUP (Figure 3-1c), NOx (Figure 3-1d), DOC (Figure 3-1 e), TSS (Figure 3-1f), and Tn (Figure 3-1g). Generally similar C-Q relationships are indicated; the largest

deviations were observed for NOx for Fall Creek (Figure 3-1d). Similar consistencies were observed for the other streams (Appendix 1). These observations are supportive of the use of the developed 2013 C-Q relationships (Table 3-2) to support first approximations of the constituent loads for the 1998-2013 period.

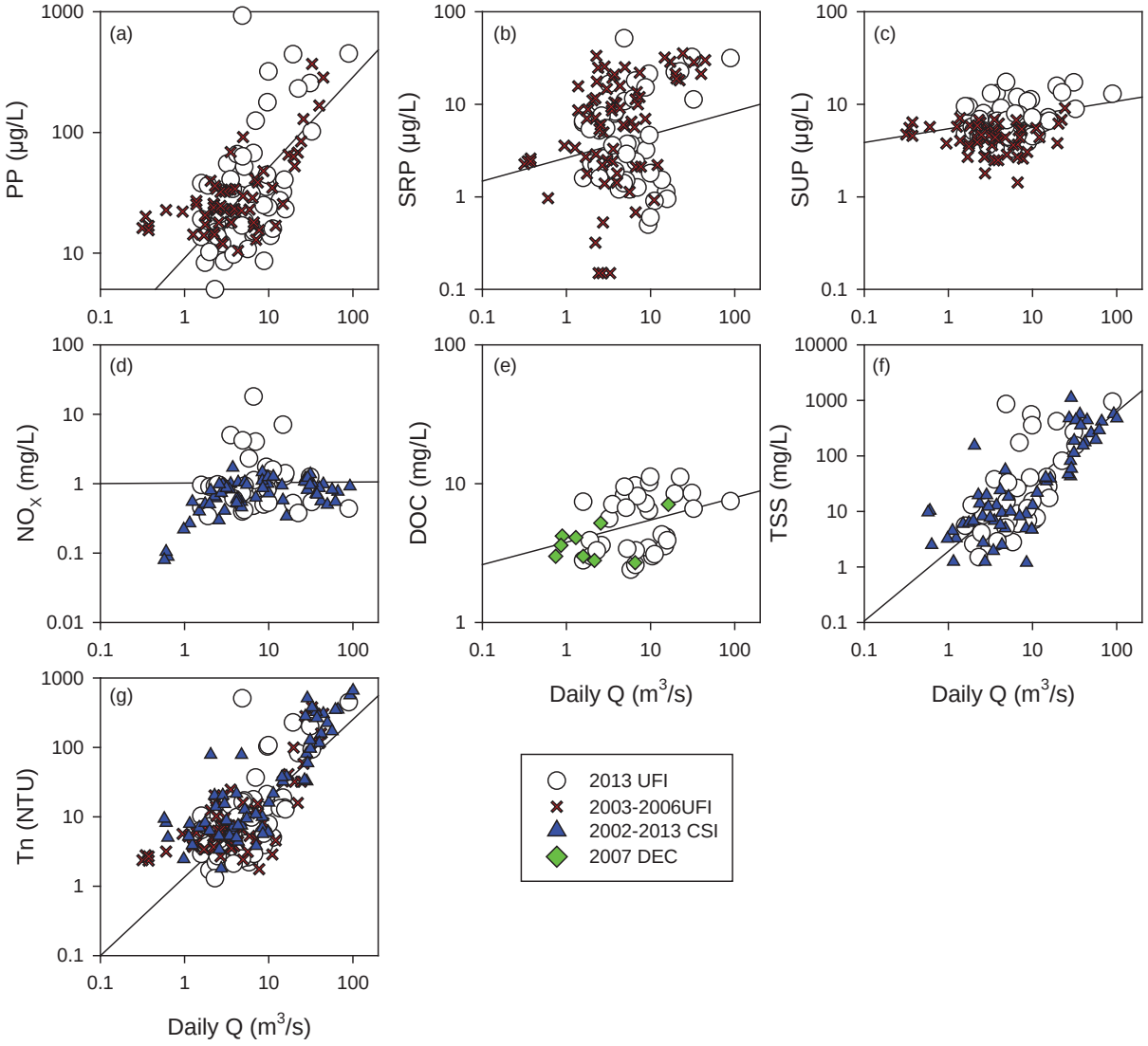

Figure 3- 1. Concentration-flow relationships for Fall Creek for selected parameters for the 2013 study interval and other historical sources for: (a) particulate P (PP), (b) soluble reactive P (SRP), (c) soluble unreactive P (SUP), (d) nitrate+nitrite (NOx), (e) dissolved organic C (DOC), (f) total suspended solids (TSS), and (g) turbidity (Tn).

Table 3- 2. Constituent concentration (C) - stream flow (Q) relationships for major tributaries to Cayuga Lake, based on 2013 observations.

		Fall Creek[1]			Salmon Creek			Cayuga Inlet Creek			Sixmile Creek		
Constituent	Strata	Equation	R^2	p-value	Equation	R^2	p-value	Equation	R^2	p-value	Equation	R^2	p-value
Particulate Constituents													
PP (g/L)	low	$=18.73Q^{0.225}$	0.08	0.02	$=7.09Q^{0.673}$	0.24	0.02	$=7.94Q^{0.427}$	0.21	0.07	$=2.59Q^{0.754}$	0.19	0.05
	high	$=2.83Q^{1.115}$	0.40	<0.01	$=1.81Q^{1.909}$	0.37	<0.01	$=1.28Q^{1.868}$	0.56	<0.01	$=9.69Q^{1.059}$	0.43	<0.01
FSS (mg/L)	low	$=4.31Q^{0.312}$	0.02	0.45	$=1.21Q^{0.875}$	0.20	0.03	$=2.97Q^{0.758}$	0.17	0.11	$=3.56Q^{0.746}$	0.15	0.09
	high	$=0.91Q^{1.483}$	0.35	<0.01	$=0.31Q^{2.312}$	0.30	<0.01	$=0.45Q^{2.296}$	0.66	<0.01	$=4.55Q^{1.463}$	0.59	<0.01
VSS (mg/L)	low	$=1.04Q^{0.174}$	0.01	0.62	$=0.47Q^{0.562}$	0.14	0.06	$=0.68Q^{0.486}$	0.16	0.12	$=1.00Q^{0.731}$	0.20	0.05
	high	$=0.20Q^{1.300}$	0.32	<0.01	$=0.09Q^{2.109}$	0.31	<0.01	$=0.07Q^{2.151}$	0.65	<0.01	$=0.65Q^{1.344}$	0.49	<0.01
Tn (NTU)	low	$=5.90Q^{0.268}$	0.03	0.42	$=2.64Q^{0.592}$	0.16	0.05	$=5.19Q^{0.734}$	0.39	0.01	$=6.49Q^{0.980}$	0.35	0.01
	high	$=0.76Q^{1.464}$	0.49	<0.01	$=0.33Q^{2.380}$	0.39	<0.01	$=0.84Q^{1.977}$	0.61	<0.01	$=7.35Q^{1.370}$	0.62	<0.01
Dissolved Constituents													
SRP (g/L)	na	$=2.64Q^{0.391}$	0.06	0.01	$=5.27Q^{0.547}$	0.13	<0.01	$=1.73Q^{0.237}$	0.09	0.08	$=4.93Q^{0.029}$	0.00	0.87
SUP (g/L)	na	$=4.58Q^{0.079}$	0.01	0.24	$=3.89Q^{0.547}$	0.37	<0.01	$=2.55Q^{0.348}$	0.47	<0.01	$=3.65Q^{0.173}$	0.18	0.01
NO_x (g/L)	na	$=1023Q^{-0.01}$	0.00	0.96	$=4113Q^{-0.01}$	0.00	0.95	$=235Q^{0.391}$	0.45	<0.01	$=125Q^{0.502}$	0.50	<0.01
DOC (mg/L)	na	$=3.79Q^{0.192}$	0.10	0.08	$=3.00Q^{0.334}$	0.23	<0.01	$=2.28Q^{0.315}$	0.41	<0.01	$=2.90Q^{0.129}$	0.11	0.15
Dissolved Si (mg/L)	na	$=2.35Q^{0.192}$	0.14	0.03	$=3.67Q^{0.087}$	0.02	0.42	$=6.01Q^{-0.028}$	0.02	0.47	$=3.99Q^{0.049}$	0.05	0.27

[1] includes P data from 2003-2006 (UFI)

Table 3-2. (cont.). Constituent concentration (C) - stream flow (Q) relationships for major tributaries to Cayuga Lake from paired data used in the development of long term concentrations (and load) estimates.

Constituent[1]	Cayuga Inlet Channel[1,2] Equation	R^2	p-value	Taughannock Creek[1] Equation	R^2	p-value
Particulate Constituents						
PP (g/L)	$=14.97Q^{0.400}$	0.28	<0.01	$=4.19Q^{0.994}$	0.59	<0.01
FSS (g/L)	$=3.87Q^{0.828}$	0.44	<0.01	$=0.79Q^{1.315}$	0.60	<0.01
VSS (mg/L)	$=1.14Q^{0.631}$	0.49	<0.01	$=0.39Q^{0.545}$	0.41	<0.01
Tn (NTU)	$=3.09Q^{1.171}$	0.74	<0.01	$=1.31Q^{1.298}$	0.68	<0.01
Dissolved Constituents						
SRP (g/L)	$=1.40Q^{0.635}$	0.28	<0.01	$=0.93Q^{0.939}$	0.40	<0.01
SUP (g/L)	$=3.89Q^{0.048}$	0.00	0.76	$=3.29Q^{0.374}$	0.25	0.03
NOx (g/L)	na[3]	na[3]	na[3]	$=713Q^{0.787}$	0.45	0.03
DOC (mg/l)	na[3]	na[3]	na[3]	$=2.97Q^{0.052}$	0.01	0.77
Dissolved Si (mg/L)	na[3]	na[3]	na[3]	$=1.24Q^{0.230}$	0.20	0.20

[1] no flow stratification due to lack of high flow samples
[2] includes P data from 2003-2006 (UFI)
[3] no data, concentrations estimated from combined inputs to the Channel

3.2.1.5. Procedures used for long-term loading rate estimates

Because of seasonal data limitation issues, a seasonal stratification approach in FLUX32 for the estimated concentrations over the 1998-2013 (16 year) interval could not be used. There was no year-round coverage (no winter season [Nov.-March] data) of observed concentration data in 2013 to justify such an approach over the long-term interval. A slightly different, but similar, estimation protocol was used to generate long-term loading rate estimates used as inputs to the water quality model. Over the 2013 April-October study interval the seasonal stratification protocol (described in Prestigiacomo et al. 2016) and the flow-based stratification protocol used here provided extremely similar estimates. The results from these two approaches were compared in the context of eleven other estimation protocols as part of Phase 1 (UFI 2014).

The final approach for load estimation was different for dissolved and particulate constituents based on flow concentration relationships and statistical performance (Appendix 1, residuals analysis). As described previously, each flow concentration relationship was stream specific but the relationships for dissolved constituents (SRP, SUP, dissolved Si, T-NH_3, NO_X, DOC) were not stratified by flow regime. Particulate constituents (PP, FSS, VSS, Tn, PAV1-4)

C-Q relationships were stratified into high and low strata based on 2013 upper quartile flow statistics for each stream.

Concentration and loading estimates for the 1998-2013 time interval for each stream were estimated as the product of concentrations (C) and stream Q (daily average), based on the continuous flow measurements near the mouths of each stream as described in Prestigiacomo et al. 2016 and the Phase I Report. Daily estimates of loads were made with FLUX32 software (FLUX 32 Load Estimation Software, version 3.31, 2013), designed to support such efforts for the common case of availability of continuous flow measurements combined with limited (e.g., biweekly) observations of concentrations. The adopted protocol (FLUX 32, Method 6) used measured concentrations for the days of constituent monitoring. Concentrations for days between monitoring were based on the natural log-transformed C-Q relationships and interpolated residuals (observed C minus the C-Q regression estimated concentrations). For dissolved constituents, no flow stratification was used. The procedure varied slightly for particulate constituents whereby for each stream, a two flow strata method was adopted, demarcated by the stream specific mean Q for the 2013 study period. For all constituents, the concentration estimates between days of observations were calculated as the sums of the C-Q based values plus the interpolated residuals. This method was applied to the continuous flow record for each stream over the 1998-2013 period. Estimates for the unmonitored (ungaged) tributaries were made as described in the Phase 1 report (UFI 2014) and Prestigiacomo et al. 2016. Example C-Q relationships used by the load estimation software from Fall Creek in 2013 are provided in Figure 3-2. The forms of P were not adjusted for bioavailability, to provide context for that priority constituent. Particulate-based metrics, including PP (Figure 3-2a), FSS (Figure 3-2b), VSS (Figure 3-2c), and Tn (Figure 3-2d), demonstrated relatively strong positive dependency on Q (Table 3-2), that was somewhat greater for the higher Q stratum. The relationships for the dissolved constituents were less strong (Figure 3-2e- i). SRP variations were not strongly dependent on Q for Fall Creek although the relationship was statistically significant (Table 3-2). Similar scatterplots for other streams and constituents can be found in Appendix 1. 2013 C-Q regression relationships and performance statistics for all monitored parameters and tributaries can be found in Table 3-2.

3.2.1.6. Example loading analysis results

The resulting daily time series of Q and estimated input constituent concentrations in 2013 (model validation year) are presented for Fall Creek in Figure 3-3 (a-j). These concentration inputs were used directly by the water quality model and are the results of loading calculations in FLUX32 as described previously. As examples, the three forms of P included here have not been adjusted for bioavailability, providing context for comparison to the other constituents. Much greater temporal increases in the particulate constituents occurred during runoff events (Figure 3-3 a-e) compared to the dissolved materials (Figure 3-3a, f-j) according to

the implemented representation. The effect on loading estimates is particularly pronounced for the particulate metrics, based on the product of Q and C. Accordingly, the effects of runoff events on the particulate constituent loads are substantially greater than for the dissolved materials. These results were consistent for Fall Creek in 1999 (Figure 3-4) which served as the model validation year and for other streams in both 2013 and 1999 (Appendix 1).

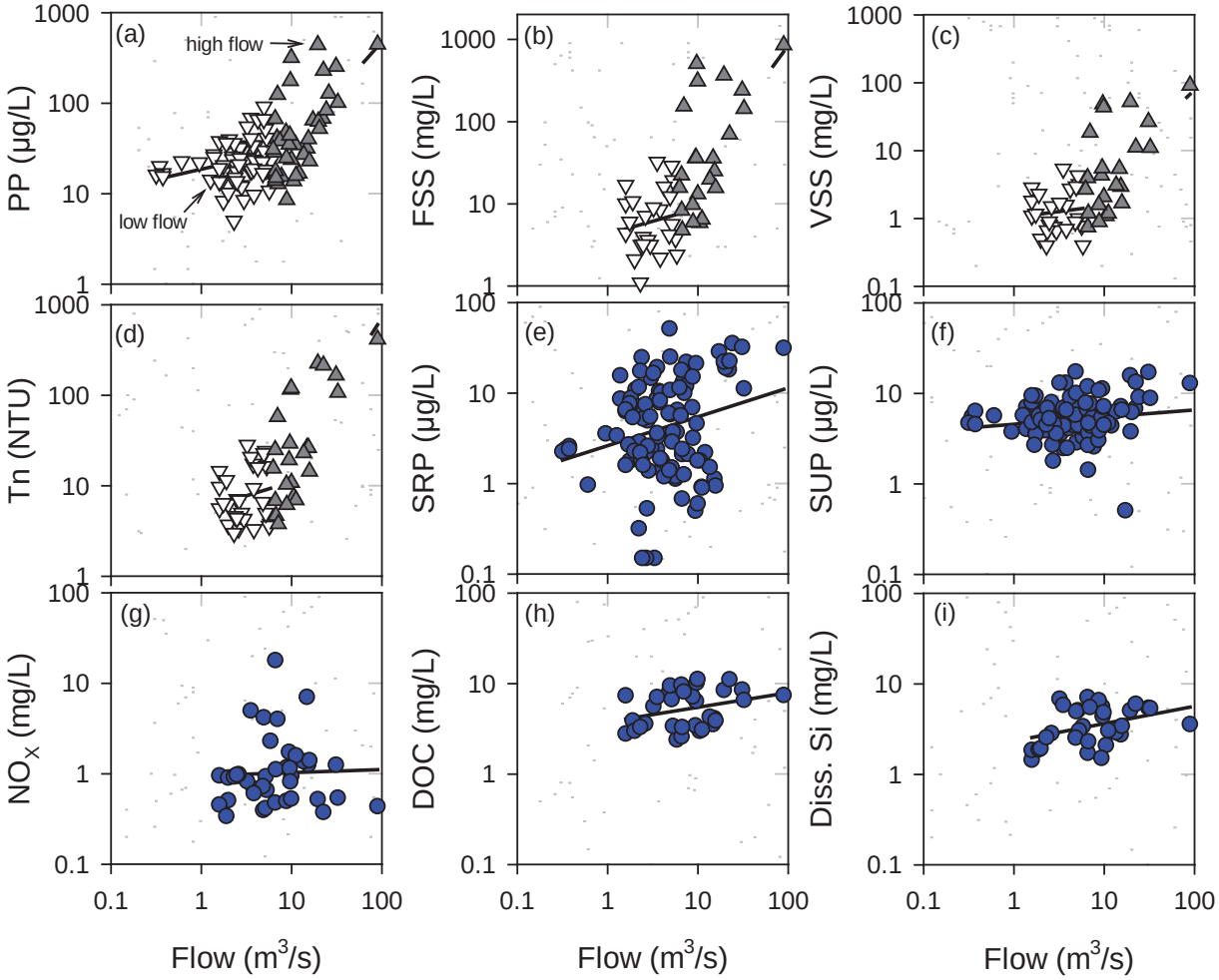

Figure 3- 2. Concentration-flow relationships for 2013 Fall Creek observations for: (a) particulate P, (b) fixed suspended solids, (c) volatile suspended solids, (d) turbidity, (e) soluble reactive P, (f) soluble unreactive P, (g) nitrate+nitrite (NOx), (h) dissolved organic carbon (DOC), and (i) dissolved silica (Si).

The C-Q based approach adopted here and the resulting generation of 16 year loading estimates (from FLUX32) supports first approximations of interannual differences in constituent loads at multiple time scales, including from seasonal to annual. Major seasonal differences for bioavailable P (P_B)) loads were obtained between 2013 and 2012, based strictly on differences in

runoff patterns (i.e., no observations in 2012; Figure 3-5 a-d). The annual estimates of these bioavailable P form loads were 130%, 58%, and 52% greater in 2013 than in 2012. This is also illustrated here for loads of the bioavailable portions of three forms of P, $PP_{L/B}$ (Figure 3-6b), $SRP_{L/B}$ (Figure 3-6c), and $SUP_{L/B}$ (Figure 3-6d). The corresponding estimates of total loads, annually and for the April-October interval, varied substantially year-to-year over the 1998-2013 period (Figure 3-6, Table 3-3), associated with variations in runoff in most years due to limited observations (Table 3-3). These support the position that major interannual differences in bioavailable P loads occur for Cayuga Lake in response to natural variations in Q.

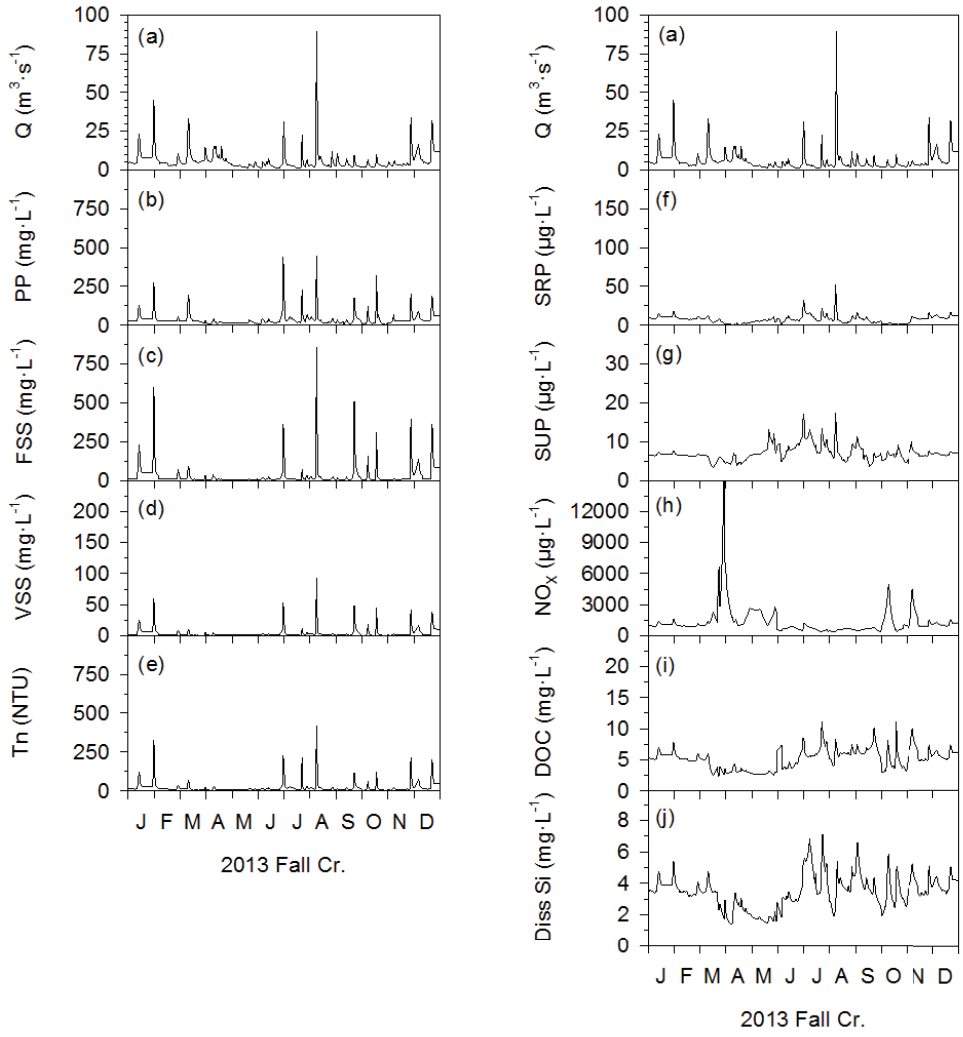

Figure 3- 3. Model calibration year (2013) time-series of inputs from FLUX32 to the model for Fall Creek of: (a) flow, (b) PP, (c) FSS, (d) VSS, (e) Tn, (f) SRP, (g) SUP, (h) NOX, (i) DOC, and (j) dissolved Si.

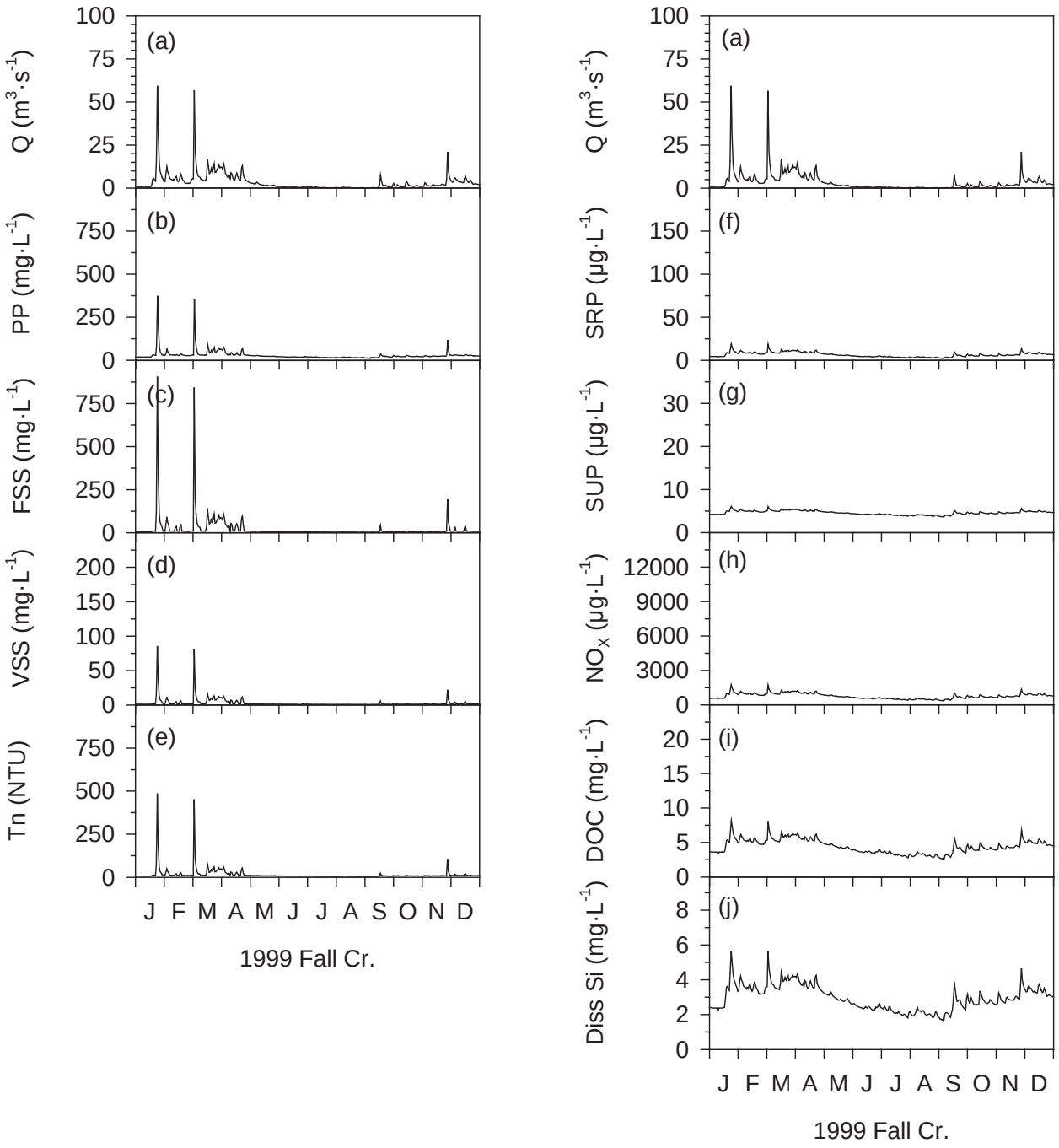

Figure 3- 4. Model validation year (1999) time-series of inputs from FLUX32 to the model for Fall Creek of: (a) flow, (b) PP, (c) FSS, (d) VSS, (e) Tn, (f) SRP, (g) SUP, (h) NOX, (i) DOC, and (j) dissolved Si.

Table 3- 3. Estimates of Q-driven interannual variations in bioavailable phosphorus loads, 1998-2013. Sums represent the summation of daily estimates from FLUX32 output.

	April - October Load (kg)				January - December Load (kg)			
Constituent	Mean	Median	Range	St. Dev.	Mean	Median	Range	St. Dev.
$PP_{L/B}$	11,500	6,800	80,400	19,500	23,150	17,350	107,970	25,400
$SRP_{L/B}$	5,700	5,130	9,900	2,900	13,500	13,900	14,600	4,100
$SUP_{L/B}$	2,450	2,200	4,300	1,100	5,416	5,700	6,100	1,650

3.2.1.7. Observations, protocols, and results for point source loading estimates

The procedures used to generate loading rates from the point sources were outlined in Phase 1 (UFI 2014). Due to lack of detailed concentration data, phosphorus was the only constituent attributed as point source inputs to Cayuga Lake in the water quality model. The procedures used in estimating daily times series of P inputs (as well as bioavailability estimates) over the 1998-2013 interval can be found in Appendix 1. A representative time series of inputs from 2013 for IAWWTP, CHWWTP, and the LSC facility is presented in Figure 3-7. P contributions from point sources were less variable annually; except for those years during treatment upgrades (see UFI 2014 and Appendix 1). A time series of these point sources for 1999 is presented in Fig 3.8 for comparison.

3.2.1.8. Loading estimates from the Seneca River

The Seneca River, at times, flows into Cayuga Lake and therefore needed to be treated as an input to Cayuga Lake during those intervals. Due to the lack of detailed concentration data, concentration data from Site 9 (site nearest to the Seneca River) was used to estimate Seneca River concentration inputs into the water quality model (Appendix 1).

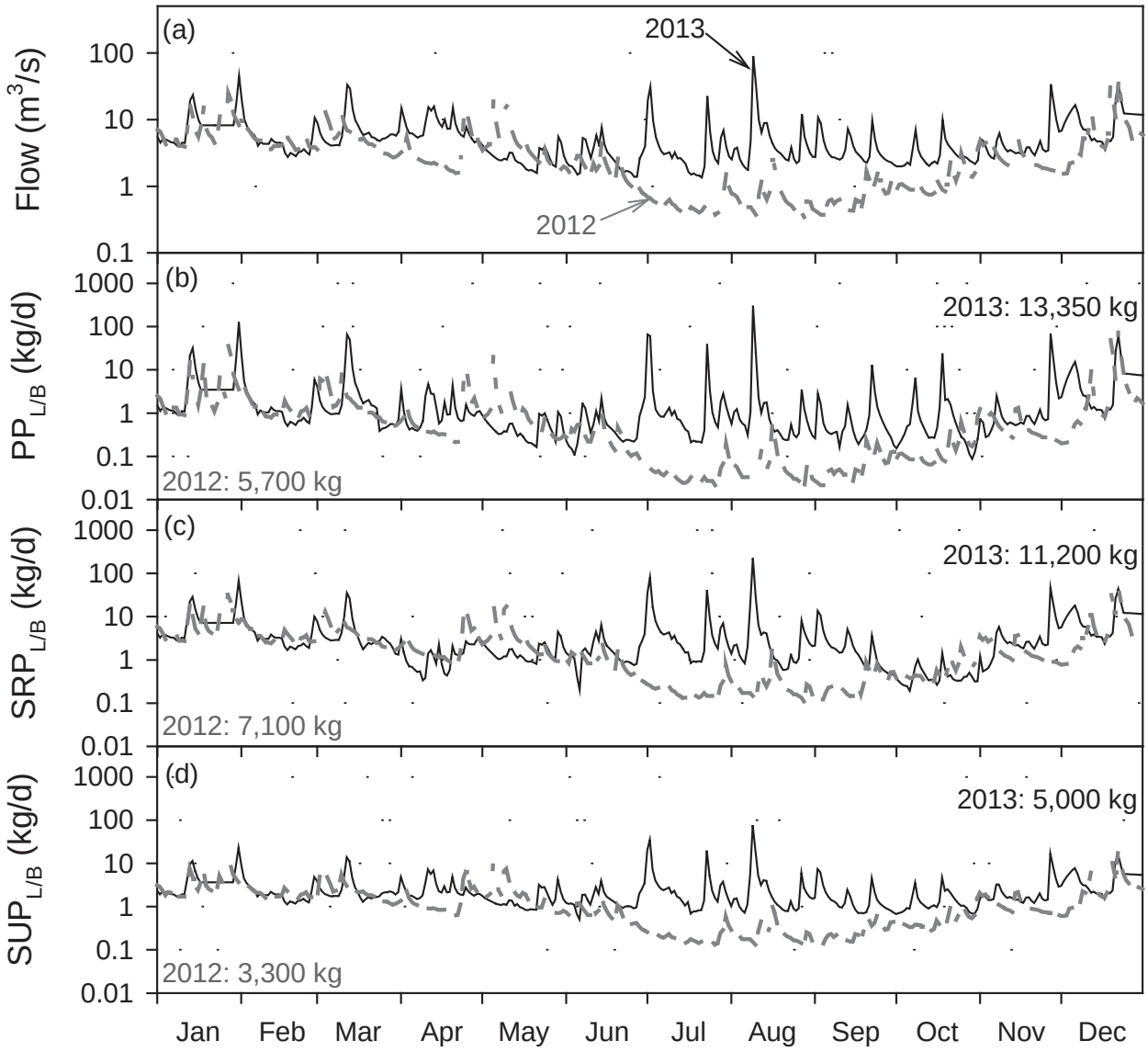

Figure 3- 5. Estimated daily time series output from FLUX32 calculations for Fall Creek loading to Cayuga Lake of forms of phosphorus for 2013 and 2012 (a dry year case) time series of: (a) flow (Q) for reference, (b) bioavailable PP ($PP_{L/B}$), (c) $SRP_{L/B}$, and (d) $SUP_{L/B}$.

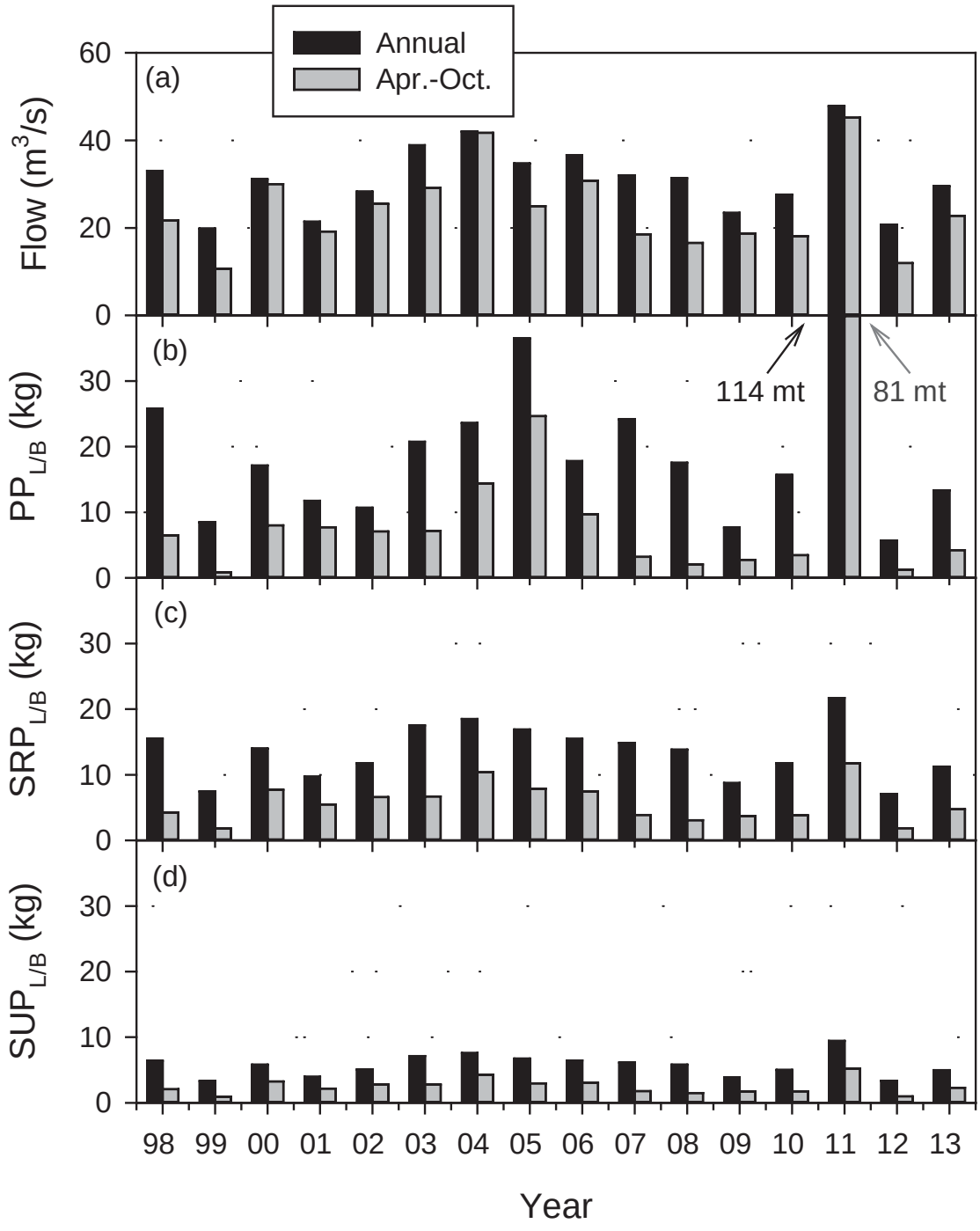

Figure 3- 6. Estimated total annual and seasonal (April-October) loads of the bioavailable portions of these forms of phosphorus from all external sources, for the 1998-2013 period: (a) total tributary flow, (b) bioavailable particulate P ($PP_{L/B}$), (c) $SRP_{L/B}$, and (d) $SUP_{L/B}$. These quantities reflect the summation of daily FLUX32 estimates for the entire year (Annual-black bar) and seasonal (April-October-gray bar).

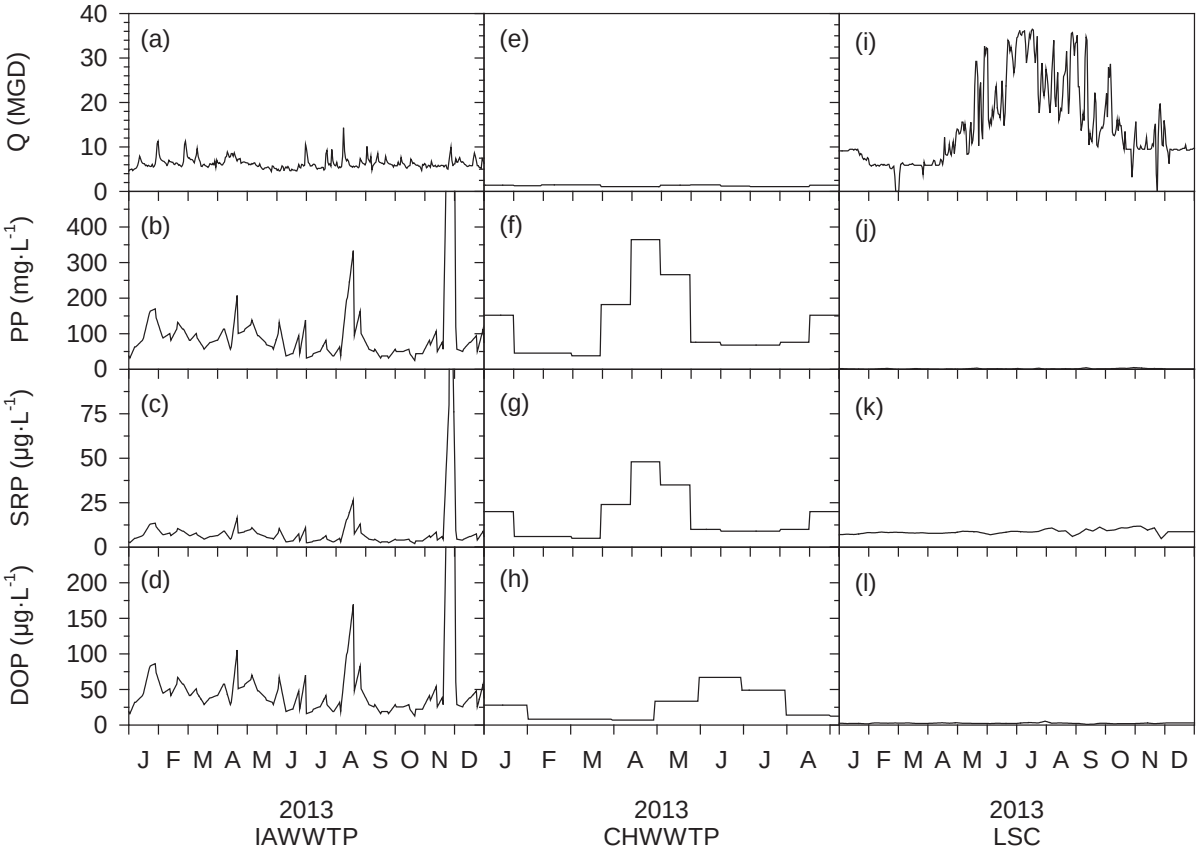

Figure 3- 7. 2013 time series of P concentrations in the three largest point sources inputs to Cayuga Lake: (a) IAWWTP flow, (b) IAWWTP PP, (c) IAWWTP SRP, (d) IAWWTP SUP, (e) CHWWTP flow, (f) CHWWTP PP, (g) CHWWTP SRP, (h) CHWWTP SUP, (i) LSC flow, (j) LSC PP, (k) LSC SRP, and (l) LSC SUP.

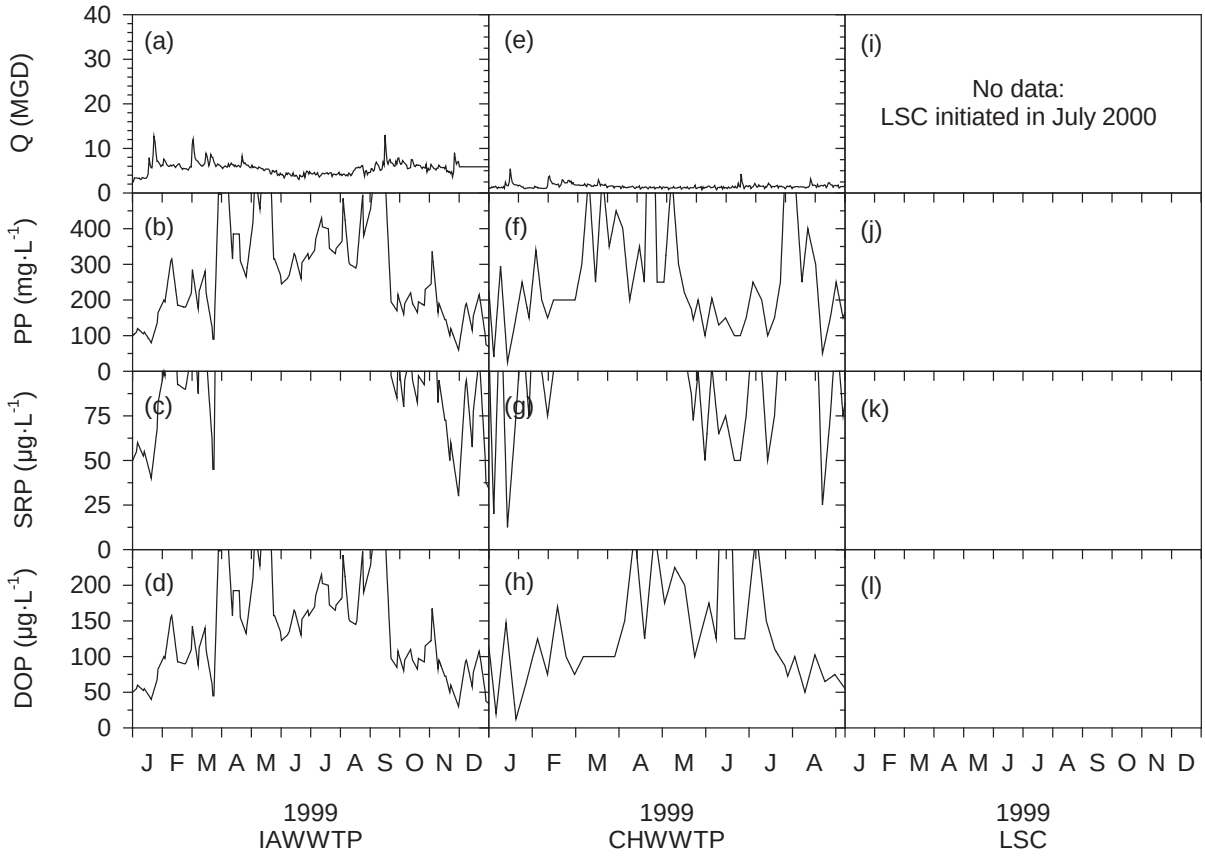

Figure 3- 8. 1999 (validation year) time series of P concentrations in the three largest point sources inputs to Cayuga Lake: (a) IAWWTP flow, (b) IAWWTP PP, (c) IAWWTP SRP, (d) IAWWTP SUP, (e) CHWWTP flow, (f) CHWWTP PP, (g) CHWWTP SRP, (h) CHWWTP SUP, (i) LSC flow*, (j) LSC PP*, (k) LSC SRP*, and (l) LSC SUP*. * *LSC was initiated in July 2000, no data for 1999.*

3.3. Summary of 2013 water quality data and loading estimates from the Cayuga Inlet Channel to Cayuga Lake (a UFI report)

3.3.1. Cayuga Inlet Channel to Cayuga Lake, summary for 2013 water quality data and loading estimates

3.3.1.1. Summary/Abstract

The Cayuga Inlet Channel (IL; 4 km), completed in 1977, receives the inflows of Cayuga Inlet, Sixmile Creek, and Cascadilla Creeks. Modifications of the tributary inputs within the Channel are known to have contributed to sediment deposition since its construction. Contemporary effects of the Channel on loading from these streams was evaluated based on additional (beyond the QAPP scopes) monitoring in 2013 with continuous instrumentation measurements (flow direction and magnitude, temperature, turbidity and specific conductance) and sampling for selected project laboratory metrics (e.g., forms of P), at a site proximate to the Channel inflow (IL). The goal was to appropriately modify tributary loads to represent the effects of the Channel. Flow velocity measurement profiles identified the complexity of the regime, with bi-directional flow (out of the Channel into the lake, or lake water flowing back into the Channel) common in low flow intervals, such as dry weather portions of summer. However, outflow from the Channel to the lake was recurring in response to runoff events. The importance of uncertainties of lake-Channel exchange, including their constituents, during dry weather in summer, was diminished by the dominance of the runoff event inputs. The Channel acted as a source of particulate constituents (e.g., particulate phosphorus; PP) during dry weather intervals and for small runoff events, suggesting inputs from Channel deposits. However, during the largest events of 2013 (e.g., July 1, July 23, August 8, and September 2) the Channel acted as a sediment sink overall, receiving greater summed loads from the tributaries than it delivered to the lake. The findings for SRP_L, was qualitatively similar, with the Channel acting as a source (compared to summed tributaries) for most of the 2013 monitoring, but a sink for the largest runoff events. In contrast, the Channel was a source of soluble unreactive phosphorus (SUP_L) throughout the study.

It was determined that during periods of low flow, concentration data at IL can be influenced by backflow from the lake in to the Channel. IL C/driver regressions and subsequent loads generated from use of April-July 5, 2013 data plus only collections that occurred during runoff event conditions for the remainder of the study period. The IL site was treated as a tributary mouth site. Representative daily concentration and loading estimates were made using the daily flow record and specific IL C/Q relationships (case 4a, see Table 3-4 and Table 3-5), in FLUX32 for the 2013 study interval and for long-term (i.e., 1998-2013) estimates. Since IL receives inputs from the Cayuga Inlet Creek, Sixmile Creek, and Cascadilla Creek, the estimates

made at IL were used in place of estimates specific to those three tributaries (UFI 2014, Prestigiacomo et al. 2016)

3.3.1.2. Background

Site IL is located near the mouth of the Cayuga Inlet Channel and was the monitoring site farthest downstream, prior to the Channel's entry to the shelf region of Cayuga Lake (Figure 3-9). The Cayuga Inlet Channel has a total watershed area of ~ 412 km^2 and receives discharge from three tributaries. In order of watershed size they are: (1) Cayuga Inlet Creek (240.81 km^2), (2) Sixmile Creek (134.11 km^2), and (3) Cascadilla Creek (36.65 km^2).

As part of the 2013 Phase I Cayuga Lake study, the mouths of Cayuga Inlet Creek and Sixmile Creek were monitored and load estimates were made for desired constituents (UFI, 2014). Loading estimates (for each constituent) for Cascadilla Creek are made here by assuming that the Cascadilla Creek load is a function of the Unmonitored load and the ratio of Cascadilla Creek watershed area (36.65 km^2) to the Unmonitored watershed area (758.18 km^2). The Unmonitored watershed area is the total area of Cayuga Lake not directly monitored in 2013 (excludes Fall Creek, Cayuga Inlet Creek, Salmon Creek, Sixmile Creek, and Taughannock Creek). For more information, please see the 2014 Phase I Report (UFI, 2014). Forty one water chemistry samples were collected at IL as part of the 2013 Cayuga Lake study during the lake monitoring portion of the program (both Biweekly and Frequent South programs). These samples were collected from near the surface (~ 0-0.5 m water depth) and analyzed for phosphorus (P), suspended solids (SS), turbidity (Tn), and minerogenic particle area per unit volume (PAV_m). In addition, a YSI data sonde with temperature (T), specific conductance (SC) and turbidity (Tn) probes was deployed at IL at ~ 0.7 m water depth from early May through October. Turbidity patterns and loading estimates were made with the field Tn (or adjusted lab Tn values), consistent with the tributary analysis in the Phase I Report (UFI 2014).

It is believed processes within the Cayuga Inlet Channel alter material loads from the three inputs; with conditions at IL more representative of the water quality and effective material loads reaching the shelf region. The analysis presented here will be used to estimate loads at IL to represent loading of the Cayuga Inlet Channel to the shelf region of Cayuga Lake. As an added complexity, the Cayuga Inlet Channel at some times is under backflow conditions when water from the lake flows upstream (south) into the channel (T. Cowen's group, 2015). This backflow effect is not uniform vertically in the water column in the Inlet Channel (e.g., bi-directional flow regime) with lake water normally at the surface overlying deeper tributary inputs. As a result, there may be cases where water quality samples collected at IL over the study interval were collected during times of backflow (i.e., lake water) and therefore would not be representative of tributary water.

3.3.1.3. General Patterns of Water Quality at IL

IL water quality was found to be highly influenced by the tributaries to the Cayuga Inlet Channel as demonstrated in Figures 3.-10 and 3-11. Figure 3-10 shows the time series for flow for Cayuga Inlet and Sixmile Creeks (Figure 3-10a), specific conductance (SC; Figure 3-10b), and flow (Q) -weighted specific conductance (Figure 3-10c). The time series for the tributaries (Cayuga Inlet and Sixmile Creeks) were generated from SC/Q relationships developed from monitoring at their respective mouths. SC at IL (from sonde measurements) was highly variable, dependent on tributary flow inputs (Figure 3-10b). During dry weather, SC at IL was 40-60 S/cm higher than the lake at Station 2. With increased flow, SC at IL decreased (i.e., dilution) often dropping below 300 S/cm. By contrast, the SC at Cayuga Lake Station 2 was consistent, narrowly ranging from ~ 400 to 425 S/cm. The SC at IL was closely approximated by the Q-weighted SC inputs from Cayuga Inlet and Sixmile Creeks (Figure 3-10c) especially during runoff events where Q-weighted SC from the tributaries was nearly identical to SC at IL.

Similarly with turbidity (Tn), the water quality at IL was found to be highly variable (positive dependency on flow) and dependent on stream inputs (Figure 3-11b). The time series for Cayuga Inlet and Sixmile Creeks were developed from Tn/Q relationships for these tributaries. During dry weather turbidity at IL was found to be 5-10 NTU higher than the inputs. During runoff events, Tn at IL increased dramatically with Tn peaks greater than 200 NTU during the four largest events over the study interval (peak Tn was ~ 1000 NTU on August 9). As with SC, the Tn at IL was closely approximated by the Q-weighted Tn inputs from Cayuga Inlet Creek and Sixmile Creek (Figure 3-11c) especially during runoff events where Q-weighted Tn from the tributaries was nearly identical to Tn at IL. The Tn at Station 2 in Cayuga Lake did not vary much over the study interval ranging from 0.7 to 4.3 NTU, but the highest Tn values at this site did occur during days shortly after runoff events. An interesting pattern of Tn was observed at IL over the mid July through October interval (Figure 3-11b-c). During this time period the Tn was extremely variable even over very short time periods (hours), displaying large swings in Tn (1-20 NTU) during dry weather conditions. It is speculated that this Tn pattern was a result of resuspension in the Channel (i.e., not due to tributary inputs) although the exact mechanism driving this pattern remains unclear. The variable Tn signature may be due to propeller turbulence from boat traffic.

3.3.2. Objectives

The objectives of this analysis were to: (1) provide insight to identify samples representative of tributary conditions at IL and appropriate to use in loading calculations (as informed by analyses by T. Cowen's group of the flow regime), (2) interrogate the IL datasonde and chemistry sample data set to provide loading estimates at IL for several cases of data usage and for several potential drivers (flow or turbidity), and (3) develop loading estimates at IL using IL data for desired water quality parameters.

3.3.3. Methods

3.3.3.1. Data Exclusions and Load Estimation Procedure

Four cases of data availability were considered and are summarized in Table 3-4. Case 1 was the simplest case whereby the load at IL was assumed to be equivalent to the sum of the three inputs to the Cayuga Inlet Channel (sum of inputs from Cayuga Inlet, Sixmile, and Cascadilla Creeks). Case 1 is the simplest and is likely to be flawed as it does not account for water quality conditions at IL from direct measurements and likely is not representative of the true loading conditions at IL because it does not account for processes within the Channel (e.g., deposition/resuspension). Case 2 assumes that all data collected at IL in 2013 were representative of tributary conditions and are acceptable for use in the estimation of IL loads. Case 2 may be a more reasonable approach; however, there are dates in the late summer through the fall (especially dry weather dates) where IL may have been influenced by backflow conditions. Case 3 represents the most conservative case of data exclusion in that only the data from April through July 5 was considered as definitely representative of tributary inputs, as determined by Cornell co-investigators (Cowen, personal communication). Case 4 includes the Case 3 data set, with the addition of IL samples collected during times of high flow (i.e., runoff events) after July 5. Case 4 probably represents the most reasonable approach as it uses verified data from the spring through early summer and data during periods of high flow which are mostly representative of tributary inputs.

Flow estimates at IL were made by summing the flows of the three inputs, Cayuga Inlet Creek, Sixmile Creek, and Cascadilla Creek. Flow estimates at Cascadilla Creek were made by assuming its flow was a function of the Unmonitored flow and the ratio of Cascadilla Creek watershed area to the Unmonitored watershed area (UFI, 2014). The three tributaries contributed flow volumes proportional to their watershed areas to the Inlet Channel over the 2013 April – October interval. Cayuga Inlet Creek was the dominant contributor of flow (~ 39 million m^3; 50%), followed by Sixmile Creek (~ 30 million m^3; 39%), and Cascadilla Creek (~ 8.3 million m^3; 11%).

3.3.3.2. Hydrograph Separation

Hydrograph separation of daily flows was used to determine days of runoff conditions in Cayuga Inlet Creek and Sixmile Creek. The method used was the local minimum method in HYSEP (Sloto and Crouse, 1996). For purposes of this analysis it was assumed that if an IL sampling day occurred during runoff conditions in either Cayuga Inlet Creek or Sixmile Creek, the conditions at IL were representative of creek inputs (i.e., not lake water) and were included for use in Case 4. A graphical representation of these results can be found in Figure 3-12. A summary of IL data used for each Case (2-4) can be found in Appendix 1. HYSEP hydrograph separation determined that 123 days over the April through October interval were under runoff

conditions. Seventeen IL sampling dates after July 5 were runoff dates and will be included in Case 4 (29 total sampling dates). Two dates, October 1 and October 7 were determined to be runoff dates by HYSEP that showed only very small increases in flow on those days, and may be in question as to whether or not IL is representative of tributaries on those dates. They were included in Case 4 analysis as runoff dates. Also, August 12 was determined to be a non-runoff date by HYSEP. Flow and Tn were still elevated from the August 8 runoff event on this date and it was therefore included as a runoff date in Case 4.

3.3.3.3. Concentration-Driver Relationships

Daily Average Concentration/Daily Average Flow

The strengths and character of the daily averaged concentration-daily averaged flow (C/Q) relationships varied by parameter and Case. For Case 2 (inclusion of all IL data), the relationships between daily Q and particulate parameters (PP, FSS, VSS, Tn, and PAV_m; Figure 3-13 and 3.11, first column) were stronger ($R^2 > 0.4$) than the relationships between daily Q and dissolved P (Figure 3-13, first column). The character and strengths (R^2) values for C/Q relationships for IL are reasonable and consistent with other Cayuga Lake tributaries (UFI, 2014). The C/Q relationships for Case 3 were substantially weaker than for Case 2 (Figure 3-13 and 3.11, middle column) because of the exclusion of data from July 5 through October 31; a period which contained three large and several small runoff events (Figure 3-12). For example, the Case 2 PP/Q regression R^2 was 0.41 and for Case 3 the PP/Q R^2 was 0.21. The strengths and character of the C/Q relationships for Case 4 were generally similar to the C/Q relationships for Case 2 (Figure 3-13 and 3.11, last column). For most parameters, in fact, the R^2 improved from Case 2 to Case 4 most likely due to a loss of data points at the low end of the C/Q relationship and increased leverage from high C/Q data. For most parameters, the intercepts decreased and slope parameters increased slightly from Case 2 to Case 4.

Daily Average Concentration/Daily Average Turbidity

The strengths and character of the daily averaged concentration-daily averaged turbidity (C/Tn) relationships varied by parameter and Case and are presented in Figures 3-15 and 3-16. For Case 2, the relationships between daily Tn and particulate parameters (PP, FSS, VSS, Tn, and PAV_m; Figure 3-15 and 3.13, first column) were stronger than the relationships between daily Tn and dissolved P (Figure 3-15, first column). The C/Tn relationships for PP, forms of SS, Tn (laboratory) and PAV_m (except PAV_{m4}) were very strong ($R^2 \geq 0.68$). For all parameters (even dissolved P), the relationships between C/Tn were better than the corresponding C/Q relationships (Figure 3-13 and 3.11). The C/Tn relationships generally became weaker in Case 3 (Figure 3-15 and 3.13, middle column) because of the exclusion of data from July 5 through October 31, although the changes were less substantial than for Case 3 C/Q. The strengths and character of the C/Tn relationships for Case 4 were generally similar to the C/Tn relationships

for Case 2 (Figure 3-15 and 3.13, last column). For most parameters, in fact, the R^2 improved from Case 2 to Case 4 most likely due to a loss of data points at the low end of the C/Tn relationship and increased leverage from high C/Tn data. For most parameters, the intercept and slope parameters were very similar between Case 2 and Case 4.

Concentration/Instantaneous Flow

The strength and character of the concentration-instantaneous flow (C/Q_I) relationships varied by parameter and Case. Like with the daily C/Q, Case 2 relationships between Q_I and particulate parameters (PP, FSS, VSS, Tn, and PAV_m; Figure 3-17 and 3.15, first column) were stronger ($R^2 > 0.4$) than the relationships between Q_I and dissolved P (Figure 3-17, first column). The PP/Q_I relationship was similar to the PP/Q relationship ($R^2 \sim 0.4$) but generally, the C/Q_I relationships for the particulate parameters were stronger (higher R^2) than daily C/Q, had lower intercepts and larger slopes. As with the other C/driver relationships, the C/Q_I relationships became substantially weaker in Case 3 (Figure 3-17 and 3.15, middle column) because of the exclusion of data from July 5 through October 31. The strengths and character of the C/Q_I relationships for Case 4 were generally similar to the C/Q_I relationships for Case 2 (Figure 3-17 and 10, last column). For most parameters, in fact, the R^2 improved from Case 2 to Case 4. For most parameters, the intercepts decreased and slope parameters increased slightly from Case 2 to Case 4 similar with the daily C/Q relationships in Figures 3-13 and 3-14.

Concentration/ Instantaneous Turbidity

The strengths and character of the concentration-instantaneous turbidity (C/Tn_I) relationships varied by parameter and Case and are presented in Figures 3-19 and 3-20. For Case 2, the relationships between Tn and particulate parameters (PP, FSS, VSS, Tn, and PAV_m; Figure 3-19 and 3.17, first column) were stronger ($R^2 \geq 0.6$) than the daily relationships between Tn and dissolved P (Figure 3-19, first column) consistent with the previous C/driver relationships. The C/Tn_I relationships for PP, forms of SS, Tn (laboratory) and PAV_m (except PAV_m 4) were strong (R^2 >0.55). For all parameters, the relationships between C/Tn_I were better than the corresponding C/Q_I relationships (Figure 3-17 and 3.15). As with the daily C/Tn regressions, the C/Tn_I relationships generally became weaker in Case 3 (Figure 3-19 and 3.17, middle column) although the changes were less substantial than for Case 3 C/Q_I. The strengths and character of the C/Tn_I relationships for Case 4 were generally similar to the C/Tn_I relationships for Case 2 (Figure 3-19 and 3.17, last column). For most parameters, the intercept and slope parameters were very similar between Case 2 and Case 4. Considering all Case 4 relationships, the C/Tn_I regressions were the strongest of all the C/driver relationships.

3.3.3.4. Methods of Load Estimation

Table 3-5 contains a summary of load calculation methods for each Case. For Cases 2-4, four different calculation techniques were employed to estimate P, SS, Tn, and PAV_m loads at IL. The four methods were: (a) defined C/Q regressions, applied the daily Q record (driver), in FLUX 32 (Method 6, Interpolation; FLUX32, 2013), (b) defined C/Tn regressions applied to the daily averaged Tn record (driver), (c) defined C/Q_I regressions applied the instantaneous Q record (driver), and (d) defined C/Tn_I regressions applied the instantaneous Tn record (driver). For both the b and d methods within Case 4, C/Q or C/Q_I, with flow as a driver were used when Tn at IL was either not available or during times when IL was suspected of being under the influence of backflow (Appendix 1).

3.3.4. Results

Please note that all results discussed below are total study interval (April through October) load estimates.

3.3.4.1. CASE 1: Load at IL is Equal to Sum of Inputs

The total P load to the Inlet Channel from the three tributaries was estimated to be 13,110 kg, 93% of which was as PP_L (12,202 kg). Total TDP_L was only 7% of TP_L. The TDP_L was estimated to be 908 kg and was dominated by SRP_L (531 kg; 58%). SUP_L for Case 1 was 378 kg (42% of TDP_L). Total TSS_L was 14,198 mt which was almost entirely as FSS_L (13,027 mt; 97%). The total Tn load was 14,164 10^6 NTU·m^3. Total $PAV_{m/L}$ was estimated to be 3,789 10^6 m^2. The ranking of total $PAV_{m/L}$ by size class contributions was: (1) size class 2 (1,370 10^6 m^2; 36%), size class 3 (1,085 10^6 m^2; 29%), size class 4 (915 10^6 m^2; 24%), and size class 1 (only 418 10^6 m^2; 11%). All Case 1 results can be found in Table 3-6.

Cayuga Inlet Creek was the dominant source of all particulate water quality parameters and for SUP_L to the Inlet Channel for the study interval. It contributed 76% of PP_L, 74% of FSS_L, 68% of VSS_L and 81% of total $PAV_{m/L}$ (range of 75%-86% for the four PAV_m size classes). Cayuga Inlet Creek contributed 47% of SUP_L. Sixmile Creek was the dominant source of TDP_L (46%) and SRP_L (52%). Sixmile Creek was the second largest contributor of PP_L (17%), TSS_L (19%), Tn_L (20%), and $PAV_{m/L}$ (8-20%). From the estimates, Cascadilla Creek was the smallest contributor for all parameters (Table 3-6).

3.3.4.2. CASE 2: Loads at IL Developed Using all IL Water Quality Data

The load estimates at IL when calculated using IL data differ substantially from Case 1 (sum of inputs). For some constituents, there were also considerable variations in estimates depending upon calculation method (a-d) used. This feature of the results will be discussed in more detail after the presentation of Case 4.

Phosphorus

TP_L estimates ranged from ~6,000 kg to ~9,000 kg (Table 3-7) and TP_L was dominated by PP_L (4,600 to 7,100 kg). For almost all constituents, Case 2c (C/Q_I regressions) yielded the highest estimates. At IL, the most directly comparable calculation method to the method used in tributary load calculations is the method used in Case 2a (FLUX 32 using daily average flows) so the comparative discussion of results here will be limited to the results of Case 2a. For Case 2a at IL, PP_L was 60% lower and TP_L was 54% lower compared to Case 1. Case 2a PP_L was 4,852 kg or 80% of TP_L at IL. This represented a decrease in the relative contribution of PP_L to TP_L compared to Case 1 where 93% of TP_L was as PP_L. These results suggest a loss (i.e., settling) of PP in the Inlet Channel.

Dissolved P_L estimates varied considerably by calculation method also. TDP_L estimates ranged from 1,200 to 1,900 kg. SRP_L was demonstrated to be the most sensitive constituent with regards to calculation method with estimates ranging from 670 to 1,500 kg. Interestingly, dissolved P_L increased at IL compared to Case 1. Case 2a TDP_L at IL was estimated to be 1,212 kg which represented a 34% increase from Case 1. Compared to Case 1, SRP_L (671 kg) increased 26% and SUP_L (378 kg) increased 43% at IL under calculation method Case 2a. It is unclear why the dissolved P would increase at IL compared to the sum of the inputs. Perhaps this reflects desorption of P from particulates in the Inlet Channel or perhaps this reflects increased contributions of dissolved P from the most proximate source, Sixmile Creek which had the highest SRP_L of the three inputs.

Suspended Solids and Turbidity

Case 2 FSS_L estimates ranged from 3,300 to 9,000 mt, however, excluding method 2c, the range was considerably narrower (3,350-3,650 mt). The range in VSS_L estimates was even narrower (420-600 mt). The range in Tn_L was large (~6,700 to >30,000 10^6 NTU·m^3) with method Case 2c being the highest by a wide margin (this will be discussed after Case 4). At IL the Case 2a FSS_L was 3,357 mt and VSS_L was 423 mt (FSS_L was 89% of TSS_L). Compared with Case 1, FSS_L and VSS_L at IL decreased 74 and 64%, respectively. Case 2a Tn_L at IL (6,740 10^6 NTU·m^3) decreased 52% compared to Case 1. These results suggest a loss (i.e., settling) of SS in the Inlet Channel. Because Tn_L is dominated by smaller particles (i.e., clays), it makes mechanistic sense that the loss in Tn_L would be smaller than the loss in FSS (-52% compared to -74%) which is comprised of an assortment of large and small particles.

Total PAV_m and PAV_m by Size Class

The loading results for PAV_m varied by method also (Table 3-7). In all cases of $PAV_{m/L}$, method Case 2c again resulted in the highest estimates among the four methods. The Case 2a total $PAV_{m/L}$ was estimated to be 1,215 10^6 m^2. The ranking of highest to lowest total $PAV_{m/L}$

contribution was: (1) PAV_{m2} (595 10^6 m^2; 49%), (2) PAV_{m3} (283 10^6 m^2; 23.3%), (3) PAV_{m1} (240 10^6 m^2; 19.8%), and (4) PAV_{m4} (96 10^6 m^2; 7.9%). The difference in Case 2a $PAV_{m/L}$ at IL when compared to Case 1 was interesting as the losses of PAV_m follow a trend consistent with their respective size class. Compared to Case 1, the loss at for Case 2a PAV_{m4} (the largest size class) was 90%. The loss for PAV_{m3} (the next smallest class) was 74%. The loss at size class PAV_{m2} was 57%. The loss for the smallest size class (PAV_{m1}) was least (43%). This trend in larger losses in bigger particles makes mechanistic sense with regards to expected faster settling rates for larger particles.

3.3.4.3. CASE 3: Loads at IL Developed Using Only IL Water Quality Data April-July 5

Case 3 probably does not represent a valid alternate case for which to evaluate loads at IL because it omits all data over the July 6 through October 31 interval including runoff event dates. The results for Case 3 varied by method and are presented in Table 3-8. For almost all constituents, the method using C/Q_I yielded the highest results. Omitting data from the second half of the study interval had a large impact on loading estimates, resulting in lower estimates when compared with estimates made using all IL data in Case 2. This was especially true in the case of particulate constituents primarily because of under-representation of C/driver relationships at high flows for Case 3.

3.3.4.4. CASE 4: Loads at IL Developed Using IL Water Quality Data April-July 5, and Runoff Event Day Samples from July 6-Otober 31

The results for Case 4 are summarized in Table 3-9. For all calculation methods (a-d), the results of Case 4 were very similar to Case 2 despite the exclusion of the 12 dry weather water quality samples over the July 6 through October 31 interval. The range in estimates between the methods in Case 4 was similar to the ranges observed for Case 2 (Table 3-7) as well. As with Case 2c, method Case 4c (C/Q_I) yielded the highest estimates, in some cases by far. The discussion here will be limited to Case 4a. A comparison of Case 1, Case 2a, and Case 4a is presented in Table 3-10.

Phosphorus

TP_L estimates ranged from ~6,000 kg to ~10,700 kg (Table 3-9). For almost all constituents, Case 2c (C/Q_I regressions) yielded the highest estimates. The Case 4a TP_L estimate was 6,104 kg (Table 6) and TP_L was dominated by PP_L (4,876 kg). TP_L and PP_L estimates from Case 4a were within 1% of the Case 2a estimates (Table 3-10). Compared to Case 1, Case 4a PP_L and TP_L at IL were 60% and 53% lower, respectively. Additionally, for Case 4a PP_L was only 80% of TP_L. This represented a decrease in the relative contribution of PP_L to TP_L compared to Case 1 (Case 1 PP_L:TP_L was 93%). These results suggest a loss (i.e., settling) of PP in the Inlet Channel.

Dissolved P_L estimates varied considerably by calculation method in Case 4. TDP_L estimates ranged from 1,200 to 2,300 kg. The dissolved P_L results for Case 4a were similar to Case 2a as well (closure within 2 %; Table 3-10). The Case 4a TDP_L estimate was 1,229 kg which was 35% higher than the Case 1 TDP_L estimate (908 kg; Table 3-6). SRP_L and SUP_L were estimated to be 683 and 545 kg, respectively. Compared to Case 1, Case 4a SRP_L estimates increased 29% and SUP_L increased 44%. As discussed in Case 2, this may reflect desorption of P from particulates in the Inlet Channel or could reflect increased contributions of dissolved P from Sixmile Creek which had the highest SRP_L of the three inputs.

Suspended Solids and Turbidity

Case 4 FSS_L estimates ranged from 3,400 to 10,500 mt, however, excluding method 4c, the range was considerably narrower (3,400-4,851 mt). The range in VSS_L estimates was smaller than FSS_L (405-643 mt). The range in Tn_L was very large (~6,700 to >38,000 10^6 NTU·m^3) with method Case 4c being the highest by a wide margin (this will be discussed subsequently). The loading estimates of SS_L for Case 4a were similar to Case 2a as well (Tables 3.8 and 3.9). The IL Case 4a FSS_L estimate was 3,390 mt and the VSS_L estimate was 420 mt (TSS_L = 3,810 mt). FSS_L was the dominant component of TSS_L (89%). Load estimates for all three forms of SS_L were all within 1% of the Case 2a estimates (Table 3-10). The Case 4a estimate of Tn_L was 6,808 10^6 NTU·m^3 which was ~1% higher than the results for the Case 2a results. Compared with Case 1, Case 4a estimates of FSS_L and VSS_L at IL decreased 74 and 64%, respectively. Tn_L decreased 52% at IL compared to Case 1. These results suggest a loss (i.e., settling) of SS in the Inlet Channel. As with Case 2a, because Tn_L is dominated by smaller particles (i.e., clays), it makes conceptual sense that the loss in Tn_L would be smaller than the loss in FSS (-52% compared to -74%).

Total PAV_m and PAV_m by Size Class

The loading results for PAV_m varied by method also (Table 3-9). In all cases of $PAV_{m/L}$, method Case 4c again resulted in the highest estimates among the four methods. For Case 4a, the total $PAV_{m/L}$ was estimated to be 1,232 10^6 m^2. The ranking of highest to lowest total $PAV_{m/L}$ contribution was: (1) PAV_{m2} (603 10^6 m^2; 49%), (2) PAV_{m3} (286 10^6 m^2; 23.2%), (3) PAV_{m1} (243 10^6 m^2; 19.6%), and (4) PAV_{m4} (101 10^6 m^2; 8.4%). For PAV_m size classes 1-3, the results from Case 4a were within 2 % of the Case 2a results (Table 3-10). For PAV_{m4}, the Case 4a results were ~ 4.7% higher than the Case 2a results. The change in Case 4a $PAV_{m/L}$ at IL when compared to Case 1 was interesting as the losses of PAV_m follow a trend consistent with their respective size class (similar to Case 2a). Compared to Case 1, the loss at for Case 2a PAV_{m4}, the largest size class, was > 89%. The loss for PAV_{m3} (the next smallest class) was 74%. The loss at size class PAV_{m2} was 56%. The loss for the smallest size class (PAV_{m1}) was the lowest of the four size classes (42%). This trend in larger losses for bigger particles makes mechanistic sense in a settling context.

3.3.5. Comparison of Case 4 Methods and Discussion of Best Case Data Usage

Constituent loading time series for all Case 4 methods can be found in Appendix 1 (Figures A1-25 – A1-27). For Case 4, the estimates from the four methods (a-d) varied and in some cases, varied substantially. Some important generalizations can be made, including that method c (C/Q_I method) yielded the highest load estimates (in some cases by far) compared with the other methods (Table 3-9). The largest discrepancy was for Tn_L. For methods Case 4a, b, d, the range in Tn_L estimates for the study interval was ~6,800 to 11,600 10^6 NTU·m^3. The estimate for Case 4c was ~38,000 10^6 NTU·m^3, more than 5-times greater than the 4a estimate and more than 3-times greater than the 4d estimate.

For Case 4d, C/Q_I estimates were used when Tn_I (driver) at IL was either not available or during times when IL was suspected of being under the influence of backflow (April-May 8 and non-runoff dates July 6-October 31, see Table 3-5). Because method Case 4d results are a combination of C/Q_I and C/Tn_I, the days of C/Q_I contribution to method Case 4d were excluded (i.e., only runoff dates were considered) and the Case 4 results were re-evaluated and are presented in Table 3-11. When considering only runoff dates over the May through October interval, two patterns become apparent. One is that methods for Cases a, b, and d provide seasonal estimates that close fairly well for most constituents. Methods 4a and 4b are nearly identical for most constituents (Table 3-11). Also, Methods 4a and 4d closed to within 15% for TP_L, PP_L, SUP_L, TSS_L, FSS_L, total PAV_m, PAV_{m2}, and PAV_{m4} which is very encouraging given the two different drivers and calculation methods used in these cases. The second obvious result is that of the four methods, Case 4c yields the highest estimates by far.

The results presented in Table 3-11 between Case 4c and 4d for Tn_L are important because they compare an estimated Tn_L (from Tn/Q_I; Case 4c) with a "known" Tn_L (Case 4d on runoff event dates is the observed load calculated by observed from data sonde-Tn_I and Q_I). In the case of Tn_L, the method 4c estimate was ~4.6 times higher than the known Tn_L (Case 4d); verifying that method 4c is over predicting compared with the other methods. There are (at least) two contributing factors causing method 4c estimates to be high compared to the other methods. First, during the 2013 study interval, the maximum sampled Q_I at IL was ~44 m^3/s (August 9 10:25 AM). However, the peak Q_I at IL over the study interval was ~172.7 m^3/s (August 9 0100 AM), approximately 4 times higher than the maximum sampled Q_I. Without timely and representative C information at the highest Q_Is it is possible that the C/Q_I developed over the limited range of sampled Q_Is was poorly defined at high flows and therefore, may be drastically over predicting C (and therefore loads) at high flows. As a note there were 86 instances of Q_I greater than the maximum sampled Q_I which delivered the vast majority of Tn_L. Second, when using LN transformed regressions, a correction to the LN transformation bias is added to the prediction. This correction is widely applied and recommended by statisticians and is calculated as ½ of the regression mean square error (mse) as described by Helsel and Hirsch (1991). Therefore, the larger the mse, the larger the correction. There are instances for large

mses (> 0.5) where the correction can result in an over-correction resulting in predicted Cs that are false high. For most cases, the mse from the C/Q_I relationships were higher than the mses from other manual regression methods (b or d) and may contribute to the discrepant Case 4c estimates.

Based on the results presented in this analysis, Case 4a represents the best case of data usage for IL loading estimates for several reasons: (1) it utilizes all IL data over the April through July 5 period verified as representative of tributary inputs (Cowen, 2015), (2) it uses IL data during runoff events over the July 6 through October 31 interval which are reasonably expected to be representative of tributary inputs, (3) the inclusion of high flow data provides characterization of water quality at this site during runoff events, (4) the inclusion of high flow data is essential to generate accurate loading estimates through improved temporal coverage and development of C/driver regression relationships, (5) it avoids using questionable IL data during dry weather intervals during the July 6 through October 31 interval, and (6) it utilizes a load estimation methodology similar to the methodology used in tributary load estimates that fits the predicted time series to the observed loads. Case 4a loading estimates were found to be similar to the Case 2a results (closed within 5%), despite excluding 12 IL samples. The closure of study interval load estimates in these two Cases strengthens the argument that Case 4a is a reasonable approach as the exclusion of the 12 dry weather samples in the questionable period had little effect on the seasonal load estimates. This was primarily due to the overwhelming contribution of runoff events on total load delivered (> 80% for all constituents). Specifically for PP_L, approximately 90% of the total study period load was delivered during runoff events.

Cases 4a, b and d had very good closure (especially during times when C/Q_I is excluded from method d) and any could be used as estimation methods. Case 4d is a valid method especially if short-term (i.e., hours) loading dynamics are required (e.g., during runoff events). The two methods using Tn as a driver (Case 4b and d); however, have limitations that make them less attractive than Case 4a on seasonal, annual, or interannual time scales. These limitations are: (1) sonde Tn data at IL is only available for 2013 May through October interval, and not available in previous years, (2) there is no Tn data over the late Fall through mid-Spring months and therefore there is no empirical data to characterize cold-weather Tn, and (3) when comparing load estimates at different locations or in different years, consistency in the methods is important because, as this analysis shows, differing calculation methodologies can result in discrepant estimates. Because the tributary load estimates were done using FLUX32 and daily flows, IL estimates should be made similarly, and therefore Case 4a should be used for IL daily load estimation. A graphical representation of the results for the a-Cases is provided in Figure 3-21. The use of C/Q_I (method c) should be avoided because this method systematically yielded the highest estimates for all cases and performed poorly when compared with the known Tn_L from the data sonde.

3.3.6. Examples of Changes in Loads at IL Due to Channel Processes

Case 4a IL loading estimates indicate changes in water quality constituents as compared to the Case 1 loads (sum of the inputs). At a seasonal time scale, particulate constituent loads were lower at IL compared to the sum of the inputs and dissolved P loads increased at IL compared to Case 1 (summarized in Table 3-10).

The timing of loading changes across the Cayuga Inlet Channel is demonstrated in Figures 3-22 - 3-24. For particulate constituents (PP; Figure 3-22b, FSS; Figure 3-23b, VSS; Figure 3-23c, Tn; Figure 3-23d, and PAV_m; Figure 3-24b-e) during dry weather periods and small runoff events, the Cayuga Inlet Channel acts as a source for these constituents (load at IL > load from sum of inputs). It is only during the largest events (i.e., runoff events of July 1, July 23, and August 8) that the loads at IL are less than the sum of the inputs and the Channel acts as a sink. Similarly with SRP_L (Figure 3-22c), the Cayuga Inlet Channel acts as source for most of the study interval and a sink during the largest runoff events. Interestingly, SUP_L at IL was found to be always higher than the sum of the inputs which means that the Cayuga Inlet Channel is always a source of SUP_L. Table 3-12 summarizes the dry weather versus event loads for the constituents in this study.

3.3.7. Conclusions and Recommendations

Case 4a represents the best case of data usage for daily IL loading estimates for several reasons (above). Case 4a loading estimates were found to be similar to the Case 2a results, despite excluding 12 dry weather IL samples over the July 6 through October 31 interval. In all cases the Case 4a results were within 5% of the Case 2a results. The closure of study interval load estimates in these two Cases strengthens the argument that Case 4a is a reasonable approach as the exclusion of the 12 dry weather samples in the questionable period had little effect on the seasonal load estimates. This was primarily due to the overwhelming contribution of runoff events on total load delivered (> 80% for all constituents).

Case 4d is a valid method especially if short-term (i.e., hours) loading dynamics are required or of interest. The two cases using Tn as a driver (Case 4b and d); however, have limitations that make them less attractive than Case 4a on a seasonal or annual time scale (above). The use of C/Q_I (method c) should be avoided because this method systematically yielded the highest estimates for all cases and performed poorly when compared to the known Tn_L (from data sonde) during runoff events. Finally, these results indicate substantial changes in water quality at IL compared to the mouths of the three tributaries, therefore, Case 1 (sum of inputs) is not a valid approach for estimating loads leaving the Cayuga Inlet Channel.

Case 4a IL loading estimates indicate changes in water quality constituents compared to the Case 1 loads (sum of the inputs). Particulate constituent loads were lower at IL compared to the sum of the inputs. PP_L decreased ~7,300 kg (-60%) at IL compared to the sum of the inputs

and this corresponded to a decrease of ~7,000 kg of TP_L (-53%). SRP_L increased by 152 kg (+29%) and SUP_L increased by 167 kg (+44%) at IL. FSS_L decreased of 9,638 mt (-74%) and VSS_L decreased 751 mt (-64%). Total SS_L decreased 10,388 mt (-73%). Tn_L decreased by 7,321 10^6 NTU·m^3 (-52%). The Case 4a results demonstrated that the losses in PAV_m were size class dependent. The largest size class, $PAVm_4$ decreased by >78% at IL compared to the sum of the inputs. The smallest size class, PAV_{m1}, decreased the least (21 %). Interestingly dissolved P_L increased at IL compared to the sum of the inputs.

The timing of loading changes across the Cayuga Inlet Channel varied in time and flow regime. For particulate constituents during dry weather periods and small runoff events, the Cayuga Inlet Channel acted as a source for these constituents (i.e., the load at IL > load from sum of inputs). It was only during the largest events (i.e., runoff events of July 1, July 23, August 8, and September 2) that the loads at IL were less than the sum of the inputs (i.e., sink). Similarly with SRP_L, the Cayuga Inlet Channel acted as source for most of the study interval and a sink only during the largest runoff events. Interestingly, SUP_L at IL was found to be nearly always higher than the sum of the inputs which means that the Cayuga Inlet Channel is always a source of SUP_L.

Table 3- 4. Cases of IL data use for loading analyses..

Case	Description	No. of Obs. at IL	Comments
1.	IL load is the sum of the tributary loads from Cayuga Inlet, Sixmile, and Cascadilla Creeks	none	not representative of loads at IL, does not account for channel processes
2.	IL C/driver regressions and subsequent loads generated from use of all data from IL	41	may contain un-representative samples if any IL collections occurred during a time of lake influence at IL
3.	IL C/driver regressions and subsequent loads generated from use of Apr.-Jul. 5 IL data only (excludes IL data from Jul. 6-Oct. 31.)	14	April through July 5 is the time period supported by Cowen's team hydrodynamic data to be representative of the tributaries at IL; may be too conservative as probably some IL collections after July are free from lake influence (especially during events)
4.	IL C/driver regressions and subsequent loads generated from use of Apr.-Jul. 5 IL data plus any collections that occurred during runoff event conditions from Jul. 6-Oct. 31	29	preferred

Table 3- 5. Summary of IL load estimation procedures and drivers used.

Case	Load Estimation Techniques [+]	Driver (s)
1.	sum of inputs	none
2.		
a.	daily Q driver, FLUX32 software	- daily flow record, Apr.-Oct.
b.	combination of case 2a; daily averaged sonde Tn driver, manual C/Tn regressions	- case 2a results, Apr.-May 8; - daily average Tn from data sonde, May 9-Oct. 31
c.	15 min Q driver, manual C/Q_I regressions	-15 minute flow record, Apr.-Oct.
d.	combination of case 2c; 15 min sonde Tn driver, manual C/Tn_I regressions	- case 2c results, Apr.-May 8 - 15 minute Tn record from data sonde, May 9-Oct. 31
3.		
a.	daily Q driver, FLUX32 software	- daily flow record
b.	combination of case 3a; daily averaged sonde Tn driver, manual C/Tn regressions	- case 3a results, Apr.-May 8; - daily average Tn from data sonde, May 9-Jul. 5; - case 3a results, Jul. 6-Oct. 31
c.	15 min Q driver, manual C/Q_I regressions	-15 minute flow record, Apr.-Oct.
d.	combination of case 3c; 15 min sonde Tn driver, manual C/Tn_I regressions	- case 3c results, Apr.-May 8; - 15 minute Tn from data sonde, May 9-Jul. 5; - case 3c results, Jul. 6-Oct. 31
4.		
a.	daily Q driver, FLUX32 software	- daily flow record, Apr.-Oct.
b.	combination of case 4a; daily averaged sonde Tn driver, manual C/Tn regressions	- case 4a results, Apr.-May 8; - May 9-Oct. 31 - runoff event dates: daily average Tn from data sonde - dry weather dates: case 4a
c.	15 min Q driver, manual C/Q_I regressions	-15 minute flow record, Apr.-Oct.
d.	combination of case 4c; 15 min sonde Tn driver, manual C/Tn_I regressions	- case 4c results, Apr.-May 8; - May 9-Oct. 31 - runoff event dates: 15 minute Tn from data sonde - dry weather dates: case 4c

[+] see Table 3-4 for data used to generate driver/C regressions

Table 3- 6. Summary of Case 1 study interval (April through October) total loads at IL.

Constituent Load	Load Units	Cayuga Inlet Creek	Tributary Sixmile Creek	Cascadilla Creek	Sum of Inputs Case 1
TP	kg	9,619	2,459	1,032	13,110
PP	kg	9,285	2,042	875	12,202
TDP	kg	334	417	157	908
SRP	kg	155	277	99	531
SUP	kg	179	140	59	378
TSS	mt	10,452	2,754	991	14,198
FSS	mt	9,657	2,470	900	13,027
VSS	mt	795	284	92	1,171
Tn	10^6 NTU·m^3	10,500	2,790	874	14,164
PAV_m total	10^6 m^2	1,657	525	157	2,338
PAV_{m1}	10^6 m^2	208	82	17	307
PAV_{m2}	10^6 m^2	639	225	55	919
PAV_{m3}	10^6 m^2	472	137	46	655
PAV_{m4}	10^6 m^2	337	81	39	457

Table 3- 7. Summary of Case 2 study interval (April through October) total loads at IL.

Constituent Load	Load Units	Sum of Inputs Case 1	Daily Q FLUX Case 2a	Daily Avg. Sonde Tn Case 2b	15min Q Regr. Case 2c	15min Tn Regr. Case 2d
TP	kg	13,110	6,064	6,018	9,013	7,169
PP	kg	12,202	4,852	4,643	7,099	5,508
TDP	kg	908	1,212	1,375	1,914	1,660
SRP	kg	531	671	809	1,548	1,118
SUP	kg	378	542	566	629	634
TSS	mt	14,198	3,780	3,940	9,606	4,125
FSS	mt	13,027	3,357	3,516	9,006	3,645
VSS	mt	1,171	423	424	600	480
Tn	10^6 NTU·m^3	14,164	6,740	6,749	32,962	11,192
PAV_m total	10^6 m^2	2,338	1,215	1,065	3,121	1,416
PAV_{m1}	10^6 m^2	307	240	239	949	326
PAV_{m2}	10^6 m^2	919	595	502	1,533	670
PAV_{m3}	10^6 m^2	655	283	223	492	287
PAV_{m4}	10^6 m^2	457	96	101	147	134

Table 3- 8. Summary of Case 3 study interval (April through October) total loads at IL.

Constituent Load	Load Units	Sum of Inputs Case 1	Daily Q FLUX Case 3a	Daily Avg. Sonde Tn Case 3b	15min Q Regr. Case 3c	15min Tn Regr. Case 3d
TP	kg	13,110	3,235	3,354	4,845	4,939
PP	kg	12,202	2,377	2,464	3,575	3,623
TDP	kg	908	858	890	1,270	1,315
SRP	kg	531	343	364	714	734
SUP	kg	378	515	526	556	581
TSS	mt	14,198	1,499	1,559	3,091	3,209
FSS	mt	13,027	1,154	1,206	2,713	2,812
VSS	mt	1,171	346	353	378	397
Tn	10^6 NTU·m^3	14,164	3,542	3,716	19,142	17,850
PAV_m total	10^6 m^2	2,338	264	276	865	4,388
PAV_{m1}	10^6 m^2	307	64	65	432	417
PAV_{m2}	10^6 m^2	919	120	125	337	351
PAV_{m3}	10^6 m^2	655	57	61	78	87
PAV_{m4}	10^6 m^2	457	23	25	18	3,533

Table 3- 9. Summary of Case 4 study interval (April through October) total loads at IL.

Constituent Load	Load Units	Sum of Inputs Case 1	Daily Q FLUX Case 4a	Daily Avg. Sonde Tn Case 4b	15min Q Regr. Case 4c	15min Tn Regr. Case 4d
TP	kg	13,110	6,104	6,011	10,714	7,575
PP	kg	12,202	4,876	4,628	8,411	5,766
TDP	kg	908	1,229	1,383	2,302	1,809
SRP	kg	531	683	820	1,639	1,164
SUP	kg	378	545	563	663	645
TSS	mt	14,198	3,810	3,841	10,481	5,322
FSS	mt	13,027	3,390	3,436	9,838	4,851
VSS	mt	1,171	420	405	643	470
Tn	10^6 NTU·m^3	14,164	6,808	6,795	38,697	11,594
PAV_m total	10^6 m^2	2,338	1,232	1,063	3,864	1,570
PAV_{m1}	10^6 m^2	307	243	256	1,303	383
PAV_{m2}	10^6 m^2	919	603	512	1,891	763
PAV_{m3}	10^6 m^2	655	286	207	511	293
PAV_{m4}	10^6 m^2	457	101	88	159	130

Table 3- 10. Summary of Case 1, Case 2a, and Case 4 study interval (April through October) total loads at IL.

Constituent Load	Load Units	Sum of Inputs Case 1	Daily Q FLUX Case 2a	Daily Q FLUX Case 4a	% Difference Cases 2a-4a	% Difference Cases 1-4a
TP	kg	13,110	6,064	6,104	0.7	-53
PP	kg	12,202	4,852	4,876	0.5	-60
TDP	kg	908	1,212	1,229	1.3	35
SRP	kg	531	671	683	1.8	29
SUP	kg	378	542	545	0.7	44
TSS	mt	14,198	3,780	3,810	0.8	-73
FSS	mt	13,027	3,357	3,390	1.0	-74
VSS	mt	1,171	423	420	-0.6	-64
Tn	10^6 NTU·m^3	14,164	6,740	6,808	1.0	-52
PAV_m total	10^6 m^2	2,338	1,215	1,232	1.4	-47
PAV_{m1}	10^6 m^2	307	240	243	1.2	-21
PAV_{m2}	10^6 m^2	919	595	603	1.2	-34
PAV_{m3}	10^6 m^2	655	283	286	1.1	-56
PAV_{m4}	10^6 m^2	457	96	101	4.7	-78

Table 3- 11. Summary of IL Case 4 loading estimates for methods a-d for runoff dates only, May 9 through October.

Constituent Load	Load Units	Case 4a	Case 4b	Case 4c	Case 4d
TP	kg	4,667	4,568	7,396	4,257
PP	kg	3,793	3,540	5,867	3,222
TDP	kg	874	1,027	1,529	1,035
SRP	kg	520	654	1,163	688
SUP	kg	354	373	365	347
TSS	mt	3,133	3,159	8,579	3,417
FSS	mt	2,805	2,846	8,140	3,151
VSS	mt	328	313	439	266
Tn	10^6 NTU·m^3	5,739	5,726	34,648	7,538
PAV_m total	10^6 m^2	1,089	919	3,350	1,056
PAV_{m1}	10^6 m^2	212	225	1,187	268
PAV_{m2}	10^6 m^2	542	451	1,647	519
PAV_{m3}	10^6 m^2	252	173	403	186
PAV_{m4}	10^6 m^2	83	70	113	84

Table 3- 12. Summary of dry weather versus runoff event loads at IL for Case 4a.

Constituent	Load Units	Flow Condition	Daily Q FLUX Case 4a	Days IL>Case 1 (%)	April-October IL- Case 1	Comments
PP	kg	dry	446	96%	+204	net export*
		event	4,430	86%	-7,530	net loss**
		overall	4,876	90%	-7,326	net loss
SRP	kg	dry	76	41%	+4	net export
		event	607	49%	+148	net export
		overall	683	46%	+152	net export
SUP	kg	dry	104	99%	+39	net export
		event	441	96%	+128	net export
		overall	545	97%	+167	net export
FSS	mt	dry	190	90%	+76	net export
		event	3,200	66%	-9,714	net loss
		overall	3,390	76%	-9,638	net loss
VSS	mt	dry	36	91%	+15	net export
		event	384	79%	-766	net loss
		overall	420	84%	-751	net loss
Tn	10^6 NTU·m3	dry	236	76%	+68	net export
		event	6,572	54%	-7,376	net loss
		overall	6,808	63%	-7,308	net loss
PAV_{m1}	10^6 m^2	dry	7.5	86%	+3.0	net export
		event	235	71%	-68	net loss
		overall	242.5	77%	-65	net loss
PAV_{m2}	10^6 m^2	dry	18.4	91%	+8.8	net export
		event	584	77%	-325	net loss
		overall	602.5	79%	-316	net loss
PAV_{m3}	10^6 m^2	dry	12.5	91%	+5.7	net export
		event	273.5	73%	-374	net loss
		overall	286	81%	-368	net loss
PAV_{m4}	10^6 m^2	dry	6.8	82%	+0.61	net export
		event	94.0	55%	-349	net loss
		overall	100.8	66%	-348	net loss

* from channel
**to channel

Table 3- 13. Summary of IL water quality data and dates used for each of the four analysis cases.

Date of Collection	Runoff Event?	Case 1 (sum of inputs)	Case 2 (use all IL data)	Case 3 (Apr.-Early Jul.)	Case 4 (Apr.-Early Jul. + events)
04/08/13		na	C2	C3	C4
04/22/13		na	C2	C3	C4
05/07/13		na	C2	C3	C4
05/21/13		na	C2	C3	C4
06/05/13		na	C2	C3	C4
06/07/13	E	na	C2	C3	C4
06/11/13	E	na	C2	C3	C4
06/13/13	E	na	C2	C3	C4
06/18/13		na	C2	C3	C4
06/20/13		na	C2	C3	C4
06/25/13	E	na	C2	C3	C4
06/28/13	E	na	C2	C3	C4
07/01/13	E	na	C2	C3	C4
07/03/13	E	na	C2	C3	C4
07/09/13	E	na	C2		C4
07/12/13		na	C2		
07/15/13		na	C2		
07/18/13	E	na	C2		C4
07/23/13	E	na	C2		C4
07/25/13	E	na	C2		C4
07/30/13	E	na	C2		C4
08/02/13	E	na	C2		C4
08/06/13		na	C2		
08/09/13	E	na	C2		C4
08/12/13	E[b]	na	C2		C4
08/15/13		na	C2		
08/20/13	E	na	C2		C4
08/23/13	E	na	C2		C4
08/27/13	E	na	C2		C4
08/29/13	E	na	C2		C4
09/03/13	E	na	C2		C4
09/06/13		na	C2		
09/10/13		na	C2		
09/13/13	E	na	C2		C4
09/17/13		na	C2		
09/19/13		na	C2		
09/24/13	E	na	C2		C4
09/27/13		na	C2		
10/01/13	E	na	C2		C4
10/15/13	E	na	C2		C4
10/29/13		na	C2		

[a] daily flows separated by HYSEP, IL is an event day if either Cayuga Inlet Creek or Sixmile Creek were under runoff conditions

[b] daily separation indicated no event, but included in analysis for Case 4; IL clearly impacted from 8/8 event on 8/12

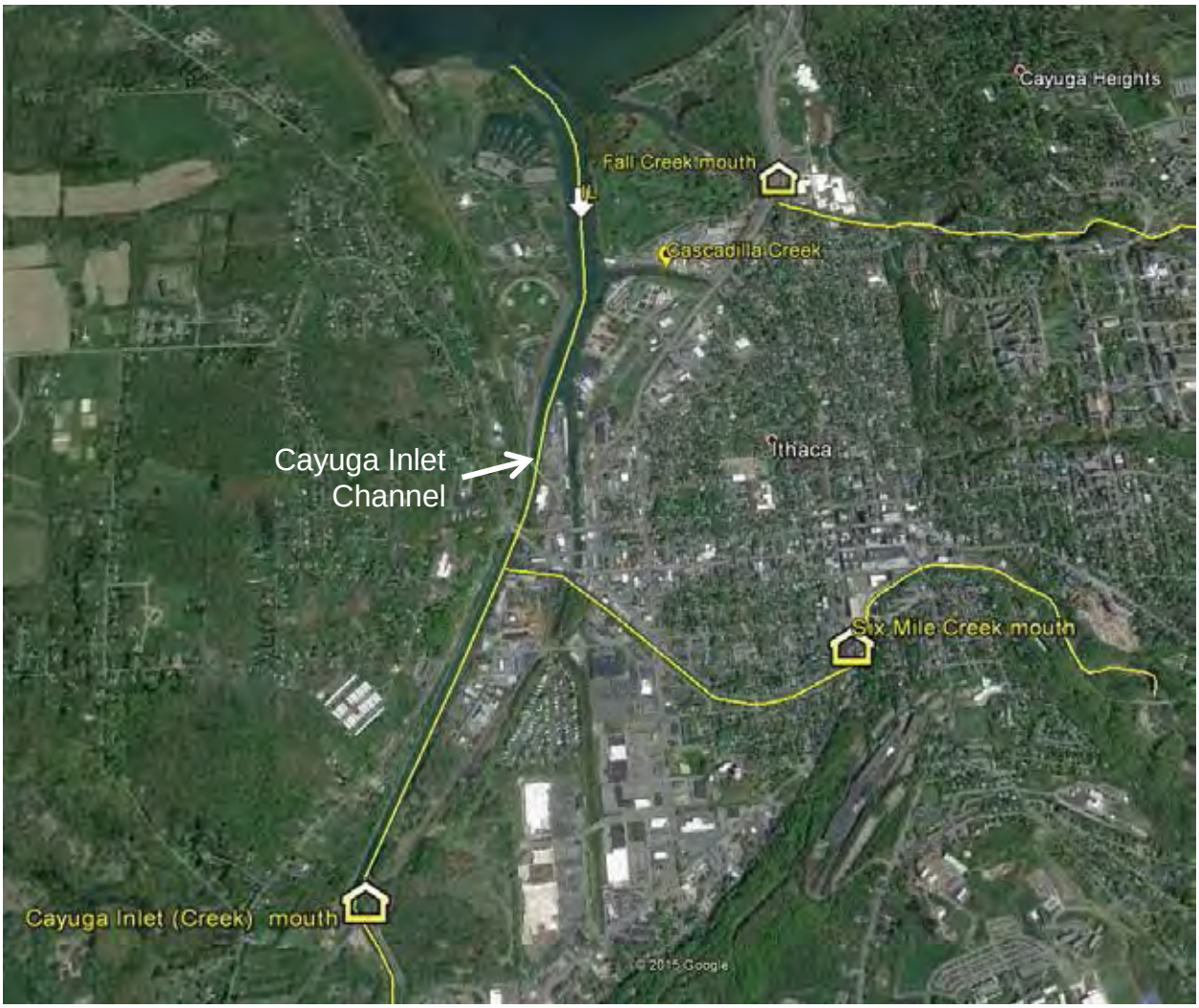

Figure 3- 9. Map of Cayuga Inlet Channel with IL, Cayuga Inlet Creek, Sixmile Creek, and Cascadilla Creek.

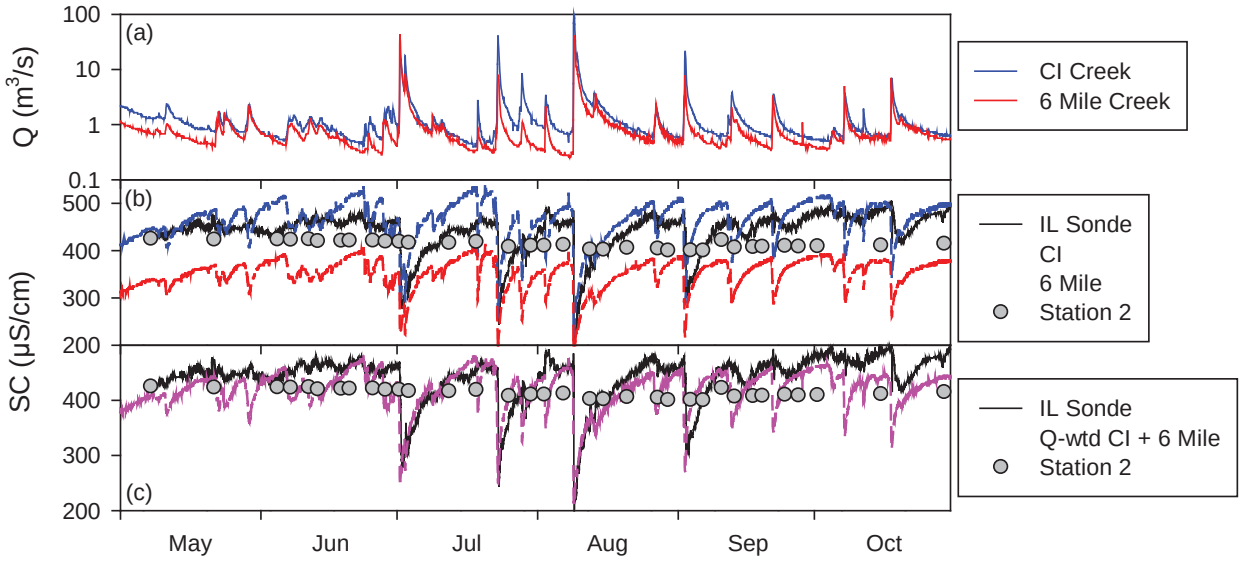

Figure 3- 10. Time series of: (a) Cayuga Inlet Creek and Sixmile Creek flow, (b) specific conductance (SC) at IL, Cayuga Inlet Creek, Sixmile Creek and Cayuga Lake Station 2, and (c) specific conductance at IL, combined Q-weighted tributary contributions (Cayuga Inlet Creek and Sixmile) and Cayuga Lake Station 2.

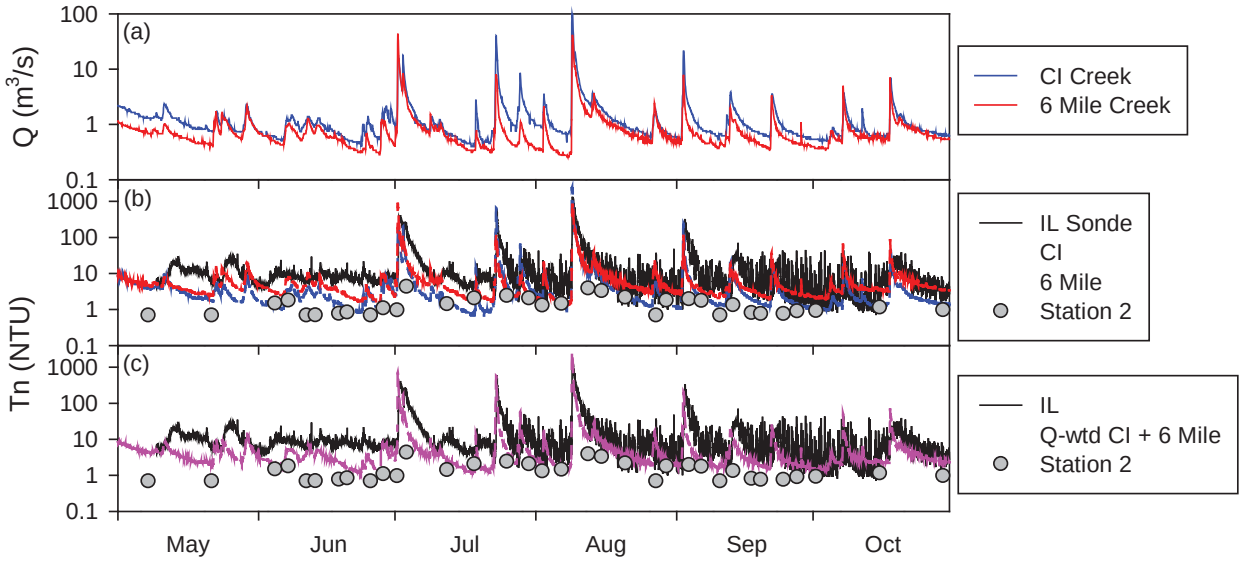

Figure 3- 11. Time series of: (a) Cayuga Inlet Creek and Sixmile Creek flow, (b) turbidity (Tn) at IL, Cayuga Inlet Creek, Sixmile Creek and Cayuga Lake Station 2, and (c) turbidity at IL, combined Q-weighted tributary contributions (Cayuga Inlet Creek and Sixmile) and Cayuga Lake Station 2.

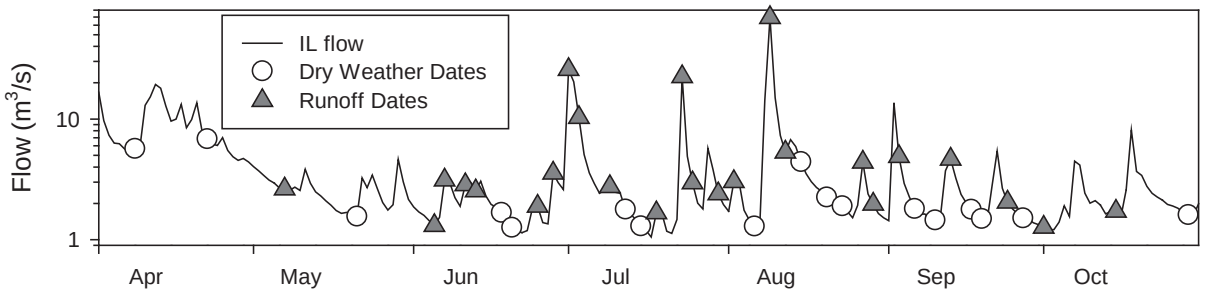

Figure 3- 12. Time series of IL flow as calculated as the sum of Cayuga Inlet Creek, Sixmile Creek, and Cascadilla Creek flow (estimates) inputs with dry weather (white circle) and runoff event (gray triangles) sampling dates identified.

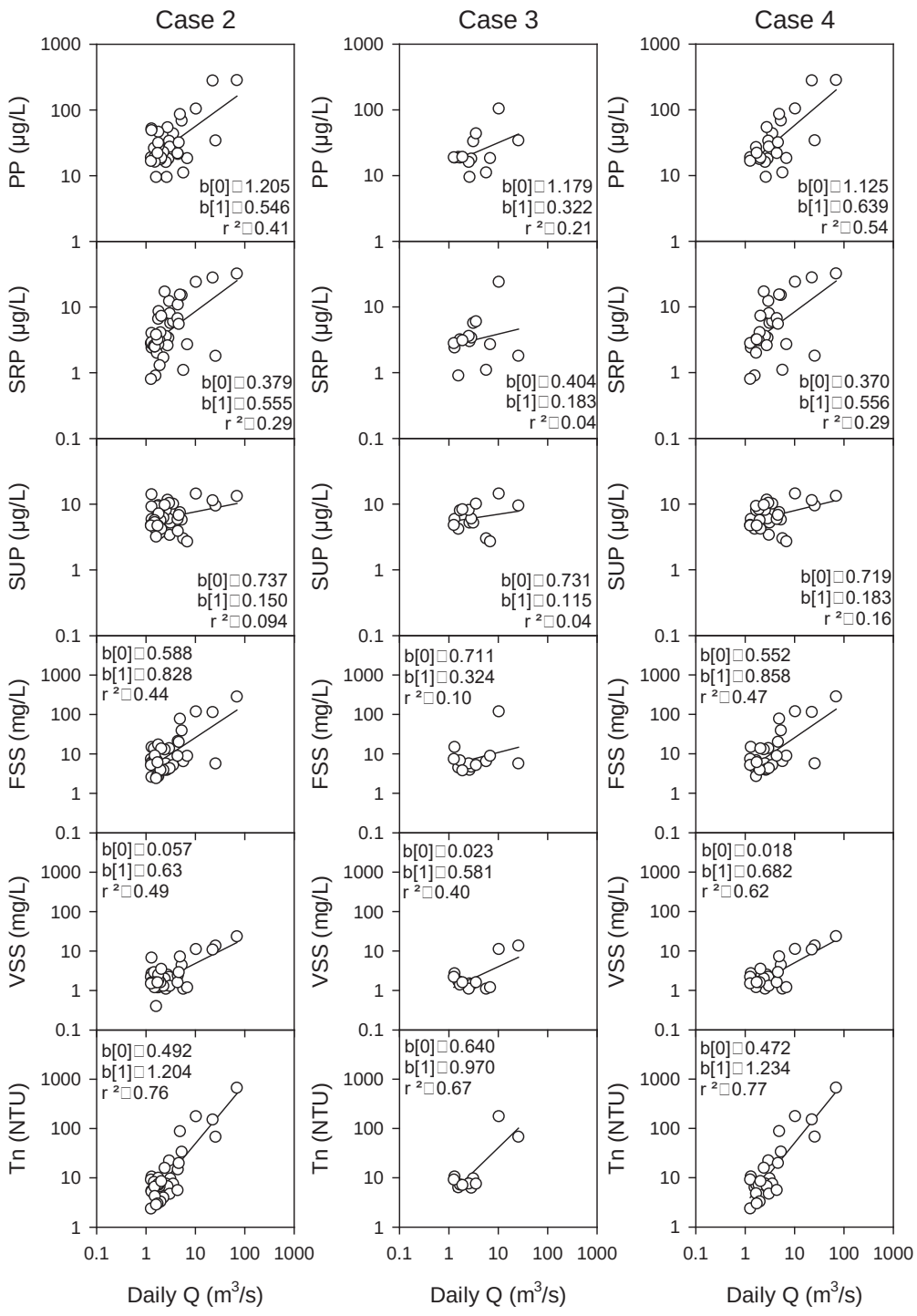

Figure 3- 13. Concentration-daily flow relationships for PP, SRP, SUP, FSS, VSS, and Tn for data cases 2-4.

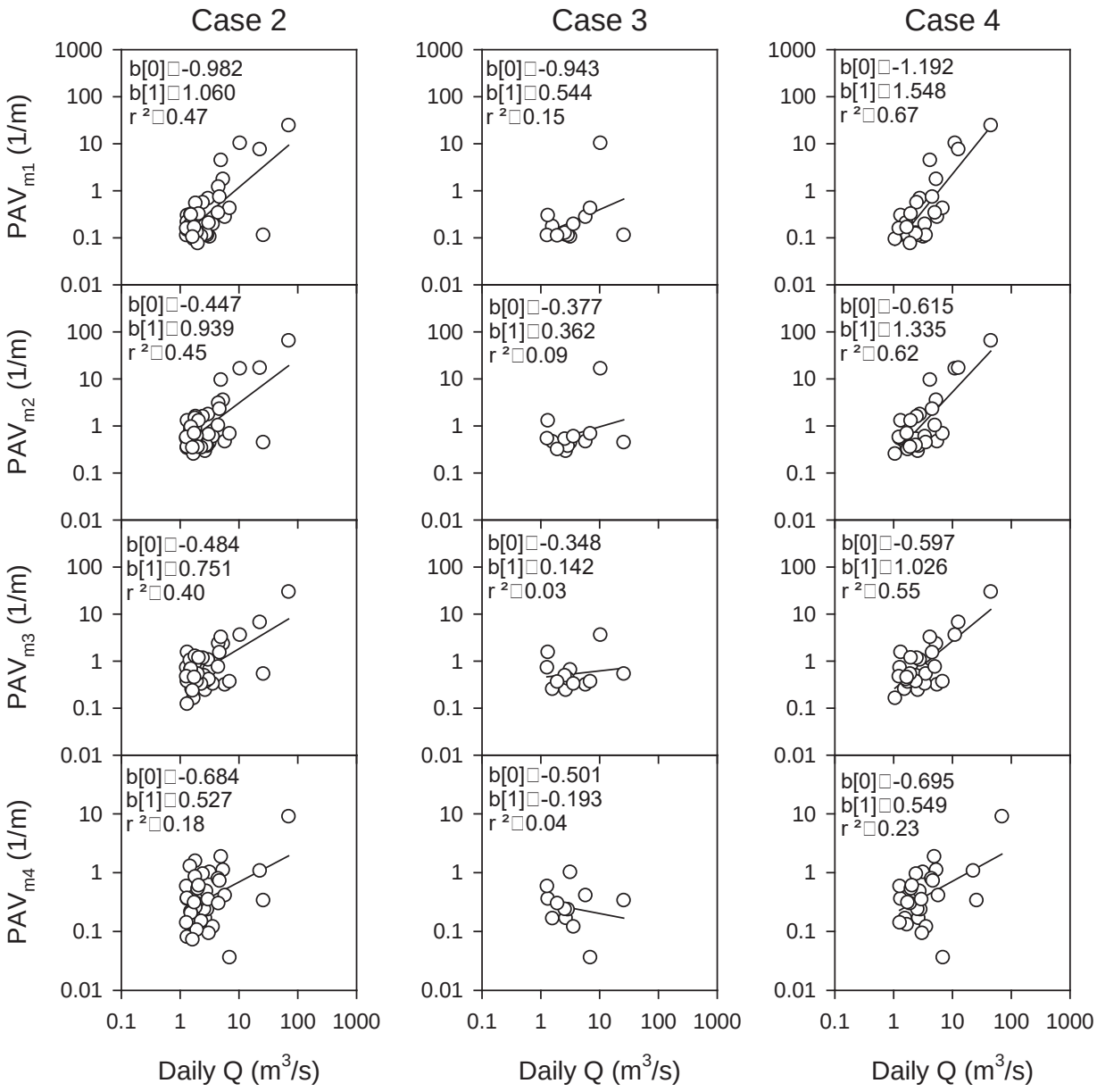

Figure 3- 14. Concentration-daily flow relationships for PAV_{m1}, PAV_{m2}, PAV_{m3}, and PAV_{m4} for data cases 2-4.

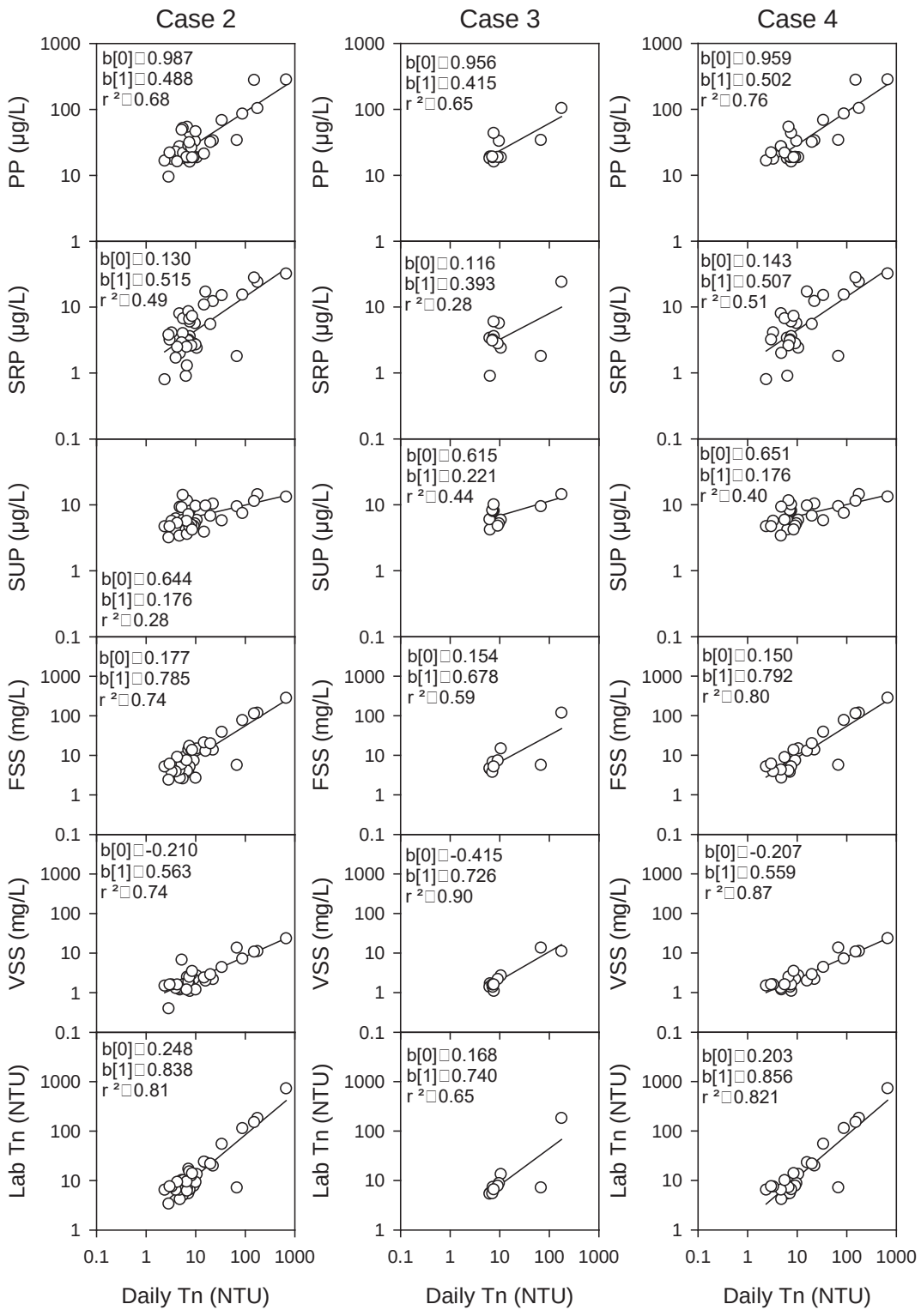

Figure 3- 15. Concentration-daily Tn (from IL sonde) relationships for PP, SRP, SUP, FSS, VSS, and Lab Tn for data cases 2-4.

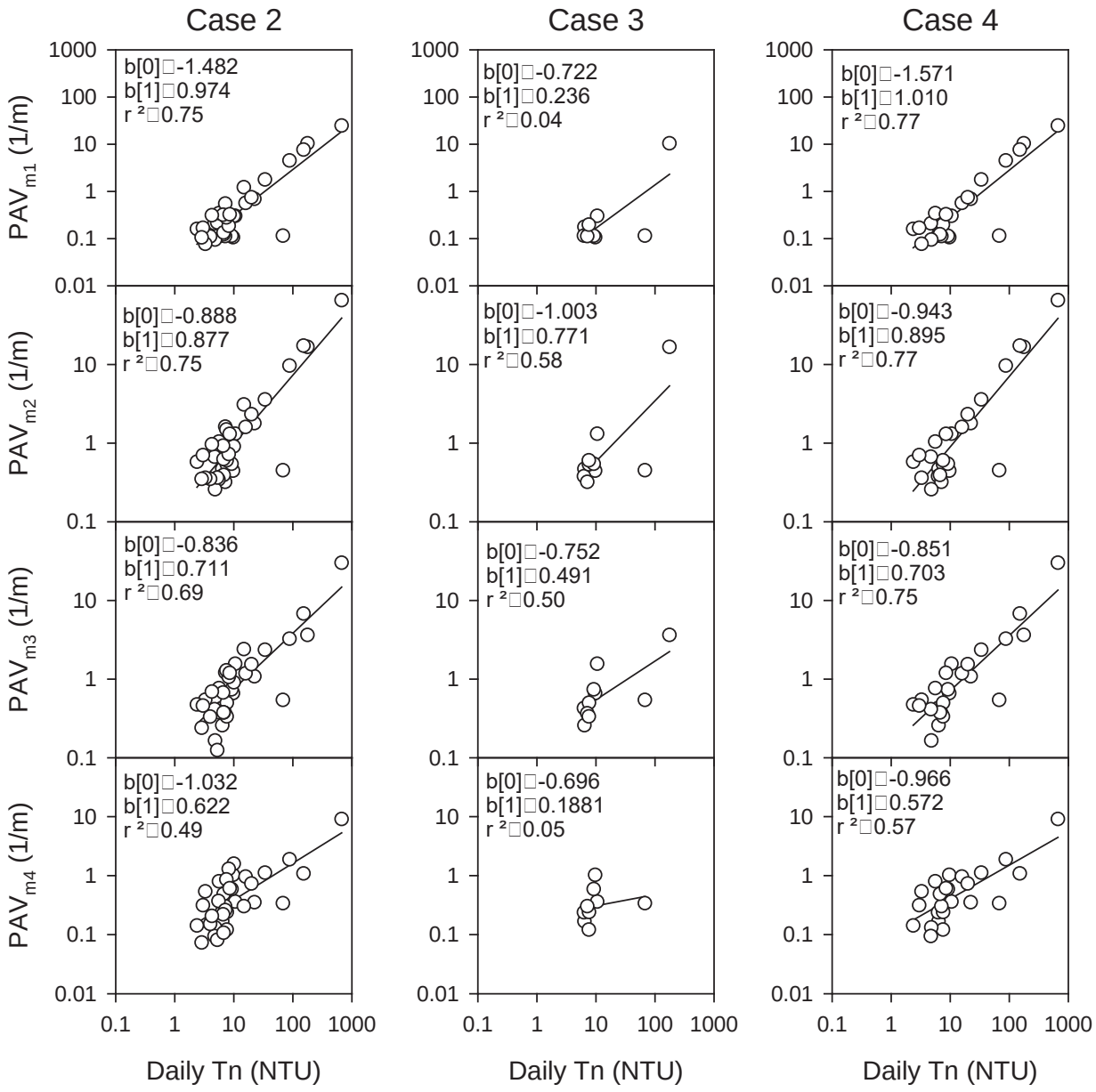

Figure 3- 16. Concentration-daily Tn (from IL sonde) relationships for PAV_{m1}, PAV_{m2}, PAV_{m3}, and PAV_{m4} for data cases 2-4.

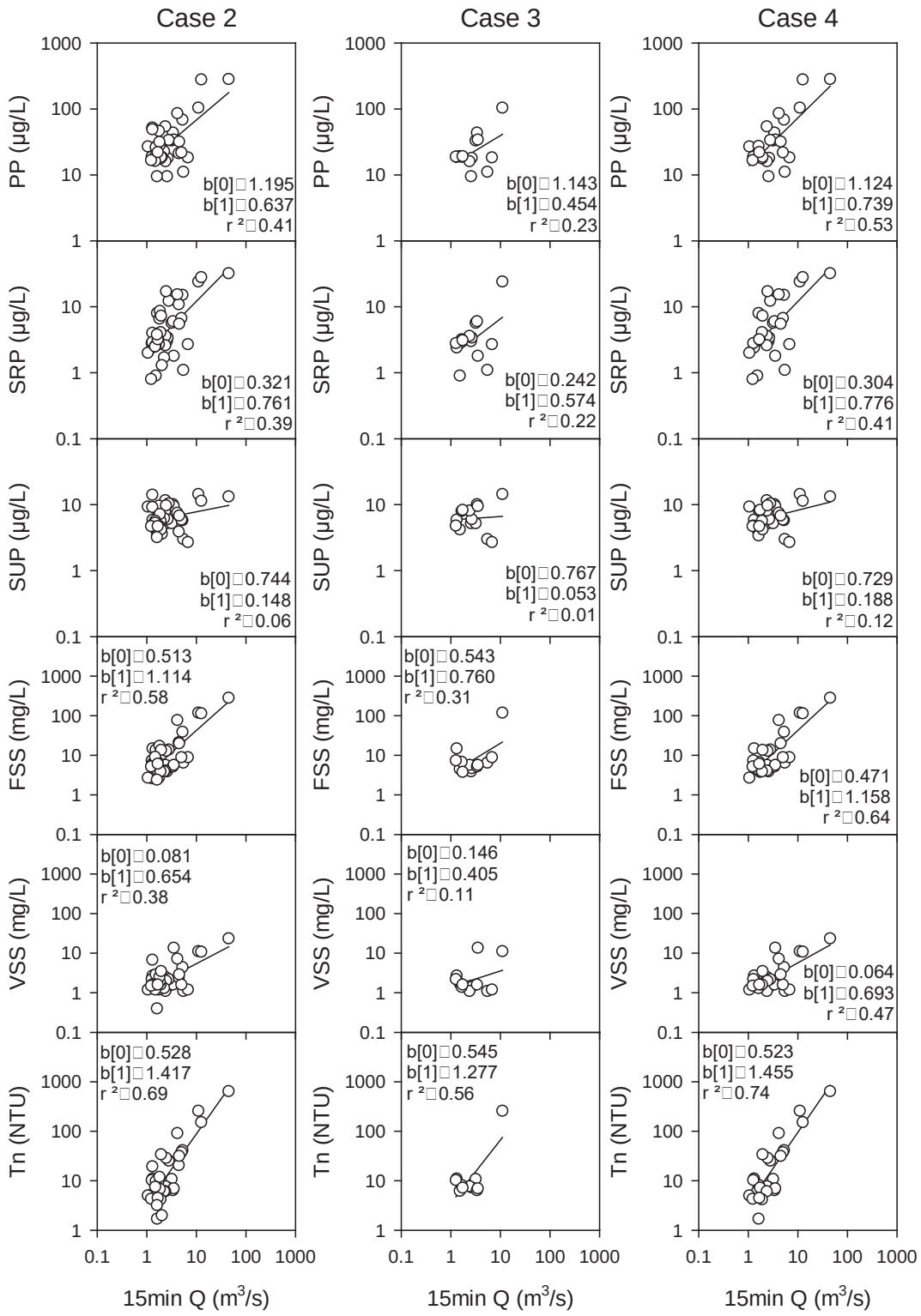

Figure 3- 17. Concentration-15minute Q relationships for PP, SRP, SUP, FSS, VSS, and Tn for data cases 2-4.

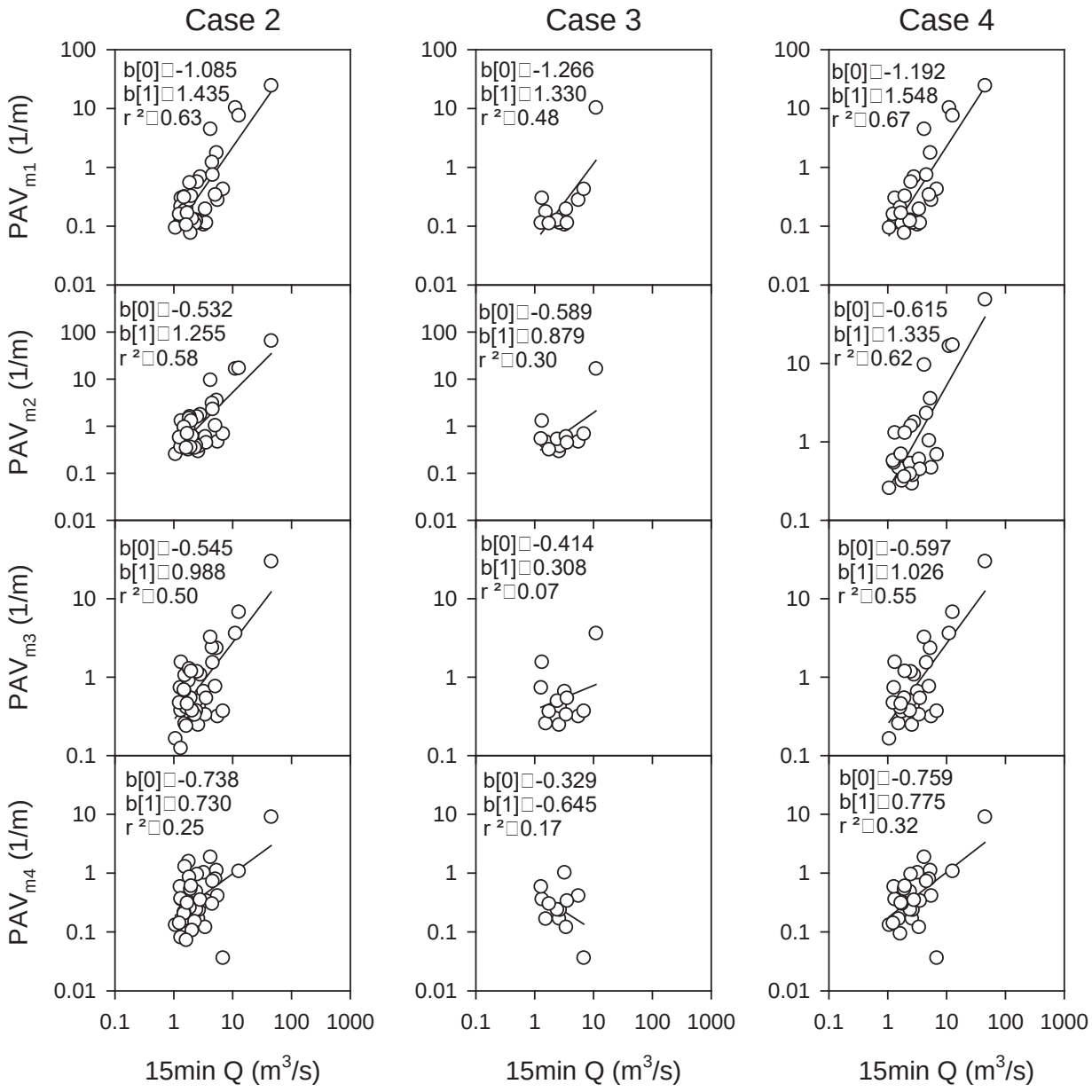

Figure 3- 18. Concentration-15minute Q relationships for PAV_{m1}, PAV_{m2}, PAV_{m3}, and PAV_{m4} for data cases 2-4.

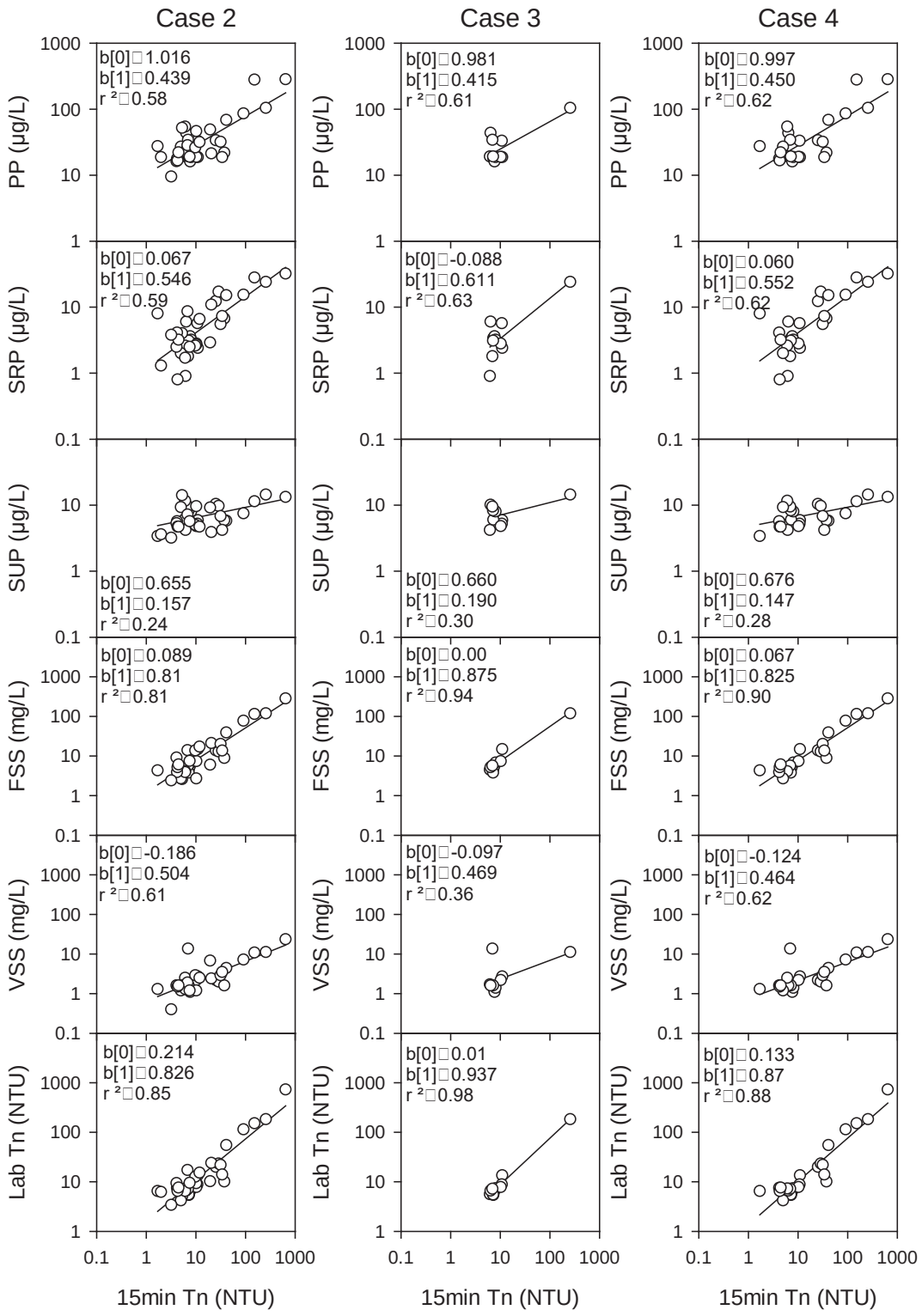

Figure 3- 19. Concentration-15minute Tn (from IL sonde) relationships for PP, SRP, SUP, FSS, VSS, and Tn for data cases 2-4.

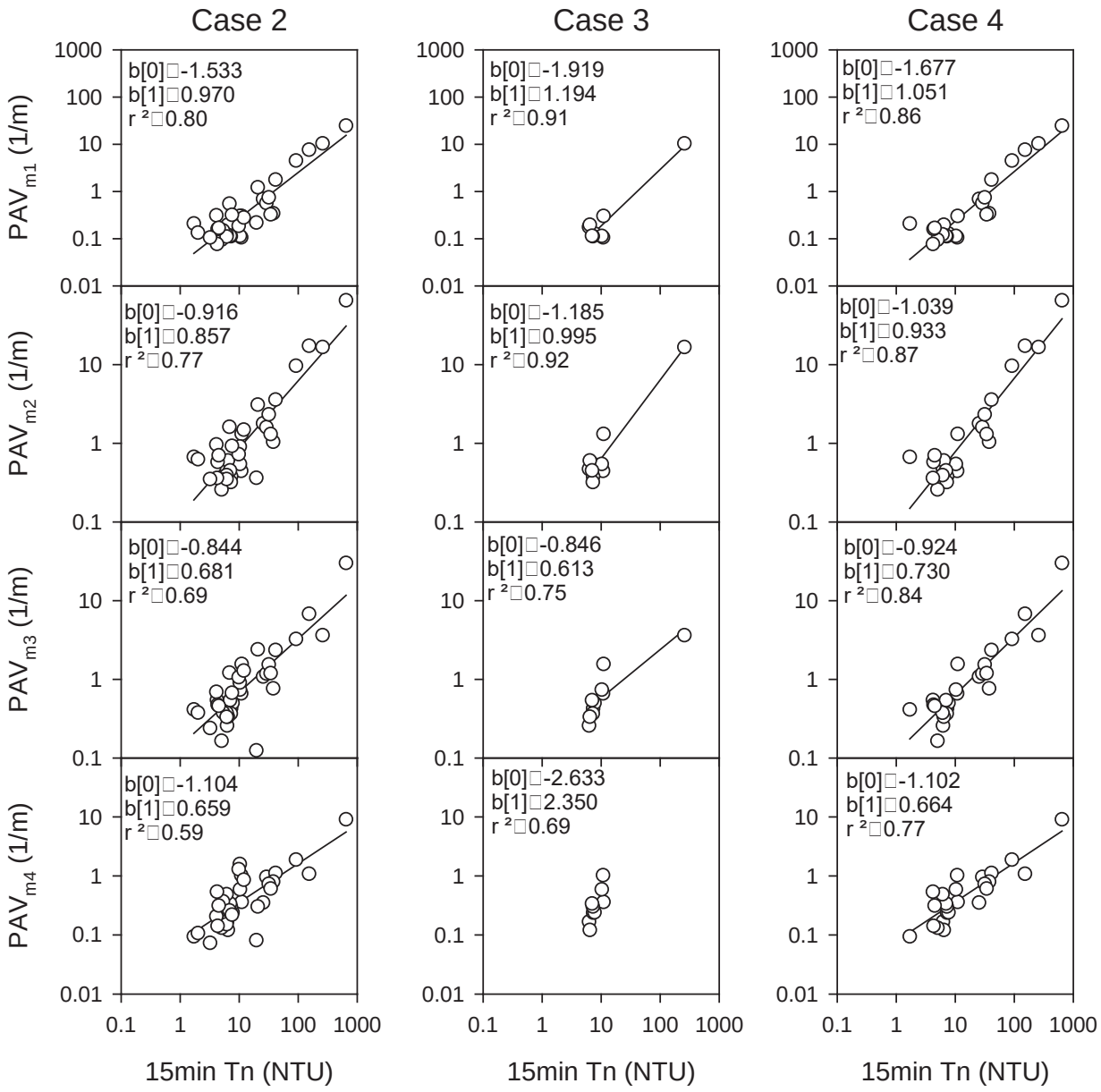

Figure 3- 20. Concentration-15minute Tn (from IL sonde) relationships for PAV_{m1}, PAV_{m2}, PAV_{m3}, and PAV_{m4} for data cases 2-4.

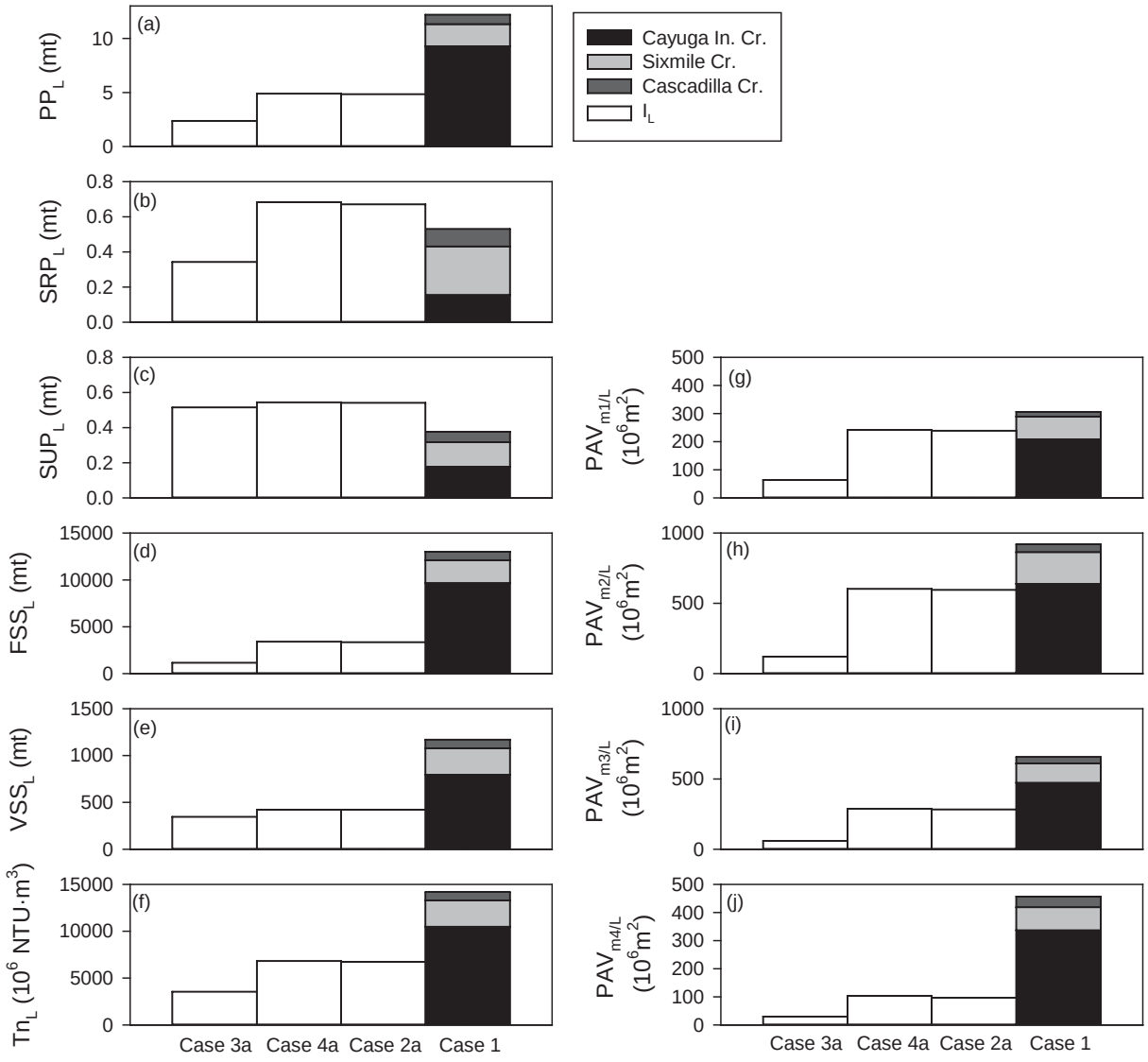

Figure 3- 21. Comparison of IL load estimates for Cases 3a, 4a, 2a, and Case 1 for: (a) PP_L, (b) SRP_L, (c) SUP_L, (d) FSS_L, (e) VSS_L, (f) Tn_L, (g) $PAV_{m1/L}$, (h) $PAV_{m2/L}$, (i) $PAV_{m3/L}$, and (j) $PAV_{m4/L}$. X-axis is arranged left to right from least to most data inclusion, Case 3a, 4a, and 2a, respectively.

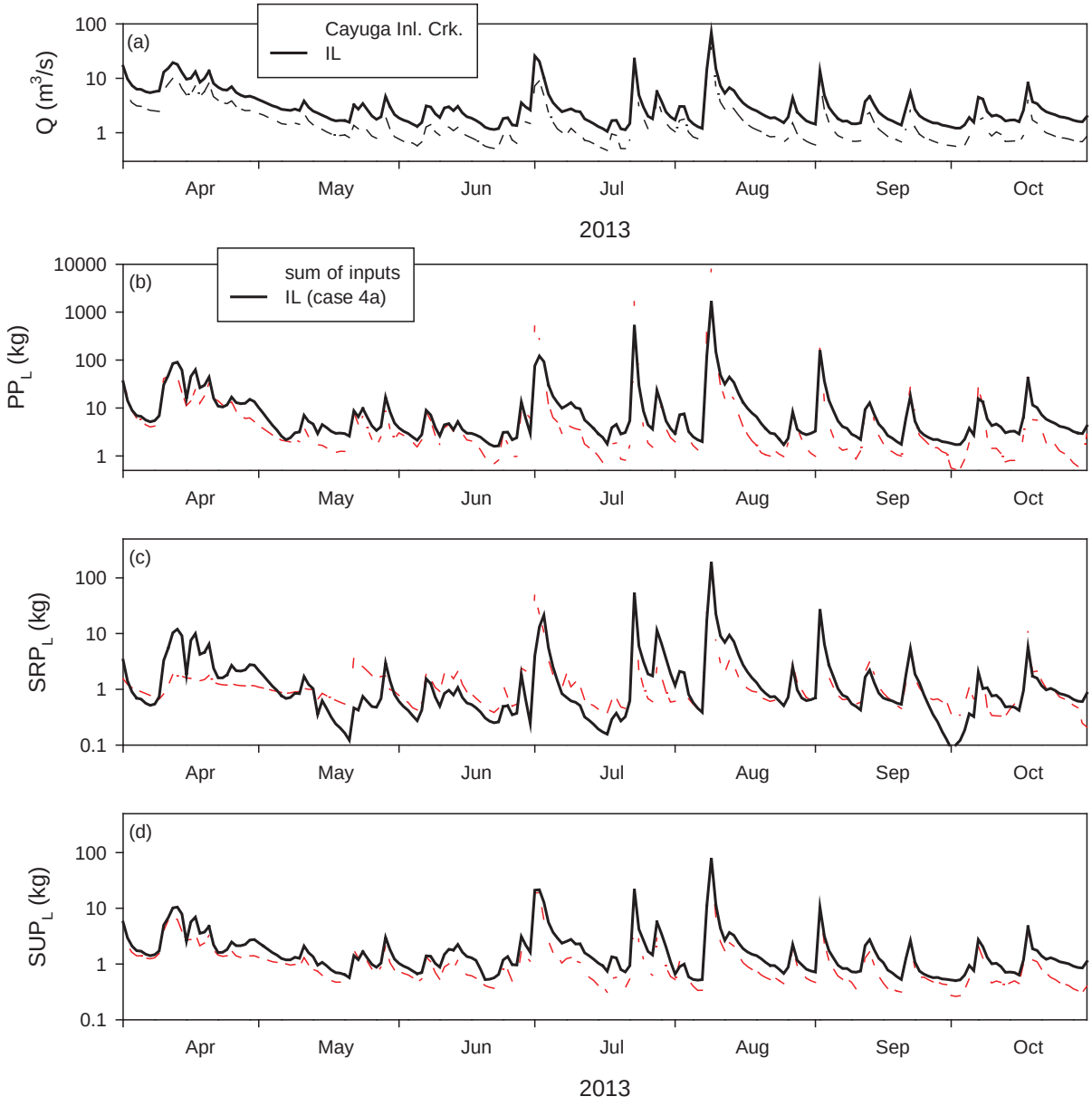

Figure 3- 22. Time series of Case 4a loads: (a) stream flow at Cayuga Inlet Creek and IL flow estimates, (b) PP_L, (c) SRP_L, and (d) SUP_L.

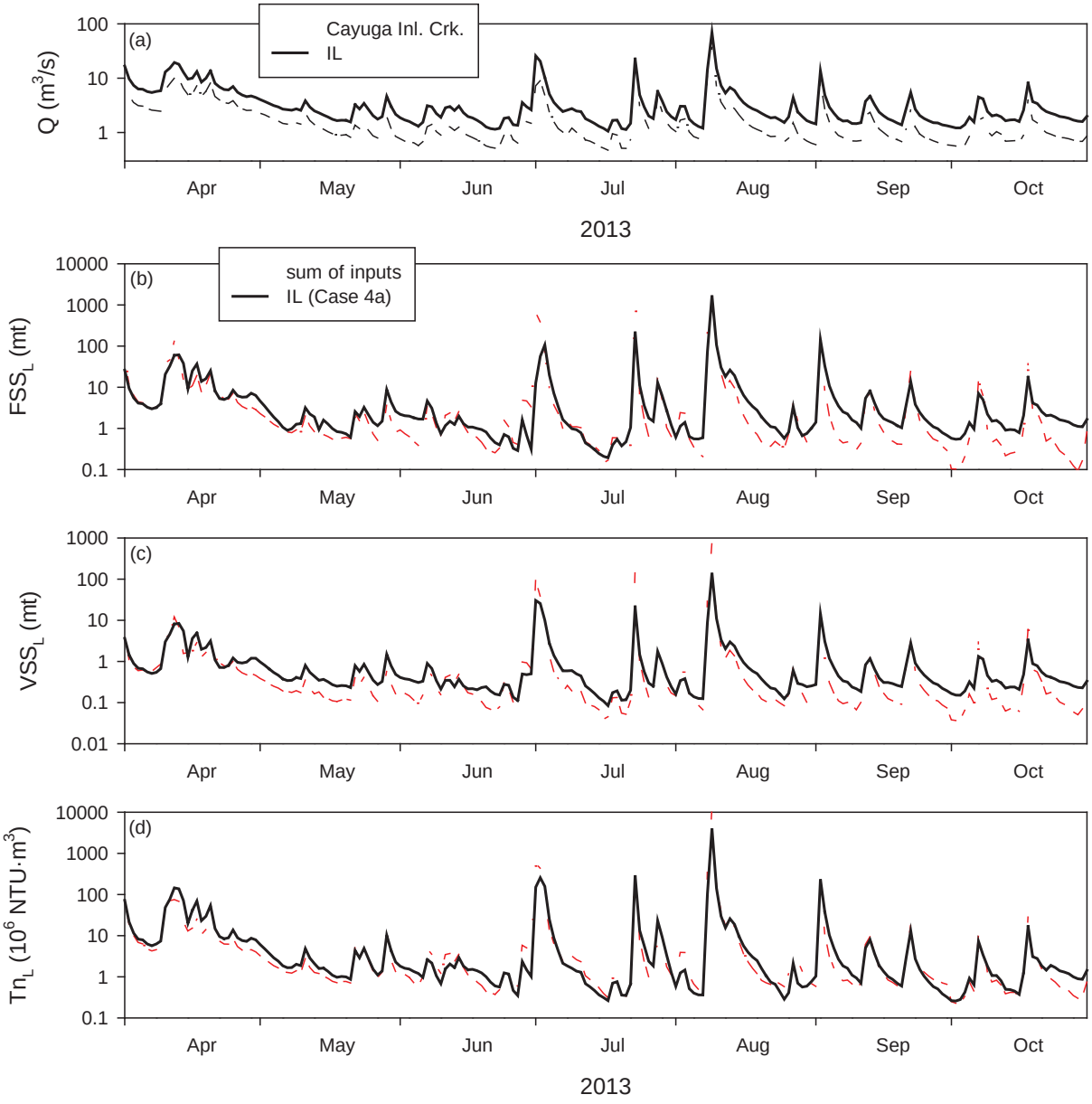

Figure 3- 23. Time series of Case 4a loads: (a) stream flow at Cayuga Inlet Creek and IL flow estimates, (b) FSS_L, (c) VSS_L, and (d) Tn_L.

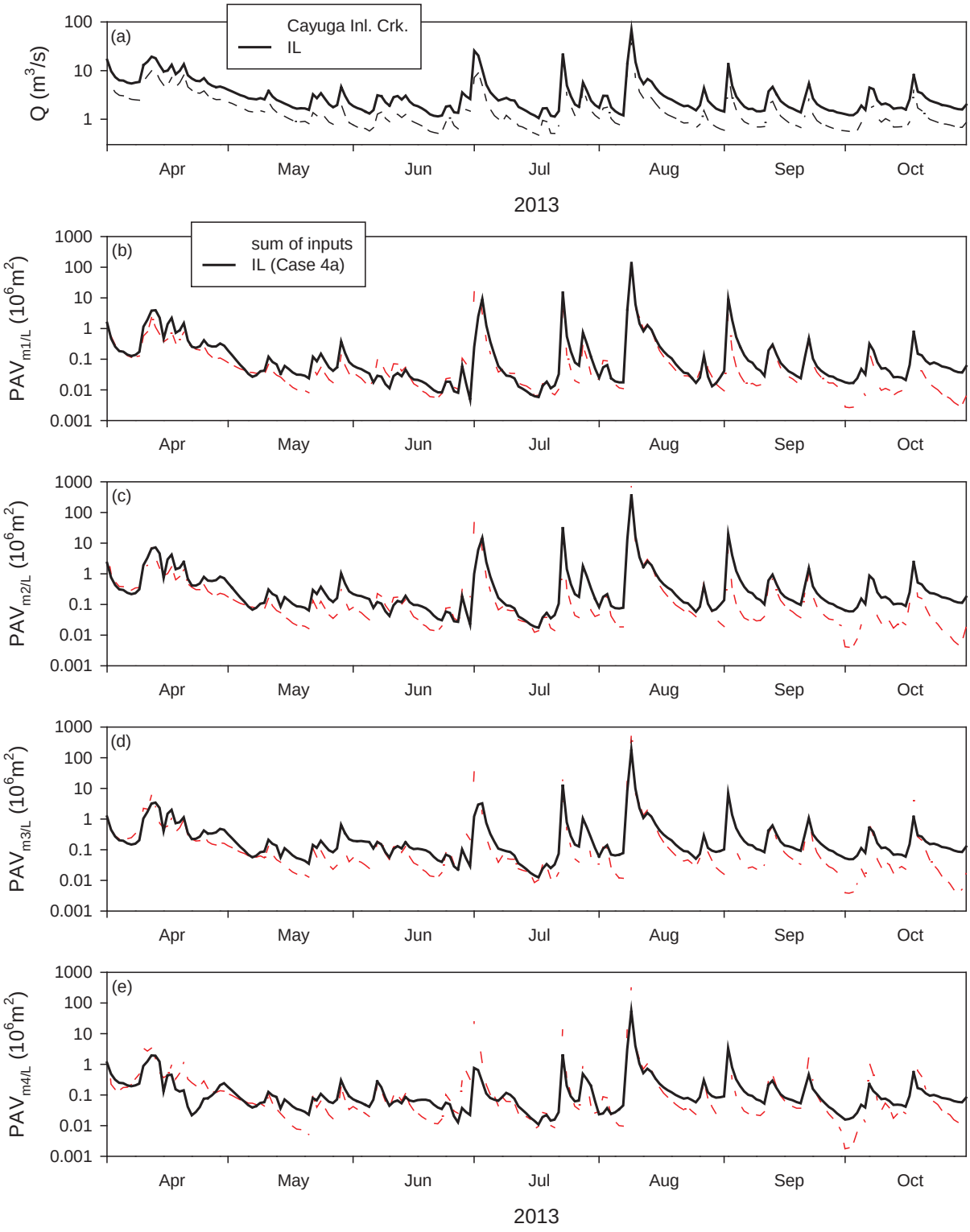

Figure 3- 24. Time series of Case 4a loads: (a) stream flow at Cayuga Inlet Creek and IL flow estimates, (b) $PAV_{m1/L}$, (c) $PAV_{m2/L}$, (d) $PAV_{m3/L}$, and (e) $PAV_{m4/L}$.

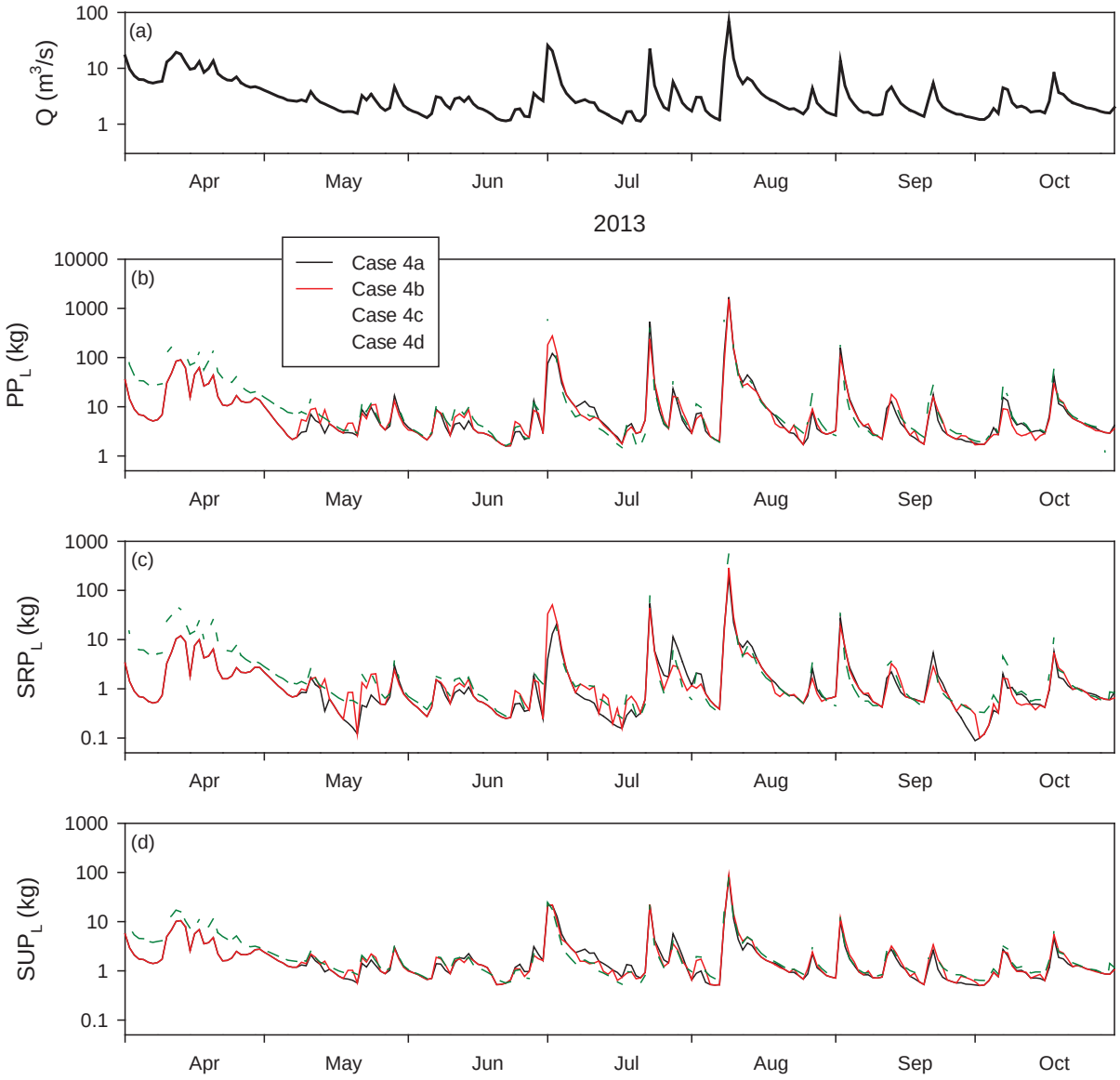

Figure 3- 25. Time series of Case 4 loads: (a) stream flow at Cayuga Inlet Creek and IL flow estimates, (b) PP_L, (c) SRP_L, and (d) SUP_L.

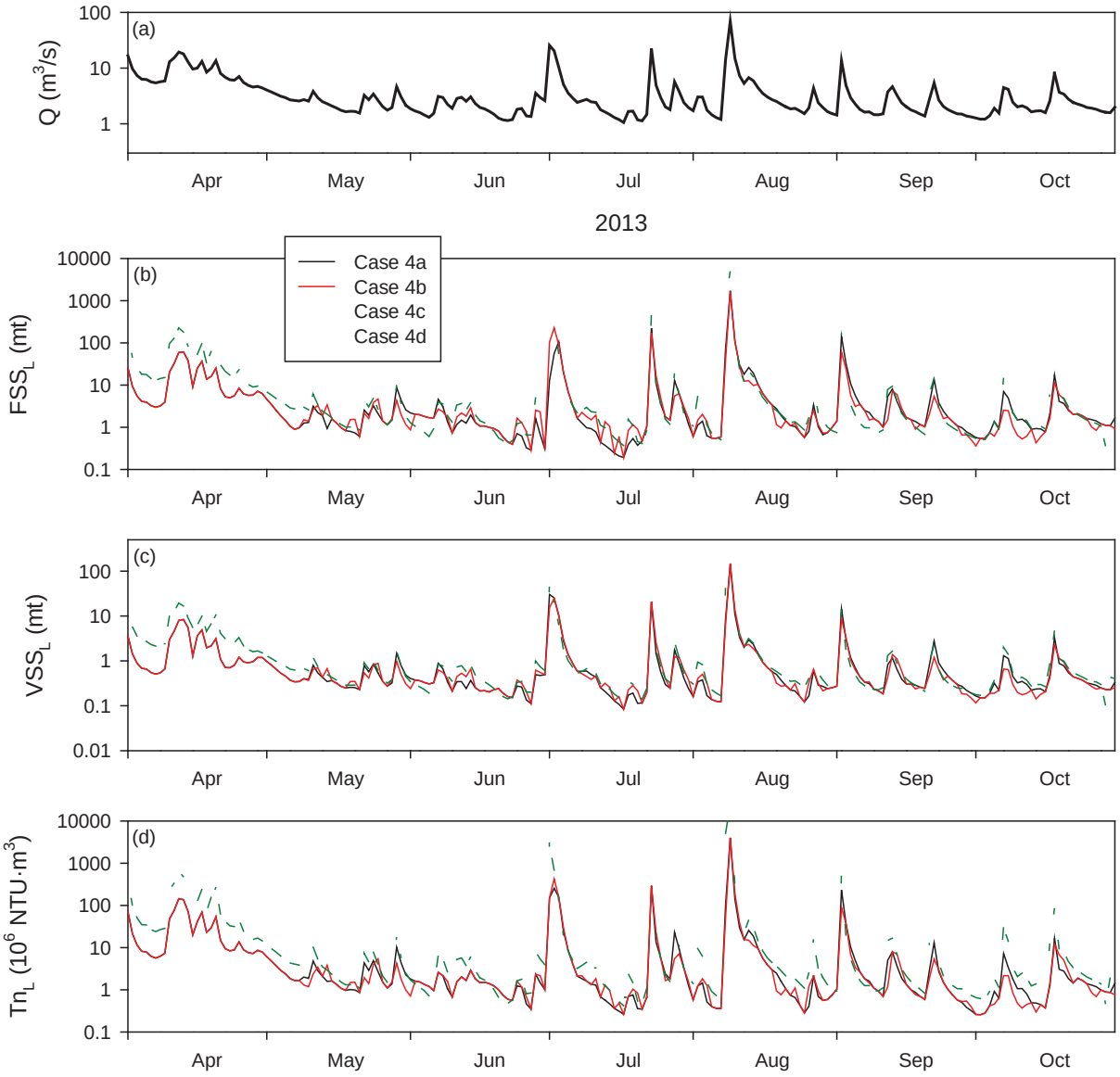

Figure 3- 26. Time series of Case 4 loads: (a) stream flow at Cayuga Inlet Creek and IL flow estimates, (b) FSS_L, (c) VSS_L, and (d) Tn_L.

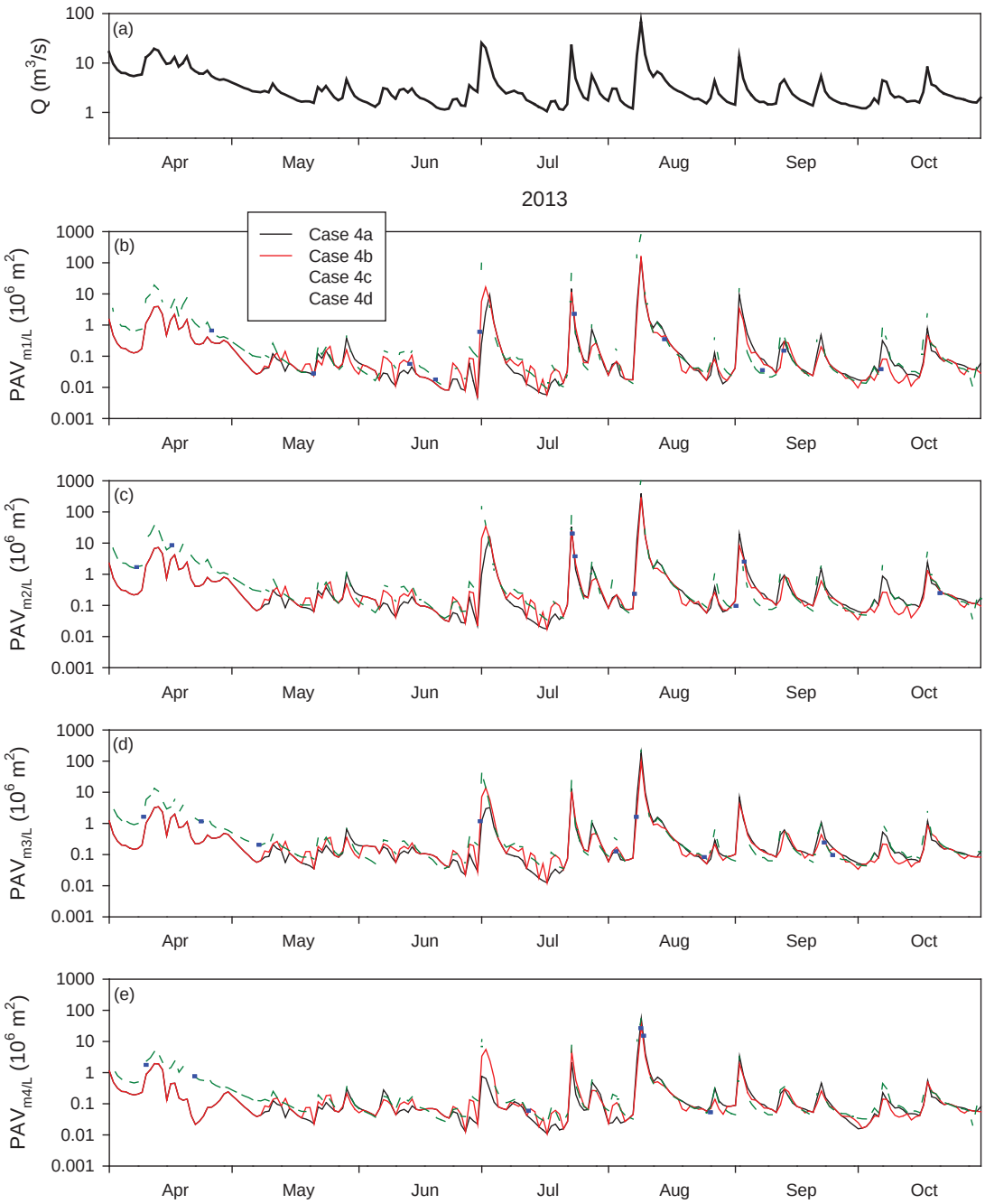

Figure 3- 27. Time series of Case 4 loads: (a) stream flow at Cayuga Inlet Creek and IL flow estimates, (b) $PAV_{m1/L}$, (c) $PAV_{m2/L}$, (d) $PAV_{m3/L}$, and (e) $PAV_{m4/L}$.

Note: The model product of this two-phase project did not address the potential changes in loading from Cayuga Inlet Channel to the lake that may occur in response to dredging of the Channel.

This page intentionally left blank

Section 4. Minerogenic Particle Characterization and Submodel

4.1. Peer-reviewed Manuscript: Effler SW and Peng F. 2014. Long-term study of minerogenic particle optics in Cayuga Lake, New York. Limnol. Oceanogr. 59(2):325–339

Selected Salient Findings:

- The dynamics of minerogenic particles in contributing to light scattering (b_p), an important regulator of Secchi depth (Z_{SD}), were evaluated from eight years (1999 – 2006) of measurements on the shelf and pelagic areas
- These particle types, together with phytoplankton, are primarily responsible for b_p and Z_{SD}
- The dominant minerogenic particle types are clay, and secondarily, calcite
- Clay levels increase following runoff events, with much greater levels of b_p, and lower Z_{SD}, observed on the shelf compared to pelagic locations
- Good closure between the summation of the two light scattering estimates for minerogenic and phytoplankton particles and bulk measurements of b_p were obtained, that will serve to quantify the relative contributions within models of these two particle types to the common trophic state metric of Z_{SD}

Limnol. Oceanogr., 59(2), 2014, 325–339
© 2014, by the Association for the Sciences of Limnology and Oceanography, Inc.
doi:10.4319/lo.2014.59.2.0325

Long-term study of minerogenic particle optics in Cayuga Lake, New York

Steven W. Effler and Feng Peng *

Upstate Freshwater Institute, Syracuse, New York

Abstract

The dynamics of light scattering by minerogenic particles in the upper waters of Cayuga Lake, New York, were characterized for the spring–autumn interval of 8 yr (1999–2006) at pelagic and nearshore sites with a scanning electron microscope interfaced with automated image and x-ray analyses (SAX). SAX results were used to estimate the minerogenic scattering coefficient (b_m) through Mie theory calculations. SAX–Mie supported a two-component model for particulate scattering (b_p) that included an organic component of scattering (b_o), estimated from a bio-optical model. The credibility of the b_m estimates and the two-component modeling approach was demonstrated through good closure of the modeling results with bulk values of b_p (estimated from measurements of the beam attenuation coefficient at 660 nm). The average of the ratio b_p : (b_m + b_o) was 1.03 (average relative error 19.4%). Two minerogenic particle types were important in regulating the dynamics of b_m—clay minerals that increased in concentration in response to runoff events, and calcium carbonate precipitated mostly on small organic particles during short-term late-summer whiting events. b_m was attributed to particles in the size range of 1–10 μm. Variations in b_m dominated the overall variations in b_p and Secchi disk depth; differences in b_m explained well those observed in b_p during dry weather intervals of low b_m. Higher b_m values, mainly associated with clay mineral particles, were observed at the nearshore site as opposed to the pelagic location; there was a positive linkage between these levels and tributary flow rate.

Light scattering by particles, a fundamental process regulating radiative transfer in water (Kirk 2011), is important in determining apparent optical properties (AOPs, depend on geometry of the light field) of interest, including clarity (Preisendorfer 1986) and the remote sensing signal (Woźniak and Stramski 2004). The total scattering coefficient (b, m^{-1}), corresponding to the integration of the volume scattering function over all directions (Kirk 2011), quantifies a central feature of the light-scattering regime. b is an inherent optical property, independent of the geometry of the light field. The magnitude and spectral features of the particulate component of scattering, b_p (which greatly exceeds that due to water), depend on multiple attributes of a particle population, including the number concentration (N), the particle size distribution (PSD), the composition of the individual particles and their shapes (Babin et al. 2003).

The particle populations of aquatic ecosystems are heterogeneous, varying in time and space and differing greatly among systems in response to an array of drivers (Stramski et al. 2004, 2007; Peng and Effler 2011). Protocols for resolving the various components of light scattering are needed to understand these differences and dynamics, and to identify their origins and drivers, objectives that are consistent with the reductionist approach advocated by Stramski and co-workers (Stramski et al. 2001, 2004, 2007). Inorganic, or minerogenic, particles are of particular interest in coastal and inland (so-called Case 2) waters because of their relatively greater contributions to b_p, compared with the open oceans (i.e., Case 1; Babin et al. 2003; Bowers and Binding 2006; Woźniak et al. 2010). Minerogenic particles have increasingly been reported to be important in influencing common optical metrics of water quality for inland waters, including Secchi depth (Z_{SD}; Swift et al. 2006; Peng and Effler 2011) and turbidity (Peng et al. 2009*b*; Peng and Effler 2010). These particles have three general origins: terrigenous (allochthonous) inputs (Kirk 1985; Peng et al. 2009*b*), re-suspension (Peng and Effler 2010), and autochthonous production (Weidemann et al. 1985).

The reductionist approach has recently been advanced (Peng et al. 2009*a*) through forward estimates of the minerogenic component(s) of b_p (i.e., $b_{m,i}$) for inland waters based on an individual particle analysis technique, scanning electron microscopy interfaced with automated image and x-ray analyses (SAX). SAX measures the light-scattering attributes of minerogenic particles (N, PSD, elemental x-ray composition, and shapes) that serve as inputs (exclusive of shape) to Mie theory calculations of the scattering efficiency factor ($Q_{bm,i}$) for the individual particles (Peng and Effler 2007). The estimates of b_m are made according to

$$b_m(\lambda) = \frac{1}{V}\sum_{i=1}^{N_m} Q_{bm,i}(m_i, \lambda, d_i)\mathrm{PA}_{m,i} \qquad (1)$$

where V is the sample volume, N_m is the number of minerogenic particles in a sampled volume of water, and $\mathrm{PA}_{m,i}$ is the projected area (m^2) of minerogenic particle i. $Q_{bm,i}$ depends on the complex refractive index (m_i, function of composition) and size (d_i) of the particle, and the wavelength of light (λ). This SAX–Mie approach supports further partitioning of b_m into contributions according to size and particularly composition (e.g., clay minerals, quartz, and calcite) of particles (Peng and Effler 2010, 2011).

Early research with the SAX–Mie approach had appropriately focused first on testing the credibility of the forward estimates of b_m for a range of particle assemblage conditions (*see* review of Peng and Effler 2012), before

* Corresponding author: fpeng@upstatefreshwater.org

4.2. **Peer-reviewed Manuscript:** Peng F and Effler SW. Characterizations of calcite particles and evaluations of their light scattering effects in lacustrine systems. Limnol. Oceanogr. (In Press; 2017).

Selected Salient findings:

- Characterization of internally produced calcite particles and their heteronuclei
- Organic particles, apparently from two size ranges, likely corresponding to pico- and nanocyanobacteria, are found to serve as the primary heteronuclei for the calcite precipitation
- Nine years of Spring – Fall monitoring in Cayuga Lake documented major interannual variations in the whiting events with respect to timing, magnitude of the light scattering signatures, and the size of the heteronuclei.
- Whiting events can have major effects on Secchi disk and remote sensing reflectance
- The relative contributions (%) of calcite, clay, and phytoplankton to particle backscattering during the whiting events show calcite was the largest contributor of the minerals (by a wide margin in most years) and phytoplankton was estimated to remain the largest contributor to particle scattering overall
- Support for the operation of the heterogeneous nucleation process in calcite precipitation in the lake
- Documentation of the general thinness of the calcite layers precipitated onto the small cyanobacteria that serve as the nuclei.
- Precipitation is active for only a portion of the summer during oversaturation of the mineral and is apparently associated with the availability of appropriate heteronuclei

Characterizations of calcite particles and evaluations of their light scattering effects in lacustrine systems

Feng Peng[1] and Steven W. Effler[*]

Upstate Freshwater Institute, P.O. Box 506, Syracuse, New York 13214

[1] Now at USG Corporation, 700 N Highway 45, Libertyville, IL 60048

[*] Correspondence: sweffler@upstatefreshwater.org

Running head: calcite and light scattering effects

Keywords: calcite ($CaCO_3$), whiting events, heteronuclei, light scattering, backscattering

4.3. **Peer-reviewed Manuscript:** Peng F and Effler SW. 2015. Quantifications and water quality implications of minerogenic particles in Cayuga Lake, New York, and its tributaries. Inland Waters. 5:403-420.

Selected Salient Findings:

- An individual particle analysis technique (SAX) was used to characterize the minerogenic particle populations of the lake and its tributaries, in the form of the total projected area per unit volume of water (PAV_m)
- PAV_m is documented to be linearly related to the mineral components of particulate phosphorus (PP_m), turbidity (Tn/m), and the light scattering coefficients, and inversely related to Secchi depth (Z_{SD})
- Clay mineral particles dominate PAV_m in this lake and its tributaries
- Levels of PAV_m are higher in a near-shore and tributary entry area (e.g., shelf) than in pelagic areas, particularly after runoff events
- The increased PAV_m is accompanied by degraded water quality, including higher PPm and Tn/m and lower Z_{SD} on the shelf compared to pelagic areas
- PAV_m measurements have an array of advantages over long-term gravimetric (long-term) data to assess the effects of minerogenic particle inputs

Article

Quantifications and water quality implications of minerogenic particles in Cayuga Lake, New York, and its tributaries

Feng Peng and Steven W. Effler*
Upstate Freshwater Institute, Syracuse, NY
** Corresponding author: sweffler@upstatefreshwater.org*

Received 23 April 2015; accepted 4 August 2015; published 9 October 2015

Abstract

An individual particle analysis technique, scanning electron microscopy interfaced with automated image and X-ray analyses (SAX), was applied to characterize the minerogenic particle populations of Cayuga Lake (New York) and its primary tributaries and quantify their effects on common water quality metrics. The primary summary metric of SAX results is demonstrated to be the total projected area of minerogenic particles per unit volume of water (PAV_m). PAV_m is documented to be linearly related to the minerogenic components of particulate phosphorus (PP_m), turbidity (T_{urb}), and the light scattering coefficient, and inversely related to Secchi depth (*SD*). SAX is demonstrated to support partitioning of PAV_m into contributions of multiple size and geochemical classes. Clay mineral particles dominated in the tributaries and the lake, although they shifted somewhat to smaller sizes (1–15 μm) in the lake. Levels of PAV_m were higher in a lake area that adjoins the tributary inputs than in pelagic waters, particularly after runoff events. This increased PAV_m degraded water quality, including higher PP_m and T_{urb} and lower SD relative to the pelagic waters, although diminished (still recognizable) signatures are documented lake-wide. Advantages of SAX over gravimetric analyses for the minerogenic particle populations of lakes include (1) improved analytical performance, (2) insights from the more robust size and composition information, (3) theoretical advantages for optical impacts, and (4) stronger relationships with water quality metrics.

Key words: clarity, lakes, minerogenic (morganic) particles, phosphorous, stream, turbidity

Introduction

Minerogenic particles (e.g., clay minerals, quartz, calcite) can have important water quality and ecological implications in lakes and reservoirs. Specific issues include (1) net sediment accumulation (Ziegler and Nisbet 1995, Gelda et al. 2013); (2) metabolic activity and composition of biological communities (Phlips et al. 1995, Newcombe 2003); (3) transport, cycling, and apportionment of forms of nutrients (Hupfer et al. 1995, Effler et al. 2014) and contaminants (O'Connor 1988, Chapra 1997); and (4) the level of light scattering and thereby optical metrics of water quality (Peng et al. 2009b, Peng and Effler 2010, Effler and Peng 2014) and the remote sensing signal (Binding et al. 2007, 2012). These particles have 3 potential general sources: terrigenous (allochthonous) inputs delivered primarily by tributaries (Kirk 1985, Peng et al. 2009b, Peng and Effler 2012), autochthonous production (Weidemann et al. 1985, Homa and Chapra 2011), and sediment resuspension (Peng and Effler 2010). Large fractions of annual sediment loads delivered by tributary streams are often input over relatively brief intervals during major runoff events (Longabucco and Rafferty 1998, Prestigiacomo et al. 2007). Short-term autochthonous production of calcium carbonate ($CaCO_3$, or calcite, precipitation), described as whiting events, occurs in summer in the epilimnia of many hardwater lakes (Homa and Chapra 2011). Predictive capability for these particles in lacustrine systems would be invaluable to quantitatively address related features of water quality issues and provide support for insightful management deliberations.

Advancement of the understanding and quantification of the effects of minerogenic particles in aquatic

DOI: 10.5268/IW-5.4.807

4.4. **Peer-reviewed Manuscript:** Gelda RK, Effler SW, Prestigiacomo AR, Peng F, Watkins, JM, Chapra S. 2016. Simulation of terrigenous particle populations in time and space in Cayuga Lake, New York, in response to runoff events. Water Air Soil Pollut. :227-365

Selected Salient Findings:

- The important effects of minerogenic particles delivered from watersheds on optical and phosphorus metrics of lacustrine water quality have been quantified through measurements of the projected area of these particles per unit volume of water (PAV_m).
- A mass balance type model for PAV_m, partitioned according to the contributions of four size classes, has been developed and tested for Cayuga Lake, supported by long-term monitoring of PAV_m in the lake and its primary tributaries.
- The model represents the source of PAV_m of tributary inputs and three in-lake loss processes: (1) size dependent settling, (2) enhancement of settling through aggregation, and (3) filter feeding by dreissenid mussels.
- The central roles of major runoff events and localized external loads of minerogenic sediment at one end of the lake in driving patterns of PAV_m in time and space are successfully simulated, including (1) the higher PAV_m levels in a shallow area ("shelf") adjoining these inputs, relative to pelagic waters, following runoff events; and (2) the positive dependence of the shelf increases on the magnitude of the event.
- The utility of PAV_m predictions to quantify the effects of these particles on optical and phosphorus concentration metrics of water quality has been established.

Water Air Soil Pollut (2016) 227:365
DOI 10.1007/s11270-016-3035-4

Simulation of Terrigenous Minerogenic Particle Populations in Time and Space in Cayuga Lake, New York, in Response to Runoff Events

Rakesh K. Gelda · Steven W. Effler · Anthony R. Prestigiacomo · Feng Peng · James M. Watkins · Steven Chapra

Received: 11 May 2016 / Accepted: 4 August 2016

Abstract The important effects of minerogenic particles delivered from watersheds on optical and phosphorus metrics of lacustrine water quality have recently been quantified through measurements of the projected area of these particles per unit volume of water (PAV_m), using an individual particle analysis technique. A mass balance type model for PAV_m, partitioned according to the contributions of four size classes, is developed and tested for Cayuga Lake, New York, supported by long-term monitoring of PAV_m in the lake and its primary tributaries. The model represents the source of PAV_m of tributary inputs and three in-lake loss processes: (1) size-dependent settling, (2) enhancement of settling through aggregation, and (3) filter feeding by dreissenid mussels. The central roles of major runoff events and localized external loads of minerogenic sediment at one end of the lake in driving patterns of PAV_m in time and space are successfully simulated, including (1) the higher PAV_m levels in a shallow area ("shelf") adjoining these inputs, relative to pelagic waters, following runoff events; and (2) the positive dependence of the shelf increases on the magnitude of the event. Analyses conducted with the model establish that settling, with aggregation enhancement, dominates the loss of PAV_m from the water column of the shelf, while mussel filtration increases in relative importance in pelagic waters. The utility of PAV_m predictions to quantify the effects of these particles on optical and phosphorus concentration metrics of water quality is established.

Keywords Minerogenic particles · Runoff events · Settling · Aggregation · Mussel filtration · Water quality

R. K. Gelda · S. W. Effler (✉) · A. R. Prestigiacomo · F. Peng
Upstate Freshwater Institute, P.O. Box 506, Syracuse, NY 13214, USA
e-mail: sweffler@upstatefreshwater.org

J. M. Watkins
Cornell Biological Field Station, Department of Natural Resources, Cornell University, 900 Shackleton Pt. Road, Bridgeport, NY 13090, USA

S. Chapra
Department of Civil and Environmental Engineering, Tufts University, 113 Anderson Hall, 200 College Avenue, Medford, MA 02155, USA

Published online: 05 September 2016

1 Introduction

Minerogenic particles, such as clay minerals, quartz, and calcite, have important water quality and ecological impacts on lakes and reservoirs. Specific issues include their effects on (1) the level of light scattering and thereby optical metrics of water quality (Peng et al. 2009a; Peng and Effler 2010; Effler and Peng 2014) and the remote sensing signal (Binding et al. 2007, 2012); (2) metabolic activity and the composition of biological communities (Phlips et al. 1995; Newcombe 2003); (3) transport, cycling, and apportionment of forms of nutrients (Hupfer et al. 1995; Effler et al. 2014) and contaminants (O'Connor 1988; Chapra 1997); and (4) net sediment accumulation (Gelda et al. 2013). These particles have three potential sources,

Section 5. Cayuga Lake Limnolog Optics Submodels (dependencies of optical metrics of water quality on constituent concentrations)

5.1. Peer-reviewed Manuscript: Effler SW, Prestigiacomo AR, Peng F, Gelda RK, Matthews DA. 2014. Partitioning the contributions of minerogenic particles and bioseston to particulate phosphorus and turbidity. Inland Waters. 4:179-192

Selected Salient Findings:

- An empirical model to partition the contributions of PAV_m and Chl-*a* to PP and Tn are developed, perform well, and perform well in tracking PP and Tn in time and space
- PAV_m is again shown to be an important component, contributing more on the shelf than in pelagic waters, particularly after PAV_m inputs from runoff events
- The particle populations supporting the analysis originate from eight years of in-lake monitoring of these portions of Cayuga Lake
- Elevated levels of PAV_m on the shelf site following runoff events caused the PAV_m to make increased contributions to PP and Tn
- These contributions to PP ($PP_{m/u}$) are not representative of trophic state

Article

Partitioning the contributions of minerogenic particles and bioseston to particulate phosphorus and turbidity

Steven W. Effler, Anthony R. Prestigiacomo*, Feng Peng, Rakesh Gelda, and David A. Matthews
Upstate Freshwater Institute, PO Box 506, Syracuse, NY 13214
** Corresponding author email: tonyp@upstatefreshwater.org*

Received 19 August 2013; accepted 8 January 2014; published 17 April 2014

Abstract

Protocols to partition the contributions of bioseston and minerogenic particles to turbidity (T_n) and particulate phosphorus (PP), as described by summations of the 2 components, are developed, tested, and applied. The analysis is based on coincident observations of T_n, PP, chlorophyll *a* (Chl), and the summation of the projected areas of individual minerogenic particles per unit volume (PAV_m) for the wide variations encountered in time and between near-shore and pelagic sites over an 8-year study of Cayuga Lake, New York. PAVm was determined from an individual particle analysis technique, scanning electron microscopy interfaced with automated image, and X-ray analyses (SAX). The partitionings are based on a stoichiometric approach that adopts Chl and PAV_m as the metrics of bioseston and minerogenic particles, respectively, and estimates developed here for stoichiometric ratios that relate T_n and PP to these 2 components. The systematically higher T_n and PP levels at the near-shore site, particularly following runoff events, are demonstrated to be a result of elevated PAV_m associated with allochthonous inputs. A reasonably good match of the partitioned 2-component summations with bulk observations is reported. Application of the 2-component PP model establishes minerogenic particles made, on average, noteworthy (~10%) to substantial (≥20%) contributions to PP. The minerogenic particle component of PP was largely responsible for the greater summer average total phosphorus (TP) concentrations at the near-shore versus the pelagic site, the interannual variations in the differences between these sites, and exceedance of the TP water quality limit at the near-shore site. Minerogenic particles were the dominant component of T_n, a finding that is demonstrated to be consistent with optical theory, based on the much greater efficiency of side-scattering for minerogenic versus organic particles.

Key words: bioavailability, bioseston, minerogenic particles, particulate phosphorus, stoichiometry, turbidity

Introduction

Minerogenic (morganic) particles play important ecologic and water quality roles in aquatic ecosystems by presenting reactive surfaces (O'Connor 1988, Hupfer et al. 1995), affecting the concentrations and stoichiometry of particulate constituents (Hecky et al. 1993, Effler et al. 2013), influencing metabolic activity (Phlips et al. 1995), contributing to net sedimentation (Bloesch 2004), and degrading optical water quality through the process of light scattering (Kirk 1985, Peng and Effler 2011). Sources of these particles to the water columns of lakes and reservoirs include allochthonous inputs from watersheds (Longabucco and Rafferty 1998), autochthonous production of oversaturated mineral phases (Yin and Johnson 1984, Homa and Chapra 2011), and sediment resuspended from bottom deposits (Bloesch 2004, Peng and Effler 2010). Water quality monitoring programs often do not include direct measurement of minerogenic particle assemblages, and those that do have primarily relied on gravimetric measurements: the mass remaining on a filter (per unit volume of sample) after exposure to a high temperature to burn off organic contributions. Such measurements have precision issues

DOI: 10.5268/IW-4.2.681

5.2. **Manuscript In Review (2016):** Effler SW, Strait CM, Effler AJP, Peng F, O'Donnell, DM, Prestigiacomo AR, O'Donnell SM, Perkins MG, Chapra S. A mechanistic model for Secchi disk depth, driven by light scattering constituents.

Selected Salient Findings:

- Secchi disk depth, like TP, suffers from interference from noteworthy or elevated levels of minerogenic particles (PAV_m), indicating false high eutrophication from contributions of PAV_m
- Heretofore, a theory based mechanistic model did not exist to quantify the effects of PAV_m on Secchi disk depth, and thereby the indicated trophic state
- Such a Secchi disk depth model was developed, successfully tested , and applied for Cayuga Lake
- Model development was supported by long-term Secchi depth and Chl-*a* observations, more recent PAV_m measurements, sophisticated optics measurements, and optics theory
- The tested model was applied to quantify the contributions of phytoplankton and PAV_m to recent light scattering and Secchi disk depths and dynamics
- The model has been integrated into the larger overall water quality model for the lake (Section 7)

A mechanistic model for Secchi disk depth, driven by light scattering constituents

Steven W. Effler*[1], Christopher Strait[1], Adam J.P. Effler[1], Feng Peng[1], David M. O'Donnell[1], Anthony R. Prestigiacomo[1], Susan M. O'Donnell[1], MaryGail Perkins[1], and Steve C. Chapra[2]

[1]*Upstate Freshwater Institute, Syracuse, NY 13224, USA*

[2]*Department of Civil and Environmental Engineerings, Tufts University, 113 Anderson Hall, 200 College Avenue, Medford, MA 02155, USA*

**Corresponding author: sweffler@upstatefreshwater.org*

Section 6. Unavailable Minerogenic Particulate Phosphorus ($PP_{m/u}$) Submodels

6.1. Peer-reviewed Manuscript: Gelda RK, Effler SW, Prestigiacomo AR, Peng F, Auer MT, Kuczynski A, Chapra, S. 2016. Simulation of the contribution of phosphorus-containing minerogenic particles to particulate phosphorus concentration in Cayuga Lake, New York. Water Air Soil Poll. 227:365-

Selected Salient Findings:

- Phosphorus (P) associated with minerogenic particles delivered from watersheds can interfere with the common use of total P (TP) concentration as a trophic state metric in lacustrine systems, particularly proximate to tributary entries, because of its limited bioavailability.
- The concentration of unavailable minerogenic particulate P ($PP_{m/u}$), where it is noteworthy, should be subtracted from TP in considering primary production potential and trophic state levels.
- A first mass balance model for $PP_{m/u}$ is developed and tested here for Cayuga Lake, New York.
- This is supported by a rare combination of detailed information for minerogenic particle level dynamics for the tributaries and lake, the bioavailability of tributary particulate P (PP), and previously tested hydrothermal/transport and minerogenic particle concentration submodels.
- The central roles of major runoff events and localized tributary loading at one end of the lake in driving patterns of $PP_{m/u}$ in time and space are well simulated, including: (1) the higher $PP_{m/u}$ concentrations in a shallow area ("shelf") adjoining the inputs, relative to pelagic waters, following runoff events, and (2) the positive dependence of the shelf increases on the magnitude of the event.
- The $PP_{m/u}$ component of P was largely responsible for the higher summer average TP on the shelf versus pelagic waters, and the exceedance of a TP water quality limit on the shelf.
- The effective simulation of $PP_{m/u}$ allows an appropriate adjustment of TP values to avoid over-representation of potential primary production levels.

Water Air Soil Pollut (2016) 227: 365
DOI 10.1007/s11270-016-3035-4

Simulation of Terrigenous Minerogenic Particle Populations in Time and Space in Cayuga Lake, New York, in Response to Runoff Events

Rakesh K. Gelda · Steven W. Effler · Anthony R. Prestigiacomo · Feng Peng · James M. Watkins · Steven Chapra

Received: 11 May 2016 / Accepted: 4 August 2016 / Published online: 5 September 2016

Abstract The important effects of minerogenic particles delivered from watersheds on optical and phosphorus metrics of lacustrine water quality have recently been quantified through measurements of the projected area of these particles per unit volume of water (PAV_m), using an individual particle analysis technique. A mass balance type model for PAV_m, partitioned according to the contributions of four size classes, is developed and tested for Cayuga Lake, New York, supported by long-term monitoring of PAV_m in the lake and its primary tributaries. The model represents the source of PAV_m of tributary inputs and three in-lake loss processes: (1) size-dependent settling, (2) enhancement of settling through aggregation, and (3) filter feeding by dreissenid mussels. The central roles of major runoff events and localized external loads of minerogenic sediment at one end of the lake in driving patterns of PAV_m in time and space are successfully simulated, including (1) the higher PAV_m levels in a shallow area ("shelf") adjoining these inputs, relative to pelagic waters, following runoff events; and (2) the positive dependence of the shelf increases on the magnitude of the event. Analyses conducted with the model establish that settling, with aggregation enhancement, dominates the loss of PAV_m from the water column of the shelf, while mussel filtration increases in relative importance in pelagic waters. The utility of PAV_m predictions to quantify the effects of these particles on optical and phosphorus concentration metrics of water quality is established.

Keywords Minerogenic particles · Runoff events · Settling · Aggregation · Mussel filtration · Water quality

R. K. Gelda · S. W. Effler (✉) · A. R. Prestigiacomo · F. Peng
Upstate Freshwater Institute, P.O. Box 506, Syracuse, NY 13214, USA
e-mail: sweffler@upstatefreshwater.org

J. M. Watkins
Cornell Biological Field Station, Department of Natural Resources, Cornell University, 900 Shackleton Pt. Road, Bridgeport, NY 13090, USA

S. Chapra
Department of Civil and Environmental Engineering, Tufts University, 113 Anderson Hall, 200 College Avenue, Medford, MA 02155, USA

1 Introduction

Minerogenic particles, such as clay minerals, quartz, and calcite, have important water quality and ecological impacts on lakes and reservoirs. Specific issues include their effects on (1) the level of light scattering and thereby optical metrics of water quality (Peng et al. 2009a; Peng and Effler 2010; Effler and Peng 2014) and the remote sensing signal (Binding et al. 2007, 2012); (2) metabolic activity and the composition of biological communities (Phlips et al. 1995; Newcombe 2003); (3) transport, cycling, and apportionment of forms of nutrients (Hupfer et al. 1995; Effler et al. 2014) and contaminants (O'Connor 1988; Chapra 1997); and (4) net sediment accumulation (Gelda et al. 2013). These particles have three potential sources,

6.2. **Peer-reviewed Manuscript:** Effler SW, Prestigiacomo AR, Peng F, Gelda RK, Matthews DA. 2014. Partitioning the contributions of minerogenic particles and bioseston to particulate phosphorus and turbidity. Inland Waters. 4:179-192 (appeared previously as subsection 5.1)

Selected Salient Findings:

- An empirical model to partition the contributions of PAV_m and Chl-*a* to PP and Tn are developed, perform well, and perform well in tracking PP and Tn in time and space
- PAV_m is again shown to be an important component, contributing more on the shelf than in pelagic waters, particularly after PAV_m inputs from runoff events
- The particle populations supporting the analysis originate from eight years of in-lake monitoring of these portions of Cayuga Lake
- Elevated levels of PAV_m on the shelf site following runoff events caused the PAV_m to make increased contributions to PP and Tn
- These contributions to PP ($PP_{m/u}$) are not representative of trophic state
- The contributions of minerogenic particles to $PP_{m/u}$ and turbidity (Tn) dominate during runoff events

Article

Partitioning the contributions of minerogenic particles and bioseston to particulate phosphorus and turbidity

Steven W. Effler, Anthony R. Prestigiacomo*, Feng Peng, Rakesh Gelda, and David A. Matthews
Upstate Freshwater Institute, PO Box 506, Syracuse, NY 13214
** Corresponding author email: tonyp@upstatefreshwater.org*

Received 19 August 2013; accepted 8 January 2014; published 17 April 2014

Abstract

Protocols to partition the contributions of bioseston and minerogenic particles to turbidity (T_n) and particulate phosphorus (PP), as described by summations of the 2 components, are developed, tested, and applied. The analysis is based on coincident observations of T_n, PP, chlorophyll *a* (Chl), and the summation of the projected areas of individual minerogenic particles per unit volume (PAV_m) for the wide variations encountered in time and between near-shore and pelagic sites over an 8-year study of Cayuga Lake, New York. PAVm was determined from an individual particle analysis technique, scanning electron microscopy interfaced with automated image- and X-ray analyses (SAX). The partitionings are based on a stoichiometric approach that adopts Chl and PAV_m as the metrics of bioseston and minerogenic particles, respectively, and estimates developed here for stoichiometric ratios that relate T_n and PP to these 2 components. The systematically higher T_n and PP levels at the near-shore site, particularly following runoff events, are demonstrated to be a result of elevated PAV_m associated with allochthonous inputs. A reasonably good match of the partitioned 2-component summations with bulk observations is reported. Application of the 2-component PP model establishes minerogenic particles made, on average, noteworthy (~10%) to substantial (≥20%) contributions to PP. The minerogenic particle component of PP was largely responsible for the greater summer average total phosphorus (TP) concentrations at the near-shore versus the pelagic site, the interannual variations in the differences between these sites, and exceedance of the TP water quality limit at the near-shore site. Minerogenic particles were the dominant component of T_n, a finding that is demonstrated to be consistent with optical theory, based on the much greater efficiency of side-scattering for minerogenic versus organic particles.

Key words: bioavailability, bioseston, minerogenic particles, particulate phosphorus, stoichiometry, turbidity

Introduction

Minerogenic (inorganic) particles play important ecologic and water quality roles in aquatic ecosystems by presenting reactive surfaces (O'Connor 1988, Hupfer et al. 1995), affecting the concentrations and stoichiometry of particulate constituents (Hecky et al. 1993, Effler et al. 2012), influencing metabolic activity (Phlips et al. 1995), contributing to net sedimentation (Bloesch 2004), and degrading optical water quality through the process of light scattering (Kirk 1985, Peng and Effler 2011). Sources of these particles to the water columns of lakes and reservoirs include allochthonous inputs from watersheds (Longabucco and Rafferty 1998), autochthonous production of oversaturated mineral phases (Yin and Johnson 1984, Homa and Chapra 2011), and sediment resuspended from bottom deposits (Bloesch 2004, Peng and Effler 2010). Water quality monitoring programs often do not include direct measurement of minerogenic particle assemblages, and those that do have primarily relied on gravimetric measurements: the mass remaining on a filter (per unit volume of sample) after exposure to a high temperature to burn off organic contributions. Such measurements have precision issues

DOI: 10.5268/IW-4.2.681

Section 7. Hydrothermal/Transport and Water Quality Modeling of Cayuga Lake

7.1. Introduction: Phosphorus, cultural eutrophication, bioavailability of phosphorus, and modeling

Cultural eutrophication remains a major contemporary water quality and ecological issue for lakes, despite advancements in the control of nutrient sources over the last four decades (Cooke et al. 2005). Control of phosphorus (P) from watershed and tributary inputs is a primary management objective because it is the nutrient limiting phytoplankton growth in the vast majority of temperate inland waters (Hutchinson 1973, Sondergaard et al. 2007, Wetzel 2001, Chapra 1997), including Cayuga Lake (Schaffner and Oglesby 1978, Effler et al. 2010), the subject of this study. Accordingly, the biogeochemistry of this element has received substantial research attention (Wetzel 2001). Phosphorus cycling is made complex by the large number of forms, processes, and transformations involved. Early studies and related models (Chapra 1997, Vollenweider 1976) to guide management often considered only the concentration of total P (TP) with respect to inputs and the in-lake pool of this critical nutrient. Partitioning of multiple forms of P became important in a management context as the differences in their potential to support primary production were recognized (DePinto et al. 1981, Reynolds and Davies 2001, Reynolds 2006, Baker et al. 2014, Joosse and Baker 2011). Phosphorus that is available to support algal and cyanobacterial production is described as bioavailable (Fishman et al. 2009, Auer et al. 1998, DePinto et al. 1981, Young et al. 1982, Young et al 1985).

Mechanistic mass balance P – phytoplankton (or eutrophication) models are widely used to guide management deliberations for lakes with eutrophication issues, and are critical tools for supporting total maximum daily load (TMDL) analyses (Cooke et al. 2005, Munoz-Carpena et al. 2006). The “mechanistic” descriptor implicitly reflects the effort to utilize realistic process-based representations of lacustrine systems in the model structure. A broad range of model complexity (e.g., number of processes and interactions considered) has been adopted in contemporary modeling efforts (Zhao et al. 2012, Hipsey et al. 2006, Gal et al. 2009, Arhonditsis et al. 2005, Flynn et al. 2015, Arhonditsis et al. 2006, Arhonditsis and Brett 2004, Chapra 1997, Robson 2014). Despite myriad differences in structural detail, these models generally share certain features, including: (1) external loading of multiple forms of P, (2) other environmental forcing conditions (e.g., light and temperature), (3) transport and mixing processes, and (4) the processes and associated kinetics that regulate P cycling and phytoplankton growth and loss processes. Additionally, a model must represent important system-specific characteristics, including prominent features of the resident biological communities. During the development of the water quality sub-model it is important to balance model representativeness with model complexity to obtain the best model reliability (Chapra 2003). This concept of parsimony has been integrated into the modeling work conducted as part of this project.

The phytoplankton community is a primary target for the simulation capabilities of mechanistic P-eutrophication models (Chapra 1997). Representative predictions of the concentration of phytoplankton biomass, and in some cases community composition, are goals of these modeling initiatives. Moreover, the interplay between zooplankton and phytoplankton dynamics (Wetzel 2001) may require representation of both communities for successful simulations. Accordingly, it may be important to have contemporary robust characterizations of both the phytoplankton and zooplankton communities to guide related structural features of a system-specific model. Phytoplankton abundance is a primary indicator of water quality indicator. Phytoplankton taxa vary with respect to nutrient requirements, growth rates, edibility by zooplankton, and end up in different places in the lake basin when they die and decompose (Reynolds 2006).

Zooplankton differ in how efficiently they consume phytoplankton, and in the taxa of phytoplankton they capture and ingest (Wetzel 2001). Water bodies with high densities of phytoplankton are turbid, affecting aesthetic quality and decreasing light penetration, with effects on the growth of rooted macrophytes and the ability of fish to locate their prey. Cyanobacteria, a common component of phytoplankton in phosphorus-enriched lakes, can cause nuisance conditions. Daphnia, a genus of cladoceran zooplankton, is a generalist, highly efficient filter-feeder with the capability of driving phytoplankton to very low densities, even when nutrient concentrations are high (Lampert et al. 1986). In contrast, herbivorous copepods are selective feeders that do not generally consume cyanobacteria and do not have a marked effect on phytoplankton densities. For these reasons, monitoring the abundance and taxonomic composition of both phytoplankton and zooplankton provides critical information for understanding the biological basis for phytoplankton response to nutrient enrichment in lakes, and for the broader impacts of plankton in the lake ecosystem. Zooplankton monitoring conducted as part of the Phase 1 work showed the zooplankton population is dominated by non-daphnid cladocerans and copepods, which migrate between the epilimnion and hypolimnion. These zooplankton are also inefficient in the mechanics of their feeding. The Phase 1 data are consistent with earlier characterizations of the zooplankton community of Cayuga Lake (Barlow and Bishop et al. 1965).

The seasonal dynamics of phytoplankton and zooplankton in Cayuga Lake in 2013 (UFI 2014) were unremarkable and largely consistent with the general Plankton Ecology Group (PEG) model description of lake plankton dynamics (Sommer et al. 1986, Sommer et al. 2012). A spring diatom bloom is typical of large lakes with a turbulent epilimnion that keeps these heavy silica-rich cells suspended. The termination of the spring bloom by a combination of silica limitation and an increase in grazing zooplankton is also typical of north-temperate zone lakes. A typical seasonal progression includes a mixed summer phytoplankton assemblage of chlorophytes, chrysophytes, and cryptophytes, followed by cyanobacteria and

dinoflagellates/zooplankton as the lake continues to warm; however, none of these groups were abundant in Cayuga Lake during 2013 (UFI 2014).

Dense populations of invasive dreissenid mussels have been demonstrated to have substantial water quality and ecological impacts associated with various aspects of their metabolism, including grazing, excretion and respiration (Higgins et al. 2010, Nalepa and Schloesser 2014). In a meta-analysis including several North American and European Lakes, mussel grazing of phytoplankton was associated with significant decreases in Chl-*a* and higher water clarity (Higgins et al. 2010). Initially, zebra mussels, which prefer shallow rocky substrates, were the dominant species. Zebra mussels have been largely replaced by quagga mussels in many deep systems (Watkins et al. 2007, Nalepa et al. 2009), as they tolerate colder temperatures, soft substrates, and reduced abundance of food. Filtering by the large biomass of deep dwelling quagga mussels was implicated in the disappearance of spring phytoplankton blooms in Lake Michigan in the early 2000's (Vanderploeg et al. 2010). The first detection of dreissenid mussels in Cayuga and Seneca Lakes was in 1991 (zebras) and 1994 (quaggas), closely following the Great Lakes expansion. By 2006, quagga mussels had largely replaced zebra mussels in Cayuga Lake and are abundant at depths extending to 100 meters (Watkins et al. 2012). This benthic survey was updated during Phase 1 CLMP investigations, resulting in detailed results of spatial distributions of dreissenid mussels as documented in the Phase 1 report (UFI 2014) and presented in subsection 7.6.3.2.

Dreissenid mussel excretion rates reported in the literature were recently reviewed by Bootsma and Liao (2014). Excretion of soluble reactive phosphorus (SRP) by dreissenid mussels at various temperatures was determined experimentally as part of Phase 1 (UFI 2014). The specific excretion rate (μmolP/gDW/hr) was calculated using the increase of SRP (concentration increase times water volume; μmolP), the dry weight biomass of the mussels (gDW), and the duration of the experiment (hours) (UFI, 2014). Phosphorus excretion by dreissenids is lower than that of other benthic macroinvertebrates and zooplankton (Sereda and Hudson 2011). Excretion by dreissenid mussels in shallow habitats of lakes has been identified as a phosphorus source enhancing growth of the nuisance algae *Cladophora* (Ozersky et al. 2009).

Partitioning external loads of P according to sources is fundamental information to support related rehabilitation initiatives, such as those guided by the TMDL analysis process or other management options (USEPA 1991). The bioavailability of P in external loads is increasingly incorporated in management and modeling initiatives (Effler et al. 2002, Effler et al. 2012, Boström et al. 1988, Lyon et al. 2006, Ekholm and Krogerus 2003, Ellison and Brett 2006). The bioavailability concept has been embraced in both the load estimation and modeling elements of this project (Prestigiacomo et al. 2016). Bioassays are conducted for the various forms of P to support estimates of the magnitudes of bioavailable P loads (Auer et al. 1998, Effler et al. 2012, Prestigiacomo et al. 2016). Accurate loading estimates also require: (1) an appropriate strategy

for sampling the tributary and point source inputs, and (2) application of appropriate calculation protocols (Defew et al. 2013). A focus on frequent sampling during runoff events is important, as a large portion of P loads carried by streams annually occurs over relatively brief intervals of high flow (Longabucco and Rafferty 1998, Richards and Holloway 1987). The development of relationships between concentrations and stream flows (Q), or other drivers such as temperature, is a central feature in supporting load calculations (Raymond and Saiers 2010, Vogel et al. 2003). These relationships provide a basis to estimate concentrations for intervals not covered by measurements.

The estimates of external loads serve to support testing of both lake water quality and watershed models. Watershed models provide critical management information, particularly for systems such as Cayuga Lake where external loads are regulated primarily by non-point sources rather than point sources. These modeling tools, once validated, can support realistic projections of loading changes to be expected by various land use management actions. Integration of these inputs to drive lake water quality projections provides an invaluable overall tool to support management deliberations related to potential improvements in lake quality.

The three common trophic state metrics are the concentrations of total phosphorus (TP), and chlorophyll *a* (Chl-*a*; a surrogate of phytoplankton biomass), and Secchi disk depth (Z_{SD}) (Chapra 1997). Phosphorus- eutrophication (P-eutrophication) models often support predictions of each of these, as they may be specified for related water quality guidelines or standards. Moreover, consistent changes in all three parameters are generally assumed (Carlson 1977, Hecky et al. 1993, Carlson and Havens 2005). For example, cultural eutrophication is expected to cause increases in Chl-*a* and TP and decreases in Z_{SD} (Wetzel 2001). Water quality standards intended to protect against cultural eutrophication are usually associated with a summer average value of one or more of these metrics, but most often TP.

There are limitations in the use of these parameters as reliable trophic state indicators and targets for management, as they can be importantly influenced by processes and constituents not directly coupled with primary production. For example, delivery of large quantities of sediment during runoff events will interfere with two of the common trophic state metrics, causing increases in TP and decreases in Z_{SD} that are not driven by increases in phytoplankton biomass. These temporarily high TP concentrations may not reflect potential for subsequent stimulation of phytoplankton growth because the dominant form of P may have only limited bioavailability (Prestigiacomo et al. 2016). A corresponding low Z_{SD} often is driven by sediment particles, rather than phytoplankton (Effler and Peng 2014, Peng and Effler 2015). The Chl-*a* measurement has no direct interference from the sediments (mostly minerogenic particles), but as a pigment it has substantial limitations as a metric of the concentration of phytoplankton biomass (Reynolds 2006). Runoff event driven sediment inputs can exacerbate challenges in interpretation of the trophic state metrics of TP (Prestigiacomo et al. 2016, Gelda et al. 2016b) and Z_{SD} (Effler and Peng 2014, Effler et al. 2016). Local impacts are encountered where large portions of the total

inflow, sediment, and multiple constituents are received along a modest portion of a lake's shoreline (Peng and Effler 2015, Gelda et al. 2016a,2016b), resulting in large differences between local nearshore and pelagic areas. Typically, phytoplankton gradients are not observed adjacent to large tributary inflows, as residence time is too short for substantial phytoplankton growth and mixing with the main body of the lake is adequate to reduce critical nutrient gradients relatively rapidly (Martin and McCutcheon 1999).

However, inorganic (or minerogenic) particles can complicate relationships between the trophic state metrics because they, like phytoplankton, have associated P and contribute to diminished Z_{SD} (Effler and Peng 2014, Effler et al. 2014). Accordingly, the effects of minerogenic particles need to be included in P-eutrophication modeling initiatives where they influence importantly the TP and Z_{SD} measurements. Otherwise, model predictions may not be reliable with respect to expectations in response to management actions. Indeed, systematic improvements in Z_{SD} are widely expected in response to management actions that are effective in reducing P loading and in-lake concentrations of P and phytoplankton biomass (Cooke et al. 2005).

7.2. Description of Cayuga Lake and watershed setting

A detailed description of Cayuga Lake and its watershed in the context of water quality and regulatory issues of concern can be found in subsections 1.1 and 7.3. Portions are repeated here for context with regard to modeling efforts. Cayuga Lake (42º 41′ 30″ N; 76º 41′ 20″ W) is the fourth easternmost of the New York Finger Lakes (Figure 7-1), and has the second largest surface area (172 km^2) and volume (9.4 x 109 m^8) of this group of lakes. The mean and maximum depths are 55 m and 133 m, respectively. This long and narrow system is positioned along a mostly north-south axis that coincides with prominent wind directions (Figure 7-1). Cayuga Lake has a warm monomictic stratification regime, stratifying strongly in summer through mid-fall, but only rarely developing complete ice cover (Schafner and Oglesby 1978). Internal seiches (e.g., lake-scale tilting of the metalimnion), internal waves (oscillations in stratified layers), and upwelling events occur in the lake in response to wind energy inputs that are promoted by its elongated shape and the prevailing wind direction (Effler et al. 2010). The average retention time of the lake, calculated by dividing its volume by the total volumetric inflow rate (e.g., completely mixed assumption, Rueda et al. 2006), is nine years.

Cayuga Lake is a P-limited mesotrophic lake (Effler et al. 2010, Schaffner and Oglesby 1978). Nearly 40% of the total tributary inflow to the lake enters the southern end, specifically from Fall Creek, Cayuga Inlet, and Sixmile Creek (Table 7-1; Figure 7-1). The localized entry of a large fraction of the tributary flow delivers locally high loads of various constituents to the southern end of the lake. In particular, large quantities of phosphorus (Prestigiacomo et al. 2016)

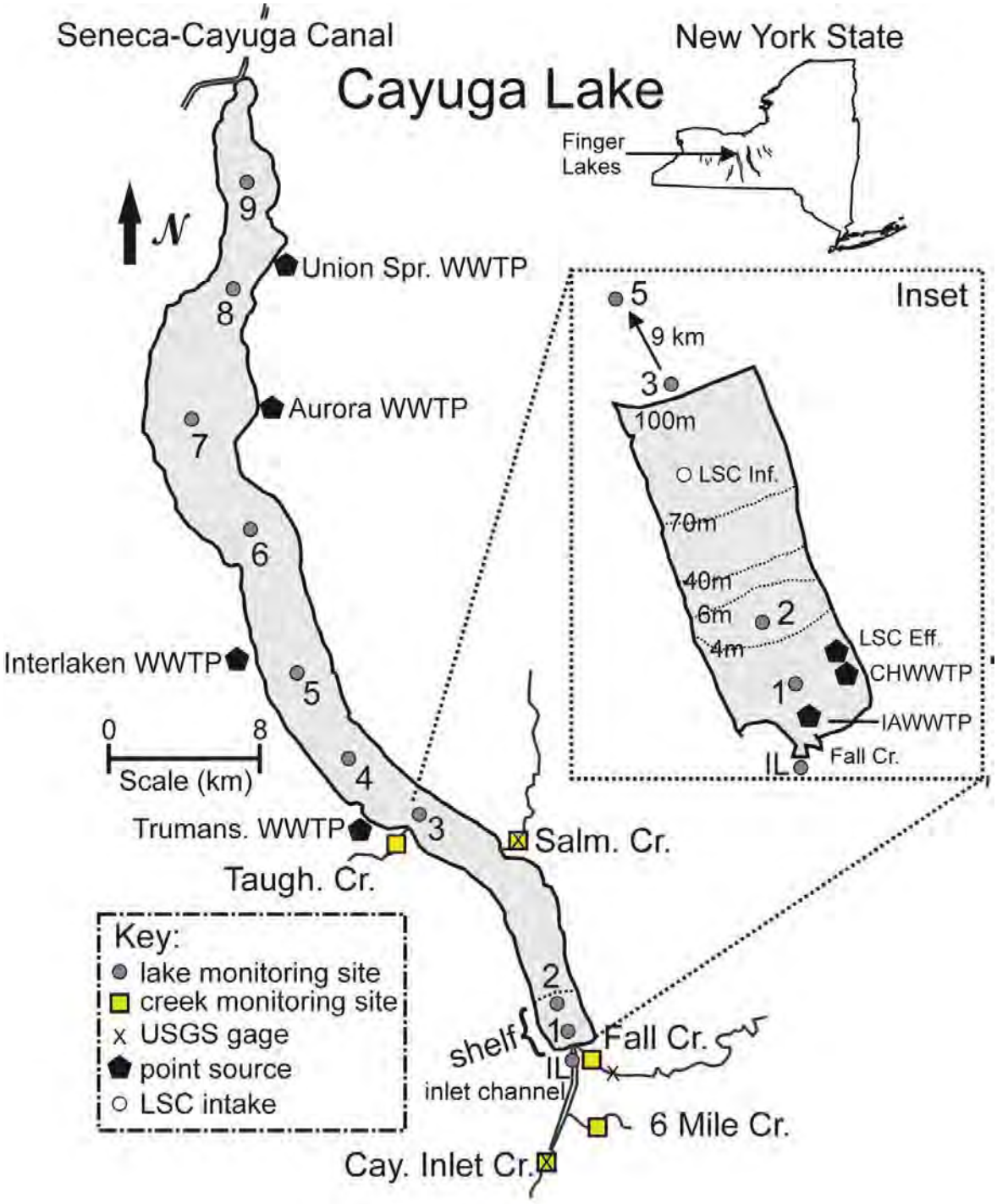

Figure 7- 1. Cayuga Lake, position within New York, and the eleven Finger Lakes. Shown are five monitored tributaries, WWTPs and Lake Source Cooling (LSC) facility discharges. Four USGS gages, and the shelf portion of the lake at its southern end.

Table 7- 1. Average stream flow, watershed areas, and land use for Cayuga Lake tributaries.

Tributary	Flow Information			Watershed		Land Use Percent[1]		
	USGS Gage	Record (years)	Mean Q (m^3/s)	Area (km^2)	%	A	F/B, R	U
Fall Creek	04234000	89	6.1	330.9	18%	49%	40%	11%
Cayuga Inlet[2]	04233255	77	2.7	240.8	13%	29%	56%	15%
Salmon Creek	0423401815	8	3.6	233.8	13%	68%	25%	7%
Taughannock Creek[3]	-	-	3.4	173.0	9%	49%	40%	11%
Sixmile Creek	04233300	19	2.1	134.1	7%	22%	63%	15%
Unmonitored Tributaries[4]	-	-	14.3	758.1	41%	62%	23%	15%
Total	**-**	**-**	**28.8**	**1870.7**	**100%**	**60%**	**26%**	**14%**

[1] A – agriculture, F/B – forest/brush, R – other rural, U – urban (from Haith et al. 2012);
[2] gage moved in 2011;
[3] ungaged, flow estimates from VSA watershed model (Archibald et al. 2014);
[4] estimated from product of total gaged flow (sum) and ungaged: gaged watershed area ratio.

and sediment (Peng and Effler 2015) are delivered to the southern end of the lake by these tributaries during runoff events. The "shelf" is the shallow (≤ 10 m), southernmost 2 km of the lake (Figure 7-1), and has generally been considered degraded relative to the pelagic zone (Oglesby 1978, Effler et al. 2010, Effler et al. 2014). Two other tributaries of noteworthy size enter the lake further north; Salmon Creek enters from the east and Taughannock Creek enters from the west (Figure 7-1). Effluent from two domestic wastewater treatment plants, Ithaca Area WWTP (IAWWTP) and Cayuga Heights WWTP (CHWWTP), and the discharge of spent cooling water from a "lake source cooling" (LSC) facility, also enter the southern end of the lake (Figure 7-1). Both WWTP facilities have been upgraded for enhanced phosphorus removal over the last decade. The LSC facility withdraws cold water from the pelagic zone at a depth of 73 meters to meet cooling demands for Cornell University and returns the spent cooling water to the "shelf" (Figure 7-1). Thirty smaller streams, draining ~ 40% of the overall watershed, flow into the lake. Agricultural land use is particularly high in the Salmon Creek watershed (68%), but is also substantial in Fall Creek and portions of the watersheds with small tributaries (Table 7-1). See Section 8 for additional land use information.

7.3. Regulatory setting

The New York State Department of Environmental Conservation listed the southern end of Cayuga Lake (e.g., shelf) as an impaired segment with respect to phosphorus and silt/sediment in 2002 ("*The Proposed Final New York State 2016 Section 303(d) List of Impaired Waters*

Requiring a TMDL/Other Strategy"). The water quality concerns identified for the shelf include high concentrations of P and sediment, which are qualitatively consistent with elevated loads of these constituents received during runoff events from the local streams (Peng and Effler 2015, Prestigiacomo et al. 2016).

The New York State guidance value for TP is a summer (June-September) average concentration of 20 μg/L. Irregular exceedance of this guidance value on the shelf (Effler et al. 2014), but not in pelagic waters, was apparently the basis for identifying elevated P levels on the shelf as a water quality management issue (cultural eutrophication). Since the late 1990s the guidance value for TP has been exceeded irregularly on the shelf, but not in pelagic waters (Effler et al. 2010). Establishment of a Total Maximum Daily Load (TMDL) for P is intended to protect the shelf from the symptoms of cultural eutrophication by maintaining the summer average TP concentration at ≤ 20 μg/L in that area.

Lake monitoring at sites on the southern shelf and in pelagic waters have been conducted since the late 1990s. In 2013, the most intensely monitored year, the number of pelagic sampling locations along the main axis of the lake was greatly increased. High frequency monitoring conducted in 2013, combined with the 1990s monitoring results have established that two trophic states metrics, TP and Z_{SD}, are significantly higher and lower, respectively, on the shelf compared with pelagic waters (UFI 2014). In addition, Chl-*a* concentrations are not significantly different between the shelf and pelagic waters (UFI 2014, Effler et al. 2010). These primary conclusions were documented as part of the Phase 1 work (UFI 2014).

Findings from the study of Cayuga Lake have supported a unified scientific position of the absence of a reliable signature of cultural eutrophication for the water column of the shelf (UFI 2014, Effler et al. 2010, 2014, Peng and Effler 2015), despite frequently high TP levels. A listing of these consistent analyses that were also integrated into the mechanistic models includes:

(1) the coupling of both high TP and lower Z_{SD} on the shelf compared to pelagic water, particularly following runoff events, but without noteworthy differences in Chl-*a* (Effler et al. 2010, 2014),
(2) high PP: Chl-*a* ratios on the shelf compared to pelagic waters (Effler et al. 2010, 2014, Peng and Effler 2015),
(3) a low bioavailable fraction value (f_{BAP} = 0.02) for a shelf PP sample collected after a major runoff event (Prestigiacomo et al. 2016, Gelda et al. 2016b),
(4) low f_{BAP} values for PP delivered in large quantities from the shelf tributaries (PP dominates TDP) during runoff events (Prestigiacomo et al. 2016, Gelda et al. 2016b),
(5) coincident and strong positive relationship of high PAV_m and $PP_{m/u}$ levels on the shelf following runoff events (Peng and Effler 2015),

(6) a successful empirical model for temporal and spatial patterns of $PP_{m/u}$ in the lake based on paired PAV_m and Chl-*a* observations (Effler et al. 2014),
(7) a validated mechanistic $PP_{m/u}$ model (Gelda et al. 2016b), for which CE-QUAL-W2 serves as the transport submodel, made clear $PP_{m/u}$ (biologically unavailable PP) is generally higher on the shelf than in pelagic waters, but particularly after runoff events, and is responsible for the irregular exceedances of the 20 g/L summer average TP standards on the shelf. Adjustment(s) for the localization of the unavailable form of P ($PP_{m/u}$) were recommended to avoid misuse of traditional TP measurements in an effort to protect against cultural eutrophication (Gelda et al. 2016b).
(8) application of the transport sub-model separately established that rapid flushing on the shelf prevails (Gelda et al. 2015), relative to phytoplankton growth rates, providing an additional feature resisting local phytoplankton blooms (Martin and McCutcheon 1999) and noteworthy shelf versus pelagic waters differences in phytoplankton
(9) the demonstrated performance of the CLM-2D model is consistent with the other above considerations, but of greater individual importance based on its more complete representation of the system.

7.4. Modeling approach: Goals and phasing

The overarching goal of this study was to develop and test a water quality P-eutrophication model for Cayuga Lake. Phase 1 included monitoring lake and tributary water quality, setup and testing of a 2-D hydrothermal/transport model, and setup and testing of a watershed/land use model. Phase 1 results were documented in the Phase 1 final report (UFI 2014). Phase 2 included enhancing the hydrothermal/transport model and development and testing of the lake water quality model. The integrated model (hydrothermal/transport with water quality; CLM-2D) is capable of supporting a phosphorus TMDL analysis for Cayuga Lake, including the southern shelf. The model incorporates the bioavailability concept for external P inputs and the potential importance of the phytoplankton, zooplankton, and dreissenid mussel communities. Sections 7.5-7.7 of this report describe the design, calibration, and validation of the water quality model as well as preliminary results from example management scenarios.

7.5. Hydrothermal/transport modeling

7.5.1. Model overview

A model is a theoretical construct that assigns numerical values to parameters and relates external inputs or forcing conditions to system variable responses (Thomann and Mueller 1987, Chapra 1997). CLM-2D is a two dimensional model composed of a hydrothermal/transport sub-model and water quality sub-models. The two-dimensional hydrothermal/transport sub-model used in CLM-2D is the hydrothermal/transport sub-model in CE-QUAL-W2, a public access model developed by the U.S. Army Corps of Engineers (Cole and Wells 2015). The

hydrothermal/transport sub-model was setup and tested during Phase 1 (version 3.70; UFI 2014; Gelda et al. 2015) and subsequently upgraded to version 3.72. Performance of the hydrodynamic sub-model, which underlies the water quality model, is documented in this report. The two-dimensional transport model simulates the thermal stratification regime and mixing/transport processes in the vertical and longitudinal dimensions. The hydrothermal/transport sub-model was calibrated for 2013 conditions, and validated for the 1998- 2012 period through continuous simulations (UFI 2014; Gelda et al. 2015). This Phase 2 report focuses on the calibration year of 2013 and two validation years, 1999 and 2006.

The time and space features of the hydrothermal/transport model are consistent with the water quality issues identified for Cayuga Lake (UFI 2014), particularly the effects of runoff events and the differences between the shelf and pelagic areas. The model is capable of representing various transport processes that may be noteworthy with regards to the water quality issues of the lake, including the residence time of local tributary inputs on the shelf, the seasonal plunging of tributaries, and vertical transport from the hypolimnion to the photic zone.

The hydrothermal/transport sub-model of CE-QUAL-W2 uses laterally averaged two dimensional (vertical and longitudinal) equations of fluid motion. Inherent in this framework is the assumption of uniform lateral mixing in each segment. For a complete treatment on hydrodynamics and transport, numerical solution schemes, and other auxiliary functions, refer to the user manual for CE-QUAL-W2 (Cole and Wells 2015).

The general data requirements of the hydrothermal/transport model are: (1) geometric data (bathymetry, model cell dimensions, elevation, area, volume); (2) meteorological data (hourly; air and dew point temperature, wind velocity and direction, cloud cover or solar radiation); (3) hydrologic data (tributary inflows, outflows, and water surface elevation); (4) temperatures of the lake and its tributaries; (5) hydrodynamic and kinetic coefficients; and (6) other data such as structural details of withdrawal works.

7.5.2. Governing equations

CE-QUAL-W2 uses laterally-averaged two-dimensional (vertical and longitudinal) equations of fluid motion (Edinger and Buchak 1975). Inherent to this framework is the assumption of uniform lateral mixing in the cross channel direction. The basic equations that describe horizontal momentum, free water surface elevation, hydrostatic pressure, continuity, equation of state, and constituent transport (temperature in this application) are presented here.

7.5.2.1. Horizontal momentum

Eq. 7- 1

$$\frac{\partial UB}{\partial t}+\frac{\partial UUB}{\partial x}+\frac{\partial WUB}{\partial z}=-\frac{1}{\rho}\frac{\partial BP}{\partial x}+\frac{\partial\left[BA_x\frac{\partial U}{\partial x}\right]}{\partial x}+\frac{\partial B\tau_x}{\partial z}$$

where

U = longitudinal, laterally averaged velocity, m/sec
B = waterbody width, m
t = time, sec
x = longitudinal Cartesian coordinate: x is along the lake centerline at the water surface, positive to the right
z = vertical Cartesian coordinate: z is positive downward
W = vertical, laterally averaged velocity, m/sec
ρ = density, kg/m^3
P = pressure, N/m^2
A_x = longitudinal momentum dispersion coefficient, m^2/sec
τ_x = shear stress per unit mass resulting from the vertical gradient of the horizontal velocity, U, m^2/sec^2

The first term represents the time rate of change of horizontal momentum, and the second and third terms are the horizontal and vertical advection of momentum. The first term on the right hand side (RHS) of Eq. 7.1 is the force imposed by the horizontal pressure gradient. The second term on the RHS is the horizontal dispersion of momentum, and the third term is the force due to shear stress.

7.5.2.2. Constituent transport

Eq. 7- 2

$$\frac{\partial B\phi}{\partial t}+\frac{\partial UB\phi}{\partial x}+\frac{\partial WB\phi}{\partial z}-\frac{\partial\left[BD_x\frac{\partial\phi}{\partial x}\right]}{\partial x}-\frac{\partial\left[BD_z\frac{\partial\phi}{\partial z}\right]}{\partial z}=q_\phi B+S_\phi B$$

where

ϕ = laterally averaged constituent concentration, g/m^3
D_x = longitudinal temperature and constituent dispersion coefficient, m^2/sec
D_z = vertical temperature and constituent dispersion coefficient, m^2/sec
q_ϕ = lateral inflow or outflow mass flow rate of constituent per unit volume, $g/m^3/sec$
S_ϕ = kinetics source/sink term for constituent concentrations, $g/m^3/sec$

Each constituent has a balance as in Eq. 7.2 with specific source and sink terms. The first term in Eq. 7.2 represents the time rate of change of constituent concentrations and the second and third terms are the horizontal and vertical advection of constituents. The fourth and fifth terms are the horizontal and vertical diffusion of constituents. The first term on the RHS is the

lateral inflow/outflow of constituents, and the second term represents kinetic source/sink rates for constituents.

7.5.2.3. Free water surface elevation

Eq. 7- 3
$$\frac{\partial B_\eta \eta}{\partial t} = \frac{\partial}{\partial x}\int_\eta^h UBdz - \int_\eta^h qBdz$$

where

B_η = time and spatially varying surface width, m
η = free water surface location, m
h = total depth, m
q = lateral boundary inflow or outflow, m^3/sec

7.5.2.4. Hydrostatic pressure

Eq. 7- 4
$$\frac{\partial P}{\partial z} = \rho g$$

where

g = acceleration due to gravity, m/sec^2

7.5.2.5. Continuity

Eq. 7- 5
$$\frac{\partial UB}{\partial x} + \frac{\partial WB}{\partial z} = qB$$

7.5.2.6. Equation of state

Eq. 7- 6
$$\rho = f\left(T_w, \phi_{TDS}, \phi_{SS}\right)$$

where

$f(T_w, \phi_{TDS}, \phi_{SS})$ = density function dependent upon temperature, total dissolved solids or salinity, and suspended solids

The six equations result in six unknowns: (1) free water surface elevation, η; (2) pressure, P; (3) horizontal velocity, U; (4) vertical velocity, W; (5) constituent concentration, ϕ; and (6) density, ρ. Lateral averaging eliminates the lateral momentum balance, lateral velocity, and Coriolis acceleration. The solution of the six equations for the six unknowns forms the basic model structure.

7.5.3. Geometric data

CLM-2D requires the same geometric data as CE-QUAL-W2 (Cole and Wells 2015). These data define the finite difference representation of a water body. The finite difference representation consists of a number of vertical layers and longitudinal segments. The grid formed by these layers and segments (cells) is called the computational grid. The geometry of the computational grid is determined by three parameters: (1) longitudinal spacing, (2) vertical spacing, and (3) average cross-sectional width. Bathymetric data were obtained from Cornell University. Segment boundaries were first established on contour maps for the lake. Dimensions for each of the computational cells were then obtained from analysis of the bathymetric data.

The computation grid was updated during the upgrade from CE-QUAL-W2 version 3.70 (as described in the Phase 1 Report; UFI 2014) to version 3.72. The model segmentation was reduced from 50 to 25 horizontal segments while the vertical spacing of layers (i.e, height) was remained at 1 meter (Figures 7-3 and 7-4). The change in segmentation significantly decreased the run time with minimal effects on the model fit (Tables 7.8 and 7.9; subsection 7.5.5. "*Review of Hydrothermal/transport Model Updates*").

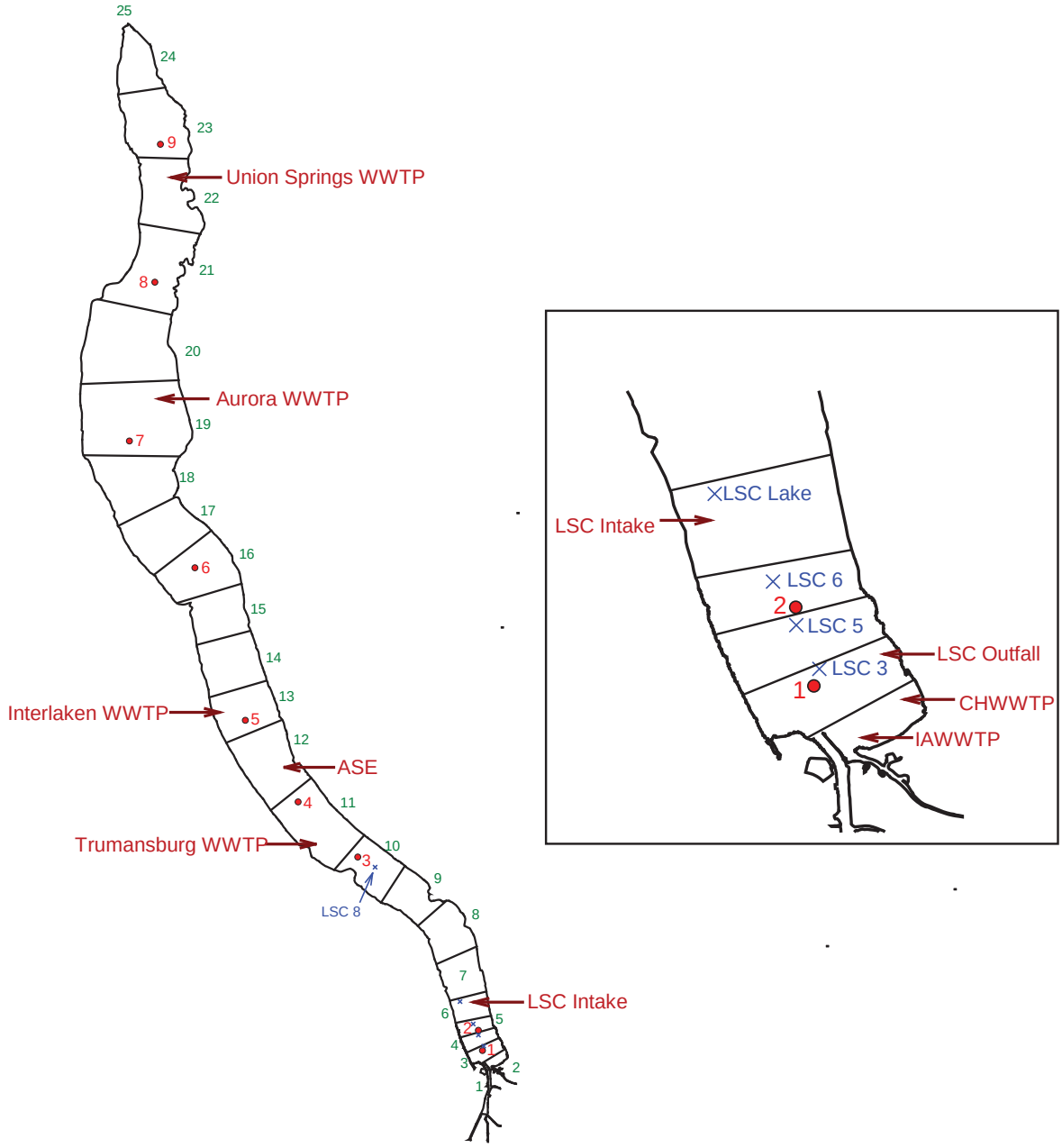

Figure 7- 2. Cayuga Lake for Phase 2 (a) longitudinal segments (25) for the entire lake as adopted in the model. Additionally, the site names (LSCx) for prior years (1998 – 2012) of monitoring, the 2013 sampling sites (circle with number) and the external inputs (arrows) to each segment are shown.

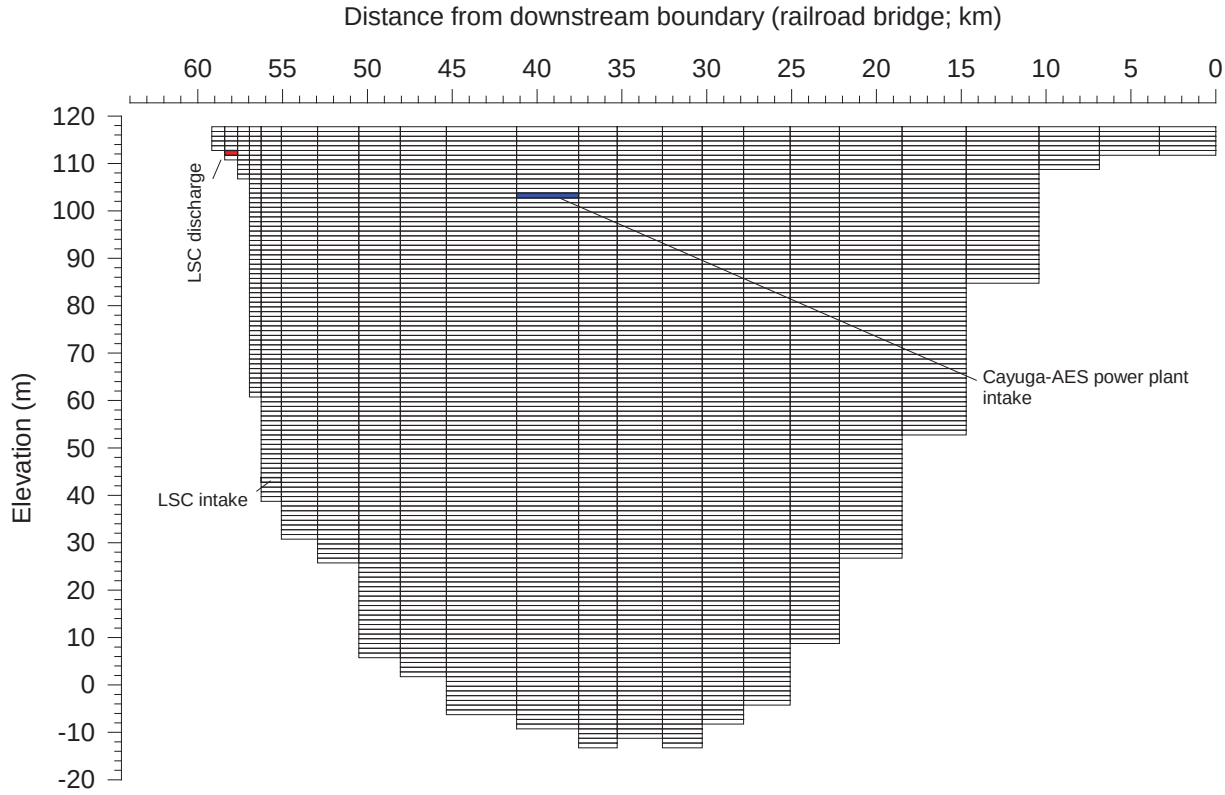

Figure 7- 3. Longitudinal and vertical computational grid of Cayuga Lake adopted in CLM-2D. Model cell with LSC intake, LSC discharge, and Cayuga-AES power plant intakes identified.

7.5.4. Development and specification of hydrothermal model drivers and coefficients

The primary drivers for CLM-2D fall into one of three types: (1) hydrologic, (2) meteorological, and (3) constituent loading (Table 7-3). Several of the major tributaries that enter the lake are presently continuously gaged by the United States Geological Survey (USGS; Table 7-3). The longest record is for Fall Creek (since 1925). Lake surface elevation is also monitored by the USGS. Estimates of overall tributary inflow and lake level are embedded in the hydrologic budget maintained within the model. Meteorological measurements are critical to drive the hydrothermal/transport sub-model. Incident light is utilized in the phytoplankton growth sub-model. These measurements are available from a proximate location on Cornell

campus (hourly since 1987), and from a site on the lake at its southern end (15 min. intervals) since 2011 (Table 7-3).

7.5.4.1. Meteorological data

CLM-2D requires hourly average air temperature, dew point temperature, wind velocity and cloud cover (or solar radiation) data to calculate surface heat exchange and wind stress. Three meteorological stations are located near Cayuga Lake; two stations belong to Cornell University (the "pile cluster" meteorological station and the Game Farm Road meteorological station) and the third station is a NOAA station that collects data from the Ithaca Airport. These data are available for different periods (Table 7-2, Appendix D of the Phase 1 report). These stations provided on-site hourly measurements of air temperature, dew point temperature, wind speed and direction, and total incident solar radiation. The meteorological inputs are presented as time-series for the calibration year of 2013 (Figure 7-4). Time-series of meteorological inputs for the validation years are available in Appendix 2 (1999 (Figure A7-1) and 2006 (Figure A7-2)).

Table 7- 2. Primary model drivers for CLM-2D.

Driver Type	Location	Availability	Notes
Meteorological	piling cluster (Cornell University)	10/27/2011-12/31/2013	10 minute frequency; missing data (T_{air} and T_{dew} 1/3/2013 – 5/13/2013 filled in from Ithaca Airport
	Game Farm Road (Cornell University)	1987-2013	Hourly frequency; missing data (0.8% days) were filled in from Ithaca Airport data
Hydrological	Fall Creek	flow record 1925-present	Temperature record 9/21/2011-11/18/2011; 5/13/2013 -11/1/2013
	Cayuga Inlet	flow record 1937-9/30/2011; 6/1/2012-present	5/9/2013-11/13/2013
	Salmon Creek	flow record 2006 - present	limited during 2013
	Sixmile Creek	flow record 1995 - present	limited during 2013
	Taughannock Creek	Pro-rated according to Fall Creek flow/watershed area	--
	ungaged inflows	Pro-rated according to Fall Creek flow/watershed area	--
temperature	Fall Creek	2013	estimated 1999, 2006
	Cayuga Inlet	2013	estimated 1999, 2006
	Salmon Creek	2013	estimated 1999, 2006
	Sixmile Creek	2013	estimated 1999, 2006
	Taughannock Creek	2013	estimated 1999, 2006
	ungaged inflows	2013	estimated 1999, 2006

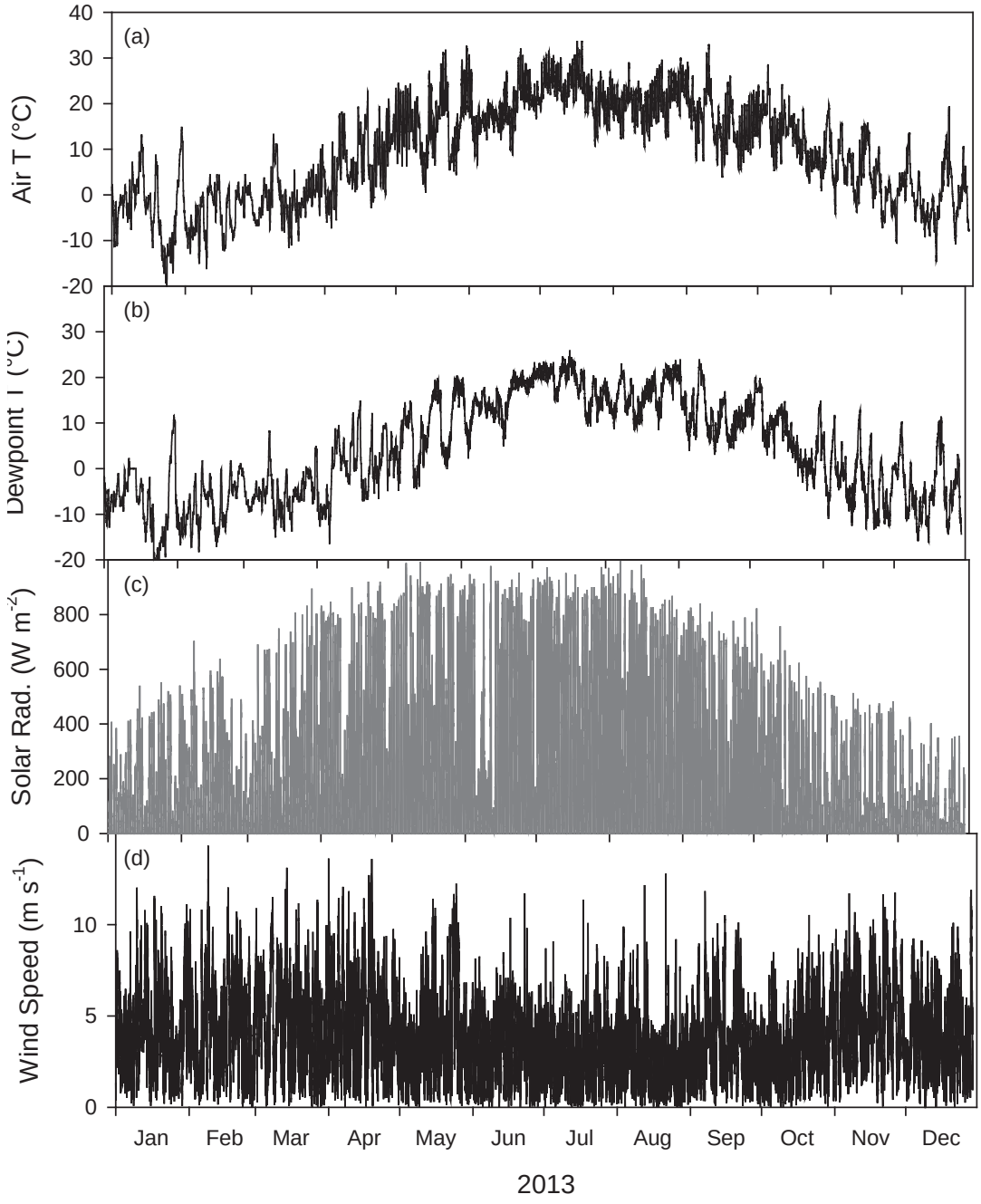

Figure 7- 4. Time-series of hourly meteorological data for Cayuga Lake for the model calibration year of 2013: (a) air temperature, (b) dew point temperature, (c) solar radiation, and (d) wind speed. This data is a combination of available data from 3 meteorological stations (see documentation in Phase 1 Report Appendix D).

7.5.4.2. Flow budget

CLM-2D requires the same meteorological data as CE-QUAL-W2 (Cole and Wells 2015). CE-QUAL-W2 (Cole and Wells 2015) requires specification of daily average inflows from tributaries, outflows, withdrawals, and water surface elevation. A hydrologic flow budget was constructed for Cayuga Lake for the period 1987 – 2013 from the available inflow and storage data. Imbalances in the hydrologic budget were attributed to uncertainty in the estimation of ungauged inflows and outflows as well as potential inflow from the Seneca River to the north end of Cayuga Lake. A summary of the tributaries monitored in this study, ranked according to watershed area, is presented in Table 7-3. A map of Cayuga Lake, including the 2013 sampling locations and the major tributaries is included as Figure 7-1.

The overall flow budget is shown in equation 7-7

Eq. 7- 7 $$Q_{in} - Q_{out,total} = \Delta$$

where:

Qin = is the sum of gaged stream flow (Qin, g), ungaged stream flow (Qin, ung;), and the point source inflows (Qin, pt.)

Qout, total = the sum of all point source outflows (Qout, pt) and outflow from the lake (Qout)

Δ = the change in water volume in the lake which is estimated from water surface elevation

Substituting into the equation

Eq. 7- 8 $$(Q_{in,g} + Q_{in,ung} + Q_{in,pt}) - (Q_{out,\ pt} + Q_{out}) = \Delta$$

USGS gaged daily flows (Qin,g, Eq. 7.8) were prorated by an adjustment factor to account for the portion of the watershed downstream of the gaging station (Table 7-4). These final adjusted flows (Figure 7-5 a-d) were used for all subsequent analyses and loading estimates. In most cases the adjustments were small (less than 8%), however the adjustment for Sixmile Creek was quite large (1.328; Table 7-4) because the Sixmile Creek gage at Bethel Grove (04233300) only accounts for 75% of the total watershed area.

Fall Creek, the largest tributary to Cayuga Lake, has a watershed area of 330.9 km2, which represents approximately 17.7 percent of the total Cayuga Lake watershed area (Haith et al. 2012). In addition to the four gaged tributaries (Table 7-3), Taughannock Creek was also monitored for constituents in Phase 1 (UFI 2014), but was ungaged for flow. Taughannock

Creek flows were estimated using Fall Creek flows and the ratio between the Fall Creek and Taughannock Creek watershed areas (Eq.7.9; Figure 7-5e).

Table 7- 3. Tributary watershed areas, flow statistics, and volume delivered in 2013 (UFI 2014).

Tributary	USGS Gage No.	Total Watershed Area (km^2)	Percent of Total Watershed (%)	Annual Mean Flow (m^3/s)	April-October Mean Flow (m^3/s)	April-October Volume (m^3)[f]
Fall Creek	04234000	330.9	17.7	5.95	4.96	9.18×10^7 (22%)
Cayuga Inlet Creek	04233255	240.8	12.9	2.69	2.09	3.86×10^7 (9%)
Salmon Creek	0423401815 [a]	233.8	12.5	3.75	2.36	4.36×10^7 (10%)
Taughannock Creek	- [b]	173.0	9.3	3.11	2.59	4.80×10^7 (11%)
Sixmile Creek	04233300	134.1	7.2	2.09	1.61	2.97×10^7 (7%)
Ungaged Tributaries	- [c]	758.2	40.5	11.98	9.28	1.72×10^8 (41%)
Total Watershed	- [d]	1870.7[e]	100	29.56	22.89	4.24×10^8

[a] Jan. 1 through Feb. 11 flows were estimated from product of Fall Creek flow and Salmon Creek to Fall Creek watershed areas, similar to Eq. 7-1.
[b] estimated from product of Fall Creek flow and Taughannock Creek to Fall Creek watershed areas.
[c] estimated from the difference between total watershed flow and monitored flow
[d] estimated from product of gaged flow and ratio of total watershed area to gaged watershed area
[e] fraction volume delivered parenthetically
[f] does not includes the Seneca-Cayuga Canal

Table 7- 4. Adjustment factors used to estimate total flows for each watershed (UFI 2014).

Tributary	USGS Gage No.	Gaged Watershed Area (km^2)	Total Watershed Area (km^2)	Percent Watershed Gaged	Adjustment Factor
Fall Creek	04234000	326.3	330.9	98.6%	1.014
Cayuga Inlet Creek	04233255	224.6	240.8	93.3%	1.072
Salmon Creek	0423401815	227.1	233.8	97.2%	1.030
Sixmile Creek	04233300	101.0	134.1	75.3%	1.328

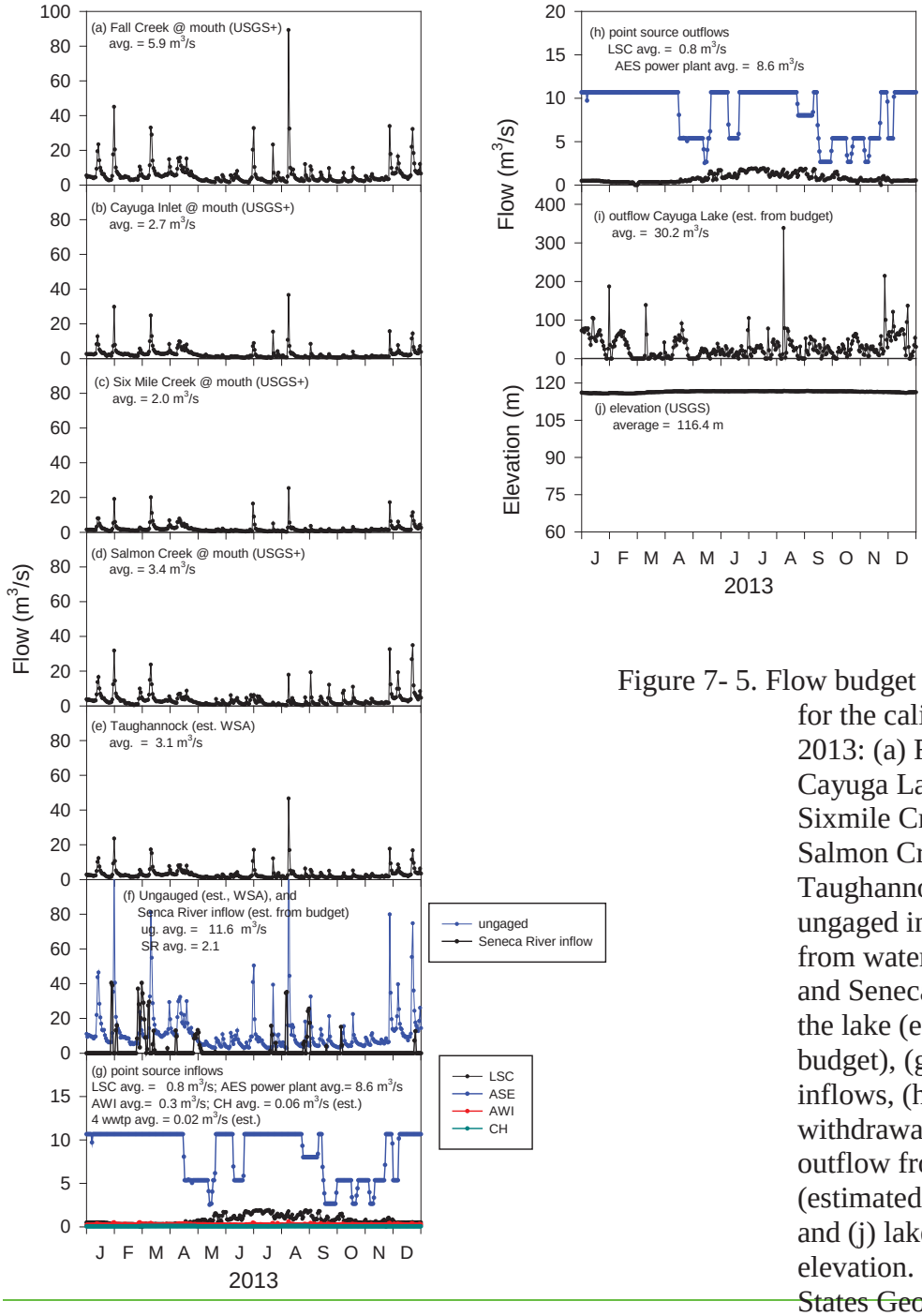

Figure 7- 5. Flow budget for Cayuga Lake for the calibration year of 2013: (a) Fall Creek flow, (b) Cayuga Lake Inlet flow, (c) Sixmile Creek flow, (d) Salmon Creek flow, (e) Taughannock Creek flow, (f) ungaged inflows (estimated from watershed area; WSA) and Seneca River inflows to the lake (estimated from flow budget), (g) point source inflows, (h) point source withdrawals, (i) overall outflow from Cayuga Lake (estimated from flow budget), and (j) lake water surface elevation. (USGS = United States Geological Survey, "+" = flow adjusted to creek mouth based on WSA).

Eq. 7- 9 $$Taughannock\ Creek\ Flow = Fall\ Creek\ Flow \cdot \frac{Taugh.Creek\ Area}{Fall\ Creek\ Area}$$

Point source inflows (Qin, pt, Eq 7.8, Figure 7-5 g) and outflows (Qout,pt, Eq. 7.8 Figure 7-5h) were measured or estimated. The change in water volume (Δ; Eq. 7.8) was estimated from a seven day average of the daily measured USGS water surface elevation (Figure 7-5 j) and Cornell's bathymetry. The total ungaged inflow (Qin, ung, Eq. 7.8) was estimated as the product of the gaged inflow times the ratio of the ungaged watershed area (from Haith et al., 2012) to the gaged watershed areas (Taughannock Creek included as gauged; Equation 7-10; Figure 7-5 f).

Eq. 7- 10 $$Total\ Ungaged\ Watershed\ Flow = Gaged\ Flow \cdot \frac{Total\ \text{Ungaged}\ Watershed\ Area}{Gaged\ Area}$$

Equation 7-8 was rearranged to solve for Qout Eq. 7.11.

Eq. 7- 11 $$Q_{out} = (Q_{in,g} + Q_{in,ung} + Q_{in,pt}) - Q_{out,\ pt} - \Delta$$

A flow budget was used to solve for outflows from the lake Qout (Figure 7-5 i). In 2013, the flow budget predicted negative outflows from the lake approximately 14% of the time. An assumption was made that allowed the negative outflows to be set to the value of the Seneca River inflow to the lake (Figure 7-5 f). The Seneca River flows into the north end of Cayuga Lake and is assumed to flow out the outlet. The USGS verified that during certain times of the year, typically Fall and Spring, the elevation of the downstream lock (Mud Lock) is adjusted (W. Coon, personal communication). This had the effect of stopping the Seneca River from short circuiting the lake. This assumption was verified by conducting a separate flow budget for 2015. In 2015, flows were measured both upstream of the Seneca River entering Cayuga Lake and downstream of Cayuga Lake's outlet. The difference between the two gages in 2015 was compared to the estimated Seneca River inflow in 2015 as calculated by the flow budget. For the April – October interval of 2015 the estimated outflows tracked the measured outflows well, corroborating the use of this flow budget technique. This update in the flow budget had little effect on the hydrothermal/transport model fits, but is more representative of actual flow conditions. The flow budgets for the validation years 1999 and 2006 are shown in Appendix 2 (Figures A7-3 and A7-4).

During hydrothermal/transport model calibration (completed in Phase 1), the ungaged flows were treated as distributed flows to the model where the model divided the flow equally among the 50 model segments. The project's Model Evaluation Group (MEG) questioned the treatment of the ungaged flows as distributed inflows since there are a number of ungaged tributaries that enter the northern and central portion of the lake. At that time, the MEG questioned whether this handling of the ungaged flows could potentially lead to a spatial bias. Unlike gaged tributaries, distributed streams are not allowed to plunge upon entry to the lake based on temperature. The concern was addressed at the time; however, subsequent modeling indicated that not only the

point of entry around the lake but also the depth of entry may be more important for the water quality constituents than it was for temperature during the hydrothermal/transport modeling.

Haith et al. (2012) documented in detail the watershed areas for 34 tributaries to Cayuga Lake. This included the five tributaries called "gaged tributaries" in the flow budget. Figure 7-6 is a modified figure from Haith et al. (2012) showing the five gaged tributaries colored in blue and the remaining 29 ungaged tributaries in yellow. The figure also shows the location of the 25 lake segments used by the water quality model in Phase 2. Watershed areas are lumped together when tributaries from multiple watersheds enter a segment. Table 7-5 summarizes the 15 ungaged watersheds currently being using to partition the ungaged flow. The ungaged flow was partitioned using the ratio of each of the 15 subwatersheds to the overall ungaged watershed area. Rather than being distributed equally around the lake, each of the 15 ungaged tributaries now enters the lake in the appropriate model segment, as the gaged tributaries do. Based on the new partitioning of the ungaged inflows, over 80% of the ungaged flow will enter the lake north of Taughannock Creek. Testing of the model showed little impact on the hydrothermal/transport model fit from redistributing the ungaged flows to the 15 ungaged tributaries (UFI, unpublished data).

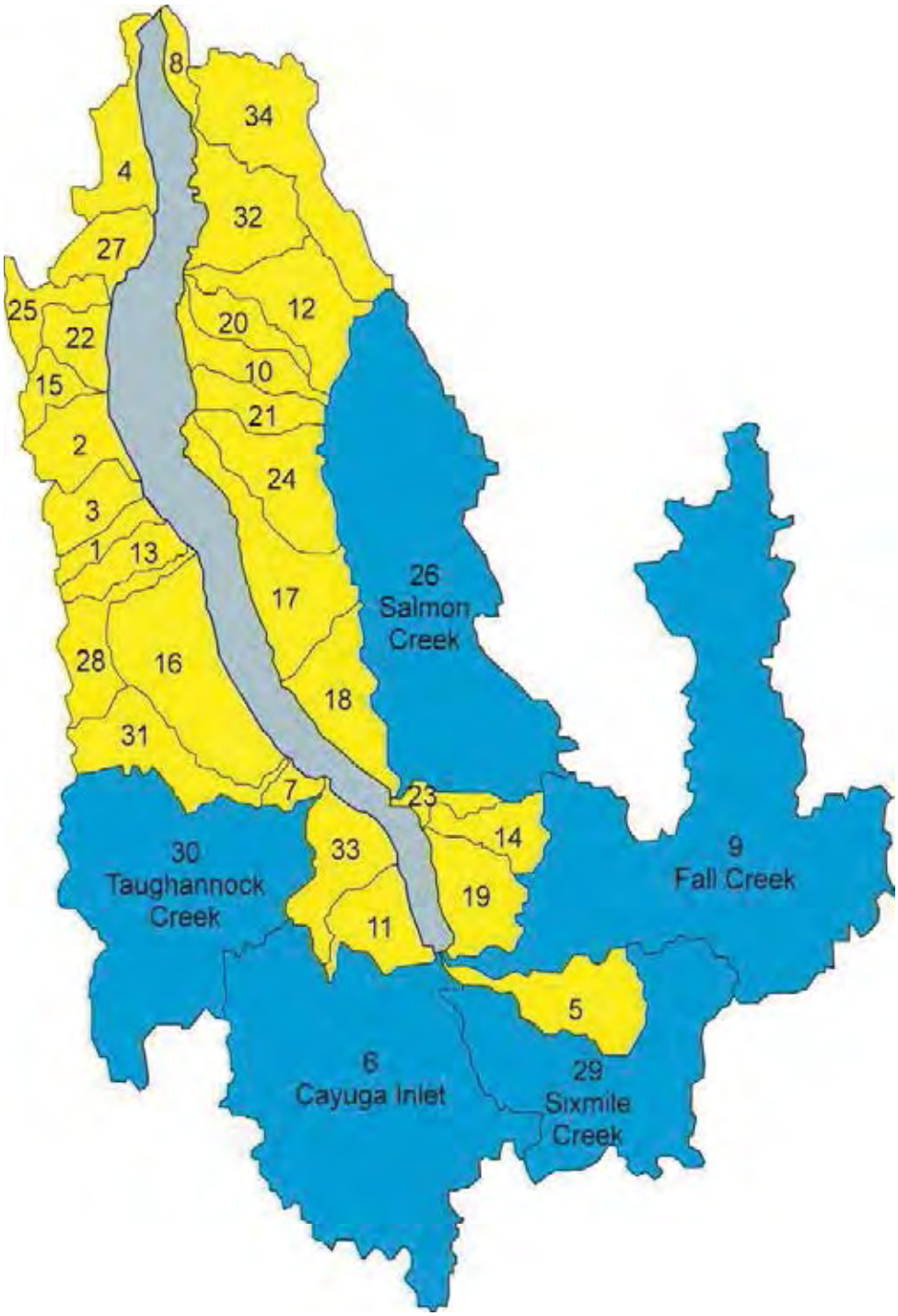

Figure 7- 6. Revised map from Haith et al. (2012; Figure 2) with gaged watersheds colored blue, ungaged watersheds colored yellow. Watershed number and related model segments are showns in Table 7-5.

Table 7- 5. The listing of the ungaged watersheds and their respective watershed areas used to partition the total ungaged inflow into 15 ungaged tributaries and the model segment that these tributaries enter the into the lake.

Ungaged tributary name	UFI 2-D model segment number	Watershed # from Haith et al. (2012)	Watershed name from Haith et al. (2012)	Watershed area from Haith et al. (2012) (ha)	Total lumped area (ha)	% of the ungaged flow
ug1	2	5	Cascadilla Ck.	3665	3665	5
ug2	7	11	Glenwood Ck. area	2484	5572	7
		19	Lansing area	3088		
ug3	8	14	Gulf Ck. area	1843	1843	2
ug4	9	33	Willow Ck. area	3052	3818	5
		23	Minnegar Ck. area	766		
ug5	11	18	Lake Ridge Point area	3409	7483	10
		31	Trumansburg Ck.	3501		
		7	Cayuga View area	573		
ug6	14	17	King Ferry Sta. area	4797	4797	6
ug7	15	28	Sheldrake Ck.	2411	9262	12
		16	Interlaken area	6851		
ug8	16	13	Grovers/Powel Creek area	1587	1587	2
ug9	17	1	Barnum Creek area	928	928	1
ug10	18	3	Bloomer/Mack Ck. area	1824	1824	2
ug11	19	21	Little Ck. area	1631	8994	12
		24	Paines Ck.	3945		
		15	Hicks Gully	1070		
		2	Big Hollow area	2348		
ug12	20	10	Glen/Dean Ck. area	1902	5051	7
		25	Red Ck.	1611		
		22	McDuffie Town area	1538		
ug13	21	12	Great Gully	3989	11186	15
		20	Lavanna area	1507		
		27	Schuyler Ck. area	1899		
		32	Union Springs area	3791		
ug14	22	4	Canoga Ck. area	2777	2777	4
ug15	23	8	Cayuga Village area	680	7031	9
		34	Yawger Ck.	6351		

7.5.4.3. Inflow temperatures

CLM-2D requires daily inputs of stream temperature. During Phase 1, the daily stream temperatures used for the distributed inflows were assumed to be the same as those measured at a USGS site near Cayuga Lake. During Phase 2, the hydrothermal/transport model was updated to use estimates of daily temperatures based on in stream measurements for 2013 and estimates for other years based on site-specific relationships. As part of the Phase 1 work, UFI routinely monitored stream temperatures on the five main tributaries during 2013. UFI had previously developed a method of estimating daily stream temperatures from daily air temperatures and a routine set of monitoring data (UFI 2001, UFI 2007). This method was used to estimate daily stream temperatures in 2013 for input to the hydrothermal/transport model (Figure 7-7.). A final assumption that the ungaged tributaries had the same temperature as Salmon Creek was based on measurements at several of the ungaged streams made on a single day.

Stream temperatures were not routinely measured for the validation years. UFI developed an air temperature - stream temperature regression for each of the streams monitored in 2013 (Figure A7-5 in Appendix 2). These regressions and the measured air temperatures for each year were used to develop stream temperatures for all the other hydrothermal/transport model years. Stream temperatures for the validation year of 1999 and 2006 are presented in Appendix 2 as Figures A7-6 and A7-.7, respectively.

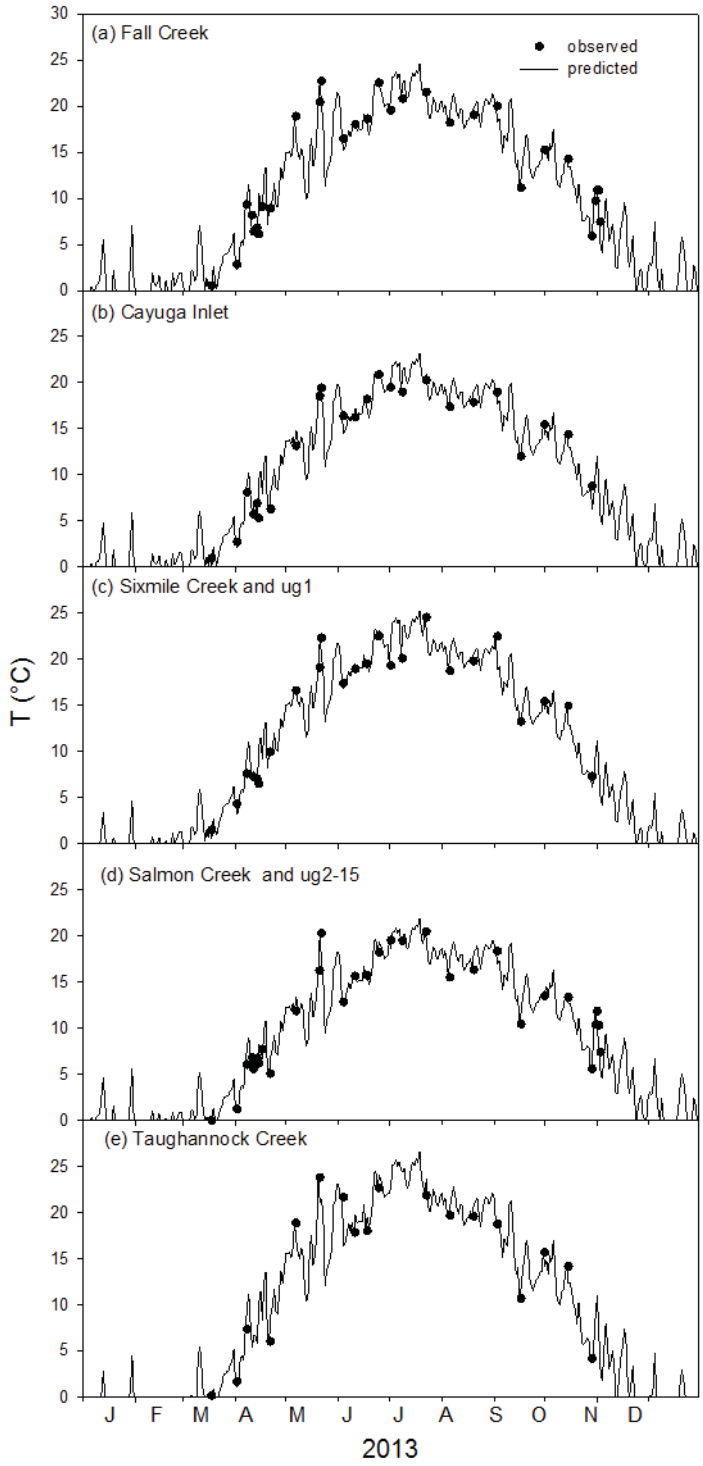

Figure 7- 7. Inflow temperature data for Cayuga Lake the calibration year of 2013: (a) Fall Creek, (b) Cayuga Inlet, (c) Sixmile Creek and ungaged tributary 1 (ug1), (d) Salmon Creek and ungaged tributaries 1-15 (ug1-15), and (e) Taughannock Creek.

7.5.4.4. Light extinction, K_d

The light extinction coefficient (K_d) for photosynthetically active radiation (PAR; 400nm—700nm) was determined by measurements of the quantum scalar irradiance light profile at the nine sampling stations in 2013 (Figure 7-8). Outside of the northern and southern shelf regions, K_d was found to be spatially homogenous. As documented previously (UFI 2014), the K_d values were generally higher in the shelf areas than in the main lake. Because only a single value of K_d can be specified in the model, the measured K_d values at Sites 3-7 were averaged to represent the pelagic lake segments. This average K_d value for the pelagic sites was doubled to represent conditions on the southern and northern lake shelves. Linear interpolation was used to generate K_d values for periods between measurements. The K_d time-series for the calibration year of 2013 is shown in Figure 7-9. Refer to Appendix 2 for time series of K_d for the validation years of 1999 (Figure A7-8) and 2006 (Figure A7-9).

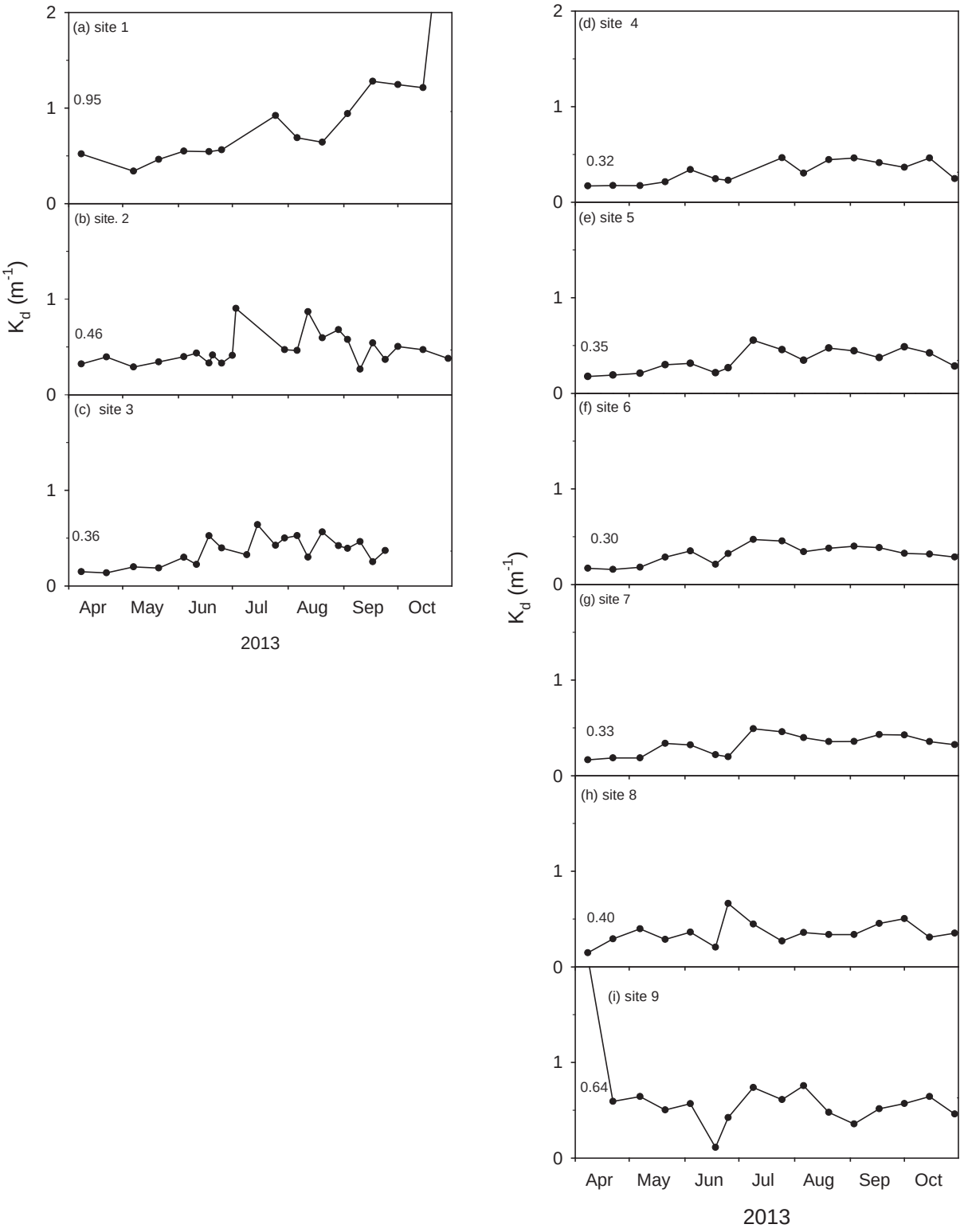

Figure 7- 8. Measured Kd values for Cayuga Lake: (a) site 1, (b) site 2, (c) site 3, (d) site 4, (e) site 5, (f) site 6, (g) site 7, (h) site 8, and (i) site 9.

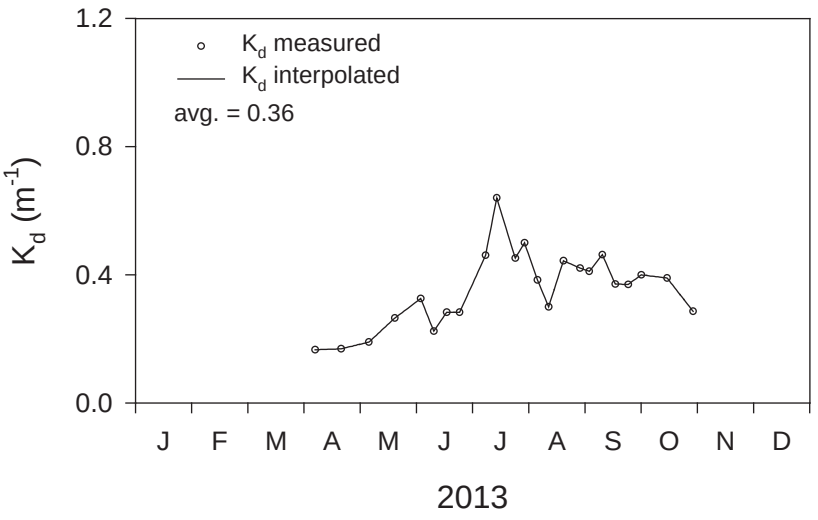

Figure 7- 9. Time series of Kd for the calibration year of 2013. Plotted values are averages from sites 3-7, located in the pelagic zone of Cayuga Lake.

7.5.4.5. Section of Validation Years

In Phase 1 the hydrothermal/transport model was calibrated for 2013 and validated for 1998-2012. In Phase 2 the upgraded hydrothermal/transport model was validated for two years, 1999 and 2006. The range of conditions observed in Cayuga Lake for precipitation, flow, phosphorus loads, and flushing rate for the model calibration year of 2013 and the model validation years of 1999 and 2006 are presented in Figure 7-10. Numbers over the bars reflect ranking over the 1998-2013 period (1-highest, 16-lowest). The two validation years represent a wide range of hydrologic conditions, with 1999 ranking as the 12th wettest summer (15th on an annual basis) and 2006 ranking as the wettest summer (7th on an annual basis). The large difference in precipitation between 1999 and 2006 (Figure 7-10a,f) was accompanied by similar differences in tributary flow rates (Figure 7-10b,g), P loading (Figure 7-10c,h), and flushing rate (Figure 7-10e). Values of these metrics for the calibration year of 2013 were generally between those measured in 1999 and 2006. The wide range of meteorological forcing conditions included in the calibration and validation data sets represents a robust test of the hydrothermal/transport model.

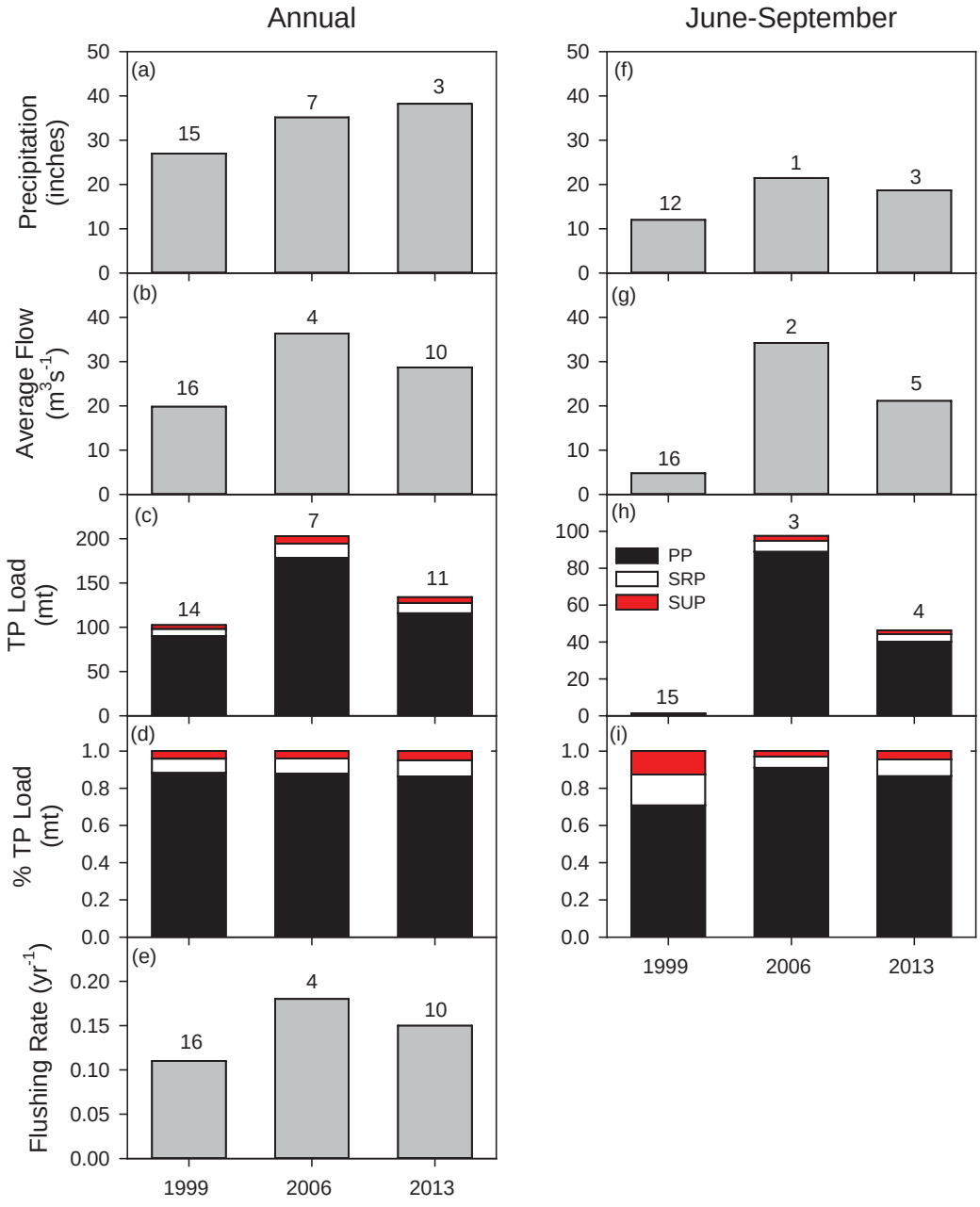

Figure 7- 10. Annual and summer (June-September) conditions for the model calibration (2013) and validation (1999, 2006) years: (a) annual precipitation (b) annual average inflow from tributaries, (c) annual TP load partitioned into PP, SRP, and SUP components, (d) composition of annual TP load, (e) flushing rate, (f) summer precipitation (g) summer average inflow from tributaries, (h) summer TP load partitioned into PP, SRP, and SUP components, and (i) composition of summer TP load. Numbers above bars reflect ranking over the 1998-2013 period (1-highest, 16-lowest).

7.5.5. Hydrothermal/transport model updates

Several important changes were made to the hydrothermal/transport sub-model since the Phase 1 report. These changes are summarized below.

1. The hydrothermal/transport sub-model was upgraded from CE-QUAL-W2 version 3.70 to version 3.72.
2. The number of model segments was reduced from 50 to 25 to reduce the run-time of the water quality model without significant negative impacts on model performance. Model run-time was reduced by > 60%.
3. The method used for calculating the root mean square error (RMSE) was modified for Phase 2. In Phase 1 a RMSE was calculated for each vertical profile, the RMSEs were averaged over time for each site, and the average RMSEs for each site were averaged to produce a single lake-wide RMSE. This method weighted all sites equally, regardless of depth or number of measurements. In Phase 2, the RMSE was calculated by pairing all of the available measurements with corresponding model output, resulting in a single lake-wide RMSE. This method gives each of the measurements equal weight, and is the approach most commonly used in water quality modeling (S. Chapra, personal communication).
4. The light extinction coefficient (Kd) has been upgraded from a single value applied to all segments (CE-QUAL-W2 model default) to separate values for pelagic and shelf (southern and northern) sites. See subsection 7.5.4.4 for additional detail.
5. The flow budget was modified to improve estimates of flow entering and leaving the lake. See subsection 7.5.4.2 for additional information.
6. A more realistic treatment of distributed flows was developed based on suggestions from the MEG. See subsection 7.5.4.2 for additional information.
7. Improved estimates of stream temperatures have been incorporated, based on local air temperature and observed stream temperatures where available. Additional information can be found in subsection 7.5.4.3.
8. The date of model initialization was changed from January 1, 2013 in Phase 1 to April 8, 2013 in Phase 2. In Phase 1, the model was initialized to a uniform temperature of 5°C. In Phase 2, the model was initialized to temperature profiles measured on April 8, 2013. This change resulted in a small improvement in the model fit.

These changes to the hydrothermal/transport sub-model were conducted sequentially and the effect of each change on RMSE was recorded. The combined effects of all these changes are presented in Table 7-6 for 2013 and Table 7-7 for 1999–2012. Items 2 and 3 above had the largest impacts on RMSE.

Table 7- 6. Root Mean Square Error (RMSE) for Phase 1 and Phase 2 hydrothermal/transport model calibration runs (2013, sites 1-9).

Site	Phase 1	Phase 2
Overall	0.89	0.82*
1	1.04	1.28
2	0.89	1.78
3	0.84	0.93
4	0.63	0.57
5	0.64	0.55
6	0.56	0.68
7	0.76	0.90
8	1.31	1.38
9	1.38	1.52

Table 7- 7. Root Mean Square Error (RMSE) for Phase 1 and Phase 2 hydrothermal/transport model validation runs, 1999-2006.

Years	Phase 1 site 3	Phase 2 Site 3
1999	1.44	0.99
2000	1.15	1.21
2001	1.37	1.36
2002	1.11	1.35
2003	1.17	1.40
2004	1.40	1.43
2005	1.22	1.55
2006	1.27	1.44
1998-2006 lumped	--	1.35
1999 only	--	0.97
2006 only	--	1.05

7.5.6. Hydrothermal/transport model calibration and validation

Model calibration is the first stage of model testing in which model coefficients not independently measured are varied within theoretically defensible ranges so that simulations of state variables match observations. According to Thomann and Mueller (1987), model calibration should not simply be considered "*a curve-fitting exercise, but should reflect wherever possible more fundamental theoretical constructs and parameters. Thus, models that have widely varying coefficients to merely "fit" the observed data are not considered calibrated…*" Independent determination of a number of key coefficients further constrains the calibration process, reducing the number of coefficients subject to variation (and thereby reducing the "degrees of freedom") and the chances that calibration is achieved with inaccurately quantified processes that are essentially compensating errors.

Model validation is the second stage of model testing. It is the demonstration of model fit for a distinctly different set of environmental conditions, with the same suite of coefficients used in calibration. However, the opportunity for rigorous validation testing does not always exist. This may be the case in systems where a narrow range of water quality conditions prevails. The existence of a long-term monitoring data set, as is the case for Cayuga Lake, is particularly beneficial, as it can be expected to include a rather wide range of natural forcing conditions. Historically, the success of model testing has relied primarily on professional judgment, influenced greatly by performance characteristics reported for similar models in the peer-reviewed literature. Increasingly, quantitative statistical treatments have been utilized (Thomann 1982), though certain features of model performance continue to remain a matter of judgment.

Once model credibility is established by successful calibration and validation testing the model can be applied to address management questions, or simulate the response to specific management scenarios. It is important to recognize that some level of uncertainty accompanies all model simulations, associated with unavoidable (though hopefully modest) uncertainty in the values of individual model coefficients and the necessarily imperfect representations of reality offered by even the best models. Further, in many cases managers want to extend the application of successfully tested models well beyond the conditions accommodated in the processes of calibration and verification. It is important to acknowledge that an added degree of uncertainty may be introduced in some cases for this type of application.

Credible application of models for management scenarios (i.e., *a priori* predictions) requires: (1) appropriate loading and other forcing function information (e.g., meteorology), (2) appropriate assumptions for ambient environmental conditions, and (3) model frameworks that appropriately accommodate regulating processes. The establishment of water quality goals by managers is also an important aspect of the model application process. The use of strictly artificial forcing and ambient environmental conditions is not recommended. Where possible, such as in the case of Cayuga Lake, system-specific and regional monitoring data should be used

to drive realistic simulations for the selected management alterations. Utilization of forcing conditions actually encountered historically with respect to hydrology and meteorology for multiple years (e.g., Gelda et al. 2015) offers the opportunity to reflect the influence of natural variability on model predictions.

The coefficients used for calibration and validation of the hydrothermal/transport model are shown in Table 7-8. These are the recommended default values except for wind sheltering (set to 1.0) and the Chezy coefficient (set to 70). Applications for numerous lakes and reservoirs under a wide variety of conditions have shown the hydrothermal/transport model generates remarkably accurate temperature predictions using default values when provided with accurate geometry and boundary conditions. The light extinction coefficient was determined from site-specific measurements of the underwater light field as outlined in Section 7.6.4.5.

Table 7- 8. Hydrothermal/transport coefficients in CE-QUAL-W2.

Coefficient	**Symbol**	**Model Values**
horizontal eddy viscosity	A_x	1 m^2/sec
horizontal eddy diffusivity	D_x	1 m^2/sec
Chezy coefficient (all segments)	C_h	70 $m^{0.5}$/sec
wind sheltering coefficient (all segments)	W_{sc}	1.0
fraction of incident solar radiation absorbed at the water surface	β	0.45
coefficient of bottom heat exchange	C_{BHE}	0.3 W/m^2/°C

7.5.7. Evaluation of Hydrothermal/transport Model Performance

Accurate simulation of temperature by the 2-D hydrothermal model is a test that the model is simulating transport of heat (and therefore mass in the water quality model) in both the vertical and longitudinal directions in the lake. Temperature also regulates a number of biological processes in the lake. The hydrothermal/transport model calibration and validation was presented in detail in Section 6 and Appendix D of the Phase 1 report. This Phase 2 report highlights the hydrothermal/transport model fit for the calibration year of 2013 and the validation years, 1999 and 2006.

The primary basis for evaluation of the hydrothermal/transport model was reproduction of vertical temperature profiles and time-series at discrete depths. Goodness of model fit was based on both visual inspection of model predictions to observed data and statistics, including RMSE. Examples of the model fit are presented for site 5 (Figure 7-11), the primary water quality monitoring site (UFI 2014), and site 3 (Figure 7-12), a site with a long-term monitoring record (1998-2012). Similar plots for 2013 at the other monitoring sites are provided in Appendix 2

(Figure A7-10). The hydrothermal model simulated T observations well for the calibration year of 2013. Several features of thermal stratification were simulated accurately, including surface temperature, mixed layer depth, near-bottom temperature, and overall profile shape. Model predictions nicely tracked the progressive deepening of the thermocline from mid-summer into the fall (Figure 7-11 and 7-12).

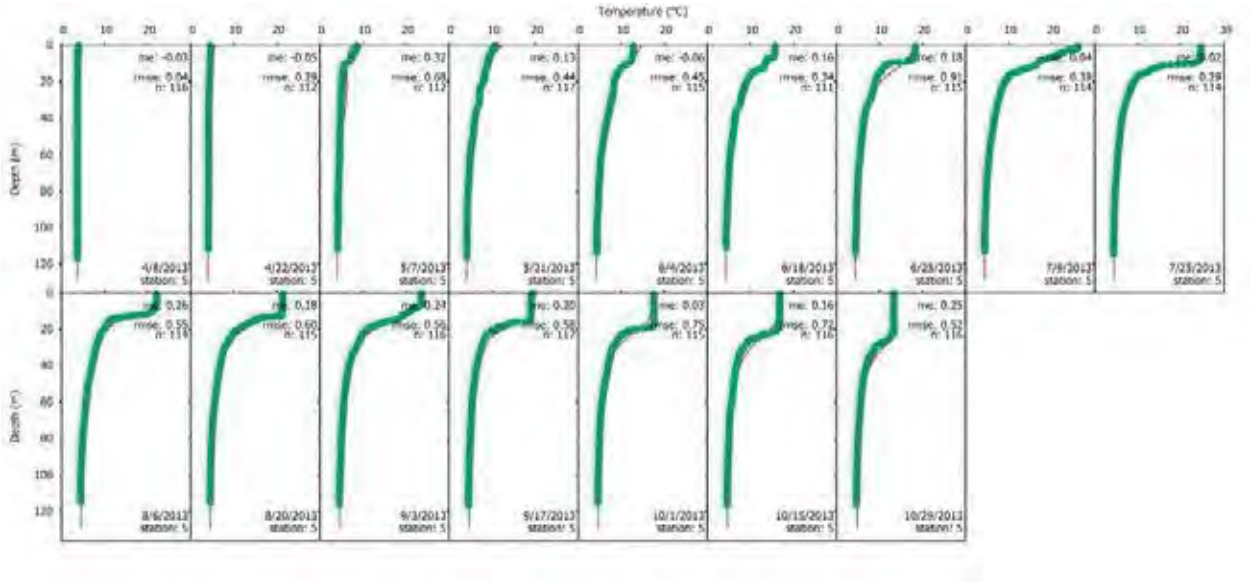

Figure 7- 11. Comparisons of predicted and observed 2013 temperature profiles for Cayuga Lake, site 5. Mean errors (me), root mean square errors (rmse), and number of observations (n) are included for reference.

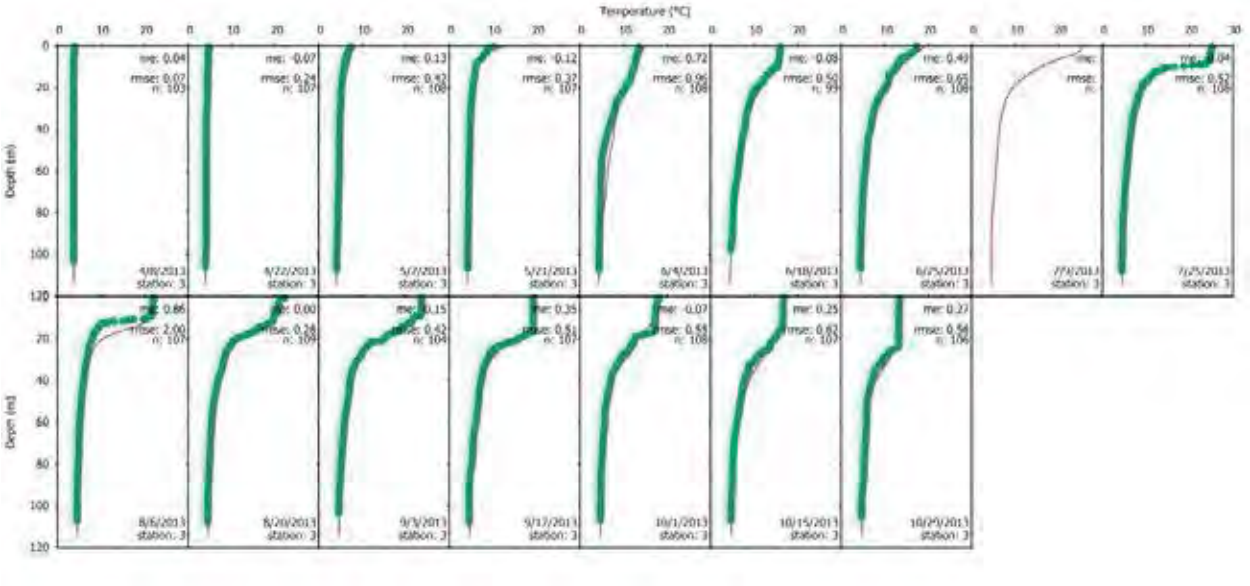

Figure 7- 12. Comparisons of predicted and observed 2013 temperature profiles for Cayuga Lake, site 3. Mean errors (me), root mean square errors (rmse), and number of observations (n) are included for reference.

Model fits for 2013 are also presented as time series, with temperature observations and simulations shown for multiple depths at each of the nine monitoring sites (Figure 7-13). The model tracked the observed temperatures reasonably well at all sites and depths, capturing the progressive warming in the upper waters over the season as evidence that the model is simulating surface heat transfer and wind mixing accurately. The model accurately predicted temperatures in the hypolimnion, most notably the rate of heating and the duration of stratification (Figure 7-13).

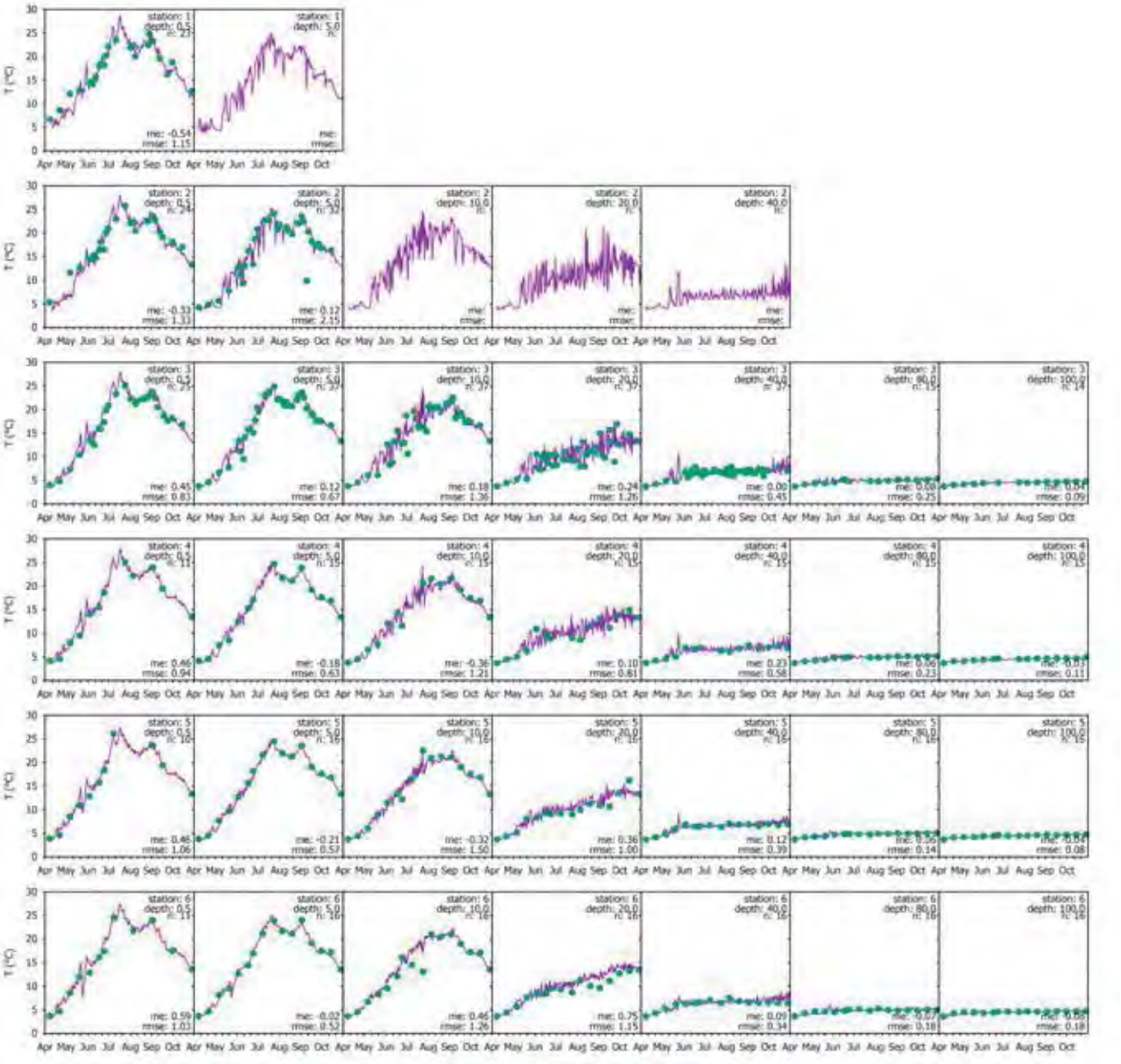

Figure 7- 13. Time series of predicted and observed temperatures for 2013 at nine monitoring sites and multiple depths (0.5, 5, 10, 20, 40, 80, and 100 meters) in Cayuga Lake. Mean errors (me), root mean square errors (rmse), and number of observations (n) are included for reference.

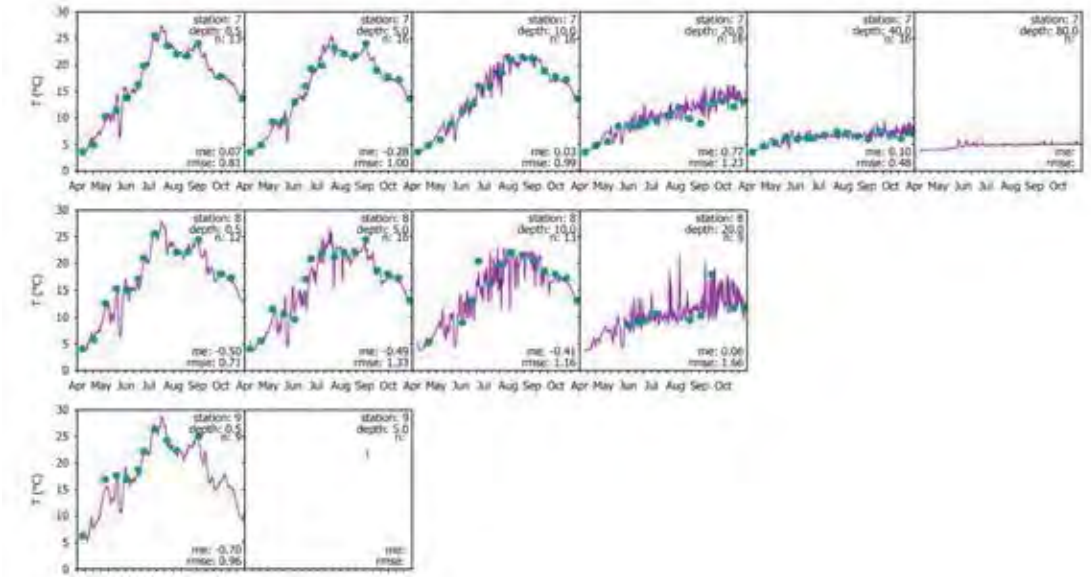

Figure 7- 13. (Continued). Time series of predicted and observed temperatures for 2013 at nine monitoring sites and multiple depths (0.5, 5, 10, 20, 40, 80, and 100 meters) in Cayuga Lake. Mean errors (me), root mean square errors (rmse), and number of observations (n) are included for reference.

The model also performed well in simulating temperatures for the two years of model validation, 1999 and 2006 (Figures 7-14 – 7-17). Under these different hydrologic and meteorological forcing conditions the model continued to accurately simulate thermal stratification (Figures 7-15 and 7-17), as well as simulating longitudinal temperature differences in the lake (Figures 7-16 and 7-18). The model performed substantially better (lower RMSE) at pelagic sites compared to shallow sites at the southern and northern ends of the lake (Tables 7-6 and 7-7). It should be noted that model performance is typically evaluated at mid-lake sites. This form of spatial variability in model performance is expected due to various processes that contribute to temperature fluctuations in these areas (e.g., seiches, tributary inflows).

A feature of thermal stratification that directly affects eutrophication is the depth of the thermocline, with shallow mixed layer depth generally associated with increased algal productivity. The thickness of the epilimnion influences the magnitude of algal productivity, such that algal productivity increases with decreasing epilimnion depth under nutrient-saturated, light-limited conditions. Model predictions of the observed seasonal increase in thermocline depth from mid-summer through fall, and also short term fluctuations associated with meteorological events, were simulated well. The primary goal of the hydrothermal/transport model is to support analysis and prediction of phytoplankton growth (e.g., eutrophication, excess

P) in Cayuga Lake. The stratification conditions which are known to affect manifestations of phytoplankton growth include duration of stratification, hypolimnetic temperature during stratification, and thickness of the epilimnion. The temperature of the hypolimnion, which is likely related to the duration of stratification, affects the rate of biochemical processes in the lower waters, such as decomposition of organic material and sediment oxygen demand. Changes or variations in hypolimnetic temperature may also affect pelagic fish and mussel populations.

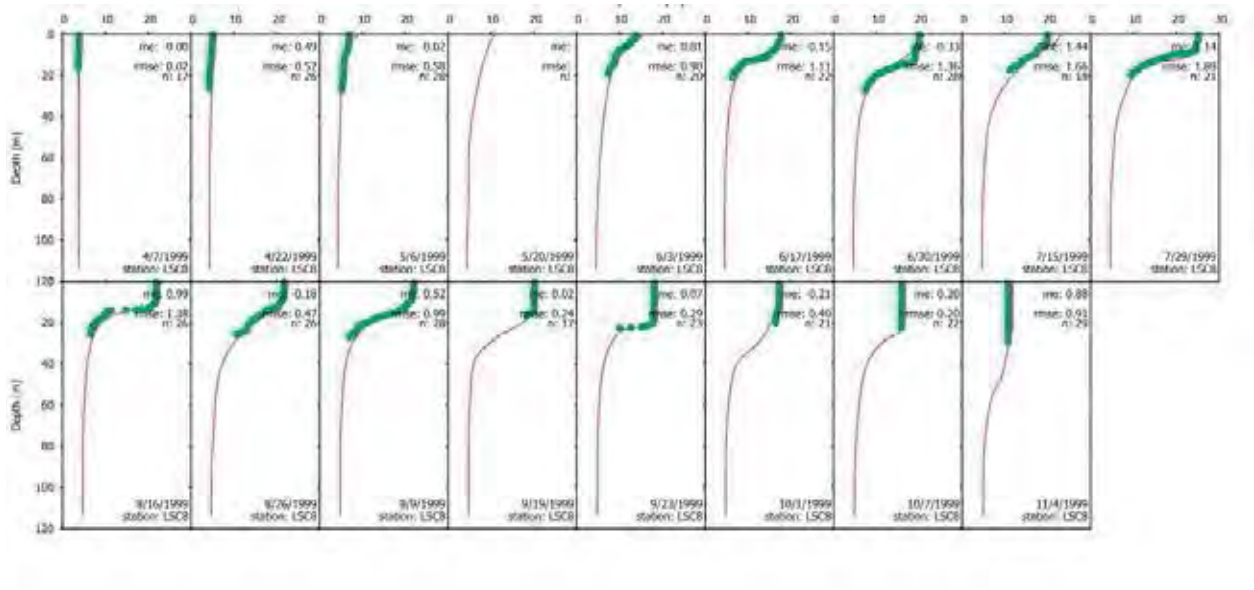

Figure 7- 14. Comparisons of predicted and observed 1999 temperature profiles for Cayuga Lake at site 3 (formerly LSC8). Mean errors (me), root mean square errors (rmse), and number of observations (n) are included for reference.

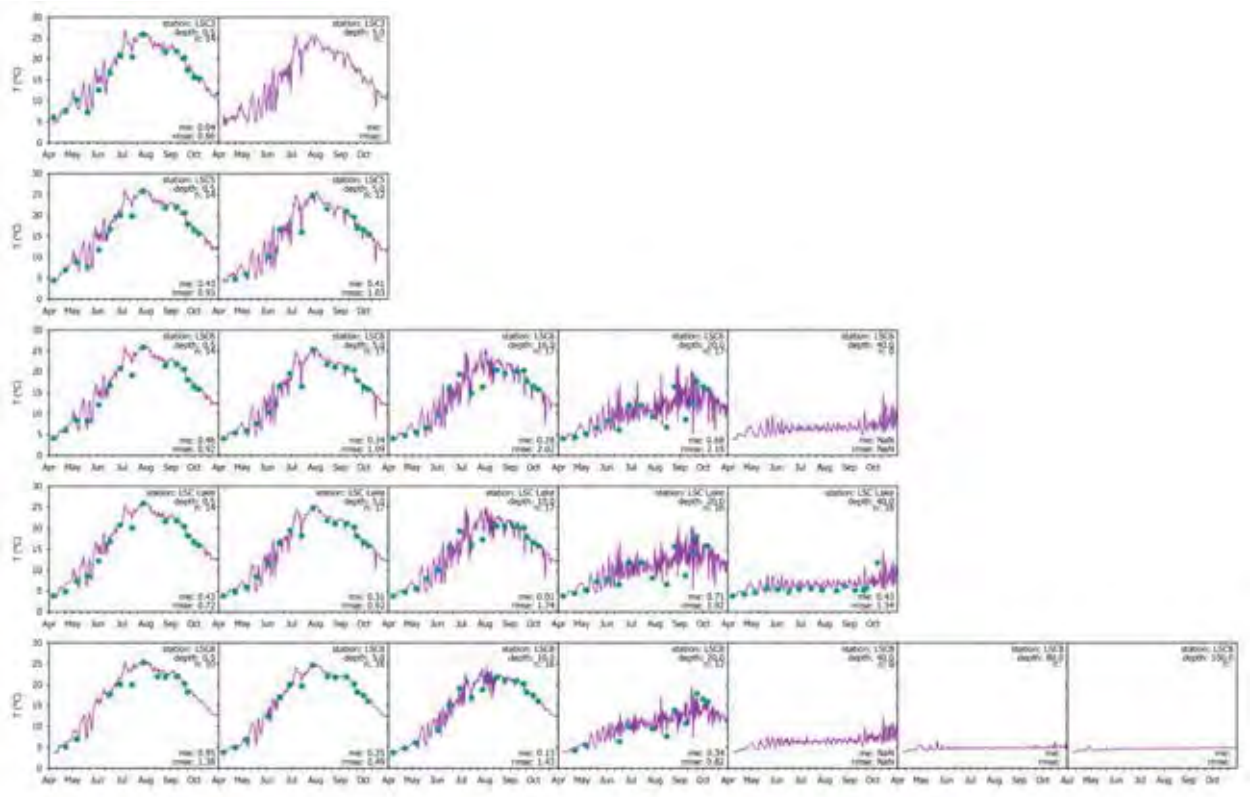

Figure 7- 15. Time series of predicted and observed temperatures for 1999 at five monitoring sites (LSC3 (site 1), LSC5 (site 2), LSC6, LSC Lake, and LSC8 (site 3)) and multiple depths (0.5, 5, 10, 20, 40, 80, and 100 meters) in Cayuga Lake. Mean errors (me), root mean square errors (rmse), and number of observations (n) are included for reference.

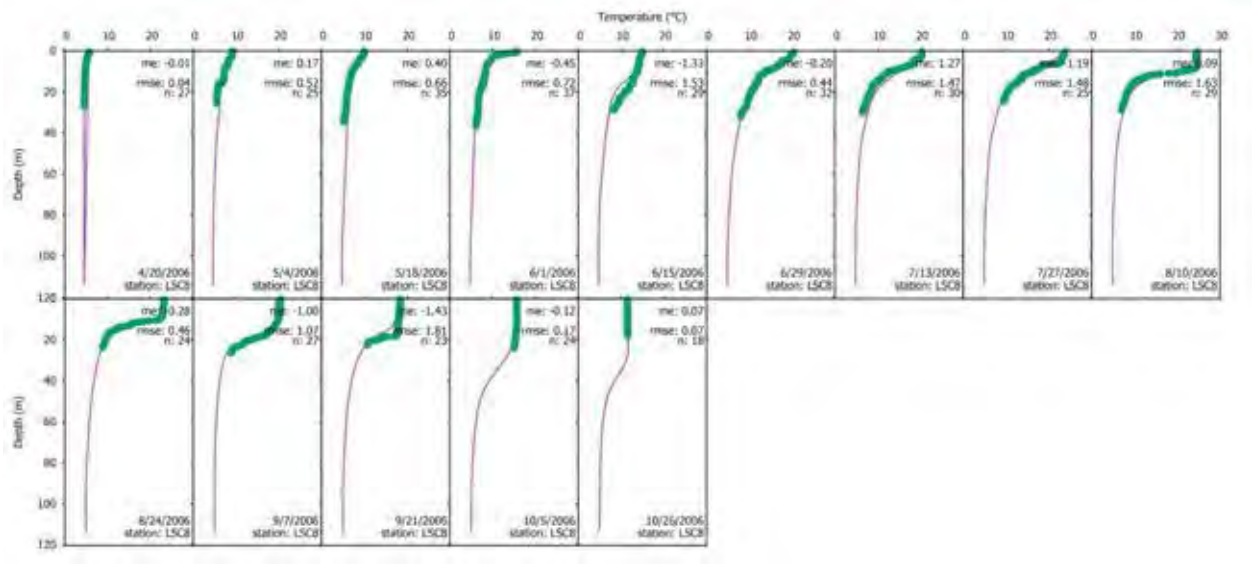

Figure 7- 16. Comparisons of predicted and observed 2006 temperature profiles for Cayuga Lake at site 3 (formerly LSC8). Mean errors (me), root mean square errors (rmse), and number of observations (n) are included for reference.

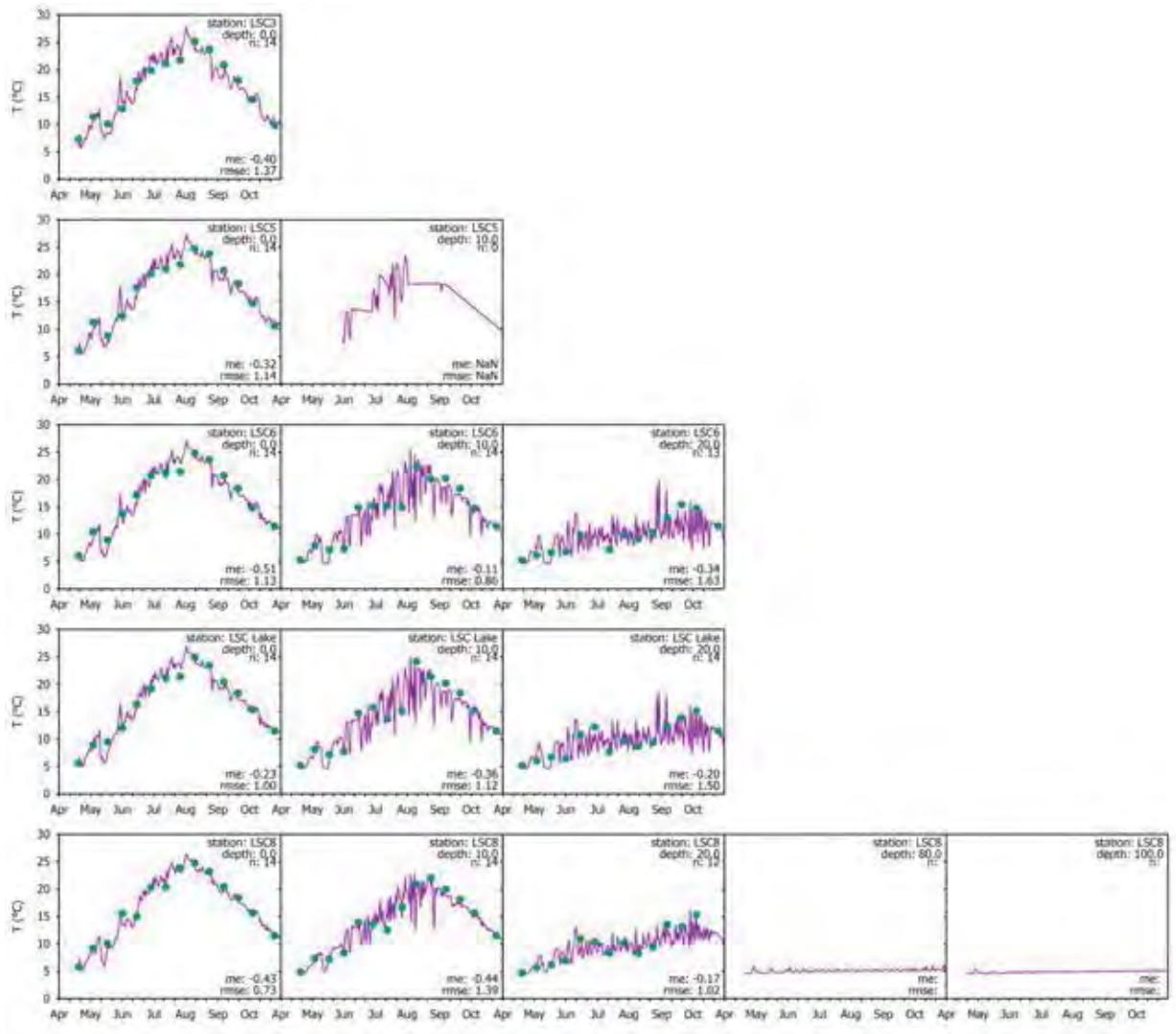

Figure 7- 17. Time series of predicted and observed temperatures for 2006 at five monitoring sites (LSC3 (site 1), LSC5 (site 2), LSC6, LSC Lake, and LSC8 (site 3)) and multiple depths (0.5, 5, 10, 20, 40, 80, and 100 meters) in Cayuga Lake. Mean errors (me), root mean square errors (rmse), and number of observations (n) are included for reference.

7.6. Nutrient-Phytoplankton water quality model

7.6.1. Conceptual framework: Background and approach

We have adopted the modeling philosophy of parsimony in development of this P-eutrophication model for Cayuga Lake. Accordingly, the model is only as complex as necessary to address the issue with credibility. The model structure and capabilities are consistent with our scientific understanding of Cayuga Lake and suitable for the regulatory task of conducting a P TMDL analysis. The overall model utilized for the Cayuga Lake project is an integrated two dimensional hydrothermal/transport and water quality model utilizing the hydrothermal/transport portion of CE-QUAL-W2 (version 3.72; Cole and Wells 2015) and a separately developed water quality model described in this section of the Phase 2 Report. The hydrothermal/transport sub-model was described in subsection 7.5. This integrated model is referred to as CLM-2D (Cayuga Lake Model - 2D). The inflow concentrations for the water quality model follow the same formatting and daily input frequency of CE-QUAL-W2. However, the model structure and state variables used in CLM-2D differ from those used in CE-QUAL-W2.

The constituents and characteristics predicted by the water quality model are described as the state variables. The overall water quality (P-eutrophication) model has a robust array of model state variables (Table 7-9) that address the water quality issues targeted by this study. The model also includes several derived constituents, which are calculated from the state variables (Table 7-10). Multiple forms of P are predicted, including particulate and dissolved fractions, which are partitioned according to labile (subject to reactions/transformations) and refractory (not subject to reactions/transformations), and organic versus inorganic, components. Phytoplankton biomass and organic carbon (C) are simulated, with multiple forms of C (dissolved versus particulate, labile versus refractory) predicted. Chlorophyll-*a* (Chl-*a*), a surrogate of phytoplankton biomass, is derived as the product of simulated phytoplankton biomass (ALG) and the Chl-*a*:ALG ratio. Two groups of phytoplankton are modeled, diatoms (ALG1) and other algal taxa (ALG2). Total phosphorus (TP) was derived by summing the simulated dissolved and particulate forms of phosphorus. Secchi disk depth (Z_{SD}) was predicted by the optics sub-model (see subsection 5.2).

Multiple metrics of sediment were simulated, including the total projected area of minerogenic particles per unit volume of sample (PAV_m), turbidity (Tn), total suspended solids (TSS), and fixed suspended solids (FSS). Optical metrics, including Tn and the attenuation coefficient for scalar photosynthetically active radiation (K_0(PAR)), were predicted by the optics sub-model. Nitrate+nitrite (NO_x) and silica (Si) were added to the Phase 1 list of model state variables because both had distinctive depletion signatures in the pelagic waters of the lake (UFI 2014). Dissolved oxygen (DO) is included as a state variable because it is needed for certain reactions. However, no effort was made to calibrate this parameter because DO is not a water quality issue for Cayuga Lake (e.g., there is no evidence of hypolimnetic depletion).

Table 7- 9. Listing of CLM-2D state variables.

Symbol	Description	Input/Output unit
T	temperature	°C
Alg1, Alg2	algae in terms of carbon	g C/L
DO	dissolved oxygen	mg O_2/L
Carbon		
LDOC	labile dissolved organic carbon	mg C/L
RDOC	refractory dissolved organic carbon	mg C/L
RPOC	labile particulate organic carbon	mg C/L
RPOC	refractory particulate organic carbon	mg C/L
CO2	carbon dioxide	mg C/L
Nitrogen		
NH_3	total ammonia	g N/L
NO_X	sum of nitrate plus nitrate plus nitrite $NO_X = NO_3 + NO_2$	g N/L
LDON	labile dissolve organic nitrogen	g N/L
RDON	refractory dissolve organic nitrogen	g N/L
LPON	labile particulate organic nitrogen	g N/L
Phosphorus		
SRP	soluble reactive phosphorus	g P/L
LDOP	labile dissolve organic phosphorus	g P/L
RDOP	refractory dissolve organic phosphorus	g P/L
LPOP	labile particulate organic phosphorus	g P/L
RPOP	refractory particulate organic phosphorus	g P/L
LPIP	labile particulate inorganic phosphorus	g P/L
RPIP	refractory particulate inorganic phosphorus	g P/L
DSi	dissolved silica	mg Si/L
Psi	particulate silica	mg Si/L
Zooplankton		
Zoo1	zooplankton carbon, modeled or fixed	mg C/L
Mussels (fixed not modeled)		
Mus_{DW}	Mussel dry weight, fixed not modeled	g DW/m^2

Table 7- 10. Listing of CLM-2D derived variables (calculated from state variables).

Symbol	Description	Input/Output unit
Chl	chlorophyll *a*	g /L
N:P	ratio of nitrogen to phosphorus	g N/ gP
Carbon		
DOC	dissolved organic carbon	mg C/L
POC	particulate organic carbon	mg C/L
TOC	total organic carbon	mg C/L
Nitrogen		
DON	dissolved organic nitrogen	g N/L
PN	particulate nitrogen	g N/L
TDN	total dissolved nitrogen	g N/L
TN	total nitrogen	g N/L
Phosphorus		
TDP	total dissolved phosphorus	g P/L
DOP	dissolved organic phosphorus	g P/L
PP	particulate phosphorus	g P/L
TP	total phosphorus	g P/L

CLM-2D includes kinetic sub-models representing algae, zooplankton, the effects of dreissenid mussels, and four major algal constituents: (1) carbon (C), (2) phosphorus (P), (3) nitrogen (N), and (4) silica (Si). Although a kinetic sub-model is also included for dissolved oxygen (DO), simulations of DO were not emphasized. Sub-models are also included for minerogenic particles and optics (e.g., Secchi depth). The conceptual frameworks of each of these sub-models are described briefly below. Mass balance equations for each of the sub-models are presented in Appendix 2. These include the source and sink terms for each state variable, exclusive of external loading and transport-based exchange. Only selected expressions are described in text.

7.6.1.1. Carbon sub-model

Dissolved components of the carbon sub-model include carbon dioxide (CO_2), labile dissolved organic carbon (LDOC), and refractory dissolved organic carbon (RDOC) (Figure 7-18). Particulate forms include zooplankton, algal carbon, labile particulate organic carbon (LPOC), and refractory particulate organic carbon (RPOC). Labile and refractory forms are differentiated by decay rates, which were determined in model calibration. Organic carbon is an important regulator of lake metabolism (Wetzel 2001). The labile portion of the DOC pool supports heterotrophic activity by aquatic bacteria. This form of metabolism can exceed primary production in certain lakes, a situation described as net heterotrophy (Hanson et al. 2003). CLM-2D uses POC as the primary metric of phytoplankton biomass. Sinks for algal carbon include grazing by zooplankton, mortality, settling, and ingestion by dreissenid mussels.

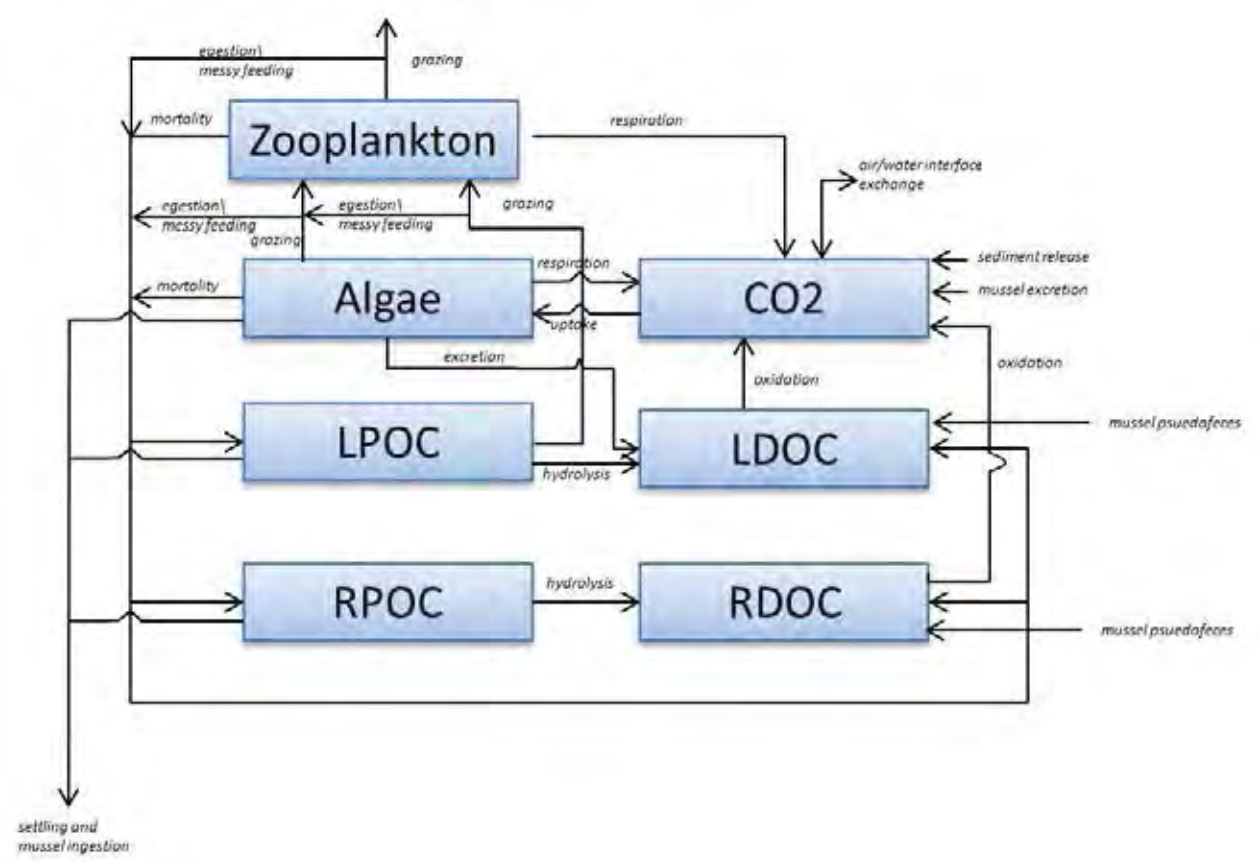

Figure 7- 18. Conceptual diagram for carbon sub-model.

7.6.1.2. Nitrogen sub-model

Dissolved forms included in the nitrogen (N) sub-model (Figure 7-19) are ammonia (NH_3), nitrate+nitrite (NO_x), labile dissolved organic nitrogen (LDON), and refractory dissolved organic nitrogen (RDON). The model also tracks four particulate forms of N: zooplankton, algae, labile particulate organic nitrogen (LPON), and refractory particulate organic nitrogen (RPON). Labile and refractory forms are differentiated by decay rates, which were determined in model calibration. Although both ammonia and nitrate can be used to support algal growth, ammonia is preferred for energetic reasons (Wetzel 2001). Ammonia concentrations are low in Cayuga Lake, and algal demand for N is met primarily by nitrate.

Algal N is lost through respiration (i.e., dark respiration) and excretion (i.e., photorespiration) processes to the NH_3 and LDON pools (Figure 7-19). Decay processes cycle N from the LDON and RDON pools to the NH_3 pool. LDON and RDON are produced from

hydrolysis of LPON and RPON and inefficient grazing of algae by zooplankton. Particulate forms of N that are lost to settling and ingestion by dreissenid mussels include algae, LPON, and RPON.

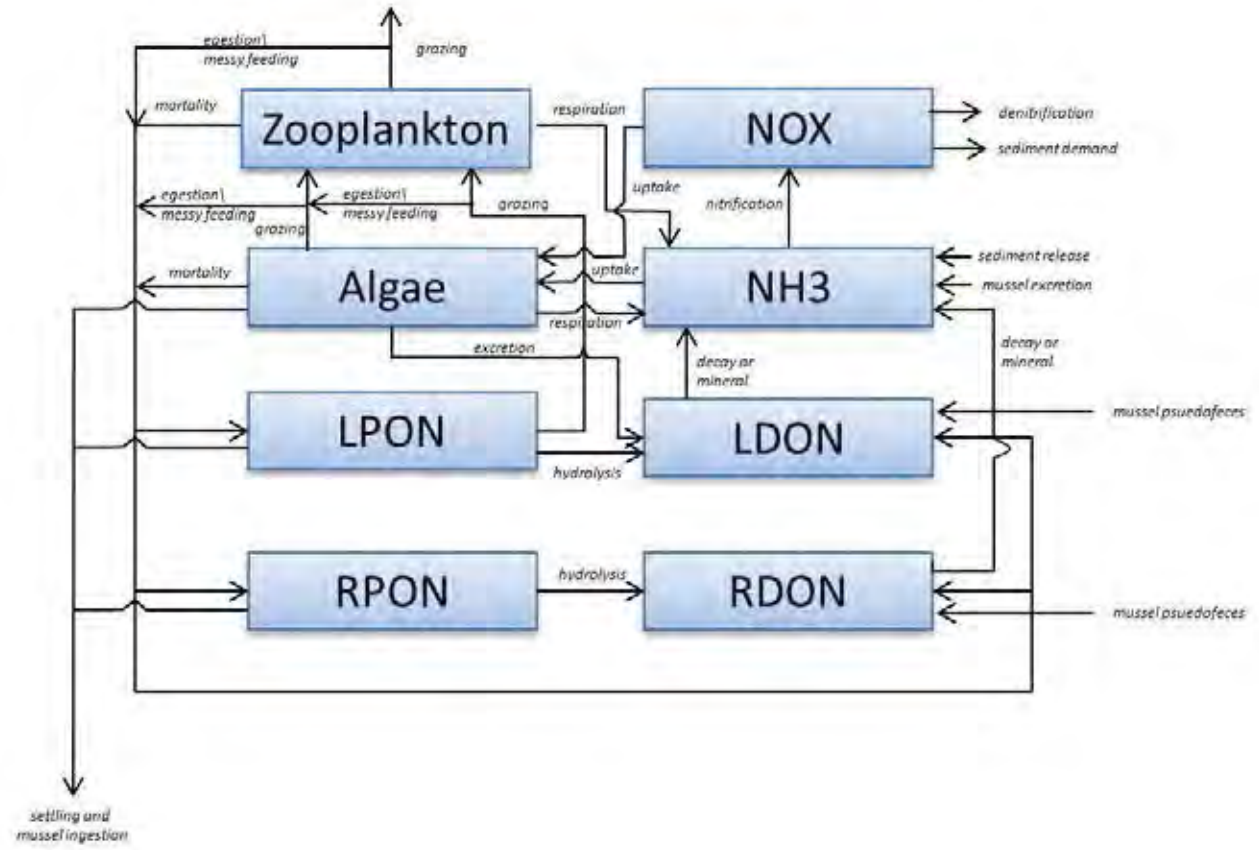

Figure 7- 19. Conceptual diagram for nitrogen sub-model.

7.6.1.3. Phosphorus sub-model

Dissolved components of the phosphorus (P) sub-model include soluble reactive P (SRP), labile dissolved organic P (LDOP), and refractory dissolved organic P (RDOP) (Figure 7-20). Particulate forms include zooplankton, algal carbon, labile particulate organic carbon (LPOC), and refractory particulate organic carbon (RPOC). Labile and refractory forms were differentiated by decay rates, which were specified according to the results of P bioavailability assays. Soluble reactive P supports algal growth, which is largely limited to the epilimnion of the lake because of limited light penetration. Sources of SRP to the water column include microbial decay of LDOP and RDOP, respiration/decay of algal phosphorus, zooplankton

respiration, and dreissenid mussel excretion. Bottom sediments represent a potential source of SRP to the hypolimnion under anaerobic conditions (i.e., depletion of both oxygen and nitrate). Because of its large oxygen-rich hypolimnion, the sediment release pathway is neither operative nor realistic for Cayuga Lake.

LDOP and RDOP are formed by hydrolysis of LPOP and RPOP, messy grazing of algae by zooplankton, and algal photorespiration (excretion). Algal respiration is partitioned according to active growth (photorespiration or excretion) and maintenance or basal (dark respiration) processes. Thus this recycle pathway is greater in the epilimnion where phytoplankton growth occurs, and is diminished in the hypolimnion where basal respiration prevails.

Particulate P in the form of algae and non-algal particles (LPOP, RPOP, LPIP, RPIP) is lost from the water column due to settling and ingestion by dreissenid mussels. Settling velocities were determined through calibration, with lower values for algal P and higher values for non-living particulate components. The external loading of PP and DOP was partitioned according to the outcome of system-specific bioavailability experiments described in the Phase 1 report (UFI 2014). Adjustments in kinetic rates to accommodate the influence of temperature in this and the other sub-models were made according to the Arrhenius function and the temperature optimum curve (Bowie et al. 1985). The primary modeling performance target for P was the summer average TP concentration in the upper waters, consistent with the NYSDEC guidance value.

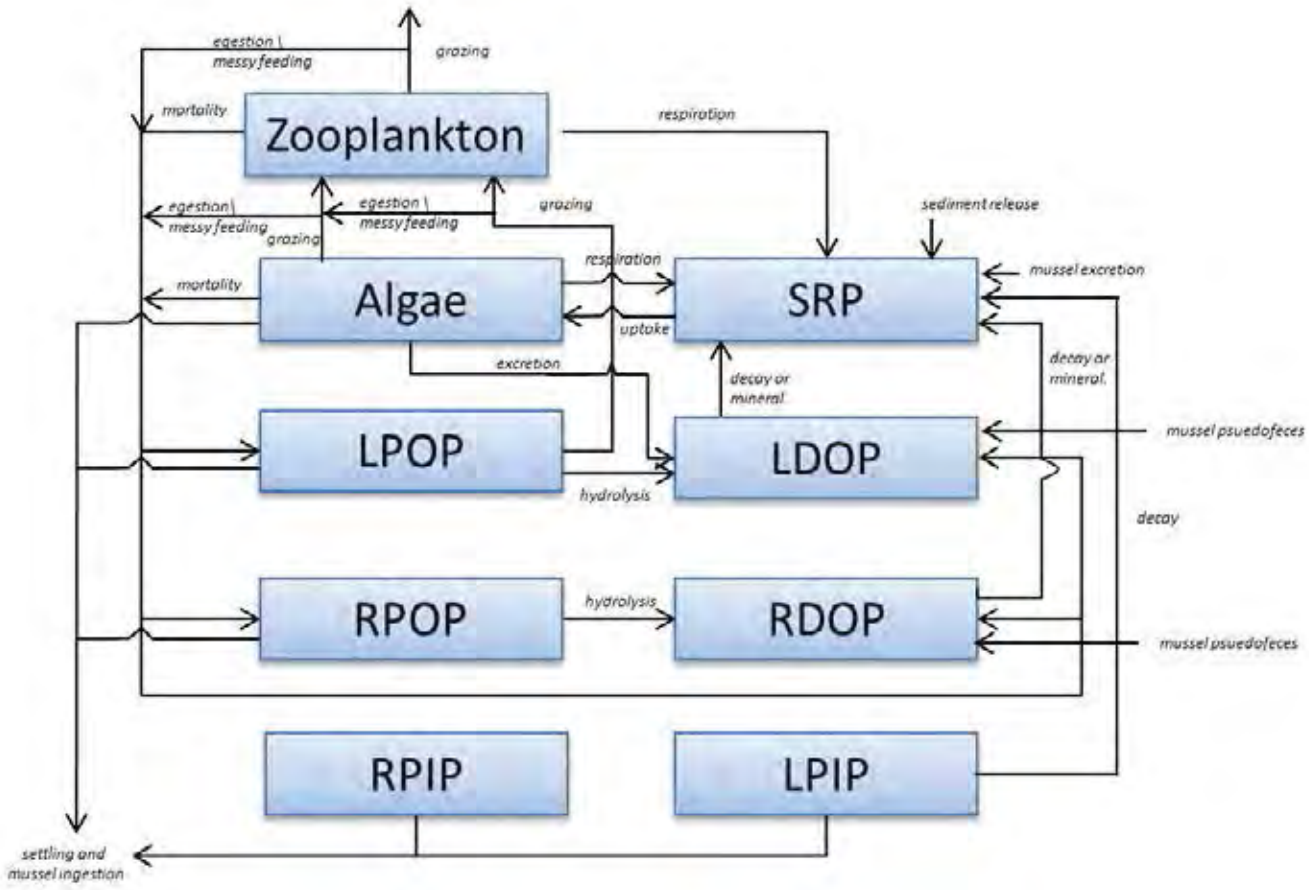

Figure 7- 20. Conceptual diagram for phosphorus sub-model.

7.6.1.4. Silica sub-model

The silica sub-model (Figure 7- 21) was included in CLM-2D to allow for simulation of diatoms as a separate algal group. Dissolved silica (DSi), which is used in the formation of diatom frustules, can limit diatom growth when depleted to low levels (Reynolds 2006). Sources of DSi to the water column include tributary loading and hydrolysis of particulate silica (PSi). Diatom mortality, zooplankton egestion, and messing feeding by zooplankton are the primary sources of Psi to the water column. PSi is lost to the water column through settling and ingestion by dreissenid mussels.

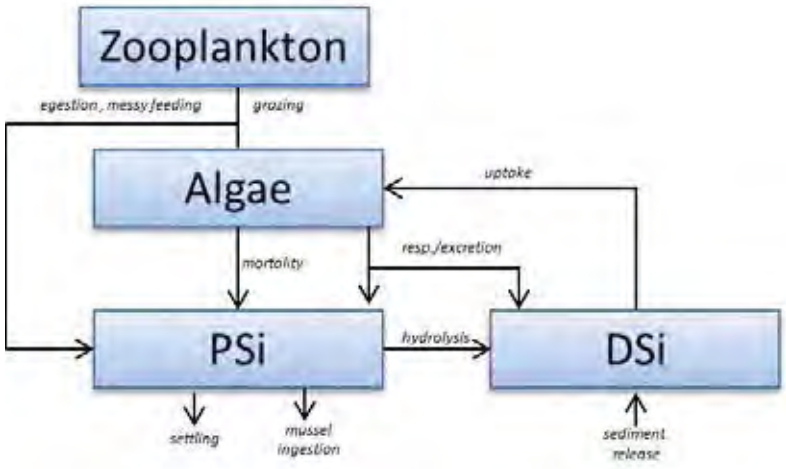

Figure 7- 21. Conceptual diagram for the silica sub-model

7.6.1.5. Dissolved oxygen sub-model

As discussed previously, modeling of dissolved oxygen (DO) was not a priority for CLM-2D because DO is not a water quality issue for Cayuga Lake. However, the DO sub-model (Figure 7-22) was operative in CLM-2D because a DO concentration is necessary for certain reaction in other sub-models. Sources of DO in the oxygen sub-model include photosynthesis (largely limited to the epilimnion) and reaeration (epilimnion, only). Oxygen sinks include algal respiration, zooplankton respiration, dreissenid mussel respiration, nitrification, and oxidation of DOC.

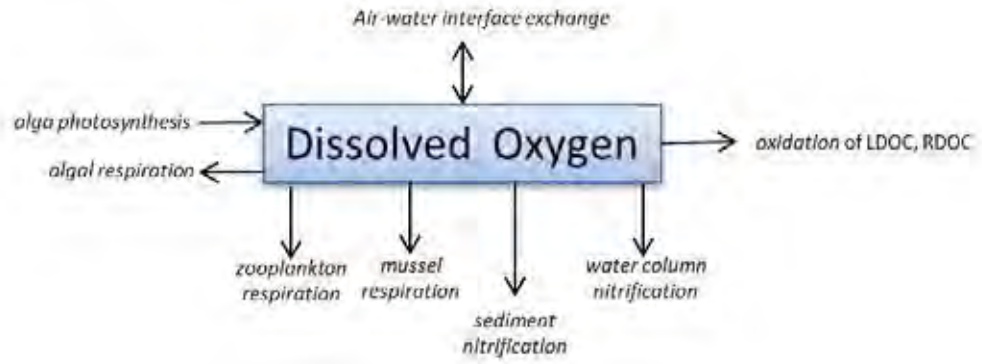

Figure 7- 22. Conceptual diagram for dissolved oxygen.

7.6.1.6. Algae sub-model

Algal biomass in lakes in the North Temperate Zone is typically limited by a combination of phosphorus availability and seasonally intense zooplankton grazing (Wetzel 2001). However, diatoms, which use dissolved silica to form frustules, can also be limited by the availability of silica. For this reason two algal groups are modeled in CLM-2D, diatoms (ALG1) and other algae (ALG2). Algal growth is limited by temperature, light and nutrient availability, as described by

Eq. 7- 12 $$\mu = \mu_{max} \cdot f(T) \cdot f(N) \cdot f(I)$$

where

μ	=	specific phytoplankton growth rates (1/d)
μ_{max}	=	maximum specific phytoplankton growth rates (1/d)
f(T)	=	temperature factor (Arrhenius type)
f(I)	=	light factor
f(N)	=	nutrient factor

A Michaelis-Menton type relationship was adopted for f(I). The f(N) term is described with a "minimum formulation"; the most severely limiting nutrient (e.g., SRP) is assumed to limit growth, in contrast to a "multiplicative" representation. The "minimum formulation" is based on "Liebig's law of the minimum", which states the nutrient in shortest relative supply will control the growth of algae. Monod kinetics were adopted to compute f(N), assuming growth rates are determined by the external (i.e., water column) concentrations of available nutrients.

Inorganic forms of carbon, nitrogen, and phosphorus are used to support algal growth. Although ammonia is the form of nitrogen preferred by algae, nitrate is used as an alternative when ammonia is unavailable. Sinks for algae include grazing by zooplankton, mortality, settling, and ingestion by dreissenid mussels. The processes of algal mortality and excretion (photorespiration) transfer algal carbon to particulate and dissolved organic forms in the water column (Figure 7- 23).

The primary metric of algal biomass in CLM-2D is particulate organic carbon (POC). The modeling goal for algal biomass was simulation of major seasonal dynamics and the summer average in the upper waters. The concentration of chlorophyll-*a* (Chl-*a*) is not simulated directly, but estimated as the product of the state variable POC and the Chl-*a*:POC ratio. Simulation of Chl-*a* was a secondary target of the initiative, at a coarse time scale of summer average. This is consistent with the known dependence of Chl-*a* on species composition, ambient light, and other environmental conditions (Reynolds 2006). Indeed, the Chl-*a*:POC ratio has been reported to be dependent on not only light availability but nutrient status (Chalup and Laws 1990, Laws and Chalup 1990, Hecky et al. 1993).

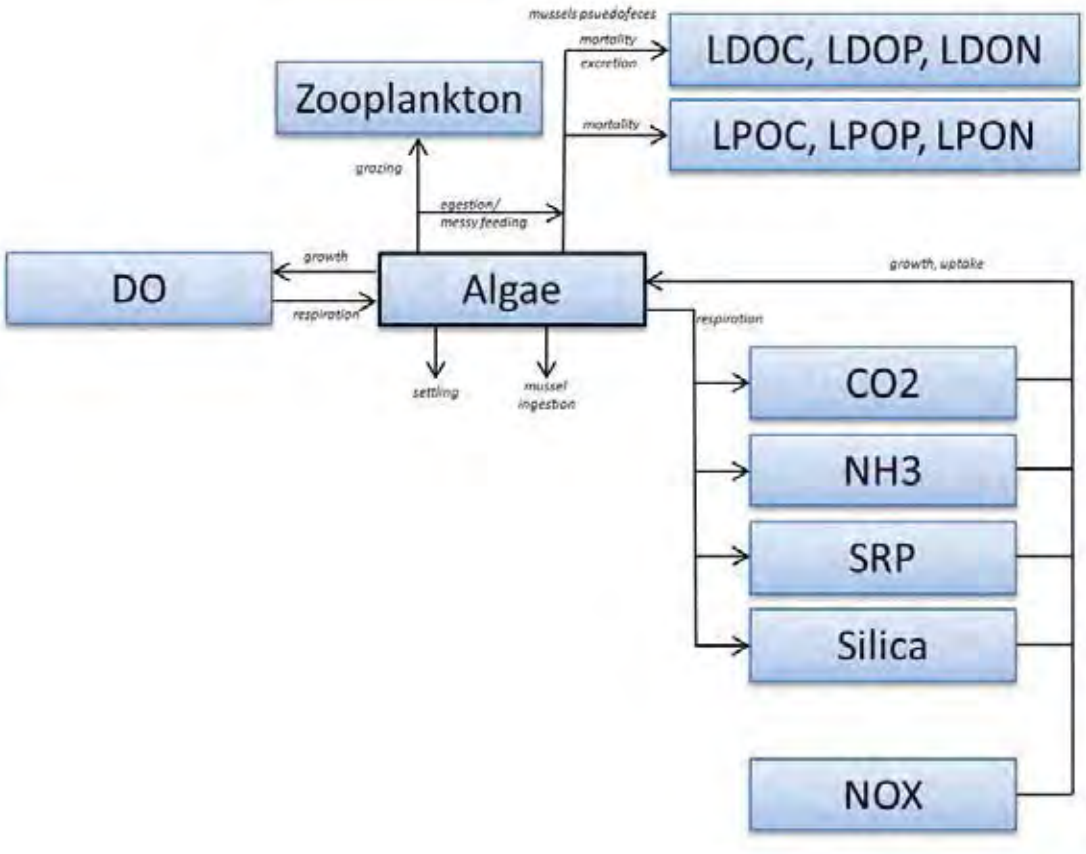

Figure 7- 23. Conceptual diagram for algae sub-model.

7.6.1.7. Zooplankton sub-model

A zooplankton sub-model was included in CLM-2D to accommodate the effects of grazing on the algal community of Cayuga Lake (Figure 7-24). Zooplankton are modeled as a single group that consumes algae, labile particulate organic matter (LPOC, LPOP, LPON), and DO. Zooplankton respiration recycles algal nutrients (CO2, NH3, SRP) back to the water column. Labile forms of dissolved and particulate organic matter are produced as a result of zooplankton mortality. Because the zooplankton community of Cayuga Lake is dominated by small taxa, it is not expected that related grazing impacts will have major effects on algal biomass.

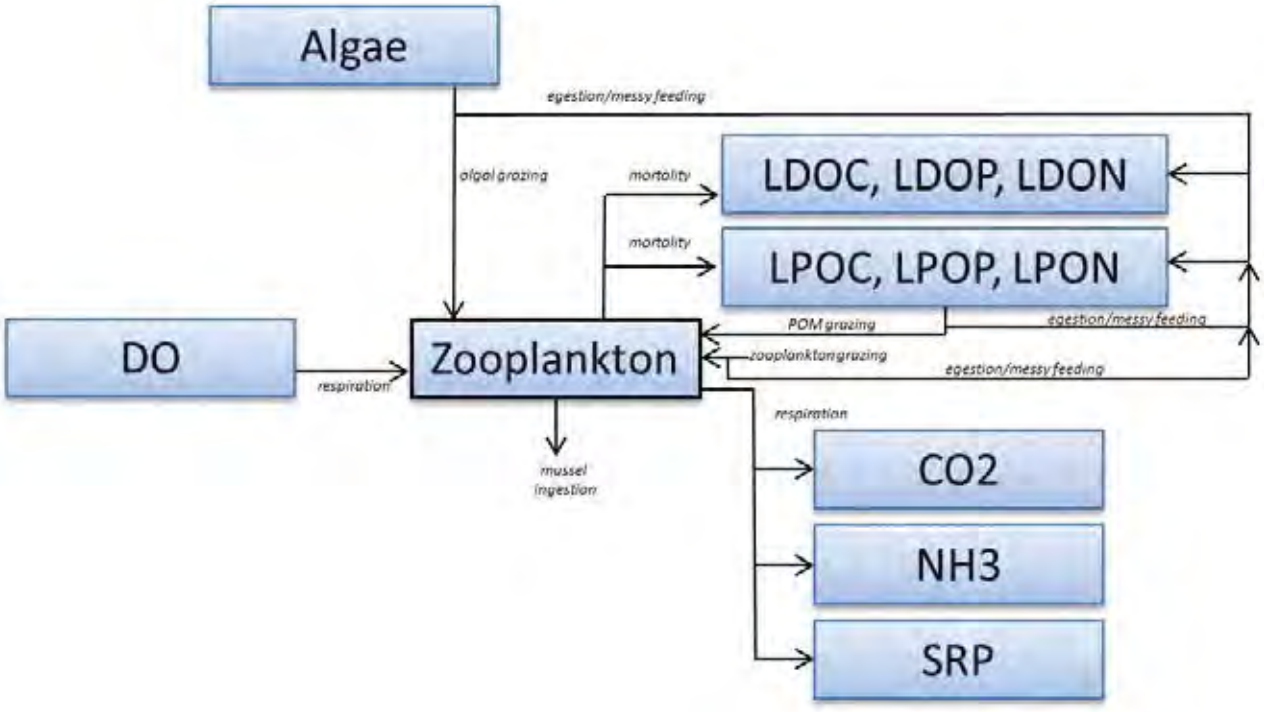

Figure 7- 24. Conceptual diagram for zooplankton sub-model.

7.6.1.8. Modeling the effects of dreissenid mussels

The water quality sub-model was updated to accommodate the water quality impacts of dreissenid mussels (zebra and quagga; Figure 7-25) found on the bottom of Cayuga Lake. The model simulates the impact of dreissenid mussels on the water column by removing particulate constituents and converting a fraction of the particulates to dissolved constituents (e.g., SRP). However, the growth and mortality of the mussels were not modeled. Instead, the mussel biomass measured in 2013 as part of Phase 1 was used as a model driver. The mussel sampling

program was described in detail in subsection 5.4.2 of the Phase 1 report (UFI 2014). In Phase 2, vertical profiles of areal density (dry weight mass per unit area of lake bottom, gDW/m2) were developed at each sampling location for both zebra and quagga mussels. A single dreissenid mussel group was formed by summing the measured biomass of the two species. These profiles were assumed to be representative of the biomass within the model segment that the sample site was located in. The data were then spatially interpolated, both vertically and horizontally, to obtain vertically detailed profiles of dreissenid mussel density for each of the 25 model segments (Figure 7-26a-w). The filtering rate of dreissenid mussels was determined through calibration, guided by laboratory experiments performed during Phase 1 (UFI 2014).

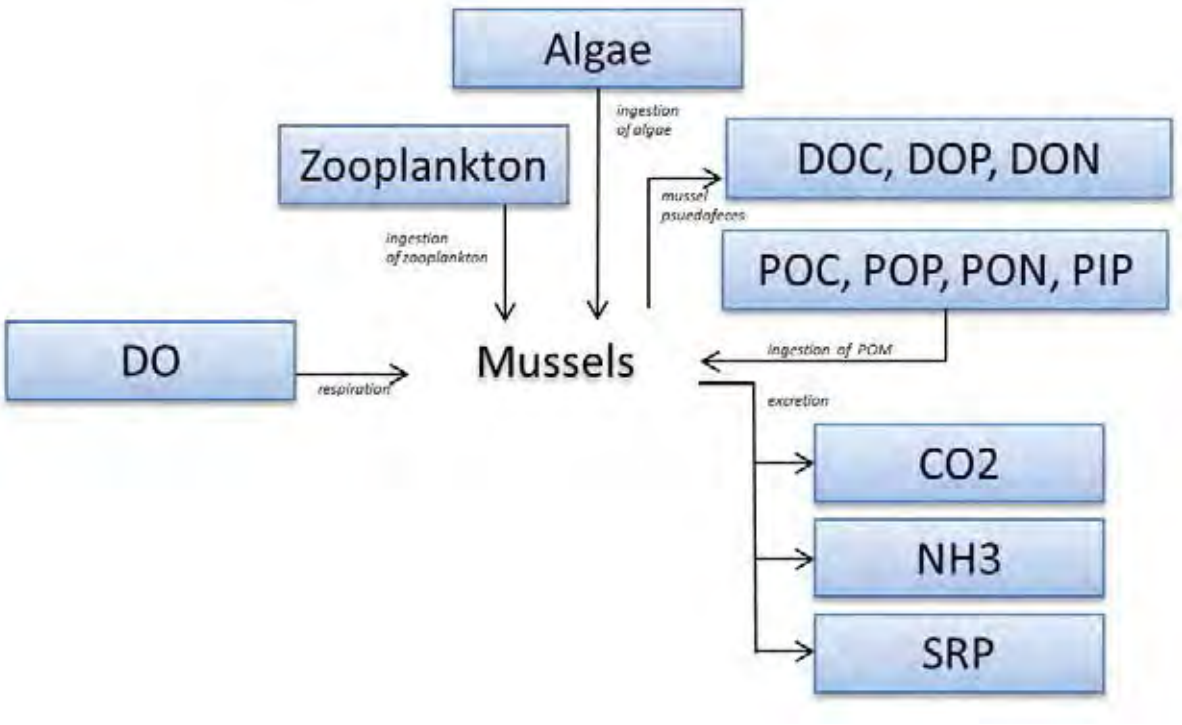

Figure 7- 25. Conceptual diagram for dreissenid mussels.

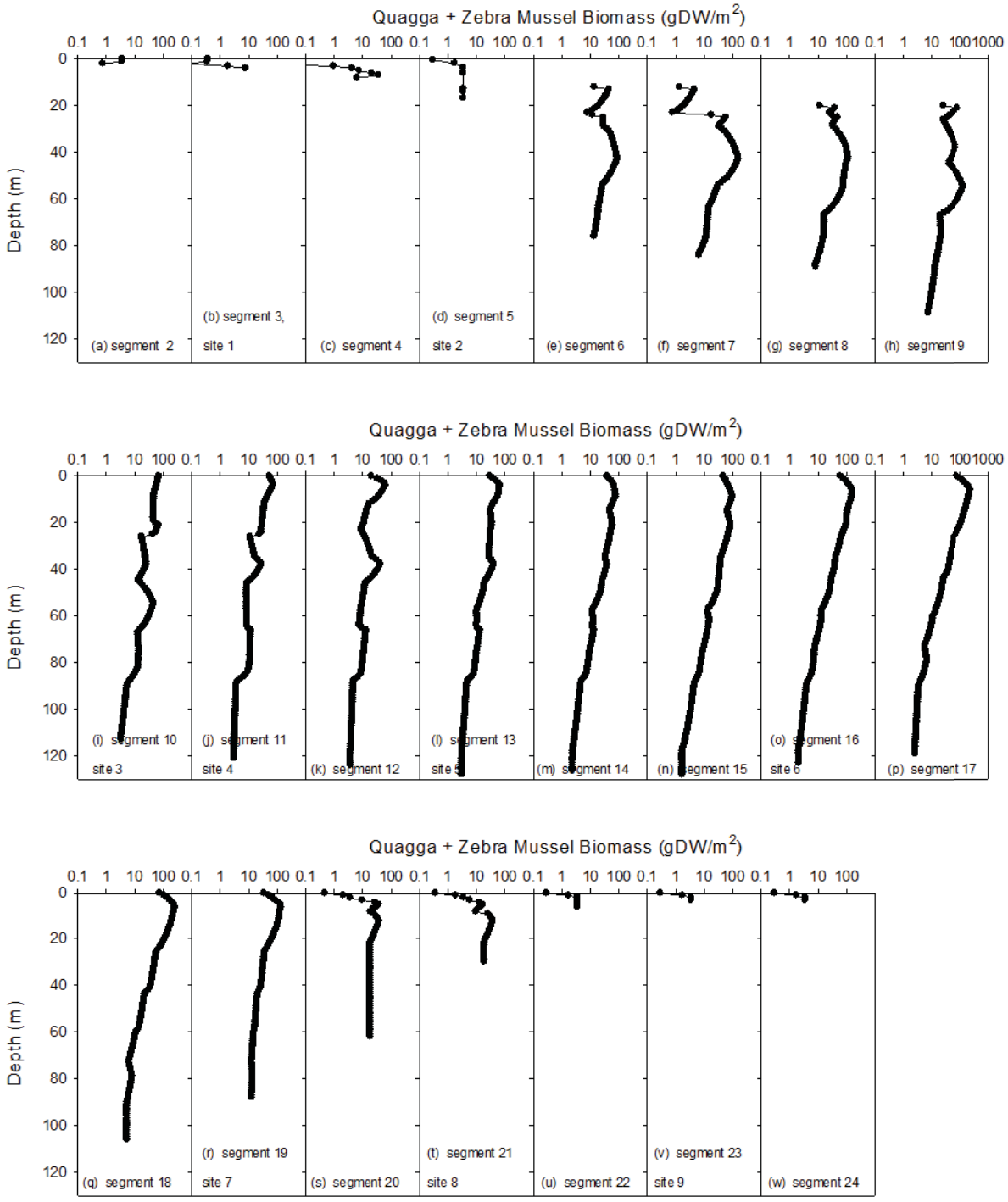

Figure 7- 26. Vertical profiles of dreissenid mussel density according to model segment. Site numbers are included for reference.

7.6.1.9. Minerogenic particle submodel

As described in the Phase 1 report (UFI 2014, Section 5) and UFI publications (Gelda et al. 2016, and Peng and Effler 2015), minerogenic particles delivered to Cayuga Lake from its watershed play an important role in metrics of water quality in the lake, including phosphorus, turbidity, clarity and light penetration. The key model state variable is the projected area of minerogenic particles per unit volume (PAV_m). The modeling approach (Gelda et al. 2016) is similar to that developed and successfully tested and applied for turbidity (Tn) in the New York City water supply reservoirs (Gelda and Effler 2007, Gelda et al. 2009, Gelda et al. 2012, Gelda et al. 2013). PAV_m was partitioned into the contributions of multiple size classes. Four size classes have been adopted in data analyses presented here (UFI 2014).

External loads of PAV_m for the same four size classes were specified by measurements for the calibration year of 2013 (Gelda et al. 2016). PAV_m – Q relationships (Figure 7-27) were applied for days without observations in 2013, as well as for model validation years. The size classes were subjected to size-dependent settling losses (Stokes' Law) and conversions to other size classes associated with aggregation/disaggregation processes (Figure 7-27). The aggregation/disaggregation processes was represented by a "net" aggregation, quantified through calibration of the sub-model to track observations of in-lake patterns. Predictions of PAV_m in time and space are the summation of the contributions for the four size classes. Predictions of particle volumes of minerogenic particles per unit volume (PVV_m) was calculated from the PAV_m size class values (Figure 7-27) assuming a particle geometry (initially spherical, but may be platelets). Predictions of PAV_m can support predictions of (Figure 7-27): (1) the minerogenic component of PP (PP_m), (2) the minerogenic component of Tn (Tn/m), and (3) levels the absorption (a_m) and scattering (b_m) coefficients for minerogenic particles, that serve as inputs to the optics sub-model (described subsequently). The predictions of PVV_m could serve to support predictions of inorganic (fixed) suspended solids (FSS).

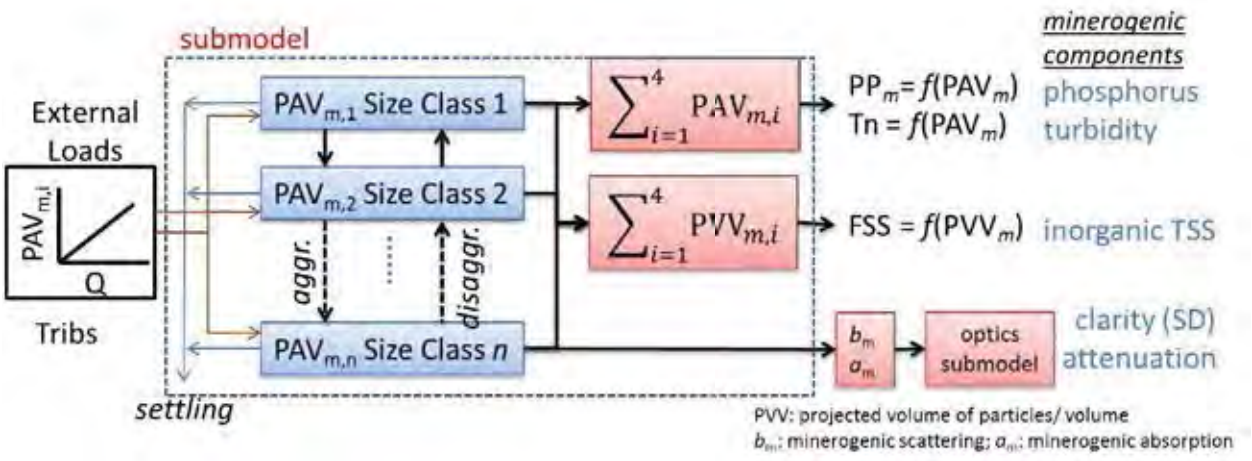

Figure 7- 27. Conceptual diagram for the minerogenic particle submodel.

7.6.1.10. Optics submodel

The optics sub-model provides predictive capabilities for optical metrics of water clarity, as represented by Secchi depth (SD) and the attenuation coefficient for scalar irradiance (K0(PAR)). SD is a primary trophic state and water quality metric of concern for lacustrine systems, including Cayuga Lake. K_0(PAR) is important as it specifies the light available at various depths to support photosynthesis and phytoplankton growth. Empirical relationships between each of these metrics and Chl-*a*, as a measure of phytoplankton biomass, have been widely adopted as part of the P-eutrophication modeling. However, in Cayuga Lake, as well as many other lakes, this is inadequate (e.g., performs poorly) because other substances contribute importantly to these optics conditions, and these do not necessarily co-vary with phytoplankton. Alternately, a mechanistic framework, one that is consistent with optical theory, is adopted.

A theoretically sound mechanistic framework is described in Figure 7-28 (refer to Table 7-11 for definition of symbols). Accordingly (moving left to right), the constituents that influence the optical measures of concern (SD and K_0(PAR)), described as apparent optical properties (AOPs) are described as the optically active constituents (OACs). The OACs are mostly state variables of the water quality model, or can be independently specified. These include measures of phytoplankton biomass (Chl-*a* or POC) and minerogenic particles (PAV_m or FSS (ISPM)). Associated components of the absorption (*a*) and scattering (*b*) coefficients, both described as inherent optical properties (IOPs), are estimated according to OAC – specific coefficients (cross-sections; Figure 7-28). The desired AOPs are predicted from IOPs using well-established equations (radiative transfer expressions; Figure 7-28). Elements of the model have been developed and successfully tested for Cayuga Lake (Effler et al. 2015b), including (1) development of cross-sections, (2) closure of the summation of absorbing components with

overall absorption, and (3) closure IOPs and AOPs through application of the radiative transfer equations.

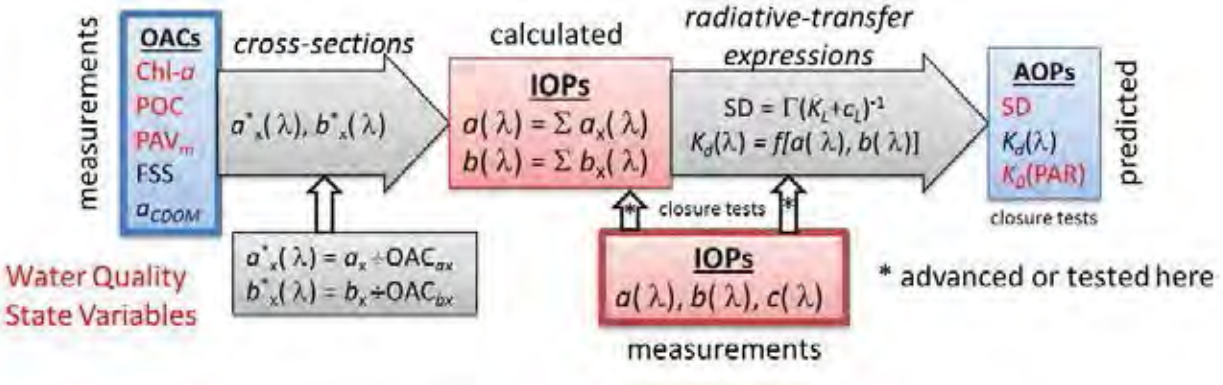

Figure 7- 28. Conceptual diagram for the optics submodel.

Table 7- 11. Specifications of symbols in the optics submodel.

Symbol	Specifications
OACs	optically active constituents
Chl-*a*	chlorophyll *a* concentration
POC	particulate organic carbon concentration
PAV_m	projected area of minerogenic particles concentration
FSS	inorganic suspended particulate material concentration (ISPM)
a_{CDOM}	absorption coefficient for CDOM
OAC_{ax}	OAC for a_x
OAC_{bx}	OAC for b_x
IOPs	inherent optical properties
$a(\lambda)$	spectral absorption coefficient
$b(\lambda)$	spectral scattering coefficient
$c(\lambda)$	spectral beam attenuation coefficient
$a_x^*(\lambda)$	spectral absorption cross-section for component
$b_x^*(\lambda)$	spectral scattering cross-section for component
a_x	absorption coefficient for component x
b_x	scattering coefficient for component x
c_L	beam attenuation illuminance coefficient
AOPs	apparent optical properties
SD	Secchi disk depth
$K_{d(\lambda)}$	spectral downwelling attenuation coefficient
K_0(PAR)	scalar attenuation coefficient for PAR
Γ	coefficient for SD radiative transfer function
K_L	downwelling attenuation illuminance coefficient

7.6.2. Water quality modeling protocols

The time step of hydrologic, material loading, and meteorological forcing function inputs to the water quality model is one day. The computational time step of the model calculations is one hour. The model was initialized by the measurements made at sites 1-9 on the first day of sampling (April 8) in 2013. Model coefficients are presented in Appendix 2 (Table A7-1). Coefficient values were selected based on earlier work on Cayuga Lake, from the literature, or based on professional judgement and well accepted limnological paradigms.

7.6.3. Development and specification of water quality model drivers

7.6.3.1. Inflow concentrations

Constituent loads are available in two forms (1) estimates based on a combination of observed concentrations (C), and those estimated from flow (Q) measurements, as described by C-Q relationships (UFI 2014), and (2) predictions from the tested watershed/land use model (SWAT version 2012). The first form utilizes the FLUX32 software that provides flow and concentration estimates at a daily time step (refer to Section 3 for details). This temporal resolution is generally consistent with the goal(s) of P-eutrophication models, and is adequate to address the short-term hydrologic and water quality issues of the shelf related to runoff events. Loading estimates for years without regular tributary monitoring of concentrations will depend primarily on the C-Q relationship developed from the 2013 data set (the most intensive available; see Section 3), but will also be informed from longer-term monitoring. Accordingly, these loading estimates are limited to the period of Q gaging.

Constituent concentrations for all tributary and point source inflows are a critical form of input for CLM-2D. Concentrations of various constituents were measured in 2013 at the mouths of five Cayuga Lake tributaries and in the inlet channel (Figure 7-1), as described in the Phase 1 QAPP (UFI 2014). The methods used to calculate loads were documented in detail in the Phase 1 final report (UFI 2014, Prestigiacomo et al. 2016) and in Section 3 of this report. The resulting loads were divided by the flows to develop tributary-specific inflow concentrations. Plots of concentrations for selected inflows and constituents are available in Appendix 2 (Figures A7-7 through A7-21). Constituent concentrations input to CLM-2D may be modified based on output from the watershed/land use model (SWAT; Section 8). For example, a SWAT management scenario that predicted a 10% reduction in TP loading for Fall Creek would be translated to CLM-2D as a 10% reduction in the TP concentrations for this inflow. Note that concentrations are modified rather than loads or flows. This represents a linkage of the models that is attractive for evaluating land use management alternatives.

7.6.3.2. In-lake calibration and validation data sets

A temporally and spatially robust dataset was collected for Cayuga Lake in 2013 to support model calibration. Details regarding the collection of these datasets are covered in detail in the Phase 1 QAPP (UFI 2013). Data analyses and summary of findings from 2013 are documented in detail in the Phase 1 final report (UFI 2014).

The validation data sets for CLM-2D rely heavily on data collected as part of Cornell University's long-term (1998-2012) monitoring program for the Lake Source Cooling facility (*https://energyandsustainability.fs.cornell.edu/util/cooling/production/lsc/default.cfm*). Data was collected at seven sites on the southern shelf and one deeper water site. Three of these monitoring sites corresponded to the locations of sites 1, 2, and 3 from the 2013 monitoring program. Measurements from these sites serve as the validation datasets for 1999 and 2006.

7.6.3.3. Summary of non-direct measurements

In the Phase 1 QAPP UFI was tasked with compiling a system-specific data set for Cayuga Lake related to the phosphorus-eutrophication issue. Related and supporting datasets and other information were obtained, compiled, and utilized in both Phase 1 and Phase 2. Table 7-12 summarizes these non-direct measurements utilized in the both phases of the project.

Table 7- 12. Non-direct measurements utilized in the Phase 1 and Phase 2 of the Cayuga Lake Modeling Project.

No.	Data Type	Source of data	How used
1.	stream flows	United States Geological Survey (USGS)	used in flow budget and as input to the model
2.	watershed areas	Haith et al. 2012	used to adjust USGS flows and partition unmonitored flows that were utilized in a flow budget and as an input to the model
3.	meteorological data	Cornell University – pile cluster data	driver of the hydrothermal/transport model
		Cornell University – Game farm Road data	
		National Oceanic & Atmosphere Administration (NOAA)	
4.	point source flows and constituents	Cornell University – LSC based lake monitoring	flow and P data as model inputs, tNH_3 as model input for WWTPs only
		IAWWTP, biweekly P data, 1995-2013, DMR data sets 2009-2013	
		CHWWTP, DMR data sets 2000-2013 for P, 2009-2013 others	
		Minor WWTP, DMR data sets 2009-2013	
		ASE power plant	
5.	stream temperatures	CSI ~2000-2013 (stream dependent)	validation of 2013 UFI air temperature vs. creek temperature regressions used to estimate creek temperatures between measurement days
6.	stream constituents	UFI 2003-2006 TP, TDP, SRP, Tn data	model inputs for years 2003-2006
		CSI ~2000-2013 (stream dependant) for TP, t-NH3, NO_X, TSS, Tn	validation of 2013 concentration/flow regressions used to estimate constituents between measurement days
		DEC 2007 TP, DOC	validation of 2013 concentration/flow regressions used to estimate constituents between measurement days
		LSC based lake monitoring data	validation data sets
7.	historical limnological information – phosphorus, clarity and plankton	earlier studies by UFI	validation data sets utilized to develop model grid
		Cornell University	
8.	bathymetric data	Cornell University	Set-up of hydrothermal/transport model

7.6.4. Water Quality Model Calibration, 2013

Model performance is evaluated primarily through comparisons of model predictions with in-lake observations. Predictions and observations are typically presented as time series of epilimnetic and hypolimnetic concentrations, and statistical results related to goodness of fit (e.g., percent error). Criteria for performance need to be sensitive to the available environmental signals. The signals are somewhat limited in low productivity systems such as Cayuga Lake relative to those available in highly eutrophic lakes and reservoirs. Reasonable criteria for lower productivity systems may include model simulations that track major recurring seasonal dynamics and the magnitudes of the Chl-*a* (POC) and dissolved nutrient pools. Matching the fine temporal structure of Chl-*a* and the pools of various forms of P is not a reasonable goal for these systems. Rather, the goal is to simulate seasonal average concentrations and also gross seasonality where possible.

Target performance thresholds for CLM-2D are provided in Table 7-13, according to parameter. The metrics are consistent with the water quality issues identified for Cayuga Lake, the goals of the Phase 2 modeling, and the potential use of the model to support a phosphorus TMDL analysis. These performance thresholds will be applied on a summer average basis, consistent with common regulatory standards and trophic state representations in the scientific literature. Spatially, conditions on the shelf will be contrasted to conditions within the pelagic waters of the lake, consistent with the findings of Phase 1. Note that performance criteria were not specified for the hypolimnion because the primary modeling targets were metrics of trophic state in the upper waters. Since hypolimnetic observations are only available for the model calibration year of 2013, the model cannot be validated for the lower waters. In cases where targeted thresholds of performance were not attained after reasonable effort, we have reported specifically on the performance issue and the results have been qualified as appropriate.

Table 7- 13. Targeted thresholds of model performance for multiple metrics of interest.

Predicted Metric	**Targeted Thresholds of Performance[1] % Error[2]**
TP	< 25%
SD	< 25%
Chl-*a*	< 50%
POC	< 30%
PAVm	< 30%

[1] summer (June-September) average values for the upper waters
[2] % Error = absolute value of (prediction – observation)/observation ×100

7.6.4.1. Model calibration fits for a pelagic site

Calibrated model fits for selected particulate parameters in 2013 are presented for the upper waters (0-10 meters) at site 5 (Figure 7-29). Observations at site 5 are generally representative of water quality conditions in the pelagic zone of Cayuga Lake (UFI 2014). The model simulation indicates the algal community was dominated by diatoms (Alg1) in late spring and early summer (Figure 7-29a) and by other algal taxa during late summer and fall (Figure 7-29b). The model matched the general magnitude of POC and captured the pattern of higher concentrations during July and August and lower concentrations during spring and fall (Figure 7-29c). The model failed to match the observed spikes in POC in early July and mid-August. This shortcoming was probably caused by non-algal (e.g., detrital) watershed contributions to POC during major runoff events. The general magnitude of Chl-*a*, and the increase from spring to summer, was simulated nicely (Figure 7-29d). However, the model did not capture the observed short-term dynamics in Chl-*a*, as expected. Observed temporal dynamics in TP concentrations on the southern shelf were matched well, including short-term increases associated with runoff events (Figure 7-29e). The model did tend to under predict TP levels on the southern shelf, potentially due to a missing source such as resuspension.

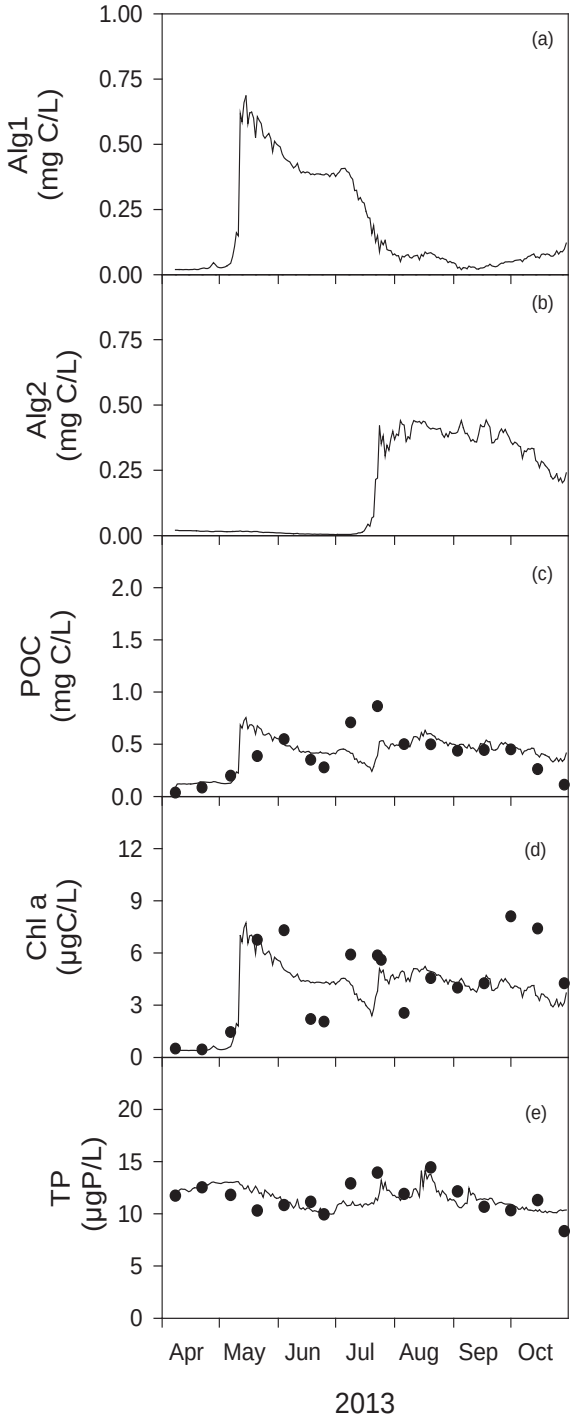

Figure 7- 29. Time series of predicted and observed upper water (0-10 meter average) concentrations of selected particulate water quality parameters for Cayuga Lake, site 5 in 2013: (a) Alg1, (b) Alg2, (c) Chl-*a*, (d) POC, and (e) TP.

Calibrated model fits for selected dissolved parameters are presented for the upper waters (0-10 meters) at site 5 (Figure 7-30). Both the magnitude of NO_x and the noteworthy seasonal depletion of this algal nutrient were simulated with a high degree of accuracy by the model (Figure 7-30a). NO_x was somewhat underpredicted during late summer and fall. The model fit to SRP measurements on the shelf was generally excellent, including the observed depletion in May (Figure 7-30b) that coincided with an increase in algal biomass (Figure 7-29d). Observed concentrations of dissolved Si were matched closely by the model (Figure 7-30c). Again, the model performed excellently in matching the observed depletion of this important diatom nutrient during May and June.

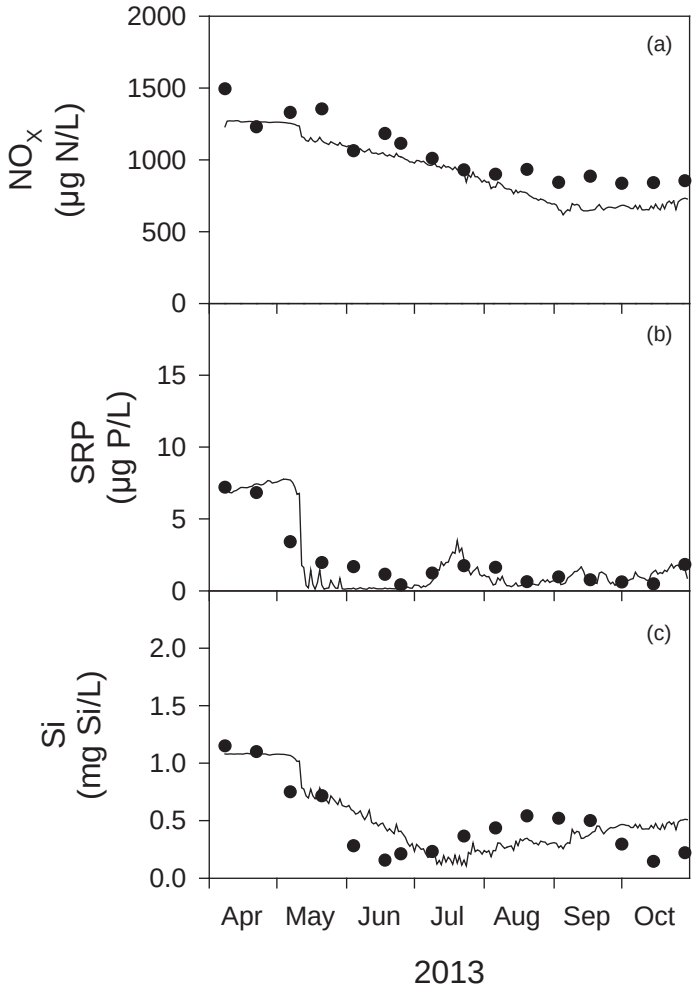

Figure 7- 30. Time series of predicted and observed upper water (0-10 meter average) concentrations of selected dissolved water quality parameters for Cayuga Lake, site 5 in 2013: (a) NO_x, (b) SRP, and (c) DSi.

Model performance was generally excellent in matching the magnitudes of particulate (Figure 7-31) and dissolved (Figure 7-32) constituents in the lower waters of Cayuga Lake. The model simulations of POC (Figure 7-31d), NOx (Figure 7-32a), SRP (Figure 7-32b), and DSi (Figure 7-32c) were particularly good. The modeled concentrations of TP in the lower waters were somewhat higher than the observations, and the trajectory of the progressive seasonal increase was not closely matched (Figure 7-31e). Although the departure of model predictions from TP observations is modest in scale (2-3 g/L), it does represent a bias toward higher TP values in the lower waters.

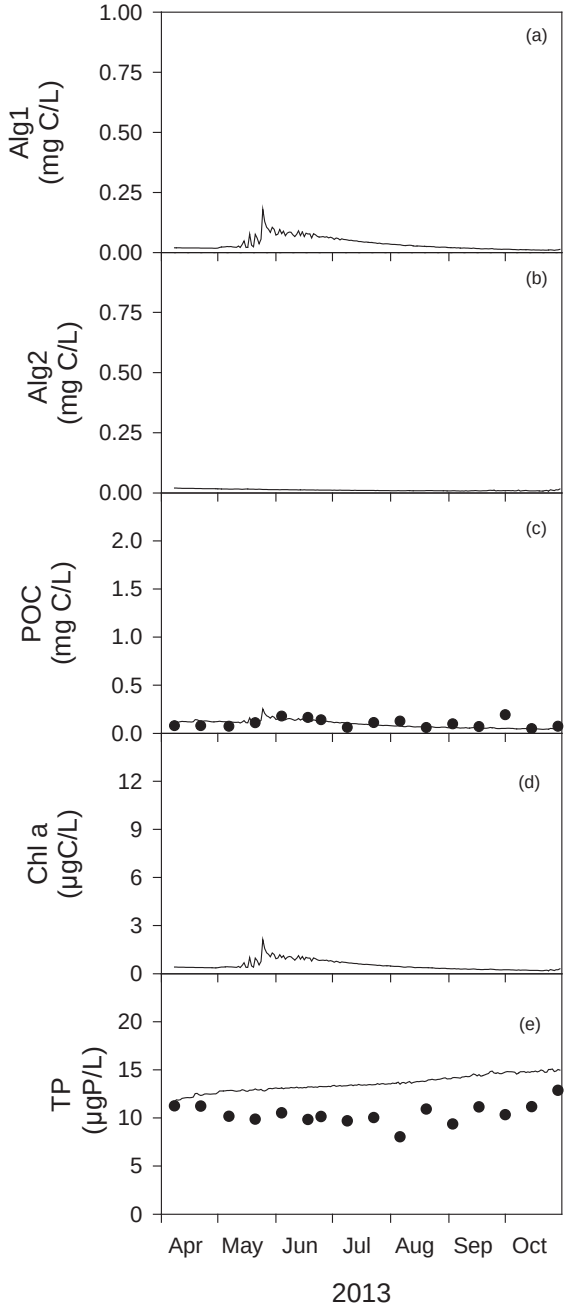

Figure 7- 31. Time series of predicted and observed lower water (20-133 meter average) concentrations of selected particulate water quality parameters for Cayuga Lake, site 5 in 2013: (a) Alg1, (b) Alg2, (c) Chl-*a*, (d) POC, and (e) TP.

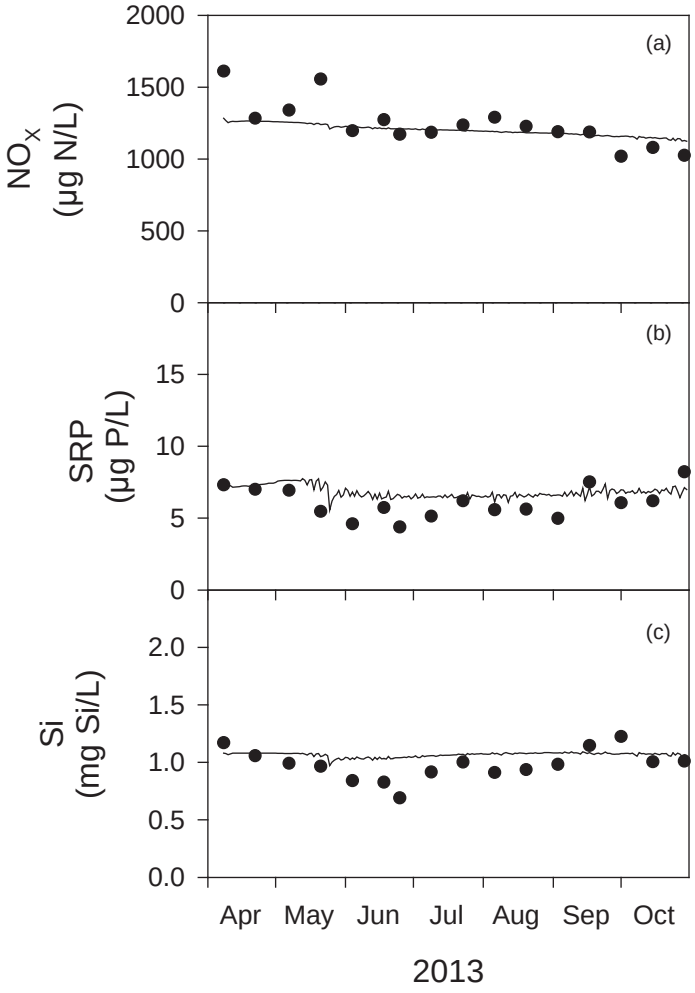

Figure 7- 32. Time series of predicted and observed lower water (20-133 meter average) concentrations of selected dissolved water quality parameters for Cayuga Lake, site 5 in 2013: (a) NOx, (b) SRP, and (c) DSi.

7.6.4.2. Model calibration fits for the southern shelf

Model calibration fits are presented in Figure 7-33 for selected particulate parameters measured in 2013 at site 1, located on the southern shelf. The model simulation indicates the algal community was dominated by diatoms (Alg1) in late spring and early summer (Figure 7-33a) and by other algal taxa during late summer and fall (Figure 7-33b). The model matched the general magnitude of POC and captured the pattern of higher concentrations during July and August and lower concentrations during spring and fall (Figure 7-33c). The model failed to match the observed spikes in POC in early July and mid-August. This shortcoming was

probably associated with non-algal (e.g., detrital) watershed contributions of POC during major runoff events. The general magnitude of Chl-*a*, and the increase from spring to summer, was simulated nicely (Figure 7-33d). However, the model did not capture the observed short-term dynamics in Chl-*a*, as expected. Observed temporal dynamics in TP concentrations on the southern shelf were matched well, including short-term increases associated with runoff events (Figure 7-33e).

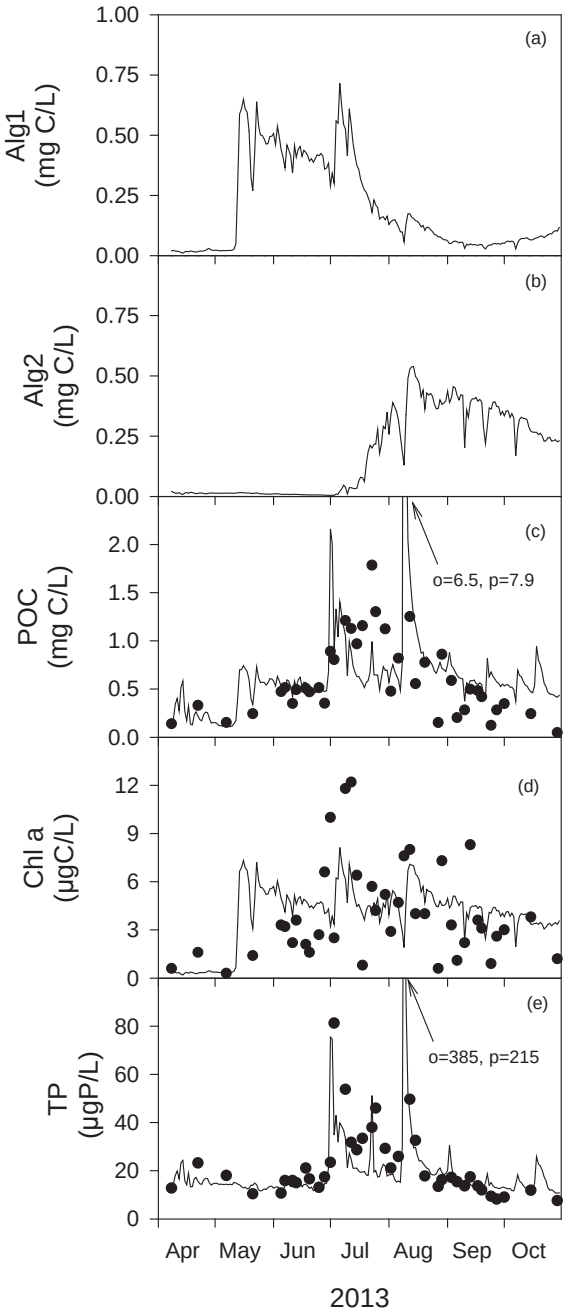

Figure 7- 33. Time series of predicted and observed upper water concentrations of selected particulate water quality parameters for Cayuga Lake, site 1 in 2013: (a) Alg1, (b) Alg2, (c) Chl-*a*, (d) POC, and (e) TP.

Model calibration fits are presented in Figure 7-34 for selected dissolved parameters measured in 2013 at site 1, located on the southern shelf. Both the magnitude of NOx and the noteworthy seasonal depletion of this algal nutrient were simulated with a high degree of accuracy by the model (Figure 7-34a). The model fit to SRP measurements on the shelf was generally excellent, including the observed depletion in May (Figure 7-34b) that coincided with an increase in algal biomass (Figure 7-33d). Two instances of high SRP in July, associated with runoff events, were under predicted by the model. Observed concentrations of dissolved Si were matched closely by the model (Figure 7-34c). Again, the model performed excellently in matching the observed depletion of this important nutrient for diatoms during May and June.

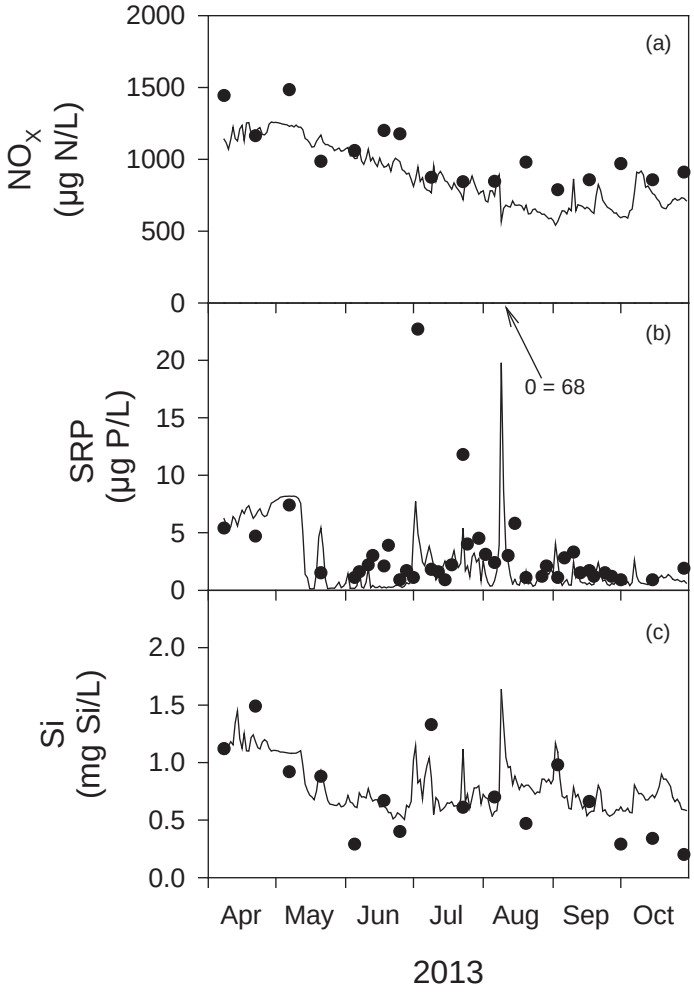

Figure 7- 34. Time series of predicted and observed upper water concentrations of selected dissolved water quality parameters for Cayuga Lake, site 1 in 2013: (a) NOx, (b) SRP, and (c) DSi.

7.6.5. Water quality model validation, 1999 and 2006

Following calibration to the robust 2013 dataset, CLM-2D was validated by applying it to two additional years (1999 and 2006) with a wide range of conditions for precipitation, flow, phosphorus loads, and flushing rate (see section 7.5.4.5). 1999 was characterized by dry conditions, with low tributary flows and associated P loads, and a long residence time. In contrast, 2006 was a wet year with high flows and loads, and a relatively short residence time. The wide range of meteorological forcing conditions included in the calibration and validation data sets represents a robust test of the water quality model.

7.6.5.1. Model validation fits for a pelagic site, 1999

Model fits for selected particulate parameters are presented for the upper waters (0-10 meters) at site 3 for the model validation year of 1999 (Figure 7-35). Although the general temporal pattern observed for Chl-*a* was captured by the model, concentrations were underestimated throughout the April-October interval (Figure 7-35d). This systematic underprediction may be associated with nutrient recycling by dreissenid mussels. The dreissenid mussel sub-model was turned off for this run because quagga mussels were assumed to be absent. However, it is likely that zebra mussels were abundant in the nearshore and actively recycling P, which would enhance algal growth. The model adequately matched both the magnitude and observed temporal pattern for TP (Figure 7-35e). The model tended to under predict TP levels during the July-September interval.

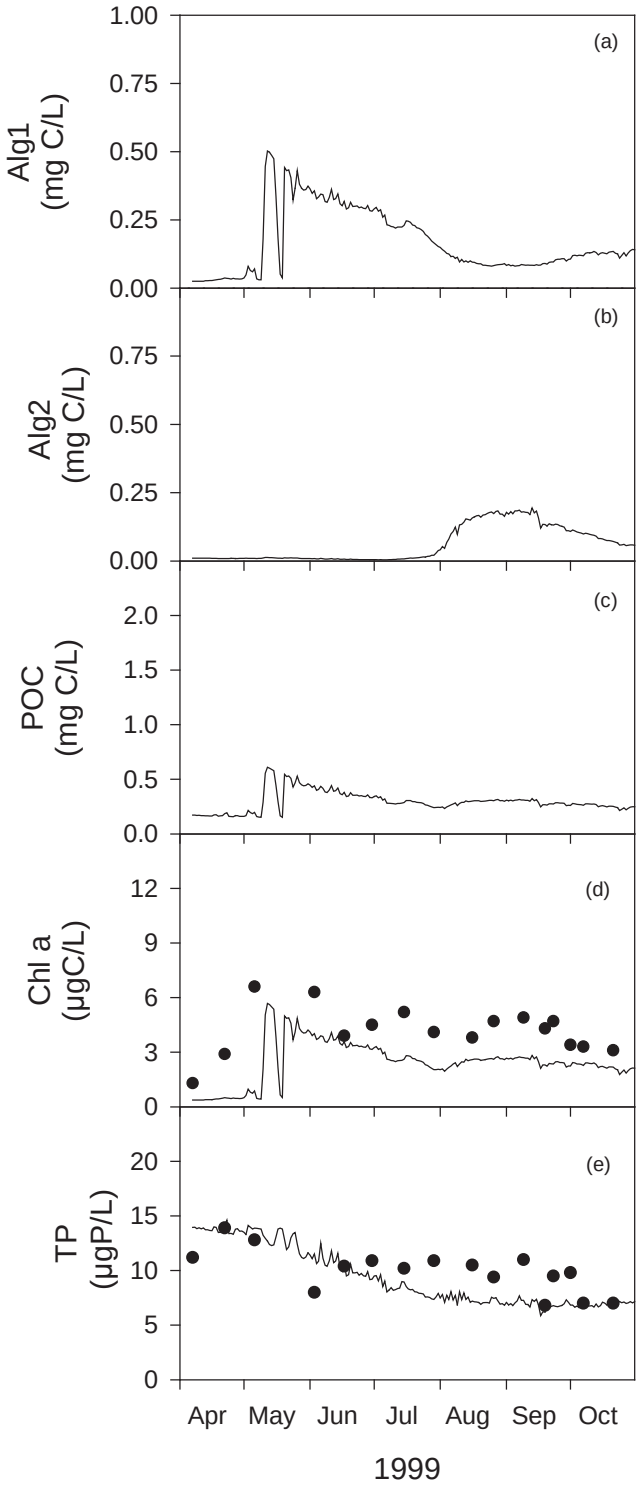

Figure 7- 35. Time series of predicted and observed upper water (0-10 meter average) concentrations of selected particulate water quality parameters for Cayuga Lake, site 3 in 1999: (a) Alg1, (b) Alg2, (c) Chl-*a*, (d) POC, and (e) TP.

Model fits for selected dissolved parameters are presented for the upper waters (0-10 meters) at site 3 (Figure 7-36). Both the magnitude of NOx and the noteworthy seasonal depletion of this algal nutrient were simulated with a high degree of accuracy by the model (Figure 7-36a). The model fit to SRP observations was quite good, including the observed depletion in May (Figure 7-36b) that coincided with an increase in algal biomass (Figure 7-35d).

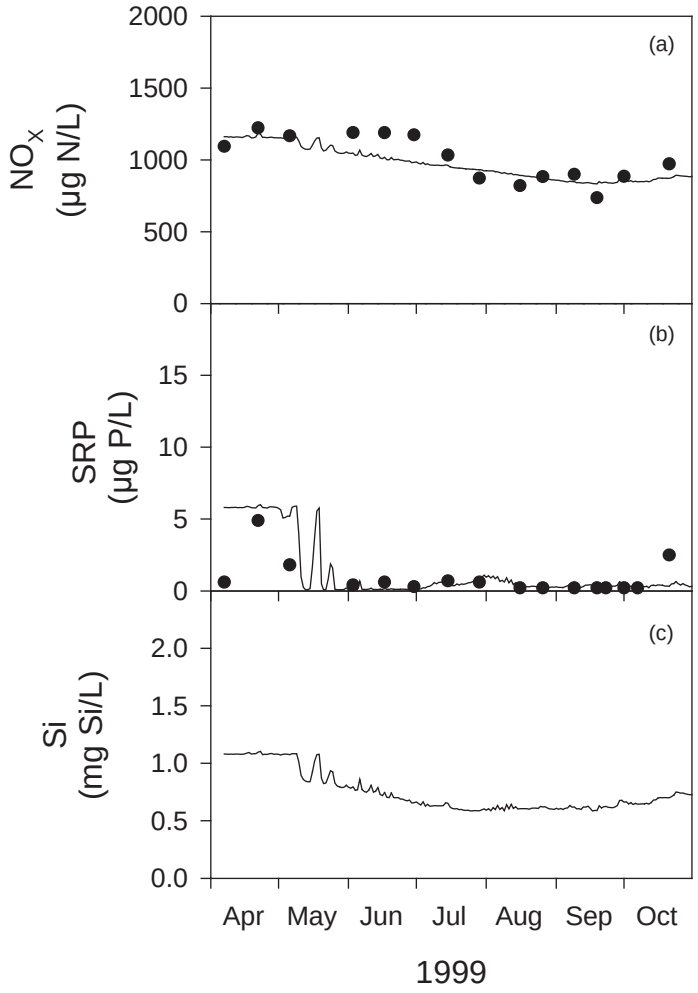

Figure 7- 36. Time series of predicted and observed upper water (0-10 meter average) concentrations of selected dissolved water quality parameters for Cayuga Lake, site 3 in 1999: (a) NO_x, (b) SRP, and (c) DSi.

7.6.5.2. Model validation fits for the southern shelf, 1999

Model fits are presented in Figure 7-37 for selected particulate parameters measured in 1999 at site 1, located on the southern shelf. The general magnitude of Chl-*a*, and the increase from spring to summer, was simulated nicely (Figure 7-37d). The model also performed impressively in capturing the short-term dynamics in Chl-*a*. The magnitude and temporal dynamics of TP on the southern shelf were also matched well by the model (Figure 7-37e).

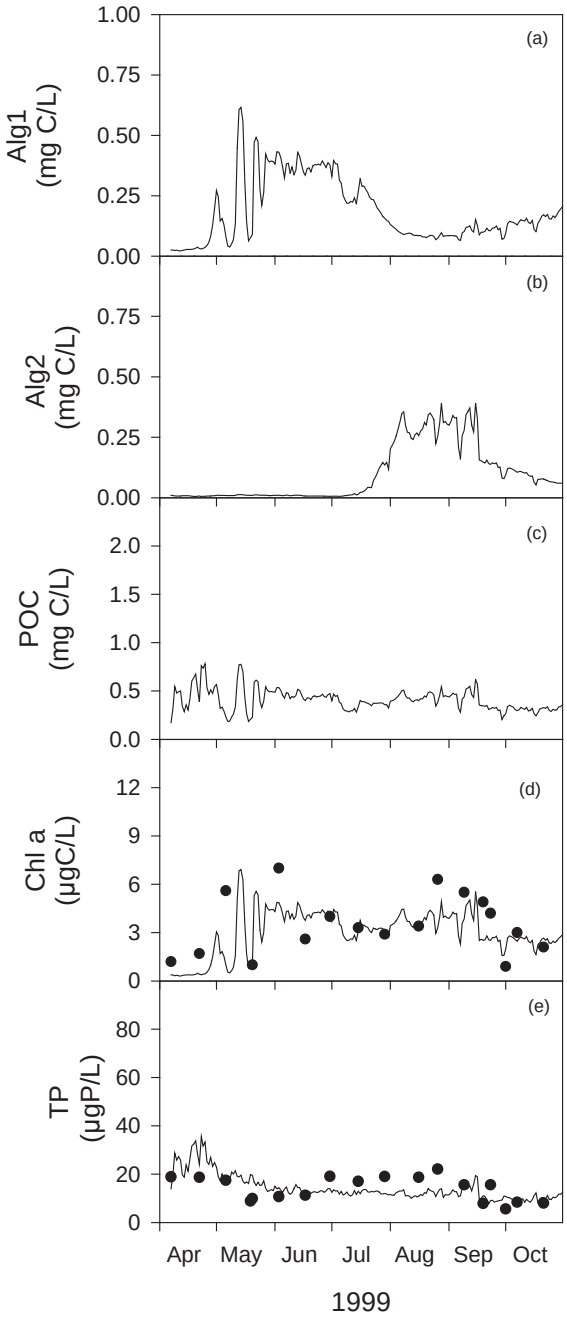

Figure 7- 37. Time series of predicted and observed upper water concentrations of selected particulate water quality parameters for Cayuga Lake, site 1 in 1999: (a) Alg1, (b) Alg2, (c) Chl-*a*, (d) POC, and (e) TP.

Model fits are presented in Figure 7-38 for selected dissolved parameters measured in 2013 at site 1, located on the southern shelf. Both the magnitude of NO_x and the noteworthy seasonal depletion of this algal nutrient were simulated with a high degree of accuracy by the model (Figure 7-38a). The model fit to SRP measurements on the shelf was generally excellent, including the observed depletion during April and May (Figure 7-38b) that coincided with an increase in algal biomass (Figure 7-37d).

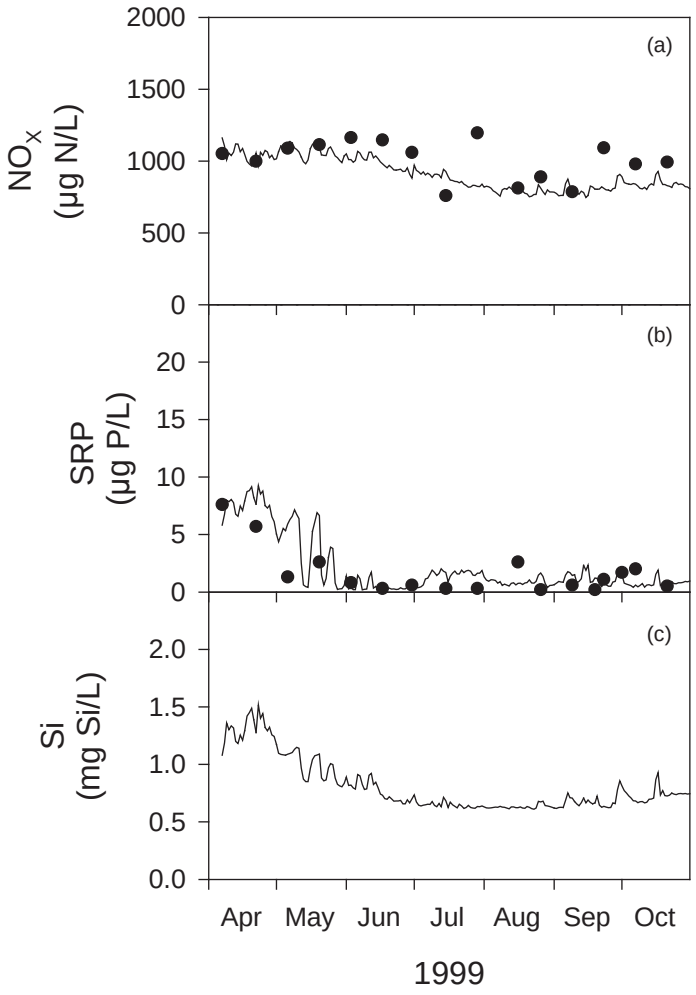

Figure 7- 38. Time series of predicted and observed upper water concentrations of selected dissolved water quality parameters for Cayuga Lake, site 1 in 1999: (a) NO_x, (b) SRP, and (c) DSi.

7.6.5.3. Model validation fits for a pelagic site, 2006

Model fits for selected particulate parameters in 2006 are presented for the upper waters (0-10 meters) at site 3 (Figure 7-39). The model generally underpredicted Chl-*a* concentrations, but did capture the observed increase from spring to summer (Figure 7-39d). The magnitude and observed temporal dynamics in TP concentrations were matched particularly well (Figure 7-39e).

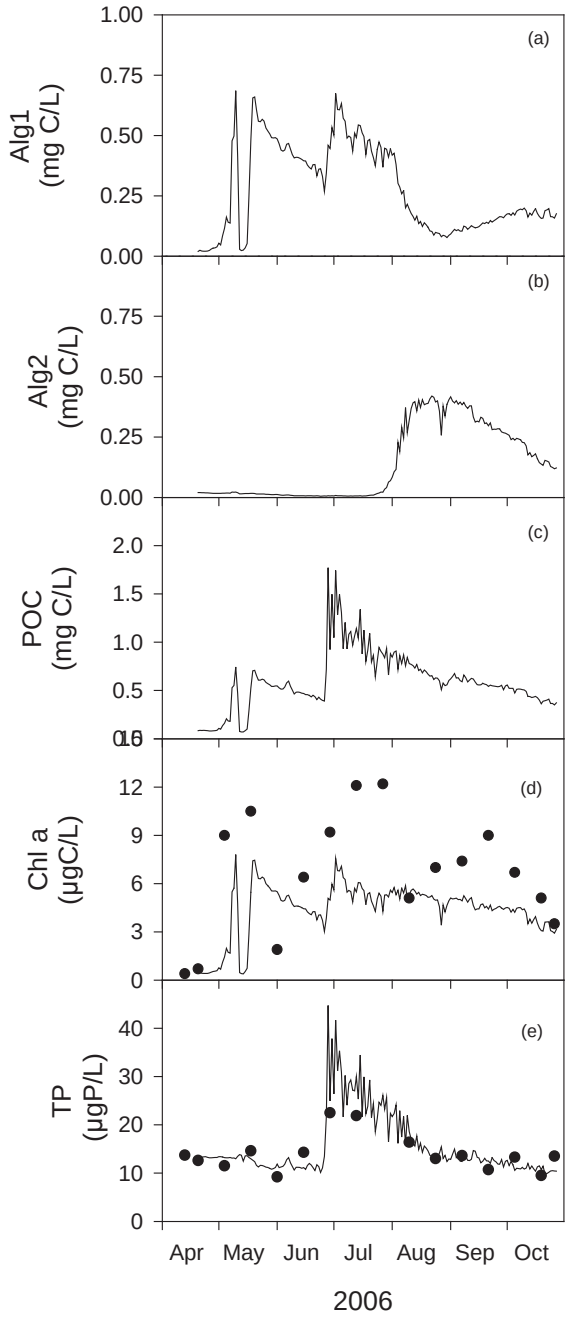

Figure 7- 39. Time series of predicted and observed upper water (0-10 meter average) concentrations of selected particulate water quality parameters for Cayuga Lake, site 3 in 2006: (a) Alg1, (b) Alg2, (c) Chl-*a*, (d) POC, and (e) TP.

Model fits are presented in Figure 7-40 for selected dissolved parameters measured in 2006 at site 3. The model fit to SRP measurements was excellent, including the observed depletion during April and May (Figure 7-40b) that coincided with an increase in algal biomass (Figure 7-39d).

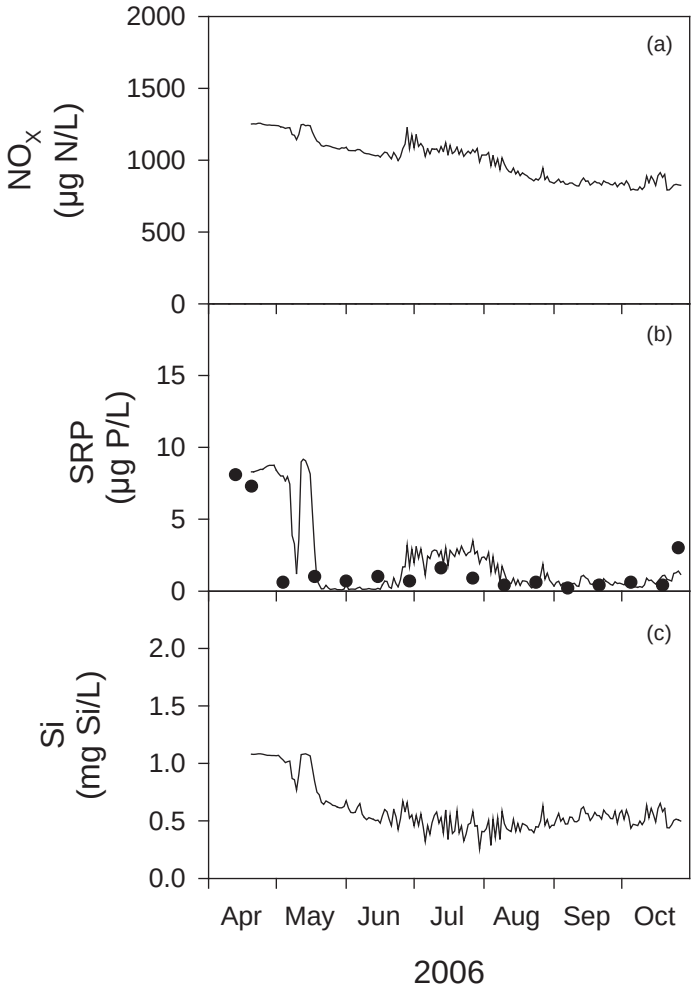

Figure 7- 40. Time series of predicted and observed upper water (0-10 meter average) concentrations of selected dissolved water quality parameters for Cayuga Lake, site 3 in 2006: (a) NO_x, (b) SRP, and (c) DSi.

7.6.5.4. Model validation fits for the southern shelf, 2006

Model fits are presented in Figure 7-41 for selected particulate parameters measured in 2006 at site 1, located on the southern shelf. The general magnitude of Chl-*a*, and the increase from

spring to summer, was simulated nicely (Figure 7-41d). The model also captured the observed short-term dynamics in Chl-*a* with an impressive degree of accuracy. Observed temporal dynamics in TP concentrations on the southern shelf were also matched well, including the short-term increase associated with an early July runoff event (Figure 7-41e). The general magnitude of TP was matched very well throughout the April-October interval of 2006.

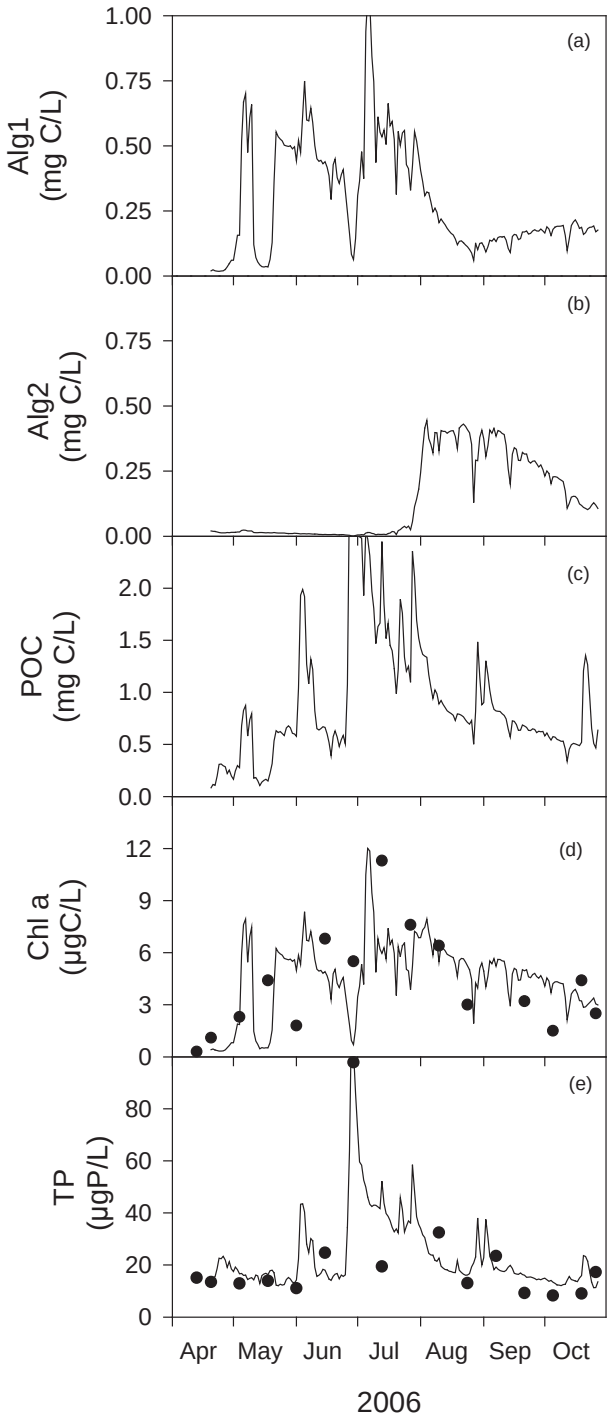

Figure 7- 41. Time series of predicted and observed upper water concentrations of selected particulate water quality parameters for Cayuga Lake, site 1 in 2006: (a) Alg1, (b) Alg2, (c) Chl-*a*, (d) POC, and (e) TP.

Model fits are presented in Figure 7-42 for selected dissolved parameters measured in 2006 at site 1, located on the southern shelf. The model fit to SRP observations on the shelf was generally excellent, including the observed depletion in April and May (Figure 7-42b) that coincided with an increase in algal biomass (Figure 7-41d). The model also captured the timing, if not the magnitude, of spikes in SRP associated with runoff events.

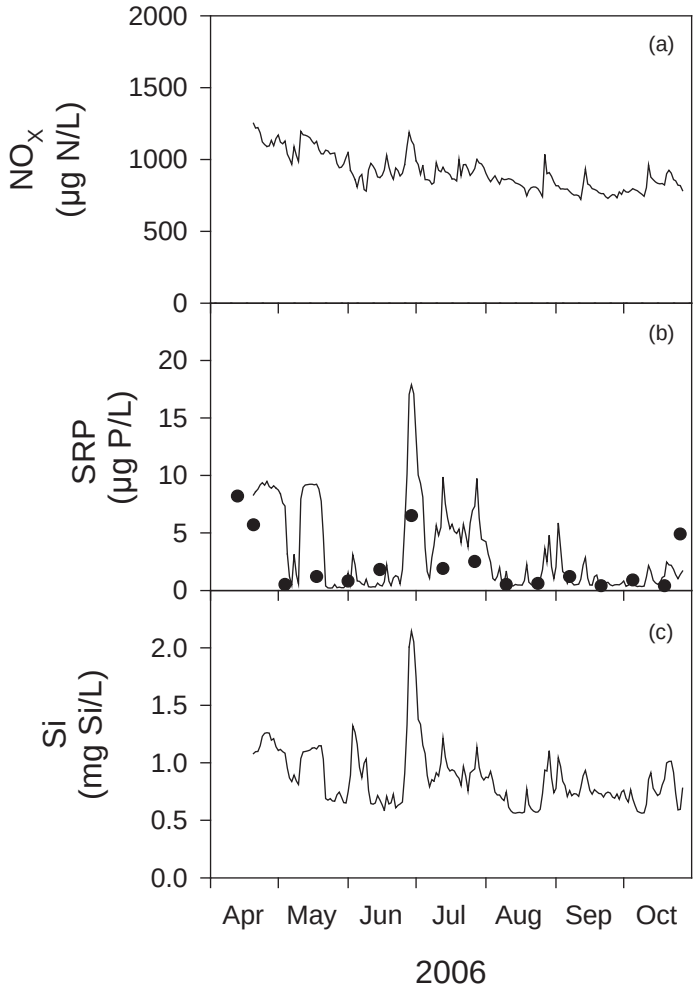

Figure 7- 42. Time series of predicted and observed upper water concentrations of selected dissolved water quality parameters for Cayuga Lake, site 1 in 2006: (a) NO_x, (b) SRP, and (c) DSi.

7.6.5.5. Comparisons with model performance criteria

Observed and predicted summer average concentrations are presented in Table 7-14 for key water quality constituents (TP, Z_{SD}, POC, SD, PAV_m) for the calibration (2013) and validation (1999, 2006) years. Model performance criteria were successfully met for TP, Chl-*a*, POC, and SD (Table 7-15). The model has been successfully validated for these parameters. Although PAVm was calibrated to closely match the observations of 2013, predictions for 1999 and 2006 did not meet the desired level of performance. This shortcoming is likely associated with the low levels of PAVm in pelagic waters and the focus of this modeling component on characterizing minerogenic particle signatures on the shelf during runoff events (Gelda et al. 2016).

Table 7- 14. Summer average upper water concentrations in Cayuga Lake (site 3) for observed and predicted parameters for calibration (2013) and validation (1999 and 2006) years.

Year	Summer Average Concentrations									
	TP		Chl-*a*		POC		SD		PAVm	
	obs.	pred.	obs.	pred.	obs.	pred.	obs.	pred.	obs.	pred.
2013	15.3	13.1	4.2	4.3	0.6	0.5	4.0	3.7	0.8	0.8
1999	9.8	8.0	4.6	2.7			3.5	4.7	1.2	0.3
2006	15.2	17.7	7.8	5.7			2.9	3.1	4.4	2.5

Table 7- 15. Comparisons of model results with performance criteria for the calibration (2013) and validation (1999 and 2006) years. Percent error is based on observed and predicted summer average concentrations in the upper waters of Cayuga Lake, site 3.

Year	Summer Average % Error				
	TP	Chl-*a*	POC	SD	PAVm
2013	15	3	11	6	8
1999	18	41	--	20	79
2006	17	27	--	8	43
Target threshold	<25%	<50%	<30%	<25%	<30%

[1] 1 % Error = absolute value of (prediction – observation)/observation ×100

7.6.6. Sensitivity analysis

Before applying the model, it is advisable to develop an understanding of its general behavior through additional model testing (Chapra 1997). A common approach for identifying important model parameters and their influence on model predictions is a sensitivity analysis. A sensitivity analysis typically consists of varying selected parameters by a specified percentage and observing variations in model predictions. We varied eight key model coefficients and two sub-models, one at a time, and observed the impact of each change on 2013 model predictions for Chl-*a*, POC, and TP (Table 7-16). The eight coefficients were varied by ± 25% from the final values used in calbration, and the 2013 model results were compared to the base case. The zooplankton and dreissenid mussel sub-models were turned off, and the resulting model predictions for 2013 were compared to the base case with these sub-models turned on. All model results are reported for the upper waters (0-10 meter average) at site 3, located in the pelagic zone.

Model predictions for 2013 were quite robust to 25% changes in most of these key coefficients (Table 7-16). However, model predictions of Chl-*a* and POC were sensitive to changes in the stoichiometric coefficients P:C and C:Chl-*a*. This is not surprising given that these stoichiometric ratios establish the composition of the modeled algal community. For example, a 25% decrease in P:C reduces algal demand for P and increases algal biomass for a fixed supply of P. The value of this ratio is particularly important in a P-limited systems such as Cayuga Lake. Similarly, a 25% reduction in C:Chl-*a* increases the Chl-*a* content per unit C, resulting in a marked increase increase in Chl-*a* but not in C. Turning off the dreissenid mussel sub-model resulted in a 14.5% decrease in Chl-*a*, suggesting that nutrient recycling by these filter feeders stimulates algal growth. The sensitivity analysis indicates that the effects of zooplankton on these water quality indicators are modest. This result is consistent with the absence of large cladoceran grazers in Cayuga Lake. Model predictions of TP were insensitive to changes in any of these coefficients or sub-models, suggesting that TP levels are regulated primarily by loading rather than in-lake processes.

Table 7- 16. Model sensitivity to changes (± 25%) to selected key calibration coefficients. Model run for 2013 with results reported for Station 3 for summer (June-September) average.

Model Runs	Coefficient	Units	Calibration Value	Coefficient Adjustment	Chl a (µg/L)	Chl a (%Chg)[1]	POC (mg/L)	POC (%Chg)[1]	TP (µg/L)	TP (%Chg)[1]
Base case					4.6		0.53		12.9	
1	µmax (alg1, alg2)	1/d	3.5, 2.5	-25%	4.5	-2.2	0.52	-1.8	13.2	2.3
				+25%	4.6	0.6	0.53	0.4	12.8	-1.2
2	Respiration (alg1, alg2)	1/d	0.06, 0.06	-25%	4.6	0.5	0.53	0.4	12.9	-0.4
				+25%	4.5	-1.0	0.52	-0.8	13.0	0.7
3	P:C (alg1, alg2)	mgP/mgC	0.01, 0.01	-25%	5.7	25.8	0.65	22.9	13.0	0.6
				+25%	3.5	-23.0	0.42	-20.5	12.9	-0.4
4	C:Chl-*a* (alg1, alg2)	mgC/ugChl	0.0904, 0.1018	-25%	6.1	33.4	0.53	0.0	12.9	0.0
				+25%	3.6	-19.9	0.53	0.0	12.9	0.0
5	Settling Vel. (alg1, alg2)	m/d	0.15, 0.10	-25%	4.8	4.4	0.54	3.7	13.2	2.2
				+25%	4.3	-4.5	0.51	-3.8	12.7	-2.2
6	½ sat. SRP (alg1, alg2)	mg/L	0.003, 0.003	-25%	4.6	1.0	0.53	0.8	12.8	-1.0
				+25%	4.5	-1.2	0.52	-1.0	13.1	0.9
7	LPOP Decay	1/d	0.025	-25%	4.5	-1.3	0.52	-1.2	12.8	-0.8
				+25%	4.6	1.2	0.53	1.0	13.0	0.7
8	LDOP Decay	1/d	0.05	-25%	4.4	-3.7	0.51	-3.2	13.3	2.7
				+25%	4.7	2.8	0.54	2.4	12.6	-2.2
9	No Zoopl.		On	Off	4.7	4.0	0.53	0.2	12.9	-0.1
10	No Mussels		On	Off	3.9	-14.5	0.50	-5.5	12.9	-0.3

1 %chg = percent change = (run – base run)/base run *100.

7.7. Example applications of CLM-2D to Cayuga Lake

Three example applications of CLM-2D are included here to demonstrate capabilities of the model for evaluating the effects of various potential management initiatives on water quality in Cayuga Lake. The first application consists of comparing predicted water quality conditions for 2013 with a scenario of zero flow to the lake from the LSC facility. In the second application, the impact of eliminating P loading from the six WWTPs that discharge to Cayuga Lake is evaluated. Finally, we assess predicted water quality impacts associated with a hypothetical 30% reduction in non-point sources of P from the watershed. In each case, the model was run with the specified changes for six years (i.e., 2013 forcing conditions repeated six times) in order to reach a steady-state condition. Predicted water quality conditions for the final year of this model run are compared to the base model predictions for 2013 (observations).

The examples presented here are entirely hypothetical and are not intended as management recommendations. Furthermore, we have not considered the extent to which any of these hypothetical examples are practical or possible. They are meant strictly as examples that demonstrate capabilities and consistencies with expectations based on our scientific understanding of Cayuga Lake.

7.7.1. Impact of removal of lake source cooling (LSC) input

In the first example application of CLM-2D we simulated the water quality effects of eliminating the flow from the LSC facility. The LSC facility transports water and ambient constituents from the hypolimnion to the southern shelf. Accordingly, elimination of this flow would reduce P loading to the shelf but also increase water residence time and reduce the flushing rate on the shelf. The model simulation indicates the net effect of eliminating the LSC flow would be a very modest degradation in water quality conditions on the shelf. Summer average concentrations of Chl-*a*, POC, and TP were predicted to increase by 1.3%, 2.4%, and 3.1%, respectively (Table 7-17). The largest increase was predicted for minerogenic particle concentrations (PAV_m), which were estimated to increase by 3.3%. In contrast, elimination of the LSC flow was predicted to result in trivial (<1%) improvements at site 5, located in pelagic waters. In summary, model simulations indicate that water quality impacts associated with the LSC facility are negligible. These results are not surprising given that the LSC contribution to P loading is also quite small.

7.7.2. Impact of removal of all point source inputs

The impact of eliminating P loading from the six WWTPs that discharge to Cayuga Lake was evaluated as the second application of CLM-2D. The six WWTPs considered are Ithaca Area WWTP, Cayuga Heights WWTP, Trumansburg WWTP, Interlaken WWTP, Aurora WWTP, and Union Springs WWTP. Because tributaries contribute approximately 97% of the P load to Cayuga Lake, elimination of these sources is not expected to result in substantial

improvements in water quality. Summer average concentrations of Chl-a, POC, and TP on the shelf were predicted to decrease by 2.1%, 1.4%, and 4.1%, respectively (Table 7-17). No change was predicted for minerogenic particle concentrations (PAV_m). Elimination of P loading from WWTPs was predicted to result in even smaller improvements in pelagic waters. Larger improvements on the shelf are consistent with the fact that the two largest WWTPs (Ithaca Area and Cayuga Heights) discharge to this area. Model simulations indicate that elimination of P loading from WWTPs located on Cayuga Lake would result in extremely small improvements in water quality. These results are consistent with point sources contributing just 3% of the P load to Cayuga Lake.

7.7.3. Impact of reduction in non-point source loads by 30%

Finally, we assess predicted water quality impacts associated with a hypothetical 30% reduction in non-point sources of P from the watershed. This reduction in P loading was applied uniformly to all of the tributaries and across all forms of P. Accordingly, the 30% reduction was applied to both bioavailable and unavailable forms of P. Tributary flows were not altered to maintain the integrity of the flow budget. Because P loading to Cayuga Lake is dominated by inputs from its tributaries, a 30% reduction in non-point source loading would be expected to result in noteworthy water quality improvements. Summer average concentrations of Chl-*a*, POC, and TP on the shelf were predicted to decrease by 13.0%, 8.3%, and 19.8%, respectively (Table 7-17). No change was predicted for minerogenic particle concentrations (PAV_m). Predicted water quality improvements were less impressive for the pelagic waters. Chl-*a*, POC, and TP concentrations at site 5 were predicted to decrease by only 5.2%, 5.1%, and 7.4%, respectively. These model results suggest a resiliency in trophic state and may reflect loss processes for P (e.g., burial) that result in disproportionate changes in loading and water quality.

Table 7- 17. Model predictions for three example applications: (1) eliminating the LSC flow, (2) eliminating P loading from six WWTPs, and (3) reducing non-point source P loads by 30%. Results are shown for sites 1 (shelf) and 5 (pelagic) as summer (June-September) averages for the upper waters (0-10 meter average).

Scenario	Chl-*a* Base case[1]	Chl-*a* Pred[2]	Chl-*a* %Chg[3]	POC Base case[1]	POC Pred[2]	POC %Chg[3]	TP Base case[1]	TP Pred[2]	TP %Chg[3]	PAV_m Base case[1]	PAV_m Pred[2]	PAV_m %Chg[3]
No LSC flow												
Site 1	5.6	5.7	1.3	0.9	0.9	2.4	23.3	24.1	3.1	5.1	5.3	3.3
Site 5	4.8	4.8	0.0	0.5	0.5	-0.1	11.6	11.6	-0.1	0.3	0.3	-0.5
No direct WTP discharge												
Site 1	5.6	5.5	-2.1	0.9	0.9	-1.4	23.3	22.4	-4.1	5.1	5.1	0.0
Site 5	4.8	4.8	-0.7	0.5	0.5	-0.7	11.6	11.5	-1.1	0.3	0.3	0.0
30% phosphorus reduction in tributary inflows												
Site 1	5.6	4.9	-13.0	0.9	0.8	-8.3	23.3	18.7	-19.8	5.1	5.1	0.0
Site 5	4.8	4.5	-5.2	0.5	0.5	-5.1	11.6	10.8	-7.4	0.3	0.3	1.1

[1] base case – predicted water quality conditions for 2013 that all scenarios are compared against
[2] Pred – predicted conditions based on the scenario specifications
3 %Chg = percent change = (run – base run)/base run *100.

Section 8. Modeling the Cayuga Lake Watershed with SWAT (submitted by T. Walter and J. Knighton, Cornell University Co-Investigators)

8.1. Approach overview

We developed a SWAT v2012 model (Neitsch et al. 2011) for the Cayuga Lake watershed to 1) estimate current precipitation driven discharge and loading of total suspended solids (TSS), Nitrate + Nitrite (NOX) and total phosphorus (TP) to Cayuga Lake, and 2) to evaluate best management practices in reducing TP loading to Cayuga Lake.

Model development and calibration was first performed for the Fall Creek watershed, a large tributary to the south end of Cayuga Lake. Fall Creek benefits from an extensive period of record of observed precipitation (NRCC 2016), streamflow (USGS 2016), and estimated water quality constituents (Prestigiacomo et al. 2016). Further, details on the spatial and temporal distributions of agricultural fertilizer applications were available for the Fall Creek watershed. These schedules were determined after discussions with experts from a number of county Soil and Water Conservation Districts (SWCDs) in the Finger Lakes region (K. Czymmek et al., personal communication, May 2015). This high level of data availability allows for more precise estimates of hydrologic model parameters that must be determined through calibration. Hydrologic parameters defining the precipitation-runoff response of the watershed derived from calibration of the Fall Creek watershed were then extrapolated to the entire Cayuga Lake watershed.

Known fertilizer spreading schemes for the Fall Creek watershed were extrapolated to the entire Cayuga Lake watershed. We assumed that the temporal distribution of fertilizer applications throughout the Cayuga Lake watershed was consistent with the management practices within Fall Creek. Further we assumed that the total mass of fertilizer applied was proportional based on area by land use. We assumed that all row crops throughout the watershed were actively fertilized as in Fall Creek with the same mass per unit area. We similarly assumed that the same proportion of pastures throughout the watershed received fertilizer spreading schedules defined for Fall Creek.

8.2. Fall Creek watershed description

The Fall Creek watershed is a small (324 km2) catchment in Tompkins County, NY USA (Latitude: 42° 28’, Longitude: 76° 27’). The watershed is composed of approximately 50% forested land and 50% active agricultural use (Figure 8-1). The dominant agricultural land uses are row crops and dairy farm pastures (Figure 8-1). The watershed climate is temperate with a

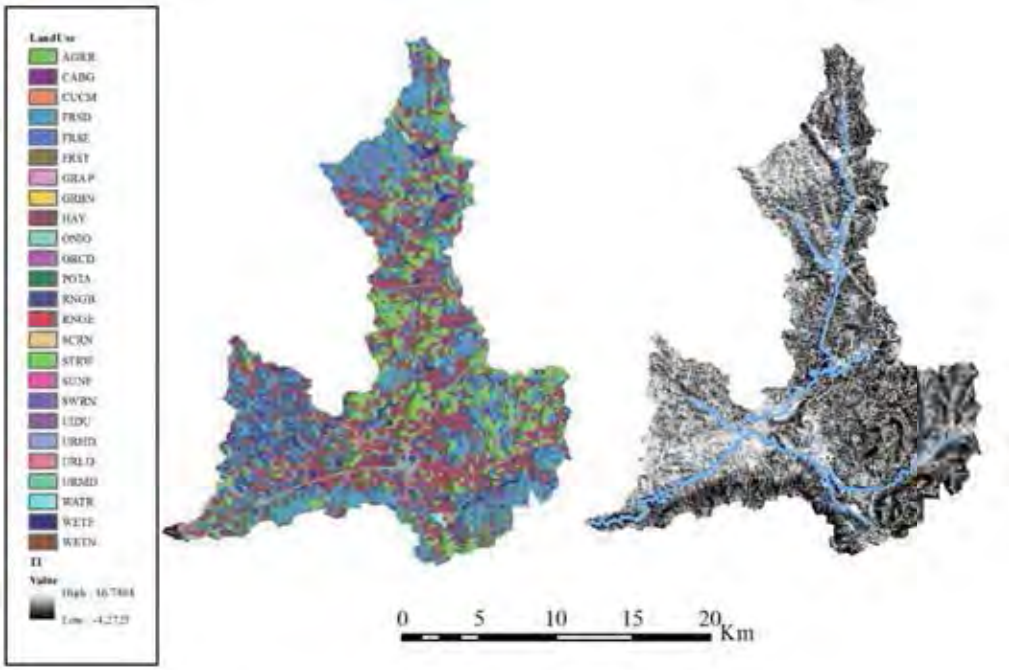

Figure 8- 1. Spatial distribution of land use and topographic wetness index throughout the Fall Creek watershed

winter freeze-thaw cycle. The steep hillslopes and highly dendritic drainage pattern of Fall Creek creates a large range of topographic wetness indices throughout the watershed (Figure 8-1).

The watershed soils are composed primarily of silt clay loam with a shallow confining layer, typically 0.5 to 1 m below the ground surface (USDA NRCS 2015). This dense restricting layer is usually found within 30 to 60 cm of the soil surface and limits percolation of water causing soils above the fragipan to saturate quickly during rain events. As a result the Fall Creek watershed typically experiences runoff as a saturation excess process (Easton et al. 2007; Dahlke et al. 2009).

The area is located in a humid continental climate and the weather varies seasonally with freezing temperatures persisting for 4 to 5 months of the year; snow cover is frequent from December to March. The Fall Creek watershed receives an annual average 94.7 cm of precipitation (NRCC 2016). The 10th and 90th percentile for hourly air temperatures is -11.6 and 17.2° C respectively (NRCC 2016).

Fall Creek is a fourth order stream that drains to the south end of Cayuga Lake. Nutrient and sediment delivery in the south end of Cayuga Lake has resulted in excessive turbidity and

aquatic plant growth which currently limits recreational use in shallow areas (NYS DEC 2015). This use impairment is in part related to agricultural runoff from the Fall Creek watershed (NYS DEC 2015).

Dairy manure is applied to all row crops and a subset of pastures within the Fall Creek watershed (Table 8-1). These schedules were determined after discussions with experts from a number of county Soil and Water Conservation Districts (SWCDs) in the Finger Lakes region (K. Czymmek et al., personal communication, May 2015). In these discussions we outlined four manure spreading schedules for pasture land and one for row crops. Dairy manure is defined as 0.7% NH3 and 0.5% soluble P by mass (ASAE 1998).

Table 8- 1. Current dairy manure application schedules within Fall Creek agricultural land

Land Use	Area (ha)	Dry Mass (kg/year)	NH_3 (kg*ha^{-1}*yr^{-1})	TDP (kg*ha^{-1}*yr^{-1})	Timing
Pasture	1300	4,290,000	23.1	16.5	year round (monthly)
Pasture	320	1,056,000	23.1	16.5	May - October
Pasture	400	3,680,000	64.4	46.0	May - October
Row Crops	5320	30,856,000	40.6	29.0	May - October

8.3. Hydrologic model selection and development

Bouraoui and Grizzetti (2014) review existing hydrologic models employed to estimate nutrient losses from agricultural land and the efficacy of nutrient runoff mitigation measures. They conclude that the Soil and Water Assessment Tool (SWAT) is 1) generally more physically based than alternative models, 2) spatially and temporally distributed 3) capable of complex fertilizer application strategies, and 4) capable of complex crop management strategies. Panagopoulos et al. (2011) demonstrate that even under data-poor conditions, prediction of spatially distributed nutrient losses with SWAT still provides some value due to the physical-basis and theoretical underpinnings of the nutrient loss models. For these reasons we use the SWAT model to simulate N and P watershed losses and to evaluate the efficacy of nutrient loss control measures. We developed the SWAT model using SWAT v2012 through the ArcSWAT extension of ESRI ArcGIS.

We utilize 30 m National Elevation Dataset (NED) digital elevation model to define watershed land surface elevations (USGS, 2016a). We obtain land-use information from the National Land Cover Database (NLCD) (Fry et al, 2011) and 30-m 2009 New York Cropland Data Layer (USDA 2010). The NLCD dataset was modified to include more specific agricultural land uses common to the Finger Lakes region of NYS such as vineyards, orchards, and vegetable farms. These additional agricultural data were obtained from the 2009 New York Cropland Data Layer at a resolution of 30 meters (USDA 2010). One land use data set was used for the entire

modeling period (1998-2010). Population growth in the watershed is consistent with this small increase in roadways; between 1950 and 1980 population increased by 10% each decade and from 1980 to present there has been a 5% increase in population in each decade (Forstall 1995). Based on these data we can assume that land use has not appreciably changed over the modeling period (1998-2010). SWAT Hydrologic Response Units (HRUs) were determined by a unique combination of landuse, soils (which includes a topographic index class), slope, and subbasin. Land use thresholds were not used to determine HRUs in the final model to preserve all types of agriculture included in the land use datasets.

A soils layer was built using TopoSWAT. TopoSWAT is an automated ArcMap tool that calls upon the Digital Soil Map of the World and includes a soil wetness class to give a more accurate representation of soil type and its propensity to generate runoff as defined by VSA hydrology (Fischer et al. 2008). We utilize SWAT-VSA (Variable Source Area) (Easton et al. 2008) to redistribute the spatial pattern of runoff generation in NY, USA based on the topographic index (TI) concept. TI was calculated as follows:

$$TI = \ln\left(\frac{\alpha}{T\tan\beta}\right) \qquad \text{Eq. 8- 1}$$

The TI is then used to define the levels of wetness for HRUs. The HRUs are divided into 10 classes of equal area. We use this definition to define a cumulative total watershed area which contributes to the VSA termed AS. We then redistribute the local storage deficit, σe, to each HRU. We define σe as follows:

$$\sigma_{e,i} = \frac{2Se\left(\sqrt{1-A_{S,i+1}}-\sqrt{1-A_{S,i+1}}\right)}{(A_{S,i+1}-A_{S,i})} - S_e \qquad \text{Eq. 8- 2}$$

The term, σe, defined at the HRU, is then used to represent the effective HRU storage which is in turn used to define the CN2 value. Redistribution of runoff generating characteristics was limited to a redistribution of the SWAT CN2 parameter, as opposed to a complete redistribution of HRU soil properties. We note that the creation of HRUs and the definition of the CN2 parameter are strongly related. As the number of HRUs increases the ability of the model to represent a non-linear rainfall-runoff response increases. The calibration of the CN2 parameter is therefore dependent on model structure. In this way the SWAT-VSA representation of the CN2 parameter may deviate substantially from the watershed CN2 parameter derived from default of tabulated values.

We first established the fertilizer distribution for Fall Creek. In order to incorporate fertilizer schedules (Table 8-1) into the SWAT framework, we assigned random HRUs, whose land use designation is Pasture, to 19 groups of three spatial sizes; 108 ha, 54 ha, and 400 ha. Twelve groups of 108 ha were assigned to Schedule 1; six groups of 54 ha were assigned to Schedule 2; and one group of 400 ha was assigned to Schedule 3 (Table 8-1). Each group under Schedules 1 and 2 was assigned a different month in which manure would be applied. As a result, each HRU

received manure applications in only one month of the year. With this method we simulate the common practice of rotating the fields in which manure is spread. All HRUs designated as Row Crops were assigned to Schedule 4. We then applied manure to these groups at the rate specified by the SWCD experts (Table 8-1).

Fertilizer spreading schemes were extrapolated to the entire Cayuga Lake watershed. We assumed the same temporal distribution of fertilizer applications throughout the Cayuga Lake watershed was consistent with the management practices within Fall Creek. Further we assumed that the total mass of fertilizer applied was proportional based on land use. We assumed that all row crops throughout the watershed were actively fertilized as in Fall Creek. We assumed that the same proportion of pastures throughout the watershed received fertilizer spreading schedules defined for Fall Creek.

The entire Cayuga Lake watershed model was developed following the same datasets and methodology as the Fall Creek watershed model (Figure 8-2). The Cayuga Lake watershed divisions were created to allow for a refined estimate of discharge and nutrient loading to the south end of Cayuga Lake based on the findings of NYS DEC (2015). The model is capable of providing the total discharge and nutrient loading to Fall Creek from the major tributaries as well as the combined total discharge and nutrient loading from all contributing watersheds.

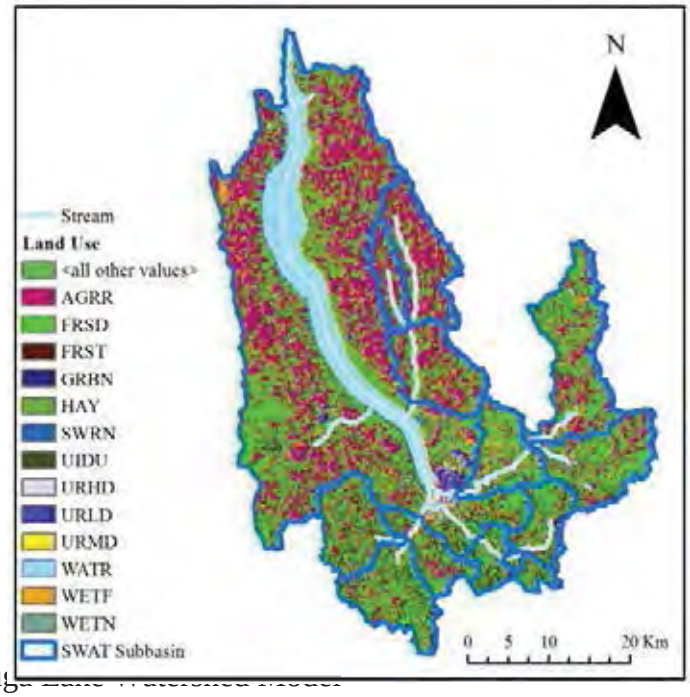

Figure 8- 2. Cayuga Lake Watershed Model

8.4. Model corroboration methodology

Model development and calibration was first performed for the Fall Creek watershed, a large tributary to the south end of Cayuga Lake. Fall Creek benefits from an extensive period of record of observed precipitation (NRCC 2016), streamflow (USGS 2016b), and estimated water quality constituents (Prestigiacomo et al. 2016). Further, details on the spatial and temporal distributions of agricultural fertilizer applications were available for the Fall Creek watershed. This high level of data availability allows for more precise estimates of hydrologic model parameters that must be determined through calibration. Hydrologic parameters defining the precipitation-runoff response of the watershed derived from calibration of the Fall Creek watershed were then extrapolated to the entire Cayuga Lake watershed.

We performed model corroboration for the period of 1998 – 2010. We corroborated our SWAT Fall Creek watershed model against observed daily flows (USGS 2016b) and estimated total suspended solids (TSS), NOX (NO3 + NO2), Particulate Phosphorus (PP), and Total Dissolved Phosphorus (TDP) loads. Sediment and nutrient load collection methodology and flow-concentration relationships are presented in Prestigiacomo et al. (2016).

For model corroboration we forced the Fall Creek model with daily precipitation, and minimum and maximum air temperatures measures at the Northeast Regional Climate Center weather station (NRCC 2016). Relative humidity, solar radiation, and wind speed were solved internally by SWATs weather generator. These weather data are available from National Oceanic and Atmospheric Association (NOAA) Global Historical Climatology Network (GHCN) of weather stations. For this model we used the meteorological station (Number USC00304174) located at Cornell University in Ithaca, NY (NRCC 2016) because of its location in the watershed and its long term data record.

We manually adjusted 19 SWAT model parameters for SWAT calibration (Table 8-2). Hydrologic parameters defining the precipitation-runoff response of the watershed derived from calibration of the Fall Creek watershed were then extrapolated to the entire Cayuga Lake watershed.

8.4.1. Flow corroboration

We corroborated the snowpack accumulation and melt through the adjustment of 5 parameters (Table 8-2). We corroborated the unsaturated zone dynamics, groundwater flow, and surface runoff through adjustment of 6 single value parameters and 1 distributed parameter (CN2) presented in Table 8-2. We manually adjusted parameter values until we were adequately reproducing both the seasonal loads of streamflow and obtaining acceptable Nash-Sutcliffe Model Efficiency (NSE) values as defined by Moriasi et al (2007).

Table 8- 2. SWAT parameters used in model corroboration

Parameter	Model	Calibrated Value	Units
SFTMP	Snowpack	1	˚C
SMTMP	Snowpack	0.5	˚C
SMFMX	Snowpack	2	mm H_2O / ˚C * day
SMFMN	Snowpack	2	mm H_2O / ˚C * day
TIMP	Snowpack	0.553	coefficient
ESCO	Water Balance	0.9	coefficient
EPCO	Water Balance	1	coefficient
SURLAG	Water Balance	0.2	days
CN_FROZ	Water Balance	0.000009	coefficient
GW_DELAY	Water Balance	1	days
ALPHA_BF	Water Balance	0.048	days
CN2	Water Balance	0.9*baseline	coefficient
USLE_K1	Sediment	0.275	coefficient
NPERCO	Nitrogen	0.4	coefficient
SDNCO	Nitrogen	1	coefficient
CDN	Nitrogen	1.4	coefficient
ERORGP	Phosphorus	0.285	coefficient
PHOSKD	Phosphorus	800	coefficient
PSP	Phosphorus	0.4	coefficient

8.4.2. TSS corroboration

SWAT incorporates the Modified Universal Soil Loss Equation (MUSLE) which estimates daily suspended sediment load based on soil types, landscape practices, and daily rainfall. We corroborate the SWAT model for against estimates of daily TSS. The form of the MUSLE equation allows one to reduce calibration to a one parameter model. In this case we modify the soil erodibility factor (USLE_K) (Table 8-2).

8.4.3. NOX corroboration

We corroborate our model estimates of NOX loads with daily estimates of in-stream NOX loads. We adjust the following parameters for nitrogen loading: NPERCO, SDNCO, and CDN. We adopt the default values for nutrient parameters CMN, and RSDCO, which control the degradation of organic material, effecting both nitrogen and phosphorus nutrient cycling. We therefore primarily adjust the parameters related to denitrification and N percolation to calibrate the SWAT model to in-stream NOX estimates.

8.4.4. Particulate and total dissolved phosphorus corroboration

SWAT estimates particulate phosphorus based on organic soil P concentrations and the estimated TSS reach loading. SWAT assumes that some proportion of the soil Organic P is

attached to sediment and runs off. We adjusted the calibration parameter ERORGP which allows the user to define the concentration of organic P that is sediment bound.

SWAT estimates TDP surface runoff as a function of the surface 10 mm TDP concentration and the rate of surface runoff generation. We adjust the PHOSKD, soil phosphorus partitioning coefficient to match estimated TDP loads for Fall Creek.

8.5. Model corroboration results

8.5.1. Flow corroboration

We obtain a daily NSE value above the recommended value of 0.5 (Moriasi et al. 20013) for 10 of the 13 years used for model corroboration (Figure 8-3a). We note here that the commonly accepted NSE of 0.5 is defined for a monthly time step which is considerably more relaxed metric than NSE calculated at a daily time step.

Seasonally, we note that our observed reproduction of flow is good for all months with some overestimation occurring from spring snowmelt. We attribute this overestimate to the simplified approach to rain on frozen soils and soil thawing approximation within SWAT. SWAT assumes that soils remain frozen only for the duration that air temperatures are below 0℃. When air temperatures exceed 0℃ soils begin infiltrating. In reality the snowmelt period likely occurs on soils that have not yet thawed resulting in a brief period of high runoff. In order to approximate this high runoff period of melt we decrease the CNFROZ parameter to generate more runoff during the spring melt period. The result is a slight over-prediction of the volume of spring snowmelt runoff (Figure 8-3b), and an under-estimate of the peak daily flow rate. This flow discrepancy affects the April loading of sediment and nutrients, and likely has a strong effect on the calculated NSE values.

8.5.2. Total suspended solids corroboration

We manually adjust the USLE_K parameter until we sufficiently reproduce the cumulative TSS load estimate for the estimated load time period (Figure 8-3c). Daily estimates of TSS are highly variable due to uncertainty in the estimation of daily flow and the relative simplicity of the MUSLE equation. We observe that we are reproducing the seasonality of TSS loading with slight over-estimation of summer loads (Figure 8-3d). There is an underestimation of April TSS loads associated with spring snowmelt. As discussed in Section 4.1, we are overestimating the volume of spring snowmelt, but slightly underestimating the peak daily flow rates.

8.5.3. NOX corroboration

Similar to the TSS, we observe that our model adequately estimates the long term trend in annual NOX loading (Figure 8-3e), and reproduces the seasonality, but underestimates the spring snowmelt NOX runoff (Figure 8-3f). SWAT assumes denitrification does not occur below some threshold soil moisture content. We corroborated NOX stream loading through a reduction of the

soil moisture threshold for the onset of denitrification. We assume that denitrification occurs when soils are at field capacity (SDNCO = 1.0). Other widely accepted theoretical models have demonstrated denitrification occurs at soil saturation levels less than field capacity (e.g. Parton et al. 1996). This simplified representation of denitrification likely produces an underestimate of the total NOX lost to denitrification in drier soils.

8.5.4. Total dissolved and particulate phosphorus

We manually adjust the PHOSKD and ERORGP parameters to reproduce the estimated TDP and PP loads for Fall Creek. We observe that the seasonality is well produced with a slight underestimation of spring P loads owing largely to the simplified snowmelt hydrology incorporated within SWAT (Figure 8-3 g-j).

8.6. Climate change: global circulation model forcing data

Bosch et al. (2014) suggests that the performance of non-point nutrient runoff reduction measures may decrease under climate change in the Northeast US.

We recommend that the benefit gained from any best management practice be evaluated over the hypothetical 40-year period of 2015 – 2055 as defined by global circulation model (GCM) simulation results downscaled for Ithaca, NY USA. This data is readily available as part of the NEX-GDDP dataset (Taylor et al. 2012) for the Representative Concentration Pathway 8.5 (RCP8.5) scenario. While a suite of simulations would be desired to represent a more complete range of possible future conditions, the GFDL-ESM2G GCM estimate of daily precipitation and temperature are approximately the average of all predictions within the NEX-GDDP dataset for Tompkins County, NY USA.

8.7. Annotation list

AS – fraction of the watershed that is effectively saturated
TI – topographic wetness index
T – transmissivity of the uppermost layer of the soil (m2d-1)
Se – total watershed storage
σ – local storage deficit of each wetness class
α – upslope contributing drainage area for the unit cell per unit of the contour line (m)
tan(β) - local topographic slope of the DEM cell

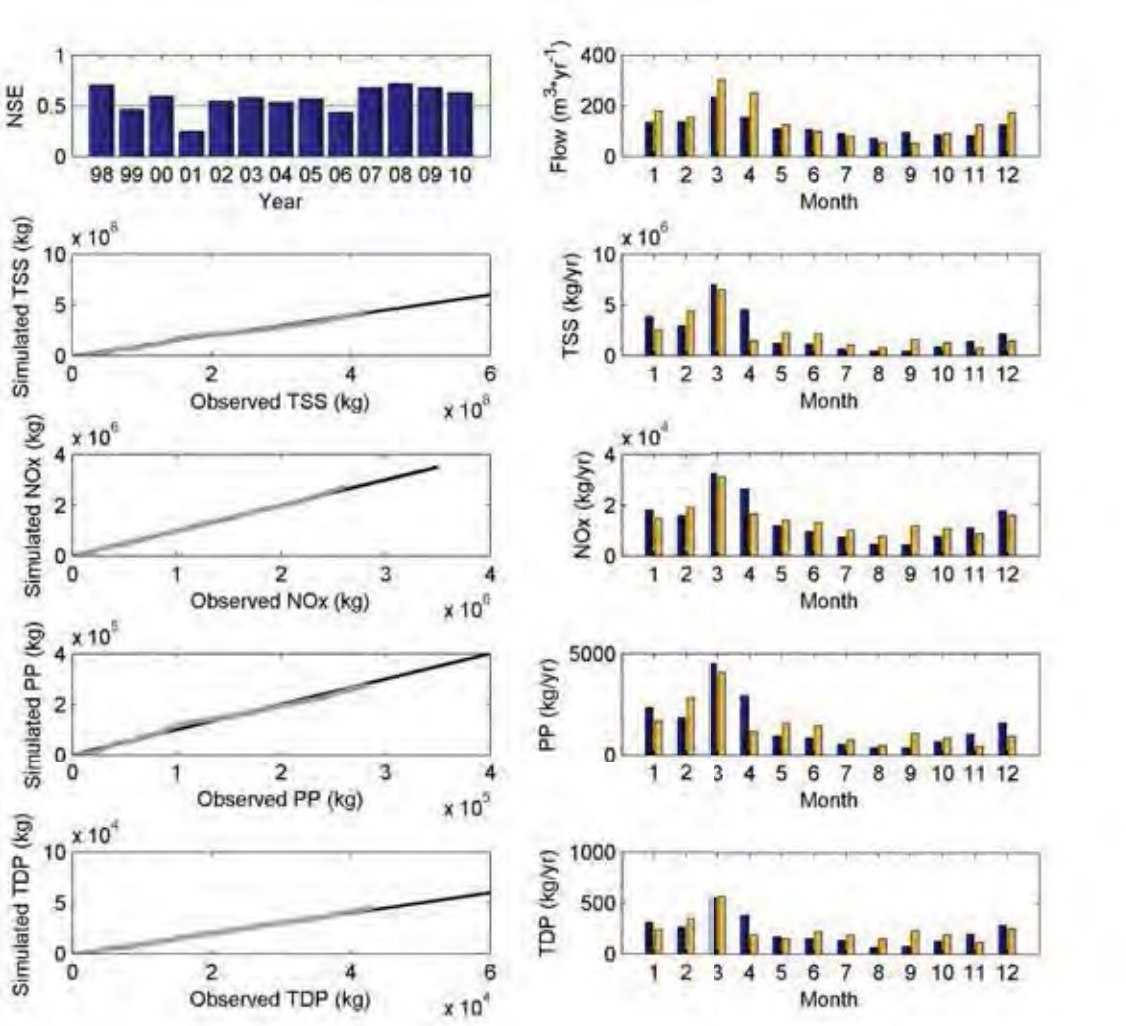

Figure 8- 3. Model corroboration for a) flow, c) total suspended solids, e) NOX, g) particulate phosphorus, and i) total dissolved phosphorus. Simulated (yellow), observed (blue).

Section 9. References

Archibald JA, Buchanan BP, Fuka DR, Georgakakos CB, Lyon SW, Walter MT. 2014. A simple, regionally parameterized model for predicting nonpoint source areas in the Northeastern US. Journal of Hydrology: Regional Studies. 1:74-91.

Arhonditsis GB, Adams-VanHarn BA, Nielsen L, Stow CA, Reckhow KH. 2006. Evaluation of the current state of mechanistic aquatic biogeochemical modeling: citation analysis and future perspectives. Environ Sci Technol. 40:6547-6554.

Arhonditsis GB, Brett MT. 2004. Evaluation of the current state of mechanistic aquatic biogeochemical modeling. Marine Ecology Progress Series. 271:13-26.

Arhonditsis GB, Brett MT. 2005. Eutrophication model for Lake Washington (USA): Part I. Model description and sensitivity analysis. Ecol Model. 187:140-178.

ASAE. 1998. Manure Production and Characteristics. P. 646-648. ASAE Standards. American Society of Agricultural Engineers

Auer MT, Tomasoski KA, Babiera MJ, Needham M, Effler SW, Owens EM, Hansen JM. 1998. Phosphorus bioavailability and P-cycling in Cannonsville Reservoir. Lake and Reserv Manage. 14:278-289.

Baker DB, Confesor R, Ewing DE, Johnson LT, Kramer JW, Merryfield BJ. 2014. Phosphorus loading to Lake Erie from the Maumee, Sandusky and Cuyahoga rivers: The importance of bioavailability. J Great Lakes Res. 40:502-517.

Barlow JP, Bishop JW. 1965. Phosphate regeneration by zooplankton in Cayuga Lake. Limnol Oceanogr. 10:R15-R24.

Bootsma HA, Liao Q. 2014. Nutrient cycling by Dreissenid mussels: Controlling factors and ecosystem response (Chapter 35). P. -775. *In:* T. F. Nalepa and D. W. Schloesser (eds). Quagga and Zebra Mussels: Biology, Impacts, and Control, Second Edition. CRC Press Taylor & Francis Group, Boca Raton, FL.

Bosch NS, Evans MA, Scavia D, Allan JD. 2014. Interacting effects of climate change and agricultural BMPs on nutrient runoff entering Lake Erie. J Great Lakes Res. 40:581-589.

Boström B, Persson G, Broberg B. 1988. Bioavailability of different phosphorus forms in freshwater systems. Hydrobiologia. 170:133-155.

Bouraoui F, Grizzetti B. 2014. Modelling mitigation options to reduce diffuse nitrogen water pollution from agriculture. Science of The Total Environment. 468:1267-1277.

Carlson RE. 1977. A trophic status index for lakes. Limnol Oceanogr. 22:361-368.

Carlson RE, Havens KE. 2005. Simple graphical methods for the interpretation of relationships between trophic state variables. Lake and Reserv Manage. 21:107-118.

Chapra SC. 1997. Surface water-quality modeling. McGraw-Hill, New York. 844 p.

Chapra SC. 2003. Engineering water quality models and TMDLs. J Water Resour Plann Manage Div ASCE. 129:247-256.

Cole,TM and SA Wells. 2014. CE-QUAL-W2: A Two-Dimensional, Laterally Averaged, Hydrodynamic and Water Quality Model, Version 3.71. Department of Civil and Environmental Engineering, Portland State University, Portland, Oregon. 792 p.

Cole,TM and SA Wells. 2015. CE-QUAL-W2: A Two-Dimensional, Laterally Averaged, Hydrodynamic and Water Quality Model, Version 3.72. Department of Civil and Environmental Engineering, Portland State University, Portland, Oregon. 797 p.

Cooke GD, Welch EB, Peterson SA, Nichols SA. 2005. Restoration and management of lakes and reservoirs. Taylor and Francis, CRC Press, Boca Raton, FL.

Dahlke HE, Easton ZM, Fuka DR, Lyon SW, Steenhuis TS. 2009. Modelling variable source area dynamics in a CEAP watershed. Ecohydrology. 2:337-349.

Defew LH, May L, Heal KV. 2013. Uncertainties in estimated phosphorus loads as a function of different sampling frequencies and common calculation methods. Mar Freshwat Res. 64:373-386.

DePinto JV, Young TC, Martin SC. 1981. Algal-available phosphorus in suspended sediments from lower Great Lakes tributaries. J Great Lakes Res. 7:311-325.

Easton ZM, Fuka DR, Walter MT, Cowan DM, Schneiderman EM, Steenhuis TS. 2008. Re-conceptualizing the soil and water assessment tool (SWAT) model to predict runoff from variable source areas. Journal of Hydrology. 348:279-291.

Easton ZM, Gérard-Marchant P, Walter MT, Petrovic AM, Steenhuis TS. 2007. Hydrologic assessment of an urban variable source watershed in the northeast United States. Wat Resour Res. 43:

Edinger,JE and EM Buchak. 1975. A hydrodynamic, two-dimensional reservoir model: The computational basis. Prepared for U.S Army Engineer Division, Ohio River, Cincinnati, OH, 94 p.

Effler AJP, Peng F, Effler SW, Strait CM, Perkins MG, Schulz KL. 2015a. Light absorption by phytoplankton and minerogenic particles in Cayuga Lake, New York. Inland Waters. 5:433-450.

Effler AJP, Strait CM, Effler SW, Perkins MG, Prestigiacomo AR, Schulz KL. 2015b. Linking CDOM patterns in Cayuga Lake, New York, USA, to terrigenous inputs. Inland Waters. 5:355-370.

Effler SW, Auer MT, Peng F, Perkins MG, O'Donnell SM, Prestigiacomo AR, Matthews DA, DePetro PA, Lambert RS, Minott NM. 2012. Factors diminishing the effectiveness of phosphorus loading from municipal waste effluent: Critical information for TMDL analyses. Wat Environ Res. 84:254-264.

Effler SW, Matthews DA, Perkins MG, Johnson DL, Peng F, Penn MR, Auer MT. 2002. Patterns and impacts of inorganic tripton in Cayuga Lake. Hydrobiol. 482:137-150.

Effler SW, Peng F. 2014. Long-term study of minerogenic particle optics in Cayuga Lake, New York. Limnol Oceanogr. 59:325-339.

Effler SW, Prestigiacomo AR, Matthews DA, Gelda RK, Peng F, Cowen EA, Schweitzer SA. 2010. Tripton, trophic state metrics, and near-shore versus pelagic zone responses to external loads in Cayuga Lake, New York. Fund Appl Limnol. 178:1-15.

Effler SW, Prestigiacomo AR, Peng F, Gelda RK, Matthews DA. 2014. Partitioning the contributions of minerogenic particles and bioseston to particulate phosphorus and turbidity. Inland Waters. 2:179-192.

Effler,SW, CM Strait, AJP Effler, F Peng, DM O'Donnell, SM O'Donnell, MG Perkins and SC Chapra. 2016. A mechanistic model for Secchi disk depth, driven by light scattering consituents. Water, Air, Soil Pollut. (in review).

Ekholm P, Krogerus K. 2003. Determining algal-available phosphorus of differing origin: routine phosphorus analyses versus algal assays. Hydrobiologia. 492:29-42.

Ellison ME, Brett MT. 2006. Particulate phosphorus bioavailability as a function of stream flow and land cover. Wat Res. 40:1258-1268.

Fischer G, Nachtergaele F, Prieler S, Van Velthuizen HT, Verelst L, Wiberg D. 2008. Global agro-ecological zones assessment for agriculture (GAEZ 2008). IIASA, Laxenburg, Austria and FAO, Rome, Italy.

Fishman DB, Adlerstein SA, Vanderploeg HA, Fahnenstiel GL, Scavia D. 2009. Causes of phytoplankton changes in Saginaw Bay, Lake Huron, during the zebra mussel invasion. J Great Lakes Res. 35:482-495.

FLUX32. US Army Corp. of Engineers. 2013. Load Estimation Software (version 3.31) [software]. Washington, D.C. Available Online: http://el.erdc.usace.army.mil

Flynn KF, Suplee MW, Chapra SC, Tao H. 2015. Model-Based Nitrogen and Phosphorus (Nutrient) Criteria for Large Temperate Rivers: 1. Model Development and Application. J Am Water Resour Assoc. 51:421-446.

Forstall,RL. 1995. New York: Population of Counties by Decennial Census: 1900 to 1990. US Bureau of the Census, Population Division.

Fry JA, Xian G, Jin S, Dewitz JA, Homer CG, LIMIN YANG, Barnes CA, Herold ND, Wickham JD. 2011. Completion of the 2006 national land cover database for the conterminous United States. Photogram Eng Remote Sensing. 77:858-864.

Gal G, Hipsey MR, Parparov A, Wagner U, Makler V, Zohary T. 2009. Implementation of ecological modeling as an effective management and investigation tool: Lake Kinneret as a case study. Ecol Model. 220:1697-1718.

Gelda RK, Effler SW, Prestigiacomo AR, Peng F, Auer MT, Kuczynski A. 2016a. Simulation of the Contribution of Minerogenic Particles to Particulate Phosphorus Concentration in Cayuga Lake, New York. Water Air Soil Pollution. 227:265-365.

Gelda RK, Effler SW, Prestigiacomo AR, Peng F, Watkins JM. 2016b. Simulations of Minerogenic Particle Populations in Time and Space in Cayuga Lake, New York, in Response to Runoff Events. Water Air Soil Pollution. 227:1-20.

Gelda RK, King AT, Effler SW, Schweitzer SA, Cowen EA. 2015. Testing and application of a two-dimensional hydrothermal/transport model for a long, deep and narrow lake with moderate Rossby number. Inland Waters. 5:387-402.

Haith DA, Hollingshead N, Bell ML, Kreszewski SW, Morey SJ. 2012. Nutrient Loads to Cayuga Lake, New York: Watershed Modeling on a Budget. Journal of Water Resources Planning and Management. 138:571-580.

Hecky RE, Campbell P, Hendzel LL. 1993. The stoichiometry of carbon, nitrogen, and phosphorus in particulate matter of lakes and oceans. Limnol Oceanogr. 38:709-724.

Hecky RE, Kilham P. 1988. Nutrient limitation of phytoplankton in freshwater and marine environments: A review of recent evidence on the effects of enrichment. Limnol Oceanogr. 33:796-822.

Higgins SN, Vander Zanden MJ. 2010. What a difference a species makes: a meta-analysis of dreissenid mussel impacts on freshwater ecosystems. Ecol Monogr. 80:179-196.

Hipsey,MR, Gal,G, Antenucci,JP, Zohary,T, Makler,V, and Imberger,JÃ. 2006. Lake Kinneret water quality modeling system. Proceedings of the 7th International Conference on HydroScience and Engineering. Drexel University College of Engineering, Philadeplphia, PA. p. 1-35. 9-10-2006.

Hutchinson GE. 1973. Eutrophication: the scientific background of a contemporary practical problem. Am Sci. 61:269-279.

Joosse PJ, Baker DB. 2011. Context for re-evaluating agricultural source phosphorus loadings to the Great Lakes. Canadian Journal of Soil Science. 91:317-327.

Lampert W, Fleckner W, Rai H, Taylor BE. 1986. Phytoplankton control by grazing zooplankton:A study on the spring clear-water phase. Limnol Oceanogr. 31:478-490.

Longabucco P, Rafferty MR. 1998. Analysis of material loading to Cannonsville Reservoir: advantages of event-based sampling. Lake and Reserv Manage. 14:197-212.

Lyon SW, McHale MR, Walter MT, Steenhuis TS. 2006. The impact of runoff generation mechanisms on the location of critical source areas. Journal of the American Water Resource Association. 42:793-804.

Martin JL, McCutcheon SC. 1999. Hydrodynamics and transport for water quality modeling. Lewis Publishers, Boca Raton, FL. 794 p.

Moriasi DN, Arnold JG, Van Liew MW, Bingner RL, Harmel RD, Veith TL. 2007. Model evaluation guidelines for systematic quantification of accuracy in watershed simulations. Transactions of the ASABE. 50:885-900.

Munoz-Carpena R, Vellidis G, Shirmohammadi A, Wallender WW. 2006. Evaluation of modeling tools for TMDL development and implementation. Transactions of the ASABE. 49:961-965.

Nalepa TF, Schloesser DW. 2014. Quagga and Zebra Mussels: Biology, Impacts, and Control, Second Edition. CRC Press Taylor & Francis Group, Boca Raton, FL. 775 p.

Nalepa TF, Fanslow DL, Lang GA. 2009. Transformation of the offshore benthic community in Lake Michigan: recent shift from the native amphipod *Diporeia* spp. to the invasive mussel *Dreissena rostriformis bugensis*. Freshwat Biol. 54:466-479.

Neitsch,SL, JR Williams, JG Arnold and JR Kiniry. 2011. Soil and water assessment tool theoretical documentation version 2009. Texas Water Resources Institute.

NRCC (Northeast Regional Climate Center). 2016. NRCC Hourly Precipitation Database. Cornell University. Available Online: http://www.nrcc.cornell.edu/page_databases.html

NYS DEC (New York State Department of Environmental Conservation). 2015. Water Quality Assessment of Cayuga Lake, Cayuga Lake, Southern End (0705-0040). Available Online: http://www.dec.ny.gov/docs/water_pdf/cornelllscpwlasmt.pdf.

Ozersky T, Malkin SY, Barton DR, Hecky RE. 2009. Dreissenid phosphorus excretion can sustain C. glomerata growth along a portion of Lake Ontario shoreline. J Great Lakes Res. 35:321-328.

Panagopoulos Y, Makropoulos C, Baltas E, Mimikou M. 2011. SWAT parameterization for the identification of critical diffuse pollution source areas under data limitations. Ecol Model. 222:3500-3512.

Parton WJ, Mosier AR, Ojima DS, Valentine DW, Schimel DS, Weier K, Kulmala AE. 1996. Generalized model for N2 and N2O production from nitrification and denitrification. Global Biogeochem Cycles. 10:401-412.

Peng F, Effler SW. 2015. Quantifications and water quality implications of minerogenic particles in Cayuga Lake and its tributaries. Inland Waters. 5:403-420.

Peng F, Effler SW. 2016a. Advancing two-component partitioning of light scattering in Cayuga Lake, New York. Limnol Oceanogr. 61:298-315.

Peng,F and SW Effler. 2016b. Characterization of calcite particles and evaluations of their optical effects in lacustrine systems. Limnol. Oceanogr. (in review).

Prestigiacomo AR, Effler SW, Matthews DA, Auer MT, Downer BE, Kuczynski A, Walter MT. 2016. Apportionment of bioavailable phosphorus loads entering Cayuga Lake, New York. J Am Wat Resour Assoc. 52:31-47.

Prestigiacomo AR, Effler SW, O'Donnell DM, Hassett JM, Michelanko EM, Lee Z, Weidemann AD. 2007. Turbidity and suspended solids levels and loads in a sediment enriched stream: implications for impacted lotic and lentic ecosystems. Lake and Reserv Manage. 23:231-244.

Raymond PA, Saiers JE. 2010. Event controlled DOC export from forested watersheds. Biogeochemistry. 100:197-209.

Reynolds CS, Davies PS. 2001. Sources and bioavailability of phosphorus fractions in freshwaters: a British perspective. Biological reviews of the Cambridge Philosophical Society. 76:27-64.

Reynolds CS. 2006. Ecology of Phytoplankton. Cambridge University Press, Cambridge. 535 p.

Richards RP, Holloway J. 1987. Monte Carlo studies of sampling strategies for estimating tributary loads. Wat Resour Res. 23:1939-1948.

Robson BJ. 2014. State of the art in modelling of phosphorus in aquatic systems: Review, criticisms and commentary. Environ Model Softw. 61:287-296.

Rueda F, Moreno-Ostos E, Armengol J. 2006. The residence time of river water in reservoirs. Ecol Model. 191:260-274.

Schaffner WR, Oglesby RT. 1978. Phosphorus loadings to lake and some of their responses. Part 1. A new calculation of phosphorus loadings and its applications to 13 New York lakes. Limnol Oceanogr. 23:120-134.

Sereda JM, Hudson JJ. 2011. Empirical models for predicting the excretion of nutrients (N and P) by aquatic metazoans: taxonomic differences in rates and element ratios. Freshwat Biol. 56:250-263.

Sommer U, Gliwicz M, Lampert W, Duncan A. 1986. The PEG-model of seasonal succession of planktonic events in fresh waters. Arch Hydrobiol. 106:433-471.

Sommer U, Adrian R, De Senerpont Domis L, Elser JJ, Gaedke U, Ibelings B, Jeppesen E, Lürling M, Molinero JC, Mooij WM. 2012. Beyond the Plankton Ecology Group (PEG) model: mechanisms driving plankton succession. Annual Review of Ecology, Evolution, and Systematics. 43:429-448.

Sondergaard M, Jeppesen E, Lauridsen TL, Skov C, Van Nes EH, Roijackers R, Lammens E, Portielje R. 2007. Lake restoration: success, failures and long-term effects. Journal of Applied Ecology. 44:1095-1105.

Taylor KE, Stouffer RJ, Meehl GA. 2012. An overview of CMIP5 and the experiment design. Bulletin of the American Meteorological Society. 93:485.

Thomann RV. 1982. Verification of water quality models. J Environ Engrg Div ASCE. 108:923-940.

Thomann RV, Mueller JA. 1987. Principles of surface water quality modeling and control. Harper & Row Publishers, NY. 644 p.

Upstate Freshwater Institute. 2001. Calibration and verification of a one-dimensional hydrothermal and eutrophication model for six Catskill/Delaware reservoirs. Submitted to the New York City Department of Environmental Protection, Valhalla, New York. Upstate Freshwater Institute, Syracuse, NY.

Upstate Freshwater Institute. 2007. Testing of a 1-D water quality model for six Croton System reservoirs, and a 2-D water quality model with sediments for New Croton Reservoir. Submitted to NYC DEP. Upstate Freshwater Institute, Syracuse, NY.

Upstate Freshwater Institute. 2014. Phase I: Monitoring and Modeling Support for a Phosphorus/Eutrophication Model for Cayuga Lake. Final Report submitted to Cornell University, Ithaca, NY. 288 p.

USDA (United States Department of Agriculture). 2010. 2010 New York Cropland Data Layer. National Agricultural Statistics Service. Available Online: http://www.nass.usda.gov/research/Cropland/SARS1a.htm

USDA (United States Department of Agriculture). 2015. Web Soil Survey. National Agricultural Statistics Service. Available Online: http://websoilsurvey.sc.egov.usda.gov/App/HomePage.htm

USEPA (United States Environmental Protection Agency). 1991. Guidance for water quality-based decisions: The TMDL process. EPA 440-4-91-001. Office of Water, Washington, DC.

USGS (U.S. Geological Survey). 2016a. National Elevation Dataset. United State Department of Interior. Available Online: http://nationalmap.gov/elevation.html

USGS (U.S. Geological Survey). 2016b. USGS 04234000 Fall Creek Near Ithaca, NY. United State Department of Interior. Available Online: http://waterdata.usgs.gov/nwis/uv?04234000

Vanderploeg HA, Liebig JR, Nalepa TF, Fahnenstiel GL, Pothoven SA. 2010. *Dreissena* and the disappearance of the spring phytoplankton bloom in Lake Michigan. J Great Lakes Res. 36:50-59.

Vogel RM, Stedinger JR, Hooper RP. 2003. Discharge indices for water quality loads. Wat Resour Res. 39:1273.

Vollenweider RA. 1976. Advances in defining critical loading levels for phosphorus in lake eutrophication. Mem Ist Ital Idrobiol. 33:53-83.

Watkins JM, Dermott R, Lozano SJ, Mills EL, Rudstam LG, Scharold JV. 2007. Evidence for remote effects of dreissenid mussels on the amphipod *Diporeia*: Analysis of Lake Ontario benthic surveys, 1972-2003. J Great Lakes Res. 33:642-657.

Watkins JM, Rudstam LG, Mills EL, Teece MA. 2012. Coexistence of the native benthic amphipod *Diporeia* spp. and exotic dreissenid mussels in the New York Finger Lakes. J Great Lakes Res. 38:226-235.

Wetzel RG. 2001. Limnology: lake and reservoir ecosystems. 3rd Ed. Academic Press, New York. 1006 p.

Young TC, DePinto JV, Flint SE, Switzenbaum SM, Edzwald JK. 1982. Algal availability of phosphorus in municipal wastewater. J Water Pollut Control Fed. 54:1505-1516.

Young TC, DePinto JV, Martin SC, Bonner JS. 1985. Algal-available particulate phosphorus in the Great Lake basin. J Great Lakes Res. 11:434-446.

Zhao,ZT, Tian Chen C., W.S.Leo and M.J.Mickelson. 2012. Modeling 2011 in Massachusetts Bay Using the Unstructured-grid Bays Eutrophication Model. 2012-13. Massachusetts Water Resources Authority, Boston, MA. 138 p.

Phase 2 Final Report Appendices

Due to large size of the Final Report Appendices, these are available upon request.